The Dissertation Committee for Saeedeh Mohebbinia Certifies that this is the approved version of the following dissertation:

Advanced Equation of State Modeling for Compositional Simulation of Gas Floods

Committee:

Kamy Sepehrnoori, Supervisor

Russell T. Johns, Co-Supervisor

Kishore Mohanty

Mojdeh Delshad

Walter G. Chapman

Advanced Equation of State Modeling for Compositional Simulation of Gas Floods

by

Saeedeh Mohebbinia, B.Che.E; M.S.E.

Dissertation

Presented to the Faculty of the Graduate School of

The University of Texas at Austin

in Partial Fulfillment

of the Requirements

for the Degree of

Doctor of Philosophy

The University of Texas at Austin

December 2013

Dedication

To my dear and loving husband, Javad,

and my wonderful parents, Masoumeh and Manouchehr

Acknowledgements

I would like to thank all those who inspired and helped me throughout this journey.

I express my sincere gratitude to my supervisors, Dr. Kamy Sepehrnoori and Dr. Russell T. Johns for their continuous guidance, support, and encouragement throughout this project. Dr. Sepehrnoori's invaluable suggestions introduced me the great area of reservoir simulation. Dr. Johns' instructive questions helped me to explore new ideas and challenge unsolved complex phase behavior problems. Their wonderful leadership and insight was the key to success of this research. I appreciate invaluable comments and feedback from my committee members, Dr. Mojdeh Delshad, Dr. Kishore Mohanty, and Dr. Walter G. Chapman.

I gratefully acknowledge the financial support from Abu Dhabi national oil company, along with the member companies of the reservoir simulation joint industry project at The University of Texas at Austin, and the gas flooding research project at EMS energy institute at Pennsylvania State University.

I would like to acknowledge the staff of the Department of Petroleum and Geosystems Engineering, Roger Terzian, Tim Guinn, Frankie Hart, Garry Miscoe, and Glen Baum who have helped me in many ways.

I am deeply grateful to be surrounded by many friends who have been helpful and supportive. Specifically, I would like to thank my great colleagues Mohsen Rezaveisi, Aboulghasem Kazeminia, Saeid Khorsandi, Javad Behseresht, Mahdy Shirdel, Hamed Darabi, and Abdoljalil Varavei for their indispensable help and knowledge sharing. I would like to thank my friends Ali Goudarzi, Ali Moinfar, Amir Frooqnia, AmirReza Rahmani, Ashwin Venkatraman, Hamid Hadibeik, Maryam Okhovat, Mehdi Haddad,

Mohsen Taghavifar, Parvaneh Karimi, and Zoya Heidari, whose moral support has been critical throughout my graduate studies.

I would like to express my deepest appreciation to my beloved husband, Javad, without whose support, I would never have found the courage to overcome all the difficulties during this research. He was always caring, supportive and patient with my long work hours. My heartfelt gratitude goes to my dear parents Masoumeh and Manouchehr for their abundant love and encouragements. Without the support of all members of my family, none of this would have been possible.

Advanced Equation of State Modeling for Compositional Simulation of Gas Floods

Saeedeh Mohebbinia, Ph.D.

The University of Texas at Austin, 2013

Supervisors: Kamy Sepehrnoori

Russell T. Johns

Multiple hydrocarbon phases are observed during miscible gas floods. The possible phases that result from a gas flood include a vapor phase, an oleic phase, a solvent-rich phase, a solid phase, and an aqueous phase. The solid phase primarily consists of aggregated asphaltene particles. Asphaltenes can block pore throats or change the formation wettability, and thereby reduce the hydrocarbon mobility. The dissolution of injected gas into the aqueous phase can also affect the gas flooding recovery because it reduces the amount of gas available to contact oil. This is more important in CO_2 flooding as the solubility of CO_2 in brine is much higher than hydrocarbons. In this research, we developed efficient and fast multi-phase equilibrium calculation algorithms to model phase behavior of asphaltenes and the aqueous phase in the compositional simulation of gas floods.

The PC-SAFT equation of state is implemented in the UTCOMP simulator to model asphaltene precipitation. The additional computational time of PC-SAFT is substantially decreased by improving the root finding algorithm and calculating the derivatives analytically. A deposition and wettability alteration model is then integrated with the thermodynamic model to simulate dynamics of precipitated asphaltenes.

Asphaltene deposition is shown to occur with pressure depletion around the production well and/or with gas injection in the reservoir domain that is swept by injected gas. It is observed that the profile of the damaged area by asphaltene deposition depends on the reservoir fluid.

A general strategy is proposed to model the phase behavior of CO_2/hydrocarbon/water systems where four equilibrium phases exist. The developed four-phase reduced flash algorithm is used to investigate the effect of introducing water on the phase behavior of CO_2/hydrocarbon mixtures. The results show changes in the phase splits and saturation pressures by adding water to these CO_2/hydrocarbon systems.

We used a reduced flash approach to reduce the additional computational time of the four-phase flash calculations,. The results show a significant speed-up in flash calculations using the reduced method. The computational advantage of the reduced method increases rapidly with the number of phases and components. We also decreased the computational time of the equilibrium calculations in UTCOMP by changing the sequential steps in the flash calculation where it checks the previous time-step results as the initial guess for the current time-step. The improved algorithm can skip a large number of flash calculation and stability analyses without loss of accuracy.

Table of Contents

List of Tables

List of Figures

Chapter 1. Introduction

1.1. PROBLEM STATEMENT

Gas flooding is the most common enhanced oil recovery (EOR) technique. Injection of a gas into the reservoir can change the phase behavior of petroleum reservoir fluids. Multiphase behavior is observed during miscible gas injection experiments. The possible phases that occur in a gas flood include a vapor phase, an oleic phase, a solvent-rich phase, and a solid phase (Huang and Tracht 1974, Shelton and Yarborough 1977, Stalkup 1978, Henry and Metcalfe 1983). The solvent-rich phase can be developed at low temperatures, typically bellow 120 °F, when the crude oil is contacted with some solvents such as carbon dioxide or a rich gas (Okuno 2009). The solid phase primarily consists of aggregated asphaltene particles. Mixing oils with a solvent incompatible with asphaltenes may lead to asphaltene destabilization and result in a sticky solid phase (Gonzalez *et al.* 2008). Water is always present, either as initial formation water or as injected water during a water-alternating-gas (WAG) cycle. Therefore, there is often an aqueous phase in contact with hydrocarbon phases in petroleum reservoirs.

Several papers have investigated the phases required to be considered for the accurate simulation of the gas floods at low temperatures at which the second liquid hydrocarbon phase can coexist with the oleic and gaseous phases. Nghiem and Li (1986) suggested to approximate three-phase regions with two-phase flash calculations to avoid complex three-phase flash calculations in these cases. However, as reported by other authors (Lim *et al.* 1992, Khan *et al.* 1992, Wang and Strycker 2000, Okuno *et al.* 2010b), considering the second liquid hydrocarbon phase (i.e. the solvent-rich phase) can significantly affect compositional simulation results. Okuno *et al.* (2010b) also showed that using two-phase approximations in the three phase regions causes discontinuities in

saturations and other physical properties during simulation, which consequently leads to smaller time-steps and in some cases failure of the simulation. Therefore, a reliable simulation of low temperature gas floods requires a phase equilibrium calculation algorithm that can handle three hydrocarbon phases.

The asphaltene deposition problem during oil production has motivated research on phase behavior modeling of asphaltenes as a function of temperature, pressure, and composition. Asphaltenes can block the pore throats or change the formation wettability by adsorbing onto the reservoir rock and thereby reduce the hydrocarbon mobility (Leontaritis *et al.* 1994). Deposition may cause serious formation damage anywhere in the reservoir domain, especially around the production well where the maximum pressure decline happens.

In spite of extensive research on asphaltene phase behavior modeling, few studies have been reported on the simulation of asphaltene precipitation problems during gas injection. The potential of asphaltene precipitation in gas flooding is not usually predicted because reservoirs often contain light oils, which have low asphaltene contents. However, light oils have lower asphaltene solubility and therefore a greater likelihood of asphaltene destabilization under physical or chemical disturbances (Sarma 2003). In some cases, the reservoir has no previous asphaltene precipitation during primary production and therefore the potential of precipitation is overlooked for gas injection (Sarma 2003). Examples are the hydrocarbon gas injection project in Rainbow Keg River "B" pool (Nagel *et al.* 1990) and CO_2 flood pilot project in Migdale in Canada (Beliveau and Payne 1991). These gas floods experienced asphaltene precipitation after gas injection into the reservoir, even though there was no prior asphaltene precipitation problem in preceding primary production or water flood phases.

In compositional reservoir simulations, cubic EOS (CEOS) models are often used in phase behavior predictions because of their simplicity and reasonable predictions of hydrocarbon mixture behavior. However, CEOS models are not as accurate for modeling mixtures containing complex and vastly different size molecules, which is the case in asphaltene containing fluids (Panuganti *et al.* 2012). CEOS models also fail to calculate accurately liquid densities. In addition, the CEOS parameters, which are tuned for critical properties, are not well defined for asphaltene molecules (Panuganti *et al.* 2012). Panuganti *et al.* (2012) showed that a CEOS, which is tuned for particular experimental data, can fail to satisfactorily predict the asphaltene onset pressure for a different gas injection composition. During gas injection, the composition of the fluid dynamically changes because of the repeated oil and gas contacts; therefore the results obtained by a CEOS may not be reliable. In general, reservoir simulators lack a comprehensive phase behavior model to simulate asphaltene precipitation under gas injection.

In the case of CO_2 flooding, CO_2 dissolution into the aqueous phase is also an important factor to be considered in simulation. The solubility of CO_2 in brine is much higher than that of hydrocarbons. Dissolution of CO_2 into the aqueous phase can affect CO_2 flooding recovery because CO_2 dissolution reduces the amount of CO_2 available to contact oil. Several authors have shown that the amount of CO_2 lost in the brine is especially important at high water saturations, e.g., for water-flooded reservoirs or CO_2 WAG processes (Yan and Stenby 2010, 2009, Enick and Klara 1992). Compositional simulators that include CO_2 dissolution into the aqueous phase usually use Henry's law or water-free flash calculations, which may not be sufficiently accurate. An accurate simulation of the CO_2 flood requires considering water in phase equilibrium calculations. CO_2 is one of the solvents that can result in three hydrocarbon phases in contact with

crude oils at low temperatures. Thus, when three hydrocarbon phases are present in equilibrium with water, a four-phase flash calculation that is robust and fast is required.

As the number of phases and components increase, flash calculation becomes more difficult to converge and computationally expensive, making it inefficient or even impractical for use in compositional simulators. Phase equilibrium computations may take a significant portion of the total execution time in compositional simulations (Stenby and Wang 1993). As reported by Chang (1990), more than 60% of the CPU time was spent on phase equilibrium calculations in conducting simulation of a miscible gas flooding (SPE fifth comparative solution project) in a three dimensional gridblock system using an IMPEC compositional simulator (UTCOMP). Therefore, when the number of phases increases, a fast and efficient phase equilibrium algorithm is essential.

Successful modeling of miscible gas flooding requires compositional models in which the transport equations, including fluid flow and mass transfer between the phases, are solved together. Coupling the transport equations is more important when miscibility is developed upon repeated contacts during fluid flow, which is normally the case in most gas injection processes. A compositional reservoir simulator, UTCOMP, has been developed by Chang (1990) at The University of Texas to model miscible gas floods. UTCOMP is capable of performing the equilibrium calculations of three hydrocarbon phases, i.e. a vapor phase, an oleic phase and a solvent rich phase using the EOS approach. The equilibrium calculations algorithm (Perschke 1988) in UTCOMP consist of stability analysis to predict the number of phases present in the gridblocks followed by flash calculations to calculate the distribution of the components between the phases. Qin *et al.* (2000) implemented a solid model (Nghiem and Coombe 1997, Nghiem 1999) in UTCOMP to predict the effects of asphaltene precipitation on fluid flow through porous media. The aqueous phase can also be included in the calculations using Henry's law.

Henry's law calculates the hydrocarbon solubility in the aqueous phase. Water is considered an inert component, which is not allowed to be in the hydrocarbon phases. UTCOMP is the base code for implementing and testing the phase behavior modules developed during this research.

1.2. RESEARCH OBJECTIVES

The main objective in this research is to study the effect of gas injection on the phase behavior of reservoir fluids with advanced EOS approaches. This will include the phase behavior modeling of asphaltene precipitation and the aqueous phase with hydrocarbon phases in different gas injection problems.

The first objective is to develop a phase behavior algorithm using the perturbed-chain statistical associating fluid theory (PC-SAFT) EOS (Gross and Sadowski 2001) to model apshaltene precipitation. PC-SAFT EOS is one of the modifications of SAFT EOS (Chapman *et al.* 1990) derived by Gross and Sadowski (2001) by adopting the hard-chain fluid instead of the hard-sphere used in the original SAFT as the reference fluid. PC-SAFT has shown promise in modeling the phase equilibrium of asphaltic crude systems (Gonzalez *et al.* 2005, Panuganti *et al.* 2012, Gonzalez *et al.* 2008, Gonzalez *et al.* 2007, Vargas *et al.* 2009). Panuganti *et al.* (2012) showed that PC-SAFT can model asphaltene precipitation under different gas injection amounts better than a CEOS.

The next goal is to couple the phase behavior algorithm with a deposition and plugging model and implement them in UTCOMP to study the effect of gas injection on asphaltene precipitation and deposition. To the best of our knowledge, no reservoir simulator uses PC-SAFT EOS to model the phase behavior of asphaltenes because of its complexity and high computational cost.

Speeding up the phase equilibrium calculations using PC-SAFT EOS is the next objective in this research. Phase equilibrium calculations using PC-SAFT EOS take more computational effort than the traditional CEOS for two reasons. First, there is no closed form for PC-SAFT EOS and therefore finding the density roots is an iterative process. Second, the algebraic equations to find the thermodynamic properties using PC-SAFT are more complex than those using a CEOS.

The next objective is to extend the available three-phase equilibrium calculation algorithm of UTCOMP to four phases using a CEOS to include the aqueous phase in the phase behavior calculations. Søreide and Whitson's modification (Søreide and Whitson 1992) of Peng-Robinson (PR) EOS (Peng and Robinson 1976) is chosen to model the aqueous phase. Their model gives reasonable predictions of the solubility of CO_2 and light hydrocarbons in water (Yan and Stenby 2009).

The last objective is to speed up the phase equilibrium calculations for CEOS. We extend the reduced flash calculations algorithm developed by Okuno *et al.* (2010b) to four phases, including three hydrocarbon phases and an aqueous phase. We also improve the equilibrium calculations algorithm in UTCOMP by changing the sequential steps in the flash calculation to skip a large number of flash calculations and stability analyses without loss of accuracy.

Chapter 2. Background

The goal of this chapter is to review the important findings published in the literature on phase behavior modeling of gas floods. The first section of this chapter briefly summarizes the equilibrium calculation concepts. In the second section, we review the basic concepts on asphaltene precipitation and deposition. Then, we explain the phase behavior modeling of asphaltene precipitation using the PC-SAFT EOS. The third section of this chapter deals with the aqueous phase modeling. Finally, the approaches for speed-up of the phase equilibrium calculations are summarized.

2.1. PHASE EQUILIBRIUM CALCULATIONS

The purpose of the phase equilibrium calculations is to predict the number and amounts of the phases and the distribution of the fluid species between the phases at equilibrium. Thermodynamic equilibrium indicates a state of balance at which the total entropy of the system comes to a maximum or, equivalently, the Gibbs free energy is a minimum based on the second law of thermodynamics.

The minimization of Gibbs free energy or the solution of equivalent equations has been the subject of a wide variety of research to formulate the phase equilibrium of mixtures. These calculations are generally performed in two main steps, as proposed by Michelsen (1982a, b). The first step is the stability analysis to determine whether the test mixture is stable or if it will split into an additional phase. The second involves flash calculations to compute the compositions and amounts of the present phases.

2.1.1. Stability analyses

A fast stability analysis algorithm was first proposed by Michelsen (1982a) based on the tangent plane criteria of Baker *et al.* (1982). A study by Baker *et al.* (1982)

showed that no point on the Gibbs free energy surface can lie below the tangent plane to the Gibbs free energy surface at a stable equilibrium. This condition can be used as a necessary and sufficient criterion for phase stability. Following this criterion, Michelsen defined the Tangent Plane Distance (TPD) as the distance between the Gibbs free energy and the tangent plane to the Gibbs free energy at a specific phase composition (Michelsen 1982a). A phase can then be stable if and only if the TPD function is nonnegative everywhere.

The TPD function is derived through a first order Taylor expansion of the Gibbs free energy around a given phase composition. At a given composition $\bar{z}$, a tangent plane to the Gibbs free energy surface can be written as (Okuno 2009)

$$\begin{aligned} T(\bar{x}) &= \bar{G}(\bar{z}) + \sum_{i=1}^{N_C}(x_i - z_i)\left(\frac{\partial \bar{G}(\bar{x})}{\partial x_i}\right)\Bigg|_{\bar{x}=\bar{z}} \\ &= \bar{G}(\bar{z}) + \sum_{i=1}^{N_C}(x_i - z_i)\left[\bar{G}_i(\bar{z}) - \bar{G}_{N_C}(\bar{z}) + \sum_{j=1}^{N_C} x_j\left(\frac{\partial \bar{G}_j}{\partial x_i}\right)\right] \\ &= \bar{G}(\bar{z}) + \sum_{i=1}^{N_C} x_i \bar{G}_i(\bar{z}) - \sum_{i=1}^{N_C} z_i \bar{G}_i(\bar{z}) \\ &= \sum_{i=1}^{N_C} x_i \bar{G}_i(\bar{z}). \end{aligned} \tag{2.1}$$

From the Gibbs-Duhem equation, the summation term in the brackets in Eq. (2.1) is zero. The dimensionless TPD function, $D_R(\bar{x})$, is obtained as

$$\begin{aligned} D_R(\bar{x}) &= \frac{1}{RT}\left[\bar{G}(\bar{x}) - T(\bar{x})\right] = \frac{1}{RT}\sum_{i=1}^{N_C} x_i\left(\bar{G}_i(\bar{x}) - \bar{G}_i(\bar{z})\right) \\ &= \sum_{i=1}^{N_C} x_i\left(\ln x_i\phi_i(\bar{x}) - \ln z_i\phi_i(\bar{z})\right) \end{aligned}, \tag{2.2}$$

where x_i is the trial composition of component i, z_i is the overall composition of component i in the test mixture, and ϕ_i is the fugacity coefficient of component i.

Michelsen's algorithm for stability analysis is based on searching for a composition at which the TPD function value becomes negative. Once the search algorithm finds such a point, the test mixture is identified as an unstable phase, which must then split into multiple phases. Otherwise, the mixture is assumed to be stable.

Two formulations have been proposed for stability analysis based on TPD criterion. One is the minimization of the TPD function in the composition space satisfying the following constraint:

$$\sum_{i=1}^{N_C} x_i = 1 \text{ and } x_i \geq 0 \quad \text{for } i = 1,...,N_C . \tag{2.3}$$

The sign of the TPD function determines the stability of the test mixture if the global minimum of the function is known. Another approach to stability analysis is to check the sign of the TPD function at stationary points. To locate the stationary points, Michelsen (1982a) proposed the following equation, which is referred to as the stationary equation:

$$\ln X_i \phi\left(\overline{x}\right) - \ln z_i \phi\left(\overline{z}\right) = 0 \quad \text{for } i = 1,...,N_C , \tag{2.4}$$

where

$$X_i = x_i \exp\left(-D_R\left(\overline{x}\right)\right) \quad \text{for } i = 1,...,N_C . \tag{2.5}$$

Eq. (2.4) is derived based on the fact that all first-order derivatives of TPD function are zeros at stationary points. Michelsen's algorithm is applicable to both single-phase and multiphase mixtures. For multiphase mixtures, the algorithm could be applied to each individual phases.

2.1.2. Flash calculations

Provided a given initial amount of components is in a closed PVT system, Duhem's theorem suggests that the equilibrium state of the system can be fully determined using any two independent properties of the system. An application of Duhem's theorem is what is known as a flash calculation. A flash calculation is used to compute the composition and amounts of different phases in a mixture, for a fixed number of moles of each component in the overall mixture, at a given temperature and pressure.

The traditional approach for flash calculation is based on the equality of chemical potentials, or equivalently, the equality of fugacities. The equilibrium condition for a multi-component system is that the chemical potential of a component, μ_i, is equal in each phase:

$$\mu_{i1} = \mu_{i2} = ... = \mu_{iN_P} \quad \text{for } i = 1, ..., N_C . \tag{2.6}$$

This criterion is true for all the components in the mixture. The chemical potential of a component is correlated to its Gibbs free energy by the following correlation:

$$\mu_i = \left(\frac{\partial G}{\partial n_i} \right)_{T,P,n_{k \neq i}} \equiv \bar{G}_i , \tag{2.7}$$

where $\bar{G}_i$ is the partial molar Gibbs free energy. A useful thermodynamic quantity, called fugacity, can be derived from the chemical potential using the following relation:

$$\mu_i = \mu_i^o + RT \ln\left(\frac{f_i}{f_i^o} \right), \tag{2.8}$$

where f_i is the fugacity of component i and f_i^o is the fugacity of the same component at a reference state. Substitution of Eq. (2.8) into Eq. (2.6) results in a more practical, but an

equivalent statement of the equilibrium condition, called the equi-fugacity equation

$$f_{i1} = f_{i2} = ... = f_{iN_P} \quad \text{for } i = 1,...,N_C . \tag{2.9}$$

In flash calculations based on solving the fugacity equations, the independent variables are K-values (i.e. equilibrium ratios) or the logarithm of *K*-values (Nghiem and Li 1984, Abhvani and Beaumont 1987). *K*-values are defined as the tendency of the components to prefer one phase over another and are given by

$$K_{ij} = x_{ij} / x_{i1} , \tag{2.10}$$

where $i = 1,...,N_C$ and $j = 2,...,N_P$. The first phase is chosen as the reference phase, arbitrarily.

One of the conventional methods to solve fugacity equations is successive substitution (SS). In SS, the equality of fugacity equations can be written in terms of *K*-values and fugacity coefficients (i.e. ϕ_{ij}) as follows:

$$\ln K_{ij}^{k+1} = \ln \phi_{i1}^{k} - \ln \phi_{ij}^{k} \quad \text{where } i = 1,...,N_C \text{ and } j = 2,...,N_P . \tag{2.11}$$

In Eq. (2.11), the superscripts show iteration steps and ϕ_{ij} is the fugacity coefficient of component *i* in phase *j*. *K*-values are updated at each iteration by solving the fugacity equations subject to material balance constraints. The material balance equations are solved to find the phase compositions for a given set of *K*-values because the fugacity coefficients are functions of the compositions. The standard algorithm to calculate the phase compositions using constant *K*-values was first proposed by Rachford and Rice (1952).

SS is considered a robust algorithm as it is a gradient method for Gibbs free energy minimization (Okuno 2009). However, the SS method becomes noticeably slow in near-critical regions (Michelsen 1982b) because this method provides a linear

convergence to the solution. A significant number of iterations are required using SS near critical regions (Mehra *et al.* 1983, Ammar and Renon 1987). Several acceleration techniques are proposed for enhancing the convergence, such as algorithms presented by Michelsen (1982b), Mehra *et al.* (1982, 1983), and Nghiem and Heidemann (1982). Perschke (1988) used the algorithm proposed by Mehra *et al.* (1983) in UTCOMP for two- and three-phase flash calculations.

Owing to its robustness, the SS algorithm has had a prominent place in phase equilibrium calculations to provide initial guesses for higher order methods such as Newton's algorithm (Ammar and Renon 1987, Michelsen 1982b, Mehra *et al.* 1982, Nghiem *et al.* 1983). SS is linearly convergent but provides a larger region of convergence compared to Newton's method (Okuno 2009). On the other hand, Newton's method is a fast and quadratically convergent iterative method only if a reasonable initial guess is provided (Okuno 2009). Therefore, using SS followed by Newton's algorithm is a common scheme in compositional reservoir simulators. One of these earliest combination methods used in compositional reservoir simulation was proposed by Nghiem and Aziz (1983).

Algorithms based on solving the fugacity equations are root-finding procedures, which are not reliable for systems with more than two phases (Michelsen 1982b). The number of critical points and stationary points of the Gibbs free energy surface increases with the number of phases in the system. Therefore, as the number of phases increases, there can be a larger number of potential solutions. Also, the solution can potentially converge to a composition where the phases have the same density and composition, which is a trivial solution (Okuno 2009). Michelsen (1982b) suggested using the minimization algorithm based on the Gibbs free energy surface for three-phase systems.

Many algorithms have been proposed in the literature to minimize the Gibbs free energy for phase split calculations (Gautam and Seider 1979, Lucia *et al.* 1985, Trangenstein 1985, 1987, Ammar and Renon 1987). Michelsen (1982b) proposed a standard algorithm for minimization of Gibbs free energy based on Newton's method. Perschke (1988) used Newton's algorithm combined with a line-search technique. The objective function in the Gibbs free energy minimization formulation is

$$G^t = \sum_{j=1}^{N_P} \sum_{i=1}^{N_C} n_{ij} \ln \mu_{ij} , \tag{2.12}$$

where G^t is the Gibbs free energy of the system and n_{ij} the number of moles of component i in phase *j*. The chemical potential is related to the fugacity using Eq. (2.8). The minimization is subject to the material balance constraints, which are given by the following equations:

$$\mathrm{n}_{ij} > 0 \quad \text{for } i = 1, 2, ..., N_C \quad \text{and} \quad j = 1, 2, ..., N_P , \tag{2.13}$$

and

$$N_i = \sum_{j=1}^{N_P} n_{ij} \quad \text{for } i = 1, 2, ..., N_C . \tag{2.14}$$

In this algorithm, n_{ij} ($i = 1, 2, ..., N_C$ and $j = 2, ..., N_P$) are used as independent variables. Because of the material balance constraint, n_{i1} is dependent on the other mole numbers and, therefore, there are $N_C \left(N_P - 1 \right)$ independent variables in the system.

The necessary and sufficient conditions to find the local minimum, x^*, of a function, *F*, are

(I) the first-order derivatives, $\nabla F \left(x^* \right)$, must be zero and

(II) the Hessian matrix, $\nabla^2 F\left(x^*\right)$, must be positive definite.

The first-order derivatives of G^t with respect to the independent variables can be written as

$$\frac{\partial}{\partial n_{ik}}\left(\frac{G^t}{RT}\right)=\sum_{j=2}^{N_P}\sum_{l=1}^{N_C}\left[\left(\frac{\partial n_{lj}}{\partial n_{ik}}\right)\ln f_{lj}+n_{lj}\left(\frac{\partial \ln f_{lj}}{\partial n_{ik}}\right)\right]+$$
$$\sum_{l=1}^{N_C}\left[\left(\frac{\partial n_{l1}}{\partial n_{ik}}\right)\ln f_{l1}+n_{l1}\left(\frac{\partial \ln f_{l1}}{\partial n_{ik}}\right)\right] \text{ for } i=1,2,...,N_C \quad \text{and} \quad k=1,...,N_P. \tag{2.15}$$

The mole numbers in Eq. (2.15) are independent, therefore

$$\left(\frac{\partial n_{lj}}{\partial n_{ik}}\right)=1, \quad \text{for } l=i \text{ and } j=k, \tag{2.16}$$

and

$$\left(\frac{\partial n_{l1}}{\partial n_{ik}}\right)=1, \quad \text{for } l=i \text{ and } k=2,3,...,N_P$$

From the Gibbs-Duhem relation, we have

$$\sum_{l=1}^{N_C} n_{lj}\left(\frac{\partial \ln f_{lj}}{\partial n_{ik}}\right)=0, \quad \text{for } j,k=1,2,...,N_P. \tag{2.17}$$

Using the Gibbs-Duhem relation, Eq. (2.15) is expressed as follows:

$$\frac{\partial}{\partial n_{ik}}\left(\frac{G^t}{RT}\right)=\ln f_{ik}-\ln f_{i1}=0 \qquad \text{for } i=1,2,...,N_C \quad \text{and} \quad k=2,3,...,N_P. \tag{2.18}$$

The Hessian matrix is also derived analytically from Eq. (2.15). The Hessian matrix for a three-phase mixture has the form

$$H = \begin{bmatrix} \frac{\partial \ln \bar{f}_2}{\partial \bar{n}_2} + \frac{\partial \ln \bar{f}_3}{\partial \bar{n}_3} & \frac{\partial \ln \bar{f}_2}{\partial \bar{n}_2} \\ \frac{\partial \ln \bar{f}_2}{\partial \bar{n}_2} & \frac{\partial \ln \bar{f}_2}{\partial \bar{n}_2} + \frac{\partial \ln \bar{f}_4}{\partial \bar{n}_4} \end{bmatrix}. \tag{2.19}$$

Newton's method can fail when the Hessian matrix is not positive definite. For this situation, the modified Cholesky decomposition is used to adjust the Hessian matrix to be positive definite (Gill and Murray 1974, Perschke 1988, Okuno 2009).

2.2. ASPHALTENES

Asphaltenes are defined as ploydisperse mixtures (i.e. mixtures containing molecules with large size differences) of the polar and high molecular weight hydrocarbon fraction of the crude oil. Conventionally, they are characterized as insoluble in light paraffinic solvents such as n-heptane and soluble in aromatic solvents such as benzene (Srivastava and Huang 1997, Vargas *et al.* 2009).

Asphaltene molecules generally contain poly-nuclear aromatic components with few alkyl groups in their aromatic rings. They also contain other components such as sulfur, oxygen, and a few specific metals (Scotti and Montanari 1998, Gonzalez 2008). Asphaltenes form a continuum of aggregates composed of self-associated molecules. Figure 2-1 shows two common asphaltene molecular structures known as continental model and archipelago model (Kuznicki *et al.*, 2008). When asphaltene concentration is large enough, asphaltenes form loose and irregular short range stacks of self-associated molecules. The length of these stacks is usually less than eight aspahltene molecules with an average aggregate size between 3 to 25 nm in diameter (Ravey *et al.* 1988, Burya *et al.* 2001).

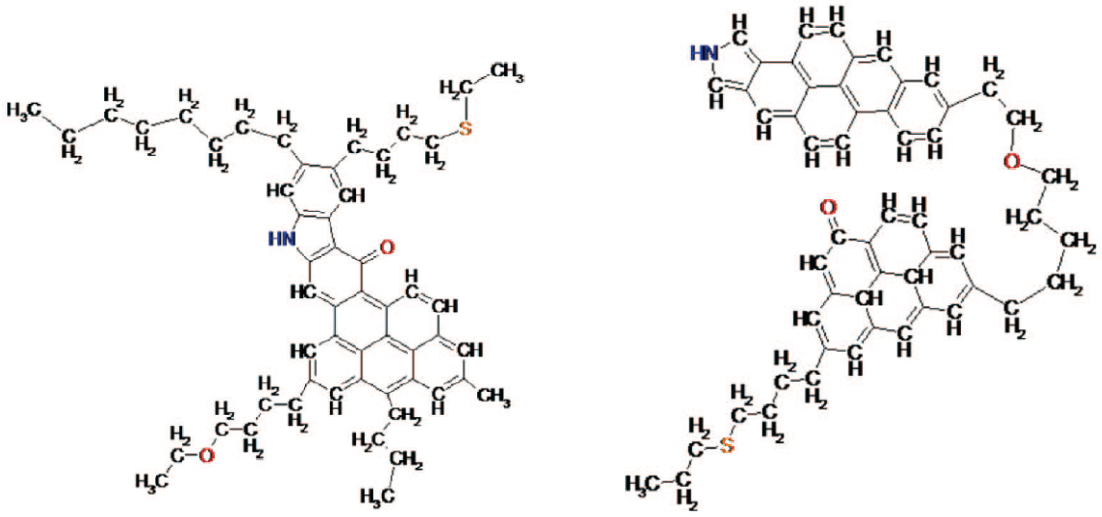

(a) (b)

Figure 2-1: Common asphaltene structural models: (a) continental model, (b) archipelago model (Kuznicki *et al*., 2008).

The carbon number in asphaltene macromolecules ranges from 40 to 80 with typical H/C ratios between 1.1 and 1.2. The density of pure asphaltenes range from 1.13 g/cm^3 to 1.20 g/cm^3 (Gonzalez 2008). An increase in the asphaltene content of the crude oil causes a pronounced increase in the oil viscosity (Werner *et al.* 1998). Usually, the sharp increase in relative viscosity of a crude oil is used to identify the onset of asphaltene destabilization when asphaltene particle aggregation occurs (Escobedo and Mansoori 1997).

2.2.1. Thermodynamics of asphaltene precipitation

Asphaltene deposition during oil production has motivated research studies on the phase behavior modeling of asphaltenes as a function of temperature, pressure, and composition. The existing thermodynamic models can be categorized in two main fundamental approaches: colloidal and solubility approaches.

Models based on the colloidal approach assume asphaltenes as suspended solid particles, which are peptized by resins in a colloidal system (Leontaritis and Mansoori 1987, Leontaritis 1988). The theory of the colloidal behavior of asphaltenes is attributed to Nellensteyn (1924). He expressed the asphaltic compounds as a hydrocarbon medium containing dispersed aggregates or flocs of asphaltenes which are stabilized by resins and other hydrocarbons absorbed on their surface. In 1987, Leontaritis and Mansoori proposed a colloidal model to predict asphaltene precipitation onset.

Based on the colloidal approach, Victorov and Firoozabadi (1996) proposed a thermodynamic micellization model in which asphaltenes are considered to exist in the crude oil within micelles. Micelles consist of an asphaltene core stabilized by protective layers of resins and components other than asphaltenes (Victorov and Firoozabadi 1996, Pan and Firoozabadi 1998b). Asphaltenes and resins in micelles are in thermodynamic equilibrium with their monomers in oil under stable conditions (Pan and Firoozabadi 1998b). As long as the micellar cores are thermodynamically stable, asphaltene particles are not problematic in crude oil. However, thermodynamic equilibrium can be disturbed by physical or chemical interactions. These interactions can dissociate the protective shell and cause asphaltene flocculation (Allenson and Walsh 1997).

According to the solubility approach, asphaltenes are dissolved in the crude oil and form a real solution (Hirschberg *et al.* 1984, James and Mehrotra 1988, Burke *et al.* 1990). In solubility models, the precipitation is considered in a solid-liquid equilibrium (SLE) or a liquid-liquid equilibrium (LLE) state. One of the SLE solubility models is the solid model proposed by Nghiem (1997). In their model, the precipitated asphaltenes were treated as a single-component solid phase; while the gaseous and oleic phases were modeled with a CEOS. Nghiem *et al.* (1997) assumed that the heaviest component in the

oil can be split into a non-precipitating component and a precipitating component (i.e., asphaltenes).

Flory-Huggins regular solution based models (Hirschberg *et al.* 1984, Rassamdana *et al.* 1996) and EOS models are other examples of the solubility approach. Li and Firoozabadi (2010) used cubic-plus-association (CPA) EOS to model asphaltene precipitation under pressure depletion and CO_2 injection processes. CPA was originally developed to model the phase behavior of systems containing associating fluids (Kontogeorgis *et al.* 1996). In this model, the physical interactions are described by a CEOS. The CEOS is incorporated with an association term describing the polar interactions between asphaltene molecules and between asphaltenes and heavy molecules.

SAFT (Chapman *et al.* 1990) is another EOS used by Ting *et al.* (2003) to model asphaltene phase behavior. This EOS, which is based on statistical mechanics, can efficiently account for molecular polydispersity. Ting *et al.* (2003) assumed that polar-polar interactions are insignificant and van der Waals forces can sufficiently explain the interactions between the molecules in asphaltic crudes. That is, they neglected the association term in SAFT. Ting *et al.* (2003) also proposed how to do fluid characterization using PC-SAFT to model asphaltene precipitation.

PC-SAFT (perturbed-chain SAFT) is one of the SAFT variants derived by Gross and Sadowski (2001). They adopted the hard-chain fluid instead of the hard-sphere used in the original SAFT as the reference fluid. PC-SAFT has shown promise in modeling the phase equilibrium of asphaltic crude systems (Gonzalez *et al.* 2005, Panuganti *et al.* 2012, Gonzalez *et al.* 2008, Gonzalez *et al.* 2007, Vargas *et al.* 2009). Panuganti *et al.* (2012) showed that PC-SAFT can predict asphaltene precipitation under gas injection much better than a CEOS. In this research, we used PC-SAFT EOS to model asphaltene

precipitation. Extended work using this model in the compositional simulator is presented in the next chapters.

2.2.2. PC-SAFT EOS

SAFT (Chapman *et al.* 1990) falls into the category of molecular EOS models based on statistical mechanics. It was developed by extending the first-order perturbation theory proposed by Wertheim (1984a, b) in which the Helmholtz free energy is expanded around the free energy of a reference fluid. Therefore, the EOS is expressed as the Helmholtz free energy of a reference fluid plus perturbation terms which correct the reference system. The reference system in SAFT was assumed as spherical segments. Gross and Sadowski (2001) developed PC-SAFT EOS by applying the perturbed chain modification to the SAFT EOS. Instead of spherical segments, they used hard-chain fluid as the reference, which is physically more realistic for chain molecules. Gross and Sadowski extended the perturbation theory of Barker and Henderson (1967) to a hard-chain reference fluid to express chain length effects on the dispersion energy of the segments. PC-SAFT EOS has received much interest in academia and industry for modeling the phase equilibrium of systems containing heavy molecules such as asphaltenes (Gonzalez *et al.* 2005, Gonzalez *et al.* 2007, Gonzalez *et al.* 2008, Gonzalez 2008, Vargas *et al.* 2009, Panuganti *et al.* 2012).

In statistical thermodynamics, an EOS is usually described by Helmholtz free energy because it is capable of describing most of the thermodynamic properties of a system. The Helmholtz free energy of a system is described by perturbation theory (Barker and Henderson 1967) as a sum of two contributions: (i) an unperturbed system (i.e. referred to as a reference system) where the only interaction between molecules is

repulsive forces and (ii) a perturbation because of attractive forces such as dispersion and association interactions. In PC-SAFT EOS, the Helmholtz free energy is expressed as

$$\tilde{a}^{res} = \underbrace{\tilde{a}^{hc}}_{\text{Reference term}} + \underbrace{\tilde{a}^{disp} + \tilde{a}^{assoc}}_{\text{Perturbation term}}, \tag{2.20}$$

where $\tilde{a}$ is the reduced Helmholtz free energy and is given by

$$\tilde{a} = \frac{A}{N\kappa T}, \tag{2.21}$$

and the superscripts *hc*, *disp*, and *assoc* denote the hard-chain, dispersion, and association contributions to the Helmholtz free energy, respectively. The term N denotes the total number of molecules, κ is the Boltzmann constant, and T is the absolute temperature. Figure 2-2 shows a schematic representation of molecule formation and different contributions to the Helmholtz free energy in PC-SAFT EOS.

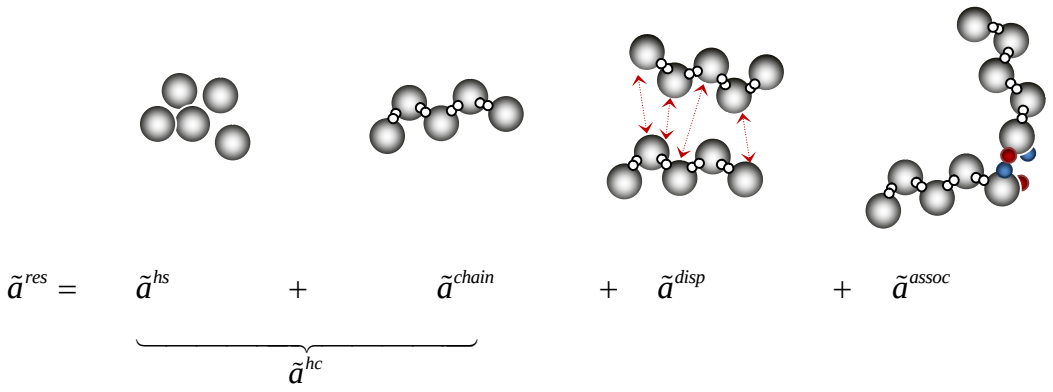

Figure 2-2: Schematic representation of the formation of molecules and different contributions to Helmholtz free energy in PC-SAFT EOS.

2.2.2.1. The hard-chain contribution

The hard-chain reference contribution consists of hard sphere and chain formation contributions. The hard-chain term is given by

$$\tilde{a}^{hc} = \bar{m}\tilde{a}^{hs} - \sum_{i=1}^{N_C} x_i \left(m_i - 1\right) \ln g_{ii}^{hs}\left(d_{ii}\right), \tag{2.22}$$

where $\tilde{a}^{hs}$ is the hard-sphere term of the Helmholtz free energy, $\bar{m}$ is the mean segment number, and g^{hs} is the hard-sphere radial distribution function. In statistical mechanics, the radial distribution function is defined as the probability of finding other molecules at a given distance from a reference molecule. It is usually determined from molecular simulations or integral calculations by evaluating the number of molecules within a distance of *r* and *r* + *dr* away from the reference molecule (Figure 2-3).

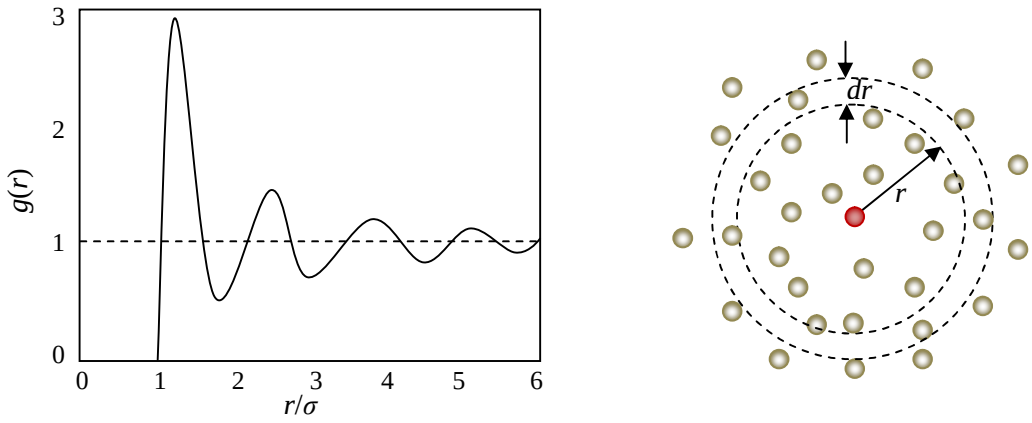

Figure 2-3: A typical radial distribution function for a mixture containing spherical particles with diameter σ.

The mean segment number in Eq. (2.22) is calculated as

$$\bar{m} = \sum_{i=1}^{N_C} x_i m_i \,, \tag{2.23}$$

where x_i is the mole fraction of component *i* and m_i is the number of segments in a chain of species *i* in the mixture. The Helmholtz free energy of the hard-sphere fluid is given by

$$\tilde{a}^{hs} = \frac{1}{\xi_0}\left[\frac{3\xi_1\xi_2}{(1-\xi_3)} + \frac{\xi_2^3}{\xi_3(1-\xi_3)^2} + \left(\frac{\xi_2^3}{\xi_3^2}\right)\ln(1-\xi_3)\right], \tag{2.24}$$

with ξ_n defined as

$$\xi_n = \frac{\pi}{6}\rho\sum_{i=1}^{N_C} x_i m_i d_i^n \quad \text{for } n = 0,1,2,3, \tag{2.25}$$

where ρ is the total number density of molecules and d_i is the temperature-dependent segment diameter of component *i*. The radial distribution function is expressed as

$$g_{ij}^{hs} = \frac{1}{(1-\xi_3)} + \left(\frac{d_i d_j}{d_i + d_j}\right)\frac{3\xi_2}{(1-\xi_3)^2} + \left(\frac{d_i d_j}{d_i + d_j}\right)^2 \frac{3\xi_2^3}{(1-\xi_3)^3} \quad \text{for } i, j = 1,\ldots,N_C. \tag{2.26}$$

The temperature-dependent segment diameter of component *i*, d_i, is calculated from

$$d_i(T) = \sigma_i\left[1 - 0.12\exp\left(-\frac{3\varepsilon_i}{\kappa T}\right)\right], \tag{2.27}$$

where σ_i denotes the temperature independent segment diameter and ε_i is the depth of square well potential of component *i*. Terms m_i, σ_i, and ε_i are the pure-component parameters which describe non-associating molecules.

2.2.2.2. The dispersion contribution

Molecular segments can exhibit attractive forces to each other. Dispersion (London) forces are the attractive forces that exist between the segments of the same

chain as well as the segments of different chains. Dispersion interactions are universal and exist whether the molecules are polar or nonpolar. In PC-SAFT EOS, the dispersion contribution to the Helmholtz free energy is given by

$$\tilde{a}^{disp} = -2\pi\rho I_1\left(\eta,\bar{m}\right)\overline{m^2\varepsilon\sigma^3} - \pi\rho\bar{m}C_1 I_2\left(\eta,\bar{m}\right)\overline{m^2\varepsilon^2\sigma^3}\,, \tag{2.28}$$

where the abbreviations C_1, $\overline{m^2\varepsilon\sigma^3}$, and $\overline{m^2\varepsilon^2\sigma^3}$ are defined as

$$C_1 = \left(1+\bar{m}\frac{8\eta-2\eta^2}{\left(1-\eta\right)^4}+\left(1-\bar{m}\right)\frac{20\eta-27\eta^2+12\eta^3-2\eta^4}{\left[\left(1-\eta\right)\left(2-\eta\right)\right]^2}\right)^{-1}, \tag{2.29}$$

$$\overline{m^2\varepsilon\sigma^3} = \sum_{i=1}^{N_C}\sum_{j=1}^{N_C} x_i x_j m_i m_j \left(\frac{\varepsilon_{ij}}{\kappa T}\right)\sigma_{ij}^3\,, \tag{2.30}$$

and

$$\overline{m^2\varepsilon^2\sigma^3} = \sum_{i=1}^{N_C}\sum_{j=1}^{N_C} x_i x_j m_i m_j \left(\frac{\varepsilon_{ij}}{\kappa T}\right)^2\sigma_{ij}^3\,. \tag{2.31}$$

In Eq. (2.29), η is the packing fraction (reduced density), which is equal to ξ_3. The parameters for a pair of unlike segments, ε_{ij} and σ_{ij}, are determined by

$$\varepsilon_{ij} = \sqrt{\varepsilon_i\varepsilon_j}\left(1-k_{ij}\right), \tag{2.32}$$

and

$$\sigma_{ij} = \frac{1}{2}\left(\sigma_i+\sigma_j\right), \tag{2.33}$$

where k_{ij} is a binary interaction parameter (BIP) between components *i* and *j*. The terms I_1 and I_2 are the integrals defined by the perturbation theory, which can be simplified to two simple power series as follows:

$$I_1(\eta,\bar{m}) = \sum_{i=0}^{6} a_i(\bar{m})\eta^i \,, \tag{2.34}$$

and

$$I_2(\eta,\bar{m}) = \sum_{i=0}^{6} b_i(\bar{m})\eta^i \,, \tag{2.35}$$

where the a_i and b_i are related to the chain length by the following equations:

$$a_i(\bar{m}) = a_{i0} + \left(\frac{\bar{m}-1}{\bar{m}}\right)a_{1i} + \left(\frac{\bar{m}-1}{\bar{m}}\right)\left(\frac{\bar{m}-2}{\bar{m}}\right)a_{2i} \,, \tag{2.36}$$

and

$$b_i(\bar{m}) = b_{i0} + \left(\frac{\bar{m}-1}{\bar{m}}\right)b_{1i} + \left(\frac{\bar{m}-1}{\bar{m}}\right)\left(\frac{\bar{m}-2}{\bar{m}}\right)b_{2i} \,. \tag{2.37}$$

The model constants a_{0i}, a_{1i}, a_{2i}, b_{0i}, b_{1i}, and b_{2i} are presented in Table 2-1 and Table 2-2 .

Table 2-1: Universal constants for Eq. (2.36) (Gross and Sadowski 2001)

i	a_{0i}	a_{1i}	a_{2i}
0	0.91056314452	-0.30840169183	-0.09061483510
1	0.63612814495	0.18605311592	0.45278428064
2	2.68613478914	-2.50300472587	0.59627007280
3	-26.5473624915	21.4197936297	-1.72418291312
4	97.7592087835	-65.2558853304	-4.13021125312
5	-159.591540866	83.3186804809	13.7766318697
6	91.2977740839	-33.7469229297	-8.67284703680

Table 2-2: Universal constants for Eq. (2.37) (Gross and Sadowski 2001)

i	b_{0i}	b_{1i}	b_{2i}
0	0.72409469413	-0.57554980753	0.09768831158
1	2.23827918609	0.69950955214	-0.25575749816
2	-4.00258494846	3.89256733895	-9.15585615297
3	-21.0035768149	-17.2154716478	20.6420759744
4	26.8556413627	192.672264465	-38.8044300521
5	206.551338407	-161.826461649	93.6267740770
6	-355.602356122	-165.207693456	-29.6669055852

2.2.2.3. The association contribution

The association contribution takes into account the specific interactions such as hydrogen bonding and electron donor-acceptor interactions. The Helmholtz energy of the association is expressed as

$$\tilde{a}^{assoc} = \sum_i x_i \left[\left(\sum_{A_i} \ln X^{A_i} - \frac{X^{A_i}}{2} \right) + \frac{M_i}{2} \right], \tag{2.38}$$

where X^{A_i} is the fraction of molecules i not bonded at site A and M_i is the number of association sites on molecule i. X^{A_i} is related to the association strength, $\Delta^{A_iB_j}$, between active sites A_i and B_i belonging to two different molecules and calculated from

$$X^{A_i} = \frac{1}{1 + \rho \sum_j x_j \sum_{B_j} X^{B_j} \Delta^{A_iB_j}}, \tag{2.39}$$

where

$$\Delta^{A_iB_j} = g_{ij}^{hs} \left[\exp\left(\frac{\varepsilon^{A_iB_j}}{\kappa T} \right) - 1 \right] \sigma_{ij}^3 \kappa^{A_iB_j} . \tag{2.40}$$

In Eq. (2.40), $\varepsilon^{A_iB_j}$ and $\kappa^{A_iB_j}$ are the association energy and association volume, respectively. Considering association term adds two more input parameters and more complexity to the EOS. Ting (2003) assumed that van der Waals forces dominate the interactions between the molecules in asphaltic mixtures and therefore they did not include the association term in PC-SAFT. This assumption is considered to be valid in this research and therefore we do not consider the association term in calculations.

2.2.3. Reversibility of asphaltene precipitation

There is a controversy in the literature about the reversibility of asphaltene precipitation. Solubility models consider asphaltene precipitation as a thermodynamically reversible process; while, according to the colloidal models, precipitation is irreversible (Peramanu *et al.* 2001, Abedini *et al.* 2011). A slow reversibility, however, is observed in laboratory works (Hirschberg *et al.* 1984, Andersen and Stenby 1996, Peramanu *et al.* 2001, Beck *et al.* 2005).

Through a set of experiments at room temperature, Rassamdana *et al.* (1996) showed that precipitation of asphaltene with respect to composition is partially reversible. Hammami *et al.* (2000) also found that precipitation is reversible. They explained that the re-dissolution is time-dependent and varies with the system physical conditions. The experiments conducted by Aske *et al.* (2002) confirm that asphaltene aggregation is almost fully reversible with re-pressurization. They reported, however, that the kinetics of re-dissolution is very slow. In summary, asphaltene precipitation is a reversible process with the kinetics of re-dissolution being a function of the physical state of the mixture. The reversibility of asphaltene precipitation supports the solubility approach and that is the approach taken in this dissertation.

2.2.4. Dynamics of asphaltene particles in porous media

Oil displacement dynamics in porous media becomes more complicated as asphaltenes start to precipitate. Asphaltene precipitation results in the first asphaltene particles called micro-aggregates. Micro-aggregates may stick together in an aggregation process and form macro-aggregates or deposit to the rock surface and wellbore tubing (Vargas 2009). Macro-aggregates can change the formation wettability by adsorbing onto the reservoir rock or block the pore throats and thus reducing the hydrocarbon mobility (Leontaritis *et al.* 1994).

Investigations show that precipitated particles can deposit in the porous medium in two different modes: (I) adsorption onto the rock surface and (II) mechanical entrapment (Minssieux 1997). Adsorption occurs because of the polar interactions between the solid particles and minerals on the rock surface. Mechanical entrapment happens when the large aggregated asphaltene particles are retained in the pore throats.

2.2.4.1. Adsorption

Several experiments have been conducted to study the adsorption of asphaltenes onto different solid surfaces (Pernyeszi *et al.* 1998, Xie and Karan 2005, Rudrake *et al.* 2009, Syunyaev *et al.* 2009). Many researchers concluded that asphaltene adsorption onto the mineral surfaces follows a Langmuir-type behavior (Collins and Melrose 1983, Dubey and Waxman 1991, Gonzalez and Travalloni-Louvisse 1993). Nghiem (1999) used a Langmuir isotherm equation to model asphaltene deposition in a compositional reservoir simulator. The Langmuir isotherm has the following form:

$$w_{ads} = \frac{w_{ads,\max} K_a C_{sus}}{K_a C_{sus} + 1}, \tag{2.41}$$

where, w_{ads} is the mass of adsorbed solids per mass of rock, $w_{ads,\max}$ is the maximum mass fraction of solids which adsorbed to the rock, K_a is the ratio of adsorption/desorption rate constants, and C_{sus} is the suspended solid concentration in the oil phase. Figure 2-4 shows the Langmuir isotherms of asphaltene adsorption on different rock.

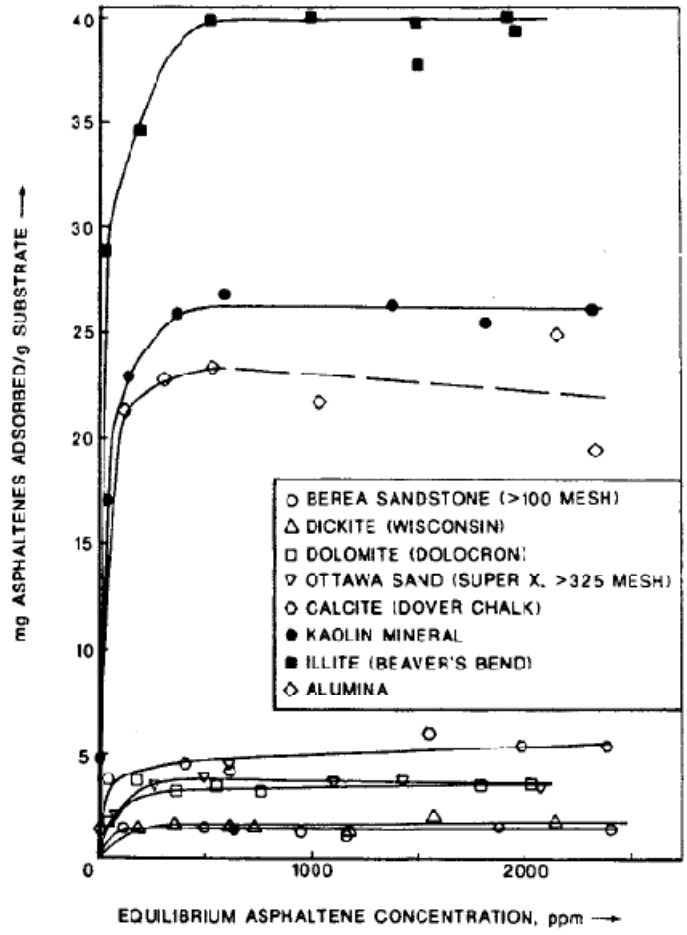

Figure 2-4: Langmuir isotherms for asphaltene adsorption on different rocks (Dubey and Waxman, 1991)

Although only a small portion of the deposited asphaltene is adsorbed (Leontaritis 1998), it can influence wettability of the formation and turn water-wet rocks into mixed-wet or oil-wet rocks. Such wettability alteration due to asphaltene adsorption has been widely studied (Collins and Melrose 1983, Crocker and Marchin 1988, Buckley *et al.* 1997).

2.2.4.2. Mechanical entrapment

A commonly used empirical model for asphaltene mechanical entrapment is an equation developed by Gruesbeck and Collins (1982) to model fine particles deposition inside porous media. In this model, the porous medium is represented as a combination of two types of pathways: (I) pluggable, and (II) non-pluggable pathways. Pluggable pathways represent a tortuous path of small pores and throats with pronounced variation in size making them prone to full plugging. In such a pluggable network, a mechanical trapping mechanism leads to pore-throat blockage as fine particles jam through the tight constrictions of the porous medium. Non-pluggable pathways, however, consist of relatively smooth and large pores and throats that are less likely to be fully plugged. The proposed equation for mechanical entrapment has the following form:

$$\frac{d\sigma_{me}}{dt} = \left(\alpha_0 + \alpha_1 \sigma_{me}\right) |u_o| \hat{C}_{sus}\,, \tag{2.42}$$

where, σ_{me} is the volume of deposited asphaltenes per initial pore volume [m^3 / m^3], α_0 and α_1 are empirical parameters [m^{-1}], u_o is the oil Darcy velocity [m/s], and $\hat{C}_{sus}$ is the precipitated asphaltene volume ration in the oil phase [m^3 / m^3]. Eq. (2.42) implies that the mechanical entrapment is a flow-dependent process and therefore deposition does not occur without fluid flow.

2.3. AQUEOUS PHASE

The dissolution of gases into the aqueous phase can affect the oil recovery (Agarwal *et al.* 1993). This is particularly important in CO_2 injection because its solubility is greater than that for hydrocarbon components. A considerable fraction of injected CO_2 can dissolve in the aqueous phase.

Compositional simulators that include gas dissolution into the aqueous phase usually use Henry's law. However, Henry's law is only applicable for solutions in which the solvent does not chemically interact with the dissolved gases (Harvey and Smith 2007). One of the gases that can react with water is carbon dioxide. When CO_2 dissolves in water, it reversibly converts to carbonic acid (H_2CO_3).

Phase behavior modeling of the aqueous systems using EOS remains a challenge owing to complicated non-idealities from the strong hydrogen bonding of water molecules. Conventional CEOSs, such as the PR EOS and Soave-Redlich-Kwong (SRK) EOS (Soave 1972), are often used in compositional reservoir simulations because of their simplicity and reasonable phase behavior predictions of hydrocarbon systems. However, they are not as accurate for modeling gas solubility in the aqueous phase, unless changes to the fluid characterization are made. Many modifications to CEOSs have been proposed in the literature to handle non-ideal mixtures containing water. Peng and Robinson (1980) modified the α-function in the original PR EOS for the water component. They also proposed two sets of BIPs between water and hydrocarbons, one set for components in the aqueous phase, and one for components in the non-aqueous phases.

Some authors introduced different mixing rules for polar asymmetric mixtures, rather than the conventional van der Waals mixing rule. Examples are the asymmetric mixing rules proposed by Huron and Vidal (1979) and Panagiotopolous and Reid (1986). Søreide and Whitson (1992) proposed a special α-term for the water component as a

function of temperature and brine salinity to predict the vapor pressure of water/brine accurately. They also used different values of BIPs between hydrocarbon components and water in the aqueous phase and in the hydrocarbon phases, as suggested by Peng and Robinson (1980).

Other authors incorporate the association concept to CEOSs to account for the effect of hydrogen bonding on the phase behavior of water-containing mixtures (Anderko 1991, Shinta and Firoozabadi 1995, Li and Firoozabadi 2009). Cubic-plus-association (CPA) EOS developed by Kontogeorgis, *et al.* (1996) is one of the EOS models being used by several researchers to model water containing mixtures. Although the association term can improve the capability of the EOS in phase behavior predictions, it causes complexity in the EOS and increases the computational time of the flash calculations as a result.

In this research, Søreide and Whitson's modification of the PR EOS (Søreide and Whitson 1992) is adopted because of its simplicity and reasonable predictions of solubilities between light hydrocarbons and water, and between CO_2 and water (Yan and Stenby 2009, 2010).

2.4. SPEED-UP OF PHASE EQUILIBRIUM CALCULATIONS

Equilibrium calculations are called millions of times during compositional simulations and therefore they can take a significant part of the total execution time. The computational time of the flash calculations increases very fast with number of components and phases. Reduced methods for phase equilibrium calculations are possible approaches to reduce the computational time. The idea behind these methods is to reduce the number of independent variables in phase equilibrium calculations. Michelsen (1986) demonstrated that the phase equilibrium calculations can be performed using only three

independent variables, regardless of the number of components in the mixture. His model, however, was limited to EOS fluid characterizations where all BIPs are zero. Michelsen's method was extended by Jensen and Fredenslund (1987) to handle non-zero BIP's of only one component using five independent variables. Later, Hendriks and van Bergen (1992) presented a different reduced approach in which the number of non-zero BIP's was not restricted. They used spectral expansion to approximate the BIP matrix. Since then, the spectral expansion method has been used by many others to handle non-zero BIP matrices (Firoozabadi and Pan 2002, Pan and Firoozabadi 2003, Nichita *et al.* 2006).

Li and Johns (2006) proposed a reduced method that uses an empirical equation for the BIPs, which makes the reduced method only a function of six parameters. Okuno *et al.* (2010c) used Li and Johns' method in a compositional simulator and showed a significant speed-up of the simulations. Okuno *et al.* (2010b) extended Li and Johns' method to three-phase flash calculations and tested the flash calculations in compositional simulation. Again, they reported a significant speed-up compared to conventional flash calculation methods, and increased robustness.

Gorucu *et al.* (2013) developed new reduced parameters based on application of Nichita's method to the Li and Johns (2006) parameters. They compared computational times for all reduced and conventional methods and showed that spectral expansion methods were significantly slower than the approach by Li and Johns.

Tie-simplex based phase behavior modeling proposed by Voskov and Tchelepi (2007) is another approach to reduce computational time of the equilibrium calculations in compositional simulation. Voskov and Tchelepi (2009) reported significant speed-up using compositional space adaptive tabulation method (CSAT), a tie-simplex based approach, compared to the standard compositional simulation. Recently, Rezaveisi et al

(2013) reported the computational efficiency of CSAT implemented in UTCOMP. The computational improvement of CSAT method reported by Rezaveisi *et al.* (2013) is not as significant as that reported by Voskov and Tchelepi (2009), although CSAFT may provide more benefit in a fully implicit simulation. In this research, we extend Li and Johns' reduced flash algorithm to a four-phase reduced flash, capable of modeling aqueous and hydrocarbon phases in a unified framework.

Chapter 3. Phase behavior calculations using PC-SAFT EOS

The objective of this chapter is to develop a fast and efficient algorithm for phase behavior modeling using PC-SAFT EOS to be implemented in UTCOMP. This algorithm provides the basis of equilibrium calculations for the simulation of asphaltene precipitation during gas injection described in the next chapter.

3.1. PURE-COMPONENT PARAMETERS

The pure-component parameters of traditional CEOSs are critical temperature, critical pressure, and acentric factor. In SAFT-type EOSs, however, the pure components are characterized by five physical parameters: (1) the number of segments in the molecule (i.e. chain length), m, (2) a size parameter, σ, (3) a segment energy parameter, ε, (4) the volume of association, $\kappa^{A_i B_i}$, and (5) the energy of association, $\varepsilon^{A_i B_i}$. The last two parameters are only required for the molecules that are self-associating. These parameters are, in general, obtained based on regression to vapor pressure and saturated liquid densities for pure components (Gross and Sadowski 2001). Table 3-1 summarizes a list of PC-SAFT parameters for the non-associating components of interest to this research. More data for the pure-component parameters can be found in Gross and Sadowski (2001).

One important feature inherent in SAFT-type EOSs is the systematic behavior of the fitted pure-component parameters (i.e. m, σ, and ε/κ), for all classes of compounds, with respect to molecular weight. There are correlations in the literature to estimate the EOS parameters for crude oil components or pseudo-component using their molecular weights (Gross and Sadowski 2001, Ting 2003, Gonzalez 2008). This characteristic is particularly important for the components whose liquid densities or vapor pressures are hard to measure.

Table 3-1: PC-SAFT pure-component parameters for non-associating components (Gross and Sadowski 2001)

Substance	m [-]	$\sigma[A^{\circ}]$	ε / k $[K]$
Carbon Dioxide	2.0729	2.7852	169.21
Nitrogen	1.2053	3.3130	90.96
Methane	1.0000	3.7039	150.03
Ethane	1.6069	3.5206	191.42
Propane	2.0020	3.6184	208.11
Butane	2.3316	3.7086	222.88
Pentane	2.6896	3.7729	231.20
Hexane	3.0576	3.7983	236.77
Heptane	3.4831	3.8049	238.40
Octane	3.8176	3.8373	242.78
Nonane	4.2079	3.8448	244.51
Decane	4.6627	3.8384	243.87
Undecane	4.9082	3.8893	248.82
Dodecane	5.3060	3.8959	249.21
Tridecane	5.6877	3.9143	249.78
Tetradecane	5.9002	3.9396	254.21
Pentadecane	6.2855	3.9531	254.14
Hexadecane	6.6485	3.9552	254.70
Heptadecane	6.9809	3.9675	255.65
Octadecane	7.3271	3.9668	256.20
Nonadecane	7.7175	3.9721	256.00
Eicosane	7.9849	3.9869	257.75

Gross and Sadowski (2001) proposed the following correlations to find the pure-component parameters of the alkane series based on their molecular weight:

$$\sigma_i = q_{01} + \left(\frac{M_i - M_{CH_4}}{M_i}\right) q_{11} + \left(\frac{M_i - M_{CH_4}}{M_i}\right)\left(\frac{M_i - 2M_{CH_4}}{M_i}\right) q_{21}, \tag{3.1}$$

$$m_i / M_i = q_{02} + \left(\frac{M_i - M_{CH_4}}{M_i}\right) q_{12} + \left(\frac{M_i - M_{CH_4}}{M_i}\right)\left(\frac{M_i - 2M_{CH_4}}{M_i}\right) q_{22}, \tag{3.2}$$

$$\left(\varepsilon_i / \kappa\right) = q_{03} + \left(\frac{M_i - M_{CH_4}}{M_i}\right) q_{13} + \left(\frac{M_i - M_{CH_4}}{M_i}\right)\left(\frac{M_i - 2M_{CH_4}}{M_i}\right) q_{23}, \tag{3.3}$$

where M_{CH_4} is the molar mass of methane ($M_{CH_4} = 16.043\ g/mol$) and q_{jk} are model constants fitted to the parameters of the pure n-alkane series (Table 3-2).

Table 3-2: Constants for the n-alkane parameter correlations (Gross and Sadowski 2001)

j	0	1	2
q_{j1}, Å	3.7039	-0.3226	0.6907
q_{j2}, mol/g	0.06233	-0.02236	-0.01563
q_{j3}, K	150.03	80.68	38.96

3.2. DENSITY ROOTS

The first step in the phase equilibrium calculations using the EOS approach is to find the density roots. The density, ρ, can be estimated from the following relation

$$\rho = \frac{P}{Z\kappa T}\left(10^{-10}\,\frac{\mathrm{m}}{\text{Å}}\right)^3, \tag{3.4}$$

where Z is the compressibility factor and the pressure, *P*, is in Pa. The compressibility factor can be derived from the residual Helmholtz energy using the following thermodynamic relation:

$$Z = 1 + \eta \left(\frac{\partial \tilde{a}^{res}}{\partial \eta} \right)_{T,x_i}, \tag{3.5}$$

which can also be written as

$$Z = 1 + Z^{hc} + Z^{disp}. \tag{3.6}$$

The hard-chain term of the compressibility factor is given by

$$Z^{hc} = \bar{m} Z^{hs} - \sum_i x_i \left(m_i - 1 \right) \left(g_{ii}^{hs} \right)^{-1} \rho \frac{\partial g_{ii}^{hs}}{\partial \rho}, \tag{3.7}$$

where

$$Z^{hs} = \frac{\xi_3}{\left(1-\xi_3\right)} + \frac{3\xi_1\xi_2}{\xi_0\left(1-\xi_3\right)^2} + \frac{3\xi_2^3 - \xi_3\xi_2^3}{\xi_0\left(1-\xi_3\right)^3}, \tag{3.8}$$

and

$$\rho \frac{\partial g_{ii}^{hs}}{\partial \rho} = \frac{\xi_3}{\left(1-\xi_3\right)^2} + \frac{d_i}{2}\left(\frac{3\xi_2}{\left(1-\xi_3\right)^2} + \frac{6\xi_2\xi_3}{\left(1-\xi_3\right)^3} \right) + \frac{d_i^2}{4}\left(\frac{4\xi_2^2}{\left(1-\xi_3\right)^3} + \frac{6\xi_2^2\xi_3}{\left(1-\xi_3\right)^4} \right). \tag{3.9}$$

The dispersion contribution to the compressibility factor is given by

$$Z^{disp} = -2\pi\rho \frac{\partial\left(\eta I_1\right)}{\partial \eta} \overline{m^2 \varepsilon \sigma^3} - \pi\rho\bar{m}\left[C_1 \frac{\partial\left(\eta I_2\right)}{\partial \eta} + C_2 \eta I_2 \right] \overline{m^2 \varepsilon^3 \sigma^3}, \tag{3.10}$$

where,

$$\frac{\partial\left(\eta I_1\right)}{\partial \eta} = \sum_{i=0}^{6} a_i\left(\bar{m}\right)\left(i+1\right)\eta^i, \tag{3.11}$$

$$\frac{\partial\left(\eta I_2\right)}{\partial \eta} = \sum_{i=0}^{6} b_i\left(\bar{m}\right)\left(i+1\right)\eta^i, \tag{3.12}$$

and the abbreviation C_2 is defined as

$$C_2 = \frac{\partial C_1}{\partial \eta} = -C_1^2 \left[\bar{m} \frac{-4\eta^2 + 20\eta + 8}{(1-\eta)^5} + (1-\bar{m}) \frac{2\eta^3 + 12\eta^2 - 48\eta + 40}{(1-\eta)^3 (2-\eta)^3} \right]. \tag{3.13}$$

Because of the algebraic complexity of the model, the above relations cannot be solved analytically to find the roots of the compressibility factor and therefore the density roots. As suggested by Gross and Sadowski (2001), the density roots of a mixture at a given pressure can be determined iteratively by adjusting the reduced density, η, in Newton-Raphson iterations. The relationship between the reduced density and the number density of the molecules is the following:

$$\rho = \frac{6}{\pi} \eta \left(\sum_{i=1}^{N_c} x_i m_i d_i^3 \right)^{-1}. \tag{3.14}$$

In Newton's iterations, the reduced density is updated according to the following equation:

$$\eta^{k+1} = \eta^k - \frac{\left(P^k - P_{sys} \right)}{\left(\partial P / \partial \eta \right)_{T,\bar{x}}}, \tag{3.15}$$

where P_{sys} is the pressure of the system, the superscript k denotes the iteration steps, and P^k is the calculated pressure at step k. The reduced density is adjusted until the difference between P^k and P_{sys} becomes less than a given stopping threshold. The stopping threshold for density root search is 10^{-10} in this research. The partial derivatives of pressure with respect to the reduced density at constant temperature and composition can be obtained from

$$\left(\frac{\partial P}{\partial \eta} \right)_{T,\bar{x}} = 10^{30} \kappa T \left[\rho \left(\frac{\partial Z}{\partial \eta} \right)_{T,\bar{x}} + Z \left(\frac{\partial \rho}{\partial \eta} \right)_{T,\bar{x}} \right]. \tag{3.16}$$

The procedure to calculate the partial derivatives $\left(\partial Z / \partial \eta \right)_{T,\bar{x}}$ and $\left(\partial \rho / \partial \eta \right)_{T,\bar{x}}$ are available in Privat *et al.* (2010). Gross and Sadowski (2001) recommended using 0.5 and

10^{-10} as the starting values of the reduced density for liquid and vapor phases, respectively. The closest packing of segments is about 0.7405; therefore, reduced density values greater than 0.7405 are physically meaningless (Gross and Sadowski 2001). Gross and Sadowski's procedure (2001) is adopted in this research to find the density roots. The flowchart for density root search is presented in Figure A-1.

To illustrate the capability of the PC-SAFT EOS to yield reliable reproductions of the molar volume (i.e. the reciprocal of density) data, we plotted the liquid molar volume of Hexatriacontane (C_{36}) and Hexadecane (C_{16}) versus temperature in Figure 3-1. To compare the PC-SAFT results with a CEOS, the results obtained by PR EOS also plotted in this figure.

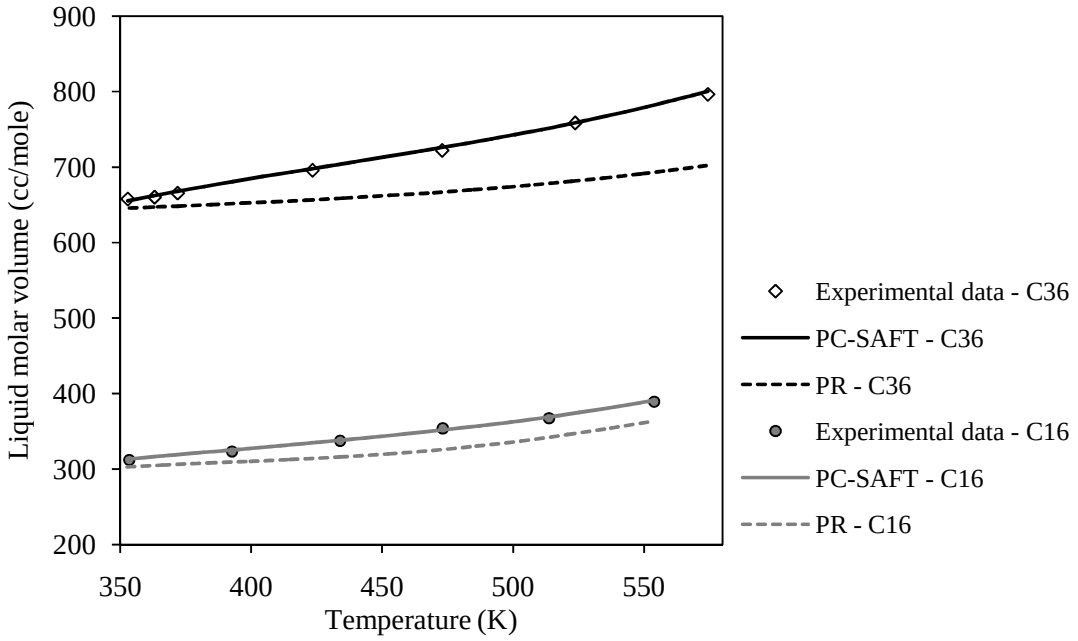

Figure 3-1: Pure-component liquid molar volume (cc/mole) of hexatriacontane (C_{36}) and hexadecane (C_{16}) versus temperature (K) at the pressure of 1 bar. The symbols represent the experimental data (Doolittle 1964) and lines are the results obtained using PC-SAFT and PR EOS.

As shown in Figure 3-1, the results obtained by the PC-SAFT EOS are in a very good agreement with the experimental data (Doolittle 1964), while PR EOS underestimates the liquid molar volumes. The difference between the simulated data by PR EOS and the experimental data becomes larger for the heavier component (i.e., Hexatriacontane, C_{36}). Although, volume shift technique can correct this deficiency, it requires more information about the system and it is not a physically consistent way to improve density.

3.3. PHASE EQUILIBRIUM CALCULATIONS

Phase behavior calculations using PC-SAFT EOS are implemented in UTCOMP within the framework of Perschke's algorithm (1988). His algorithm is a sequential implementation of stability analyses and flash calculations described in the following sections. The calculations start with single phase stability analysis to test the stability of the mixture at the overall composition. If the mixture is identified to be unstable, two-phase flash calculation is initiated to find the amounts and compositions of the resulting equilibrium phases. If the mixture with the overall composition is found to be stable, the mixture is concluded to be a single-phase fluid and no further calculations would be done. After two-phase flash calculation is completed, the stability of one of the resulting phases is tested. If the stability analysis indicated the test phase as unstable, the mixture is assumed to be a three-phase mixture and then a three-phase flash calculation is begun to find the compositions of the equilibrium phases. Otherwise, it is concluded that the fluid is a stable two-phase mixture. The stability analysis result is generally used as the initial guess for subsequent flash calculations.

Fugacity coefficients, the derivatives of fugacity, compressibility factor, and phase density are developed using PC-SAFT EOS and implemented in the Perschke's

algorithm. The Perschke's algorithm, however, is changed in this work in order to speed up the equilibrium calculations. The speed up procedure will be explained in Chapter 6.

3.3.1. Phase stability analysis

Stability analysis is a search for a trial composition at which the Gibbs free energy of the system is less than that of a single-phase mixture of the overall hydrocarbon composition $\bar{z}$. To express this condition mathematically, a function known as the tangent plane distance (TPD) can be defined as follows:

$$\Delta G = \sum_{i=1}^{N_C} y_i \left[\mu_i(\bar{y}) - \mu_i(\bar{z}) \right]. \tag{3.17}$$

A phase is stable only if ΔG is positive for any set of mole fractions at a given pressure and temperature. In this research, the stationary point method (Michelsen 1982a) is implemented to carry out the stability analysis. In the stationary point method, the objective is to solve the following nonlinear equations to locate the stationary points:

$$\ln Y_i + \ln \phi_i(\bar{y}) - h_i = 0 \quad \text{for } i = 1,...,N_C, \tag{3.18}$$

where Y_i is the trial composition and the mole fraction $\bar{y}$ is defined as

$$y_i = \frac{Y_i}{\sum_{s=1}^{N_C} Y_s} \quad \text{for } i = 1,...,N_C, \tag{3.19}$$

and

$$h_i = \ln z_i + \ln \phi_i(\bar{z}) \quad \text{for } i = 1,...,N_C. \tag{3.20}$$

The summation of the variable $\bar{Y}$ is calculated for evaluating the stability of the phase resulting from the solution of Eq. (3.18). If this summation is larger than one, the

phase is concluded to be unstable, otherwise it is considered a stable phase. Eq. (3.18) is solved using successive substitutions followed by Newton-Raphson iterations. The updating equations used during the successive substitution iterations are

$$Y_i^{k+1} = \exp\left[h_i - \ln\phi_i\left(\overline{y}\right)\right] \quad \text{for } i = 1,...,N_C . \tag{3.21}$$

In Newton-Raphson, the residual variable, r_i, is defined as

$$r_i = \ln Y_i + \ln\phi_i\left(\overline{y}\right) - h_i \quad \text{for } i = 1,...,N_C . \tag{3.22}$$

The independent variables, Y_i, are then identified from these nonlinear equations using

$$\overline{Y}^{k+1} = \overline{Y}^{k} - \left(J\right)^{-1}\overline{r}\,, \tag{3.23}$$

where J is the Jacobian matrix comprised of $N_C \times N_C$ elements, which are calculated as

$$j_{is} = \left(\frac{\partial r_i}{\partial Y_s}\right)_{Y_{m(m\neq s)}} = \frac{1}{\sum_{r=1}^{N_C} Y_r} + \frac{\partial}{\partial Y_s}\left[\ln\left(y_i\phi_i\left(\overline{y}\right)\right)\right]_{Y_{m(m\neq s)}} \tag{3.24}$$

The calculation procedure for stability analyses using stationary point method can be summarized as follows:

1. Calculate h_i from Eq. (3.20).
2. Estimate values for Y_i.
3. Calculate $\phi_i\left(\overline{y}\right)$ where y_i is given by Eq. (3.19).
4. Check for the convergence of the successive substitution iteration by comparing the residuals with a stopping criteria, ε_{SA} ,

   $$\max\left|r_i\right| \le \varepsilon_{SA} \quad \text{for } i = 1,...,N_C . \tag{3.25}$$

The stopping criterion for stability analysis is chosen to be 10^{-8} throughout this research.

5. If the latter inequality is not satisfied, i.e. successive substitution did not converge, check for switching to the Newton-Raphson iteration using the criterion,

$$\max|r_i| \le \varepsilon_{switch} \quad \text{for } i = 1,..., N_C . \tag{3.26}$$

6. If the switching criterion is not satisfied, update the variable Y_i using Eq. (3.21) and go back to step (3). Otherwise, go to step (7) to start Newton-Raphson iteration.
7. Calculate the elements of the Jacobian J, using Eq. (3.24).
8. Update variable Y_i using Eq. (3.23).
9. Calculate the residuals in Eq. (3.22) and check for the convergence by satisfying Eq. (3.25).
10. If it is not converged, go back to step (7).

When the above algorithm converges to a solution, the solution must be analyzed to check for stability. First, we need to make sure the iterations have not converged to a trivial solution, i.e. a solution where the composition $\bar{y}$ is equal to the test composition, $\bar{z}$. For a nontrivial solution the following condition must be met:

$$\left[\sum_{i=1}^{N_C}\left(y_i - z_i\right)^2\right]^{1/2} \ge \frac{\varepsilon_{trivial}}{N_C}, \tag{3.27}$$

where $\varepsilon_{trivial}$ is 10^{-8}.

If the result is identified as a trivial solution or if the iterations did not converge within the allowed maximum number of iterations, another guess for $\bar{Y}$ is made and the entire procedure is repeated.

A second check for stability is performed, if the condition of Eq. (3.27) is satisfied. A phase is considered unstable if

$$\left(\sum_{i=1}^{N_C} Y_i\right) - 1 \geq \varepsilon_{stab.} \,. \tag{3.28}$$

If calculations did not converge to a nontrivial solution satisfying the condition of Eq. (3.28) using all initial guesses, the phase is considered stable. For single-phase stability analysis, vapor-like and liquid-like phases can be used as initial guesses for $\overline{Y}$:

$$Y_i = z_i K_i \quad \text{for } i = 1,...,N_C \,, \tag{3.29}$$

and

$$Y_i = \frac{z_i}{K_i} \quad \text{for } i = 1,...,N_C \,. \tag{3.30}$$

If the critical properties and acentric factor of the components are available, the *K*-values can be computed using Wilson's correlation (Wilson 1969):

$$K_i = \frac{P_{ci}}{P} \exp\left[5.37\left(1+\omega_i\right)\left(1-\frac{T_{ci}}{T}\right)\right] \quad \text{for } i = 1,...,N_C \,. \tag{3.31}$$

For multiple phases, Michelsen (1982a) recommended using the lightest and the heaviest components as pure phases, e.g.

$$Y_1 = 0.999 \text{ and } Y_i = \frac{0.001}{N_C - 1} \quad \text{for } i = 2,...,N_C \,, \tag{3.32}$$

$$Y_{N_C} = 0.999 \text{ and } Y_i = \frac{0.001}{N_C - 1} \quad \text{for } i = 1,...,N_C - 1 \,. \tag{3.33}$$

In addition, Michelsen used the arithmetic mean of existing phase compositions and also an ideal gas mixture as initial guesses:

$$Y_i = \frac{1}{2}\left(x_{i2} + x_{i3}\right) \quad \text{for } i = 1,..., N_C\,, \tag{3.34}$$

$$Y_i = \exp\left(h_i\right) \quad \text{for i=1,...,N}_C\,. \tag{3.35}$$

3.3.2. Flash calculations

The procedure for flash calculations in UTCOMP consists of accelerated SS (ACSS) iterations (Mehra *et al.* 1983) followed by the minimization of the Gibbs free energy (Trangenstein 1987). In the ACSS iterations, K-values are updated using the following equation:

$$K_{ij}^{k+1} = K_{ij}^{k} \exp\left(-\lambda^{k+1} \frac{f_{i2}}{f_{ij}} \right), \tag{3.36}$$

where λ^{k+1} is an acceleration factor and the subscript *i* and *j* are component and phase indices. Phase two is arbitrarily selected as the reference phase. The acceleration factor is calculated from a recursive equation as follows:

$$\lambda^{k+1} = \frac{\lambda^{k} \sum_{j=3}^{N_P} \sum_{i=1}^{N_C} \left(r_{ij}^{k}\right)^2}{\left| \sum_{j=3}^{N_P} \sum_{i=1}^{N_C} \left(r_{ij}^{k-1} r_{ij}^{k}\right) - \sum_{j=3}^{N_P} \sum_{i=1}^{N_C} \left(r_{ij}^{k}\right)^2 \right|}, \tag{3.37}$$

where

$$r_{ij} = \ln\left(\frac{f_{ij}}{f_{i2}} \right) \quad \text{for } i = 1,..., N_C \text{ and } j = 3,..., N_P\,. \tag{3.38}$$

For $k = 0$, the value of λ^1 is set to 1.0. The acceleration factor is kept between 1.0 and 3.0. Given the overall composition and the updated *K*-values, the amounts and composition of the phases are determined by solving Rachford-Rice equations.

The ACSS method is switched to the minimization of the Gibbs free energy algorithm when the error of the equi-fugacity equations becomes less than a switching criterion:

$$\max\left|\ln f_{ij} - \ln f_{i2}\right| \le \varepsilon_{switch} \quad \text{for } i = 1,...,N_C \text{ and } j = 3,...,N_P . \tag{3.39}$$

The switching criterion for flash calculations is 10^{-4} in this research. In the method based on minimization of Gibbs free energy, two conditions must be satisfied to find a local minimum: (1) the first partial derivatives of the Gibbs free energy function must be zero, and (2) the matrix of the second partial derivatives (Hessian matrix) must be positive definite.

Referring to Eqs. (2.18), the first condition leads to the equi-fugacity equations. The Hessian matrix can be determined by taking the derivatives of equation (2.18) with respect to the independent mole numbers as follows

$$\frac{\partial^2}{\partial n_{lj}\partial n_{ik}}\left(\frac{G^t}{RT}\right) = \frac{\partial \ln f_{ik}}{\partial n_{lj}} + \frac{\partial \ln f_{i1}}{\partial n_{l1}} \quad \text{for } i,l = 1,...,N_C \text{ and } j,k = 2,...,N_P . \tag{3.40}$$

The resulting Hessian matrix is a symmetric matrix of rank $\left[N_C\left(N_P - 1\right)\right]^2$. The partial derivatives required to find the elements of the Hessian matrix are evaluated analytically, which are described in the next sections. The main steps required to minimize the objective function are summarized in the following:

1. Make an initial guess for the independent mole numbers.
2. Calculate the dependent mole numbers from material balance Eq. (2.14).
3. Calculate the fugacity coefficients for each phase.
4. Calculate the first partial derivatives of the fugacity coefficients with respect to the independent variables Eq. (2.18).

5. Set the elements of the Hessian matrix using the partial derivatives of the fugacity coefficients.
6. Decompose the Hessian matrix using modified Cholesky decomposition method and check if it is positive definite.
7. Check the convergence criteria of the flash calculations using either

$$\max\left|\ln f_{ij} - \ln f_{i2}\right| \le \varepsilon_{flash} \quad \text{for } i = 1,...,N_C \text{ and } j = 3,...,N_P, \tag{3.41}$$

or

$$\max\left|\frac{\Delta n_{ij}^{k}}{n_{ij}^{k}}\right| \le \varepsilon_{flash} \quad \text{for } i = 1,...,N_C \text{ and } j = 3,...,N_P. \tag{3.42}$$

where ε_{flash} is 10^{-8}. If the convergence criteria are met, then stop the calculations, and if not, then go to step 8.

8. Calculate the descent direction and the step length using line-search technique based on the Newton directions.
9. Update the mole numbers.
10. Return to step 3.

3.3.3. Fugacity coefficient

One of the most useful quantities in phase equilibrium calculations is the fugacity coefficient. The fugacity coefficient can be derived from the residual chemical potential according to the following equation (Gross and Sadowski 2001):

$$\ln\phi_k = \frac{\mu_k^{res}(T,v)}{\kappa T} - \ln Z, \tag{3.43}$$

where v is the molar volume and μ_k^{res} is the residual chemical potential, which can be obtained from

$$\frac{\mu_k^{res}(T,v)}{\kappa T} = \tilde{a}^{res} + (Z-1) + \left(\frac{\partial \tilde{a}^{res}}{\partial x_k}\right)_{T,v,x_{i\neq k}} - \sum_{j=1}^{N_C} x_j \left(\frac{\partial \tilde{a}^{res}}{\partial x_j}\right)_{T,v,x_{i\neq j}}. \tag{3.44}$$

The derivative of the residual Helmholtz energy with respect to mole fraction at constant temperature and constant volume is given by

$$\left(\frac{\partial \tilde{a}^{res}}{\partial x_i}\right)_{T,v,x_{k\neq i}} = m_i \tilde{a}^{hs} + \bar{m}\left(\frac{\partial \tilde{a}^{hs}}{\partial x_i}\right)_{T,v,x_{k\neq i}} + \left(\frac{\partial \tilde{a}^{chain}}{\partial x_i}\right)_{T,v,x_{k\neq i}} + \left(\frac{\partial \tilde{a}^{disp}}{\partial x_i}\right)_{T,v,x_{k\neq i}}. \tag{3.45}$$

The hard-sphere derivative term is calculated as

$$\begin{aligned}\left(\frac{\partial \tilde{a}^{hs}}{\partial x_i}\right)_{T,v,x_{k\neq i}} = {} & \frac{-\xi_{0,x_i}}{\xi_0}\tilde{a}^{hs} + \frac{1}{\xi_0}\left[\frac{3\left(\xi_{1,x_i}\xi_2 + \xi_1\xi_{2,x_i}\right)}{(1-\xi_3)} + \frac{3\xi_1\xi_2\xi_{3,x_i}}{(1-\xi_3)^2} + \frac{3\xi_2^2\xi_{2,x_i}}{\xi_3(1-\xi_3)^2} + \right. \\ & \left. \frac{\xi_2^3\xi_{3,x_i}(3\xi_3-1)}{\xi_3^2(1-\xi_3)^3} + \left(\frac{3\xi_2^2\xi_{2,x_i}\xi_3 - 2\xi_2^3\xi_{3,x_i}}{\xi_3^3} - \xi_{0,x_i}\right)\times\ln(1-\xi_3) + \left(\xi_0 - \frac{\xi_2^3}{\xi_3^2}\right)\frac{\xi_{3,x_i}}{(1-\xi_3)}\right],\end{aligned} \tag{3.46}$$

where the abbreviations ξ_{n,x_i} are defined as

$$\xi_{n,x_i} = \left(\frac{\partial \xi_n}{\partial x_i}\right)_{T,v,x_{k\neq i}} = \frac{\pi}{6}\rho m_i d_i^n. \tag{3.47}$$

The derivative of the chain term in Eq. (3.45) is given by

$$\left(\frac{\partial \tilde{a}^{chain}}{\partial x_i}\right)_{T,v,x_{k\neq i}} = (1-m_i)\ln g_{ii}^{hs} - \sum_k \left[\frac{x_k(m_k-1)}{g_{kk}^{hs}}\left(\frac{\partial g_{kk}^{hs}}{\partial x_i}\right)_{T,v,x_{m\neq i}}\right], \tag{3.48}$$

with

$$\left(\frac{\partial g_{kk}^{hs}}{\partial x_i}\right)_{T,v,x_{j\neq i}} = \frac{\xi_{3,x_i}}{(1-\xi_3)^2} + \frac{d_k}{2}\left(\frac{3\xi_{2,x_i}}{(1-\xi_3)^2} + \frac{6\xi_2\xi_{3,x_i}}{(1-\xi_3)^3}\right) + \frac{d_k^2}{4}\left(\frac{4\xi_2\xi_{2,x_i}}{(1-\xi_3)^3} + \frac{6\xi_2^2\xi_{3,x_i}}{(1-\xi_3)^4}\right). \tag{3.49}$$

The derivative of the dispersion contribution to the Helmholtz energy is calculated as

$$\left(\frac{\partial \tilde{a}^{disp}}{\partial x_i}\right)_{T,v,x_{k\neq i}} = -2\pi\rho\left[I_{1,x_i}\overline{m^2\varepsilon\sigma^3} + I_1\left(\overline{m^2\varepsilon\sigma^3}\right)_{x_i}\right] -$$
$$\pi\rho\left[\left(m_i C_1 I_2 + \bar{m}C_{1,x_i}I_2 + \bar{m}C_1 I_{2,x_i}\right)\overline{m^2\varepsilon^2\sigma^3} + \bar{m}C_1 I_2\left(\overline{m^2\varepsilon^2\sigma^3}\right)_{x_i}\right], \tag{3.50}$$

with

$$\left(\overline{m^2\varepsilon\sigma^3}\right)_{x_i} = 2m_i\sum_k x_k m_k\left(\frac{\varepsilon_{ik}}{\kappa T}\right)\sigma_{ik}^3, \tag{3.51}$$

$$\left(\overline{m^2\varepsilon^2\sigma^3}\right)_{x_i} = 2m_i\sum_k x_k m_k\left(\frac{\varepsilon_{ik}}{\kappa T}\right)^2\sigma_{ik}^3, \tag{3.52}$$

$$C_{1,x_i} = C_2\xi_{3,x_i} - C_1^2\left[m_i\left(\frac{8\eta-2\eta^2}{(1-\eta)^4}\right) - m_i\left(\frac{20\eta-27\eta^2+12\eta^3-2\eta^4}{(1-\eta)^2(2-\eta)^2}\right)\right], \tag{3.53}$$

$$I_{1,x_k} = \sum_{i=0}^{6}\left[a_i \times i \times \xi_{3,x_k}\eta^{i-1} + a_{i,x_k}\eta^i\right], \tag{3.54}$$

$$I_{2,x_k} = \sum_{i=0}^{6}\left[b_i \times i \times \xi_{3,x_k}\eta^{i-1} + b_{i,x_k}\eta^i\right], \tag{3.55}$$

$$a_{i,x_k} = \frac{m_k}{\bar{m}^2}a_{1i} + \frac{m_k}{\bar{m}^2}\left(3-\frac{4}{\bar{m}}\right)a_{2i}, \tag{3.56}$$

and

$$b_{i,x_k} = \frac{m_k}{\bar{m}^2}b_{1i} + \frac{m_k}{\bar{m}^2}\left(3-\frac{4}{\bar{m}}\right)b_{2i}. \tag{3.57}$$

3.3.4. Derivatives of the fugacity

The analytical derivative expressions of the fugacity coefficient for the PC-SAFT EOS do not appear in open literature. We derived those derivatives based on standard thermodynamic relations and summarized some of the results in this section. More details on the derivatives can be found in Appendices A and B.

3.3.4.1. Derivatives of the fugacity with respect to mole number

The partial derivatives of the fugacity with respect to mole number are required in both flash calculations and determination of the cumulative volume derivatives in pressure equations. From the definition of the fugacity coefficient of a component in mixtures, we have

$$\ln\frac{f_i}{P} = \ln\left(\phi_i x_i\right). \tag{3.58}$$

The fugacity coefficient is a function of temperature, pressure, and mole fractions. Therefore, it is easier here to calculate the partial derivatives with respect to mole fractions and then convert them to the mole number derivatives. The mole number derivatives of $\ln\left(\phi_i x_i\right)$ are related to the mole fraction derivatives as follows:

$$\left(\frac{\partial \ln\left(\phi_i x_i\right)}{\partial n_j}\right)_{T,P,n_{k\neq j}} = \frac{1}{n_T}\left(\left(\frac{\partial \ln\left(\phi_i x_i\right)}{\partial x_j}\right)_{T,P,x_{k\neq j}} - \sum_m x_m \left(\frac{\partial \ln\left(\phi_i x_i\right)}{\partial x_m}\right)_{T,P,x_{k\neq m}}\right), \tag{3.59}$$

where n_T is the total number of moles in the corresponding phase. Taking the derivatives of Eq. (3.43) at constant temperature and pressure results in

$$\left(\frac{\partial \ln\phi_i}{\partial x_j}\right)_{T,P,x_{k\neq j}} = \left[\frac{\partial}{\partial x_j}\left(\frac{\mu_i^{res}\left(T,v\right)}{\kappa T}\right)\right]_{T,P,x_{k\neq j}} - \frac{1}{Z}\left(\frac{\partial Z}{\partial x_j}\right)_{T,P,x_{k\neq j}}. \tag{3.60}$$

The compressibility factor appears in both Eq. (3.60) and the chemical potential expression in Eq. (3.44). Therefore, we should start by taking the derivatives of the compressibility factor. The calculations of the chemical potential derivatives are then straightforward, which are presented in Appendix A. Referring to Eq. (3.6) we have

$$\left(\frac{\partial Z}{\partial x_j}\right)_{T,P,x_{k\neq j}} = \left(\frac{\partial Z^{hc}}{\partial x_j}\right)_{T,P,x_{k\neq j}} + \left(\frac{\partial Z^{disp}}{\partial x_j}\right)_{T,P,x_{k\neq j}} . \tag{3.61}$$

The left hand side of Eq. (3.61) is given by

$$\left(\frac{\partial Z}{\partial x_j}\right)_{T,P,x_{k\neq j}} = \left(10^{-10}\frac{\mathrm{m}}{\text{Å}}\right)^3 \frac{-P}{\kappa T \rho^2}\left(\frac{\partial \rho}{\partial x_j}\right)_{T,P,x_{k\neq j}} , \tag{3.62}$$

where the only unknown is the derivative of the density with respect to mole fraction, $\left(\partial\rho/\partial x_j\right)_{T,P,x_{k\neq j}}$.

The partial derivatives of the hard-chain term of the compressibility factor, $\left(\partial Z^{hc}/\partial x_j\right)_{T,P,x_{k\neq j}}$, are obtained as follows:

$$\left(\frac{\partial Z^{hc}}{\partial x_j}\right)_{T,P,x_{k\neq j}} = \left(\frac{\partial \bar{m}}{\partial x_j}\right)_{T,P,x_{k\neq j}} Z^{hs} + \bar{m}\left(\frac{\partial Z^{hs}}{\partial x_j}\right)_{T,P,x_{k\neq j}} - \left(m_j - 1\right)\left(g_{ii}^{hs}\right)^{-1}\rho\frac{\partial g_{ii}^{hs}}{\partial \rho}$$
$$-\sum_i x_i\left(m_i - 1\right)\left[\rho\frac{\partial g_{ii}^{hs}}{\partial \rho}\left(\frac{\partial\left(g_{ii}^{hs}\right)^{-1}}{\partial x_j}\right)_{T,P,x_{k\neq j}} + \left(g_{ii}^{hs}\right)^{-1}\left(\frac{\partial}{\partial x_j}\left(\rho\frac{\partial g_{ii}^{hs}}{\partial \rho}\right)\right)_{T,P,x_{k\neq j}}\right]. \tag{3.63}$$

The derivative of the mean segment number to the mole fractions is simply given by

$$\left(\frac{\partial \bar{m}}{\partial x_j}\right)_{T,P,x_{k\neq j}} = m_j . \tag{3.64}$$

Referring to Eq. (3.8), the hard-sphere contribution is a function of $\xi_n \left(n = 0,...,3\right)$; therefore, from the chain rule we have

$$\left(\frac{\partial Z^{hs}}{\partial x_j}\right)_{T,P,x_{k\neq j}} = \sum_{n=0}^{3}\left(\frac{\partial Z^{hs}}{\partial \xi_n}\right)\left(\frac{\partial \xi_n}{\partial x_j}\right)_{T,P,x_{k\neq j}}, \tag{3.65}$$

where,

$$\left(\frac{\partial \xi_n}{\partial x_j}\right)_{T,P,x_{k\neq j}} = \frac{\xi_n}{\rho}\left(\frac{\partial \rho}{\partial x_j}\right)_{T,P,x_{k\neq j}} + \frac{\pi}{6}\rho m_j d_j^n . \tag{3.66}$$

The partial derivatives $\partial Z^{hs} / \partial \xi_n$ are given as follows:

$$\frac{\partial Z^{hs}}{\partial \xi_0} = \frac{-3\xi_1\xi_2}{\xi_0^2\left(1-\xi_3\right)^2} + \frac{\xi_3\xi_2^3 - 3\xi_2^3}{\xi_0^2\left(1-\xi_3\right)^3}, \tag{3.67}$$

$$\frac{\partial Z^{hs}}{\partial \xi_1} = \frac{3\xi_2}{\xi_0\left(1-\xi_3\right)^2}, \tag{3.68}$$

$$\frac{\partial Z^{hs}}{\partial \xi_2} = \frac{3\xi_1}{\xi_0\left(1-\xi_3\right)^2} + \frac{3\xi_2^2\left(3-\xi_3\right)}{\xi_0\left(1-\xi_3\right)^3}, \tag{3.69}$$

$$\frac{\partial Z^{hs}}{\partial \xi_3} = \frac{1}{\left(1-\xi_3\right)^2} + \frac{6\xi_1\xi_2}{\xi_0\left(1-\xi_3\right)^3} + \frac{\xi_2^3\left(8-2\xi_3\right)}{\xi_0\left(1-\xi_3\right)^4}, \tag{3.70}$$

Again, the only unknown in Eq. (3.66) and therefore Eq. (3.65) is the derivative of the density with respect to mole fraction. The first derivative in the summation term of Eq. (3.63) is determined as

$$\left(\frac{\partial\left(g_{ii}^{hs}\right)^{-1}}{\partial x_j}\right)_{T,P,x_{k\neq j}} = \frac{-1}{\left(g_{ii}^{hs}\right)^2} \times \left(\frac{\partial g_{ii}^{hs}}{\partial x_j}\right)_{T,P,x_{k\neq j}}, \tag{3.71}$$

where

$$\left(\frac{\partial g_{ii}^{hs}}{\partial x_j}\right)_{T,P,x_{k\neq j}} = \sum_{n=0}^{3} \frac{\partial g_{ii}^{hs}}{\partial \xi_n} \times \left(\frac{\partial \xi_n}{\partial x_j}\right)_{T,P,x_{k\neq j}} . \tag{3.72}$$

The partial derivatives $\frac{\partial g_{ii}^{hs}}{\partial \xi_n}$ are given by

$$\frac{\partial g_{ii}^{hs}}{\partial \xi_0} = \frac{\partial g_{ii}^{hs}}{\partial \xi_1} = 0, \tag{3.73}$$

$$\frac{\partial g_{ii}^{hs}}{\partial \xi_2} = \frac{3d_i}{2\left(1-\xi_3\right)^2} + \frac{d_i^2 \xi_2}{\left(1-\xi_3\right)^3}, \tag{3.74}$$

and

$$\frac{\partial g_{ii}^{hs}}{\partial \xi_3} = \frac{1}{\left(1-\xi_3\right)^2} + \frac{3d_i \xi_2}{\left(1-\xi_3\right)^3} + \frac{3}{2}\frac{d_i^2 \xi_2^2}{\left(1-\xi_3\right)^4} . \tag{3.75}$$

The term $\rho \frac{\partial g_{ii}^{hs}}{\partial \rho}$ in Eq. (3.63) is also a function of $\xi_n \left(n = 0,...,3\right)$; therefore

$$\left(\frac{\partial}{\partial x_j}\left(\rho \frac{\partial g_{ii}^{hs}}{\partial \rho}\right)\right)_{T,P,x_{k\neq j}} = \sum_{n=0}^{3}\left[\frac{\partial}{\partial \xi_n}\left(\rho \frac{\partial g_{ii}^{hs}}{\partial \rho}\right)\left(\frac{\partial \xi_n}{\partial x_j}\right)_{T,P,x_{k\neq j}}\right], \tag{3.76}$$

where the partial derivatives $\frac{\partial}{\partial \xi_n}\left(\rho \frac{\partial g_{ii}^{hs}}{\partial \rho}\right)$ are given by

$$\frac{\partial}{\partial \xi_0}\left(\rho \frac{\partial g_{ii}^{hs}}{\partial \rho}\right) = \frac{\partial}{\partial \xi_1}\left(\rho \frac{\partial g_{ii}^{hs}}{\partial \rho}\right) = 0, \tag{3.77}$$

$$\frac{\partial}{\partial \xi_2}\left(\rho \frac{\partial g_{ii}^{hs}}{\partial \rho}\right) = \frac{d_i}{2}\left(\frac{3}{\left(1-\xi_3\right)^2} + \frac{6\xi_3}{\left(1-\xi_3\right)^3}\right) + \frac{d_i^2 \xi_2}{2}\left(\frac{4}{\left(1-\xi_3\right)^3} + \frac{6\xi_3}{\left(1-\xi_3\right)^4}\right), \tag{3.78}$$

$$\frac{\partial}{\partial\xi_3}\left(\rho\frac{\partial g_{ii}^{hs}}{\partial\rho}\right)=\frac{-1}{\left(\xi_3-1\right)^2}+\frac{3d_i\xi_2-2}{\left(\xi_3-1\right)^3}-\frac{3d_i\xi_2\left(d_i\xi_2-6\right)}{2\left(\xi_3-1\right)^4}-\frac{6d_i^2\xi_2^2}{\left(\xi_3-1\right)^5}. \tag{3.79}$$

Taking the derivatives of the dispersion term of the compressibility factor in Eq. (3.10) results in

$$\left(\frac{\partial Z^{disp}}{\partial x_j}\right)_{T,P,x_{k\neq j}}=-2\pi\frac{\partial\left(\eta I_1\right)}{\partial\eta}\overline{m^2\varepsilon\sigma^3}\left(\frac{\partial\rho}{\partial x_j}\right)_{T,P,x_{k\neq j}}$$

$$-2\pi\rho\times\overline{m^2\varepsilon\sigma^3}\left(\frac{\partial}{\partial x_j}\left(\frac{\partial\left(\eta I_1\right)}{\partial\eta}\right)\right)_{T,P,x_{k\neq j}}$$

$$-2\pi\rho\frac{\partial\left(\eta I_1\right)}{\partial\eta}\left(\frac{\partial\overline{m^2\varepsilon\sigma^3}}{\partial x_j}\right)_{T,P,x_{k\neq j}}-\pi\bar{m}\left[C_1\frac{\partial\left(\eta I_2\right)}{\partial\eta}+C_2\eta I_2\right]\overline{m^2\varepsilon^2\sigma^3}\left(\frac{\partial\rho}{\partial x_j}\right)_{T,P,x_{k\neq j}}$$

$$-\pi\rho m_j\left[C_1\frac{\partial\left(\eta I_2\right)}{\partial\eta}+C_2\eta I_2\right]\overline{m^2\varepsilon^2\sigma^3}$$

$$-\pi\rho\bar{m}\left[\frac{\partial\left(\eta I_2\right)}{\partial\eta}\left(\frac{\partial C_1}{\partial x_j}\right)_{T,P,x_{k\neq j}}+C_1\left(\frac{\partial}{\partial x_j}\left(\frac{\partial\left(\eta I_2\right)}{\partial\eta}\right)\right)_{T,P,x_{k\neq j}}\right]\overline{m^2\varepsilon^2\sigma^3}$$

$$-\pi\rho\bar{m}\left[\left(\frac{\partial C_2}{\partial x_j}\right)_{T,P,x_{k\neq j}}\eta I_2+C_2\left(\frac{\partial\eta}{\partial x_j}\right)_{T,P,x_{k\neq j}}I_2+C_2\eta\left(\frac{\partial I_2}{\partial x_j}\right)_{T,P,x_{k\neq j}}\right]\overline{m^2\varepsilon^2\sigma^3}$$

$$-\pi\rho\bar{m}\left[C_1\frac{\partial\left(\eta I_2\right)}{\partial\eta}+C_2\eta I_2\right]\left(\frac{\partial\overline{m^2\varepsilon^2\sigma^3}}{\partial x_j}\right)_{T,P,x_{k\neq j}}. \tag{3.80}$$

The unknowns in Eq. (3.80) are calculated through Eqs (3.81)-(3.87). The reduced density, η, is equal to ξ_3 whose derivative is given by Eq. (3.66).

$$\left(\frac{\partial I_2}{\partial x_j}\right)_{T,P,x_{k\neq j}}=\sum_{i=0}^{6}b_{i,x_j}\eta^i+\sum_{i=0}^{6}\left[b_i i\eta^{i-1}\left(\frac{\partial\eta}{\partial x_j}\right)_{T,P,x_{k\neq j}}\right], \tag{3.81}$$

$$\left(\frac{\partial}{\partial x_j}\left(\frac{\partial(\eta I_1)}{\partial \eta}\right)\right)_{T,P,x_{k\neq j}} = \sum_{i=0}^{6} a_{i,x_j}(i+1)\eta^i + \sum_{i=0}^{6}\left[a_i(i+1)i\eta^{i-1}\left(\frac{\partial \eta}{\partial x_j}\right)_{T,P,x_{k\neq j}}\right], \tag{3.82}$$

$$\left(\frac{\partial}{\partial x_j}\left(\frac{\partial(\eta I_2)}{\partial \eta}\right)\right)_{T,P,x_{k\neq j}} = \sum_{i=0}^{6} b_{i,x_j}(i+1)\eta^i + \sum_{i=0}^{6}\left[b_i(i+1)i\eta^{i-1}\left(\frac{\partial \eta}{\partial x_j}\right)_{T,P,x_{k\neq j}}\right], \tag{3.83}$$

$$\left(\frac{\partial \overline{m^2\varepsilon\sigma^3}}{\partial x_j}\right)_{T,P,x_{k\neq j}} = 2m_j\sum_i x_i m_i\left(\frac{\varepsilon_{ij}}{\kappa T}\right)\sigma_{ij}^3, \tag{3.84}$$

$$\left(\frac{\partial \overline{m^2\varepsilon^2\sigma^3}}{\partial x_j}\right)_{T,P,x_{k\neq j}} = 2m_j\sum_i x_i m_i\left(\frac{\varepsilon_{ij}}{\kappa T}\right)^2\sigma_{ij}^3, \tag{3.85}$$

$$\left(\frac{\partial C_1}{\partial x_j}\right)_{T,P,x_{k\neq j}} = \left(\frac{\partial C_1}{\partial \eta}\right)\left(\frac{\partial \eta}{\partial x_j}\right)_{T,P,x_{k\neq j}} + m_j\frac{\partial C_1}{\partial \bar{m}}, \tag{3.86}$$

$$\left(\frac{\partial C_2}{\partial x_j}\right)_{T,P,x_{k\neq j}} = \left(\frac{\partial^2 C_1}{\partial \eta^2}\right)\left(\frac{\partial \eta}{\partial x_j}\right)_{T,P,x_{k\neq j}} + m_j\frac{\partial^2 C_1}{\partial \eta\partial \bar{m}}. \tag{3.87}$$

The terms $\frac{\partial C_1}{\partial \eta}$, $\frac{\partial C_1}{\partial m}$, $\frac{\partial^2 C_1}{\partial \eta^2}$, and $\frac{\partial C_1^2}{\partial \eta\partial \bar{m}}$, which are functions of the known parameters $\bar{m}$ and η, are determined as follows

$$\frac{\partial C_1}{\partial \eta} = -C_1^2\times\left[\bar{m}\frac{8+20\eta-4\eta^2}{(1-\eta)^5} + (1-\bar{m})\frac{40-48\eta+12\eta^2+2\eta^3}{(1-\eta)^3(2-\eta)^3}\right], \tag{3.88}$$

$$\frac{\partial C_1}{\partial \bar{m}} = -C_1^2\times\left[\frac{8\eta-2\eta^2}{(1-\eta)^4} - \frac{20\eta-27\eta^2+12\eta^3-2\eta^4}{\left[(1-\eta)(2-\eta)\right]^2}\right], \tag{3.89}$$

$$\frac{\partial^2 C_1}{\partial \eta^2} = \frac{2}{C_1}\left(\frac{\partial C_1}{\partial \eta}\right)^2 - C_1^2[\bar{m}\frac{60+72\eta-12\eta^2}{(1-\eta)^6} + (1-\bar{m})\frac{-6\eta^4-48\eta^3+288\eta^2-480\eta+264}{(1-\eta)^4(2-\eta)^4}], \quad (3.90)$$

$$\frac{\partial C_1^2}{\partial \eta \partial \bar{m}} = 2\frac{C_2}{C_1}\frac{\partial C_1}{\partial \bar{m}} - C_1^2\left[\frac{-4\eta^2+20\eta+8}{(1-\eta)^5} - \frac{2\eta^3+12\eta^2-48\eta+40}{(1-\eta)^3(2-\eta)^3}\right], \quad (3.91)$$

Substitution of Eq. (3.62) and the derivatives of the hard-chain and dispersion terms of the compressibility factor into Eq. (3.61) results in a linear equation in which the only unknown is $\left(\partial\rho / \partial x_j\right)_{T,P,x_{k\neq j}}$. The derivative of the compressibility factor is then calculated from Eq. (3.62) using $\left(\partial\rho / \partial x_j\right)_{T,P,x_{k\neq j}}$.

3.3.4.2. Derivatives of the fugacity with respect to pressure

The derivatives of the fugacity with respect to pressure are required to determine the cumulative volume derivatives with respect to pressure in pressure equations. To calculate these derivatives, we need to follow a procedure similar to that used in the previous section to calculate the derivatives with respect to mole number. The detailed procedure can be found in Appendix B.

3.3.4.3. Analytical derivatives versus numerical derivatives

We evaluated the analytical derivatives of the fugacity and compressibility factor by comparing them with the numerical derivatives. To compute the numerical derivatives with respect to mole fractions, a forward difference approximation is employed as follows:

$$\left(\frac{\partial f_i(T,P,\bar{x})}{\partial x_j}\right)_{T,P,x_{k\neq j}} \approx \left.\frac{\Delta f_i}{\Delta x_j}\right|_{T,P,x_{k\neq j}} = \frac{f_i\left(T,P,\left[x_1,...,x_j+h,...,x_{N_C}\right]\right)-f_i(T,P,\bar{x})}{h}, \quad (3.92)$$

$$\left(\frac{\partial Z(T,P,\bar{x})}{\partial x_j}\right)_{T,P,x_{k\neq j}} \approx \left.\frac{\Delta Z}{\Delta x_j}\right|_{T,P,x_{k\neq j}} = \frac{Z\left(T,P,\left[x_1,...,x_j+h,...,x_{N_C}\right]\right)-Z(T,P,\bar{x})}{h}, \quad (3.93)$$

where h represents a small change in x_j while $x_{k\neq j}$ are kept constant. The mole fraction derivatives are then converted to the mole number derivatives based on Eq. (3.59). The numerical derivatives with respect to the pressure are determined as

$$\left(\frac{\partial f_i(T,P,\bar{x})}{\partial P}\right)_{T,\bar{x}} \approx \left.\frac{\Delta f_i}{\Delta P}\right|_{T,\bar{x}} = \frac{f_i(T,P+h,\bar{x})-f_i(T,P,\bar{x})}{h}, \quad (3.94)$$

$$\left(\frac{\partial Z(T,P,\bar{x})}{\partial P}\right)_{T,\bar{x}} \approx \left.\frac{\Delta Z}{\Delta P}\right|_{T,\bar{x}} = \frac{Z(T,P+h,\bar{x})-Z(T,P,\bar{x})}{h}, \quad (3.95)$$

where h is an infinitesimal change in pressure.

To compare the numerical and analytical derivatives, we made a synthetic mixture containing C_1, C_2, and nC_5 with the overall compositions of 0.4, 0.2, and 0.4 (mixture 1), respectively. The pure-component parameters and BIPs are given in Table 3-3.

Table 3-3: Pure-component parameters and BIPs for mixture 1.

	Overall composition	PC-SAFT parameters			Binary interaction parameters	
	Z	σ (Å)	ε/κ (K)	m	$kC_{1,j}$	$kC_{2,j}$
C_1	0.4	3.7039	150.03	1.0000	0.0000	0.0027
C_2	0.2	3.5206	191.42	1.6069	0.0027	0.0000
nC_5	0.4	3.7729	231.2	2.6896	0.0206	0.0086

Through two-phase flash calculations at 100 °F and 1300 psia, we calculated the partial derivatives of the compressibility factor and component fugacities for each phase. The partial derivatives of the compressibility factor and fugacity with respect to mole numbers are matrices containing $N_P \times N_C$ and $N_P \times N_C^2$ elements, respectively. In order to compare the numerical and analytical derivatives with respect to mole number, the differences between the results obtained by the two methods are calculated for each element of the matrices. Then, the maximum differences are plotted in Figure 3-2 and Figure 3-3 for different values of *h* in log-log scale.

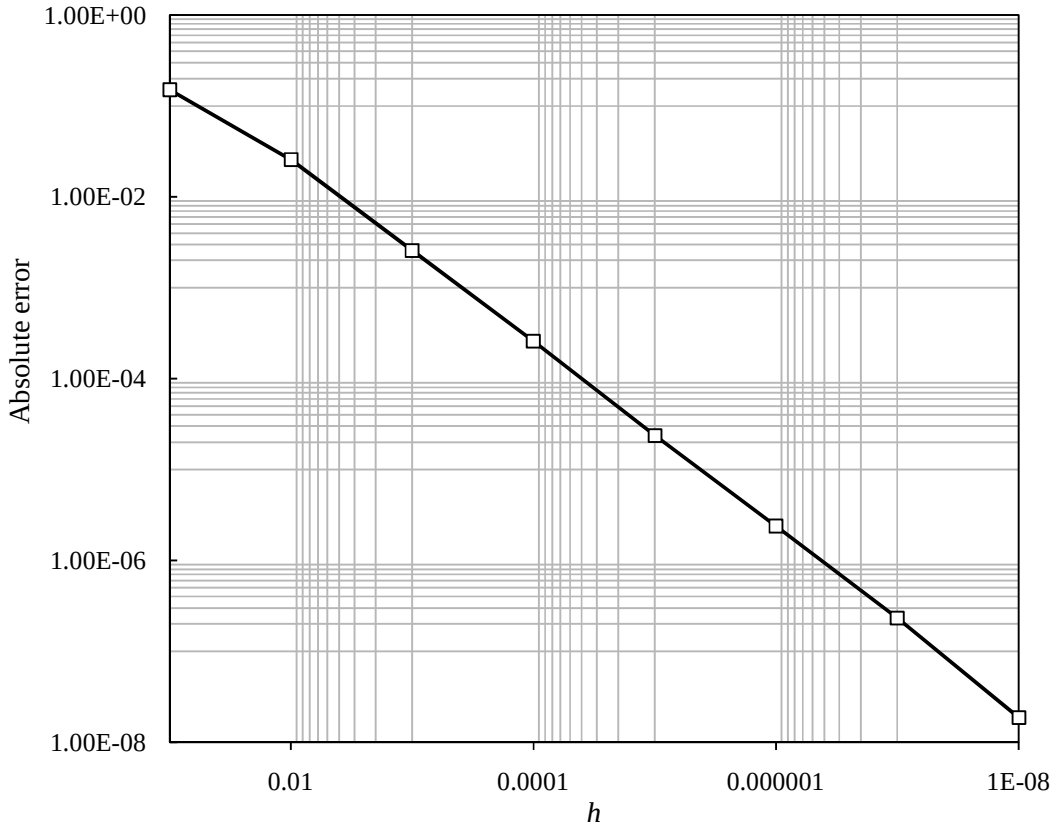

Figure 3-2: Maximum difference between the numerical and analytical derivatives of the compressibility factor with respect to mole numbers for mixture 1 at 100 °F and 1300 psia.

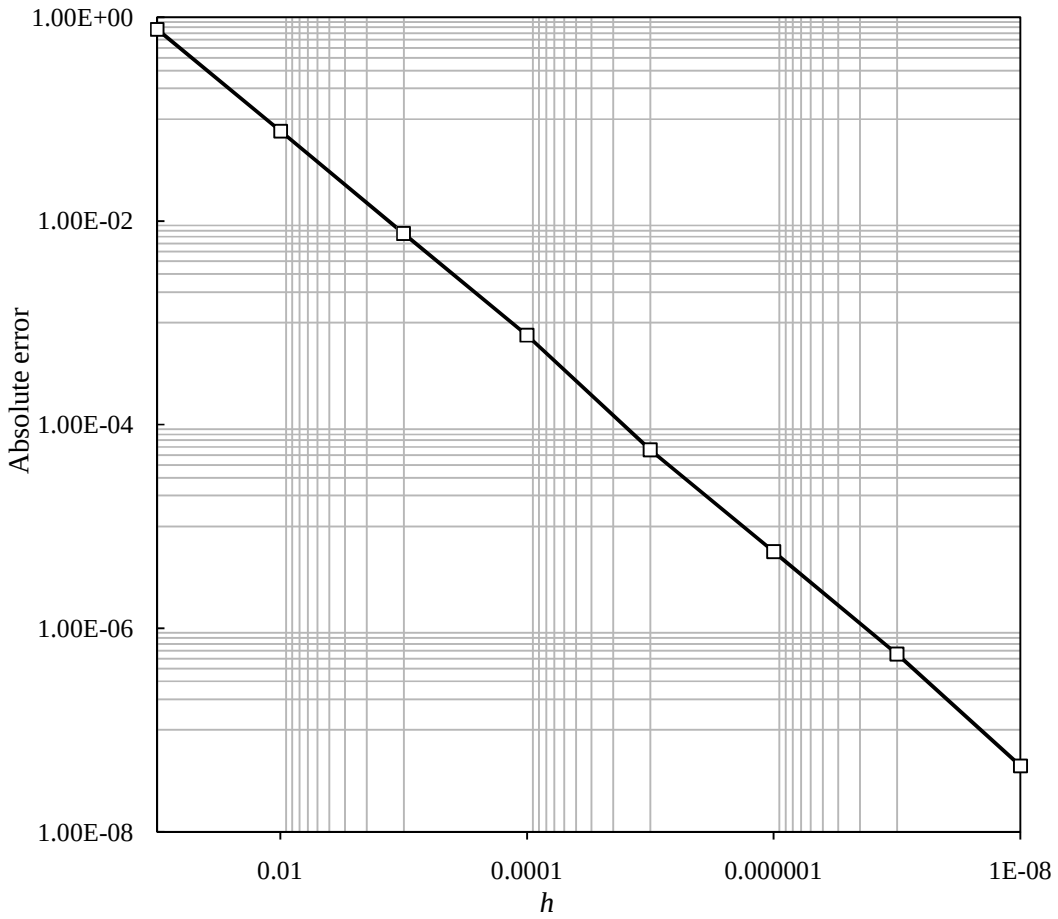

Figure 3-3: Maximum difference between the numerical and analytical derivatives of the fugacity coefficient with respect to mole numbers for mixture 1 at 100 °F and 1300 psia.

Results show that by decreasing the value of the variable *h*, the maximum differences between the numerical and analytical derivatives approach 10^{-8} for both compressibility factor and fugacity derivatives. The maximum differences between numerical and analytical derivatives with respect to pressure are plotted in Figure 3-4 and Figure 3-5.

To determine the numerical derivatives, h is chosen as a fraction (h') of the pressure. The maximum differences between the numerical and analytical derivatives with respect to pressure approach 10^{-9} for both compressibility factor and fugacity derivatives. These results confirm the validity of the analytical partial derivatives derived in this research.

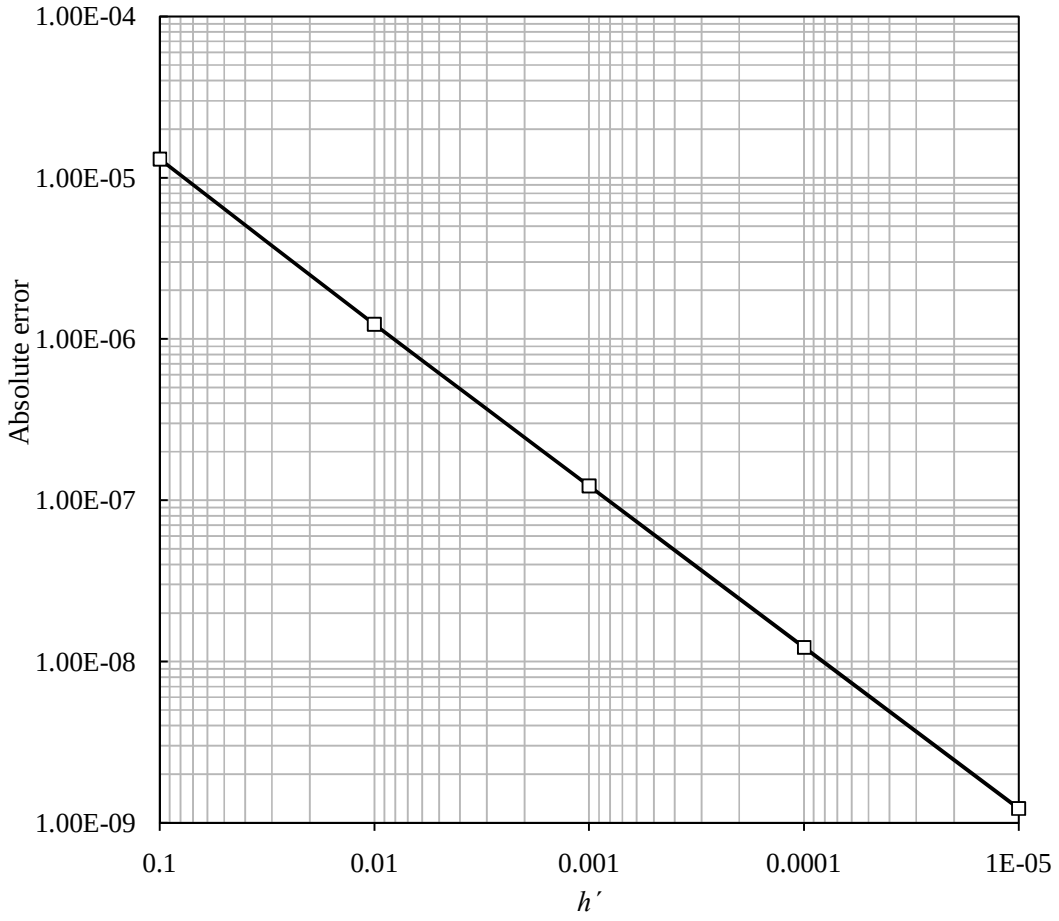

Figure 3-4: Maximum difference between the numerical and analytical derivatives of the compressibility factor with respect to pressure for mixture 1 at 100 °F and 1300 psia.

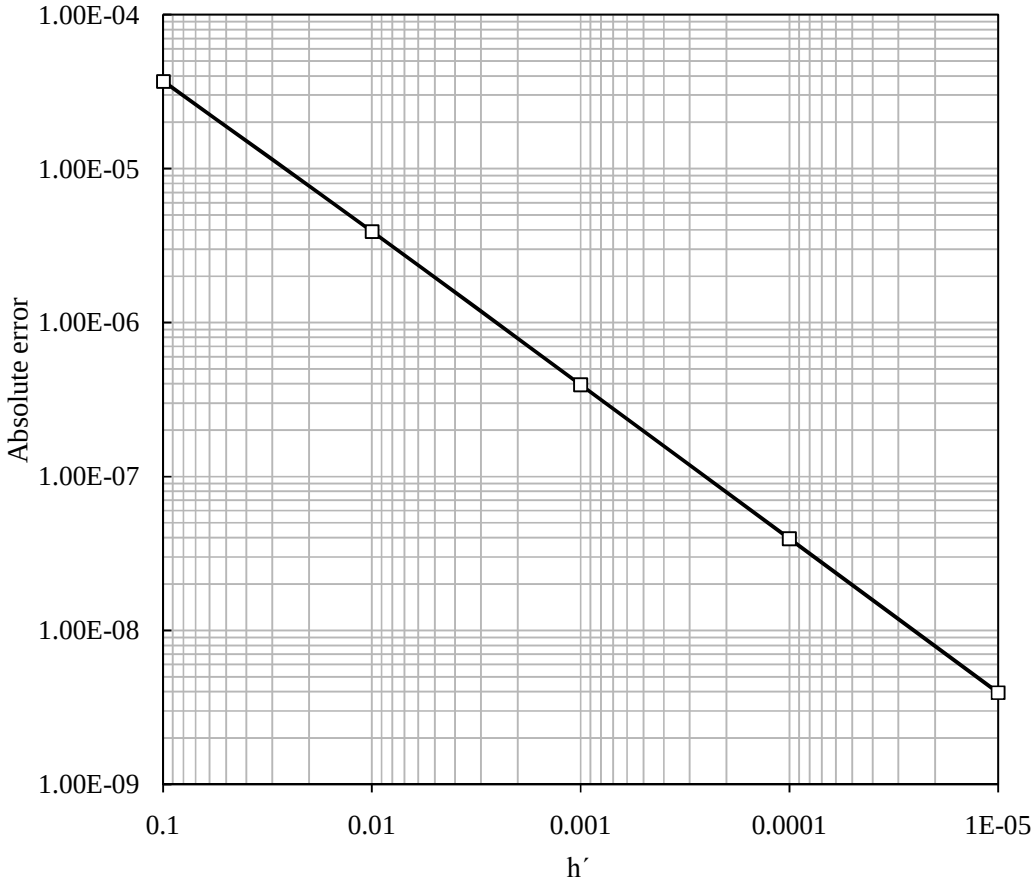

Figure 3-5: Maximum difference between the numerical and analytical derivatives of the fugacity with respect to pressure for mixture 1 at 100 °F and 1300 psia.

Besides accuracy, using the analytical derivatives instead of the numerical ones can save a significant computational time in phase equilibrium calculations. To show this, we calculated the total computational time of the equilibrium calculations, including stability analysis and flash calculations, for the same ternary mixture using both kinds of derivatives. The computational time is plotted in Figure 3-6 for different number of components ranging from 3 to 10. To have similar cases with different number of components, the last component is split to multiple components with the same physical properties.

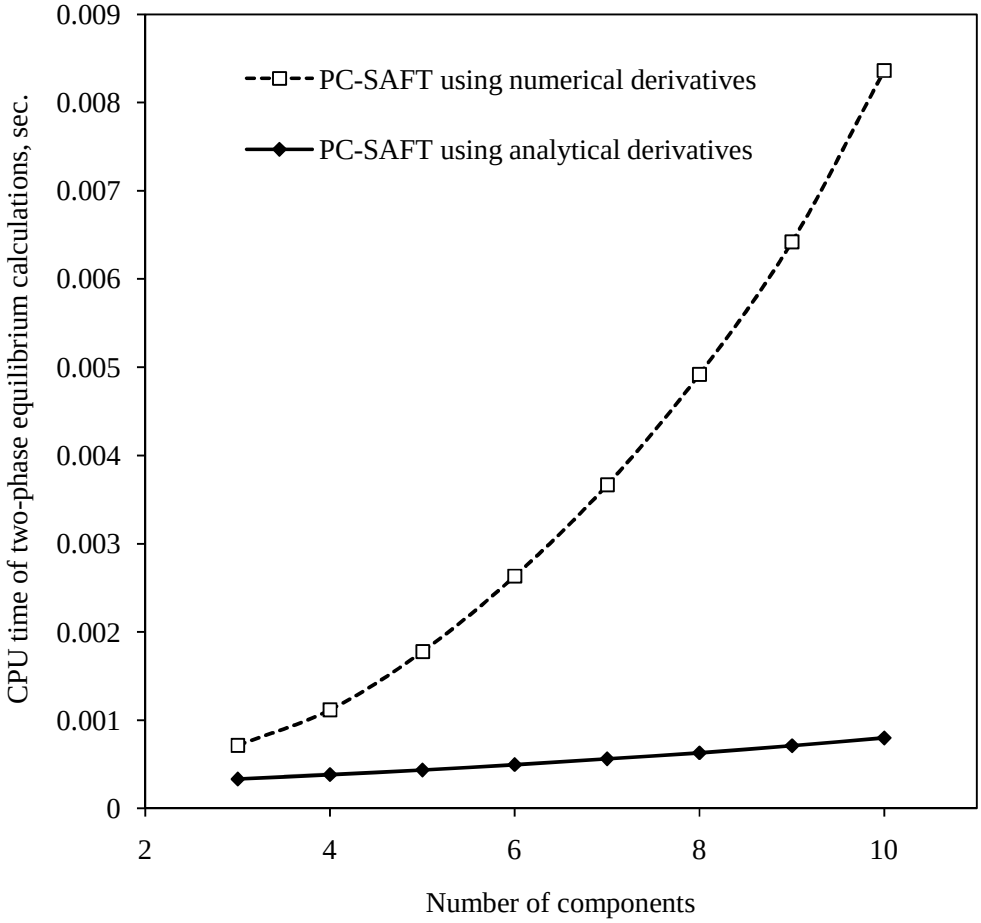

Figure 3-6: Total computational time of the two-phase equilibrium calculations (including stability analyses and flash calculations) for mixture 1 using PC-SAFT EOS.

Referring to Figure 3-6, the curve of the CPU time for the equilibrium calculations using analytical derivatives is flatter and considerably smaller than by using the numerical derivatives. One of the required quantities to find the partial derivatives of the fugacity is the density root, which is determined iteratively in the PC-SAFT model. As mentioned earlier, the numerical derivatives with respect to mole fractions are estimated using the finite difference approach by making an infinitesimal change in the composition of interest. By changing the composition, the density roots must be

recalculated to find the fugacity values at the new compositions. Therefore, constructing the Hessian matrix with the numerical derivatives leads to a significant computational effort to search for the PC-SAFT density roots for each element of the Hessian matrix. The analytical derivatives, however, require finding the density roots only one time. This is the primary reason that the CPU time curve using the analytical derivatives is more constant with N_C than when the numerical derivatives are used.

3.4. EQUILIBRIUM CALCULATIONS SPEED-UP

Phase equilibrium calculations using PC-SAFT EOS take more computational effort than the traditional CEOSs for two reasons: first, there is not a closed form for PC-SAFT EOS and finding the density roots is an iterative process and second, the algebraic equations to find thermodynamic properties from PC-SAFT EOS are more complex than those calculated from a CEOS.

An EOS can give multiple roots at a given pressure and temperature. In phase equilibrium calculations, we need to search for a root that gives the minimum Gibbs free energy for the corresponding phase. In CEOSs, liquid and vapor roots are found simultaneously. However, because the root finding procedure in PC-SAFT is iterative, the two roots must be determined separately. Therefore, in order to find the fugacity of a phase, we need to perform two iterative root finding processes. This fact causes a significant increase in computational time of the flash and stability analysis calculations, which require finding the fugacity coefficient several times.

Yan *et al.* (2011) suggested ruling out the search for vapor density root at high pressures. They set a limit pressure, P_{limit}, above which only liquid-like density roots can exist. In this way, they search for only one density root, which is a liquid-like root. They also suggested using the density results from a previous calculation as the initial estimate

for the new density calculation. They used this procedure for the simplified version of PC-SAFT EOS implemented in a slim tube simulator. Their improved algorithm reduces the CPU-time ratio of simplified PC-SAFT to SRK EOS by 3 for components ranging from 3 to 12 in number.

In this research, we did not exclude the vapor-like density root. Our experience shows that after one iteration of the flash calculation, the identity of the density root for each phase is specified. Therefore, we need to search for both density roots only for the first iteration of the flash calculation. The remaining calculations require searching only near the root determined in the previous iteration. This algorithm automatically rules out one of the density roots, whether it is a liquid or a vapor phase.

Using previous results as the initial guess for finding the density root also reduces the number of root finding iterations to only a few. This procedure, which is similar to that proposed by Yan *et al.* (2011), is not limited to high pressure systems. We applied this procedure to the PC-SAFT EOS in its complete form.

3.4.1. Case study 1, CPU-time of PC-SAFT in standalone calculations

To show the speed-up obtained by improving the root finding process, the total CPU-time of the two-phase equilibrium calculations for mixture 1 is plotted in Figure 3-7 with and without the speed-up procedure.

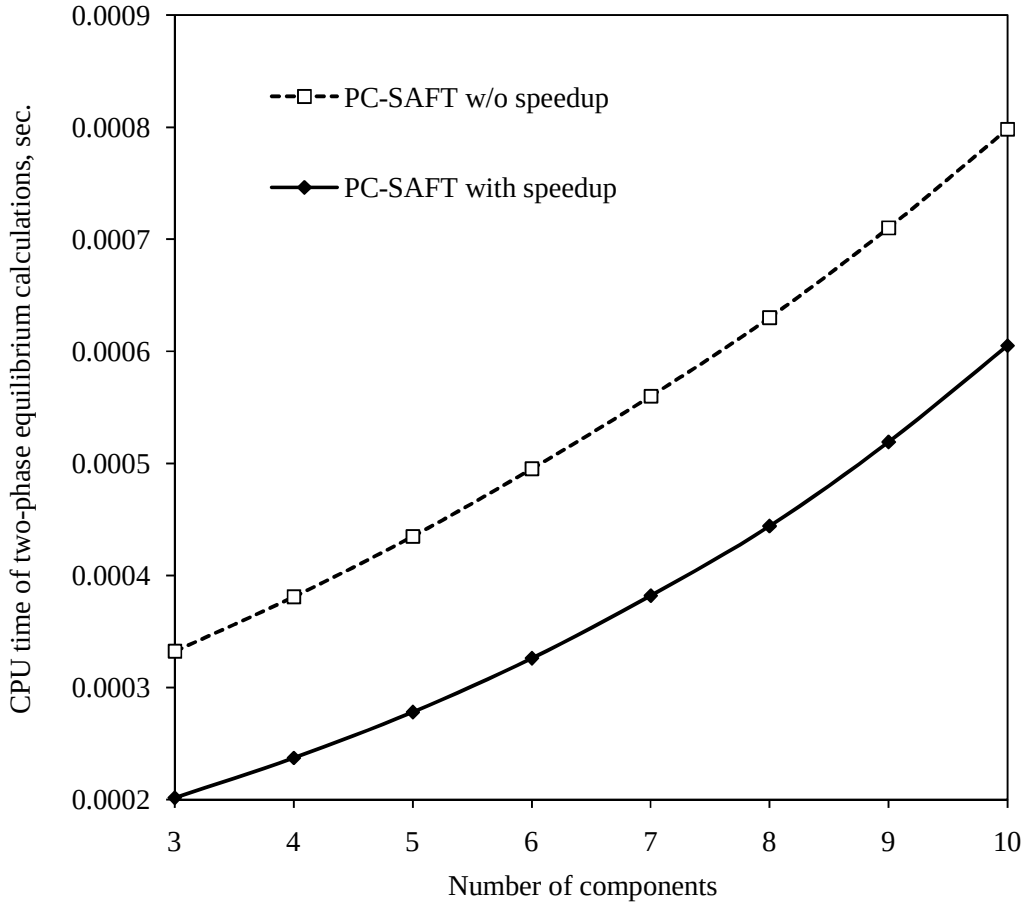

Figure 3-7: CPU time for two-phase equilibrium calculations (stability analyses and flash calculations) for mixture 1 at 100 °F and 1300 psia. All derivatives are calculated analytically in both cases.

The speed-up obtained for the test case is plotted in Figure 3-8 in terms of the percentage decrease in the total computational time of the equilibrium calculations.
In this case, the improvement in the root finding procedure can save about 25-40% of the CPU-time. The effect of this improvement is more pronounced for mixtures with a small number of components. The negative slope of the speed-up curve in Figure 3-8 implies that a larger proportion of the total CPU-time is spent on solving the density roots at a fewer number of components.

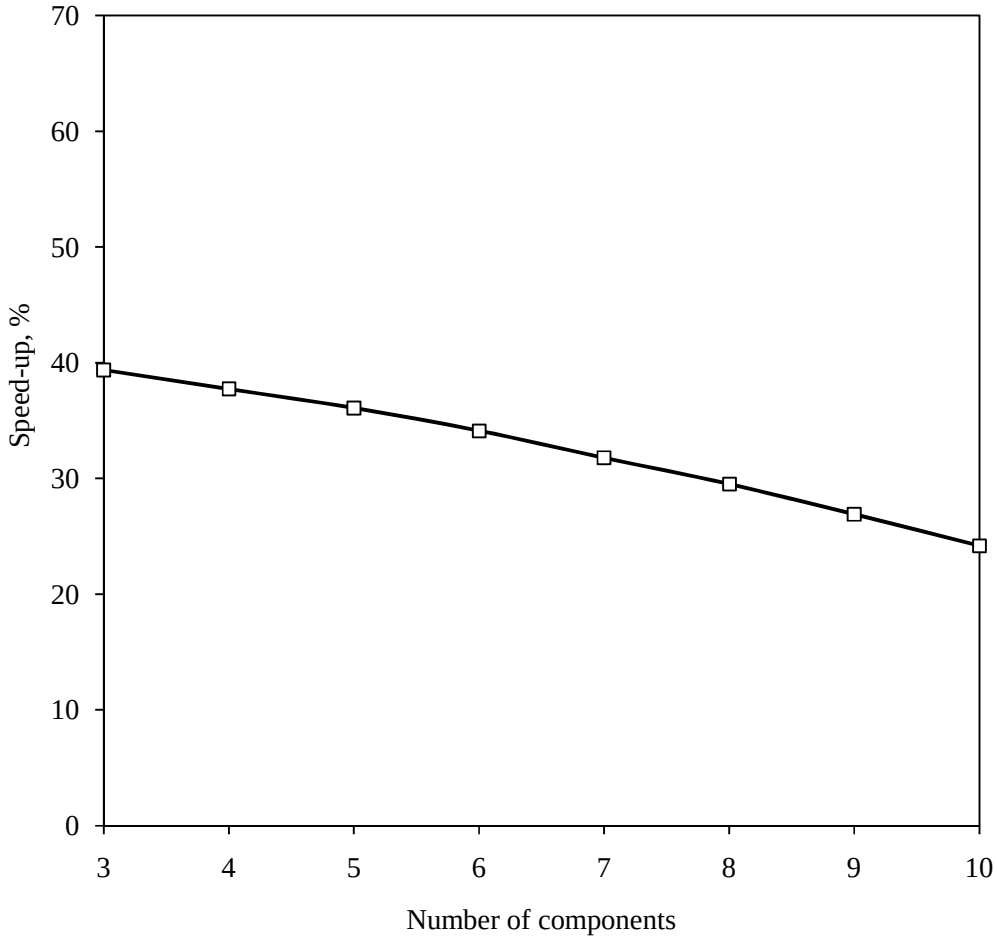

Figure 3-8: The speed-up obtained by improving the root finding procedure in phase equilibrium calculations of mixture 1 at 100 °F and 1300 psia.

The total speed-up obtained by improving root finding algorithm and using the analytical derivatives, instead of the numerical derivatives, is plotted in Figure 3-9. As shown, these improvements reduced the computational time of the equilibrium calculations by 70-90%.

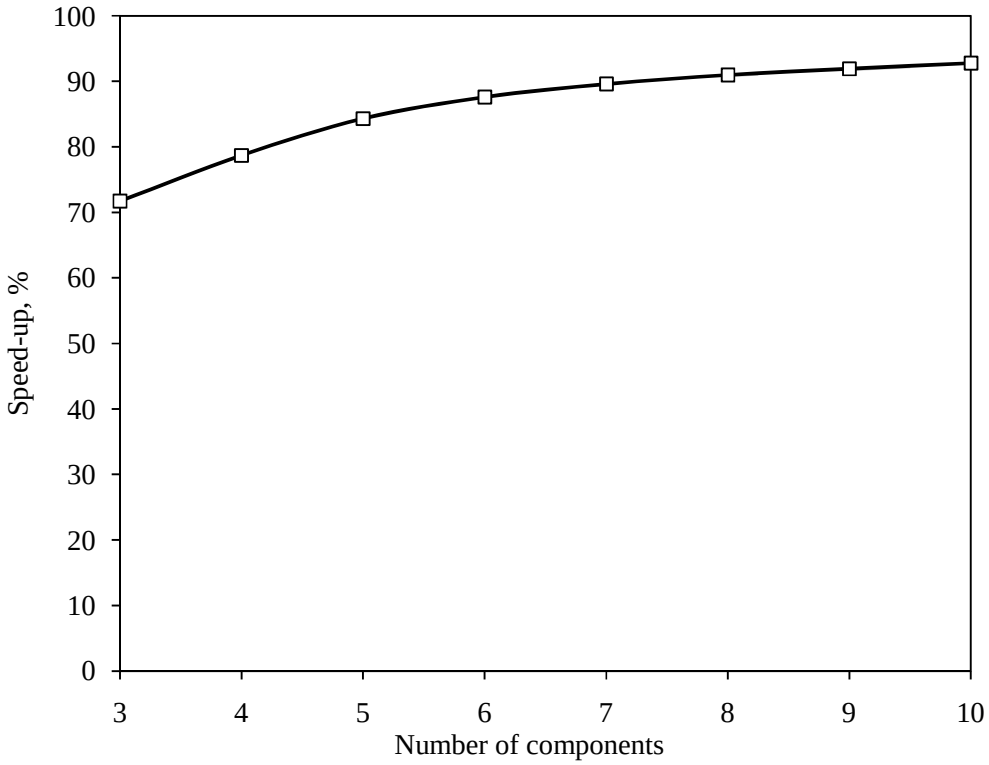

Figure 3-9: Total speed-up obtained by improving root finding procedure and using the analytical derivatives, instead of the numerical derivatives, in phase equilibrium calculations of mixture 1 at 100 °F and 1300 psia.

We compared the CPU time of the equilibrium calculations using PC-SAFT and PR EOS. The ternary mixture of $C_1/C_2/nC_5$ is used again with PR input parameters reported in Table 3-4. Similar binary interaction parameter sets (Table 3-3) are used for both PC-SAFT and PR.

Table 3-4: Peng-Robinson (PR) EOS pure-component parameters of mixture 1

Component	$T_c(K)$	$P_c(psi)$	ω
C_1	190.6	667.2	0.008
C_2	305.4	708.3	0.98
nC_5	469.6	489.4	0.251

Figure 3-10 shows the comparison of the CPU time of the flash calculations using PC-SAFT and PR EOS for different number of components. In Figure 3-10, the speed-up procedure is adopted to perform equilibrium calculations using PC-SAFT. All derivatives are calculated analytically.

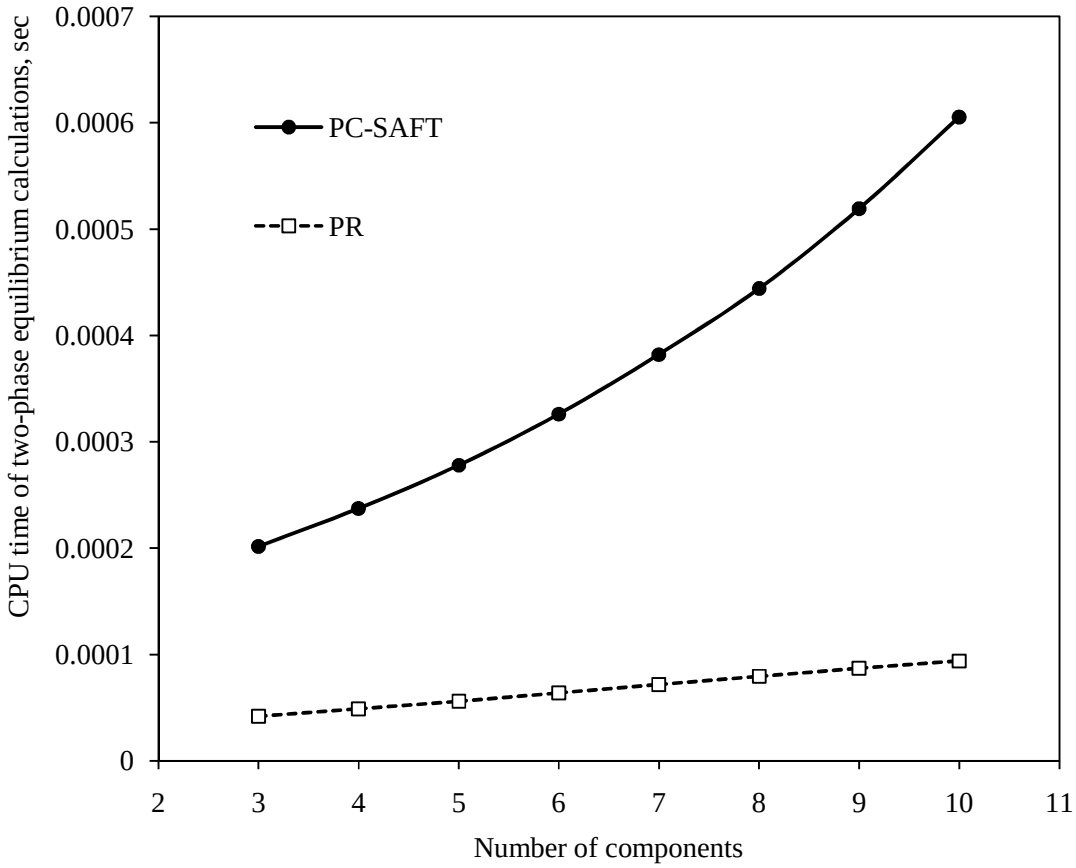

Figure 3-10: CPU time of the equilibrium calculations using PC-SAFT and PR EOS.

The CPU time ratio of PC-SAFT to PR EOS is plotted in Figure 3-11. Referring to this figure, PC-SAFT in batch calculations takes about 5-6 times more CPU time than PR EOS for components ranging from 3 to 10 in number.

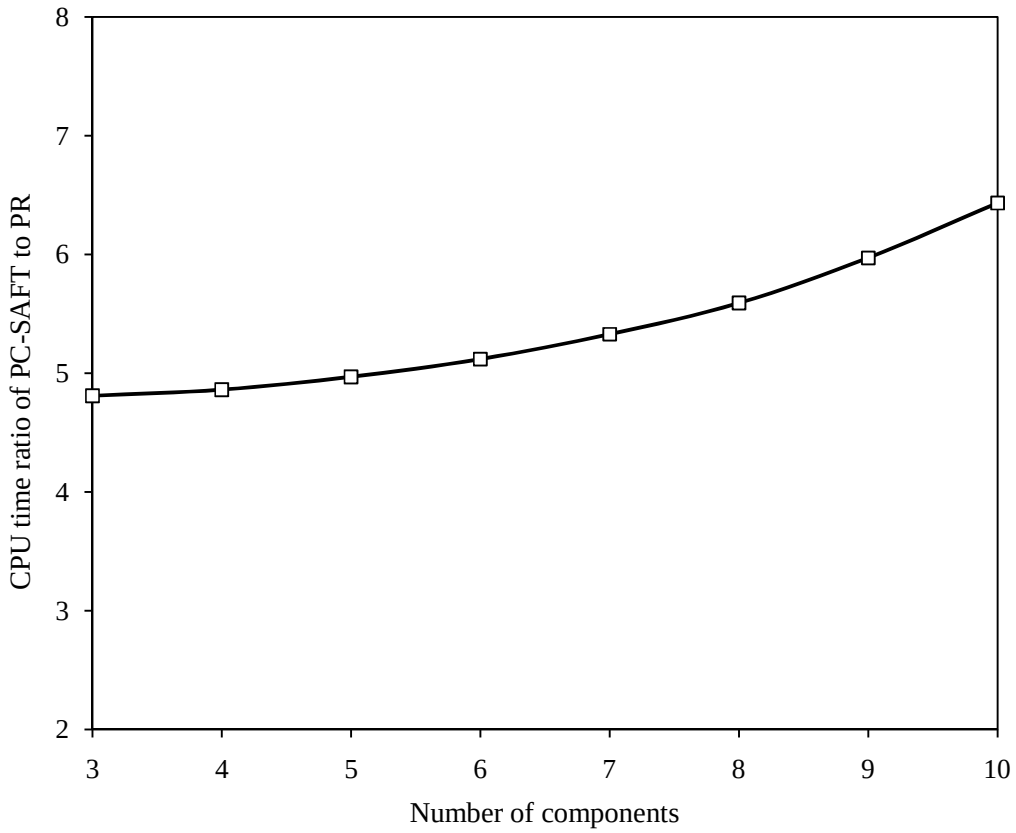

Figure 3-11: CPU time ratio of PC-SAFT to PR EOS

3.4.2. Case study 2, CPU-time of PC-SAFT in simulation

In compositional simulation, the CPU-time ratio of PC-SAFT to PR EOS is even less because the equilibrium calculations are only a part of the total CPU-time for the simulation. Also, in simulations, we can take advantage of the previous time-step results for the initialization of the flash calculations and potentially skip many stability analyses. Figure 3-12 plots the total CPU-time of the simulation for one pore volume (PV) gas injection in a two dimensional gridblock system. The reservoir properties are summarized in Table 3-5.

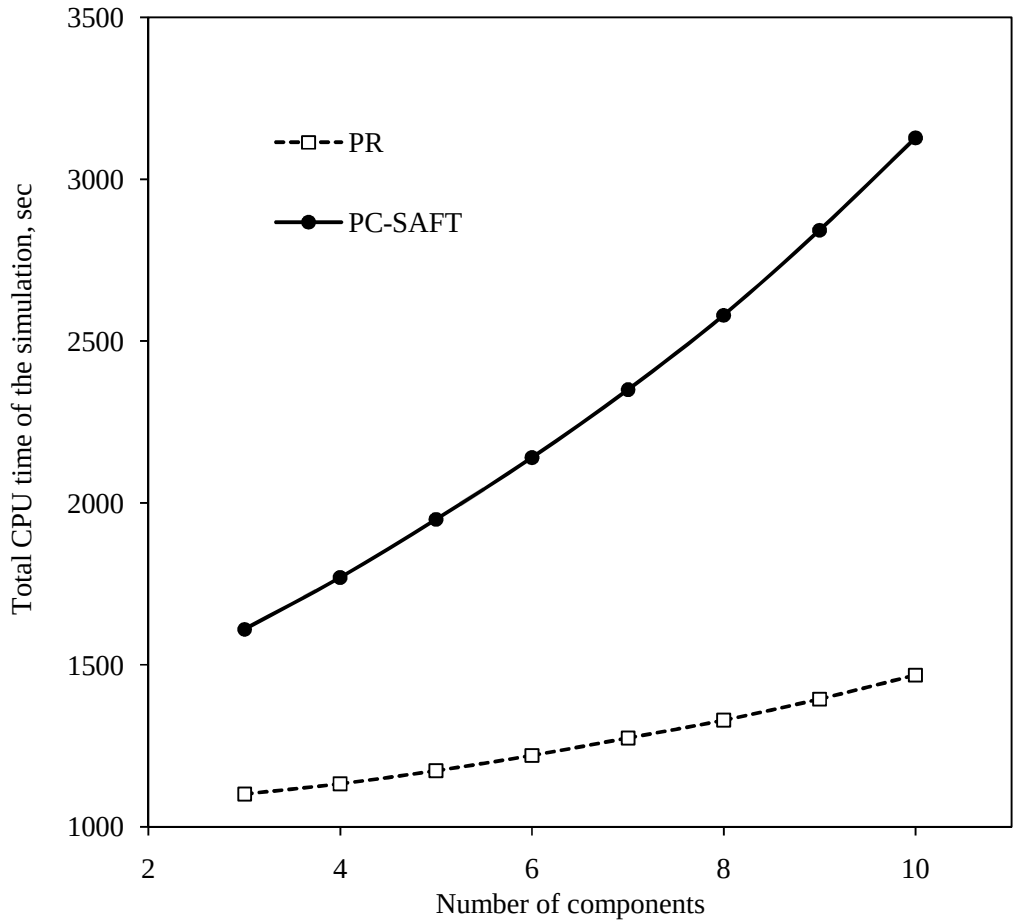

Figure 3-12: Total CPU time for the simulation of case study 2 using PC-SAFT and PR EOS

Figure 3-13 plots the CPU-time ratio of PC-SAFT to PR EOS. The results show that in this case study, the simulation implementing PC-SAFT takes about 1.5-2.1 times more CPU time than that using PR EOS, which is a reasonable computational time. The results of these simulations confirm the feasibility of applying PC-SAFT model in compositional simulation.

Table 3-5: Reservoir properties for case study 2.

Reservoir fluid	$C_1/C_2/nC_5$
Injected gas	C_1 and C_2
Initial overall composition	[0.1 0.2 0.7]
Composition of the injected gas	[0.99 0.01]
Number of gridblocks	20×20
Constant bottomhole injection pressure	2400 psia
Constant bottomhole production pressure	1500 psia
Initial reservoir pressure	2000 psia
Reservoir temperature	100 °F
Initial water saturation	0.25
Porosity	0.25
Homogeneous permeability in x and y directions	100 mD
Relative permeability model	Corey's model
Constant gridblock size at x and y directions	25 ft

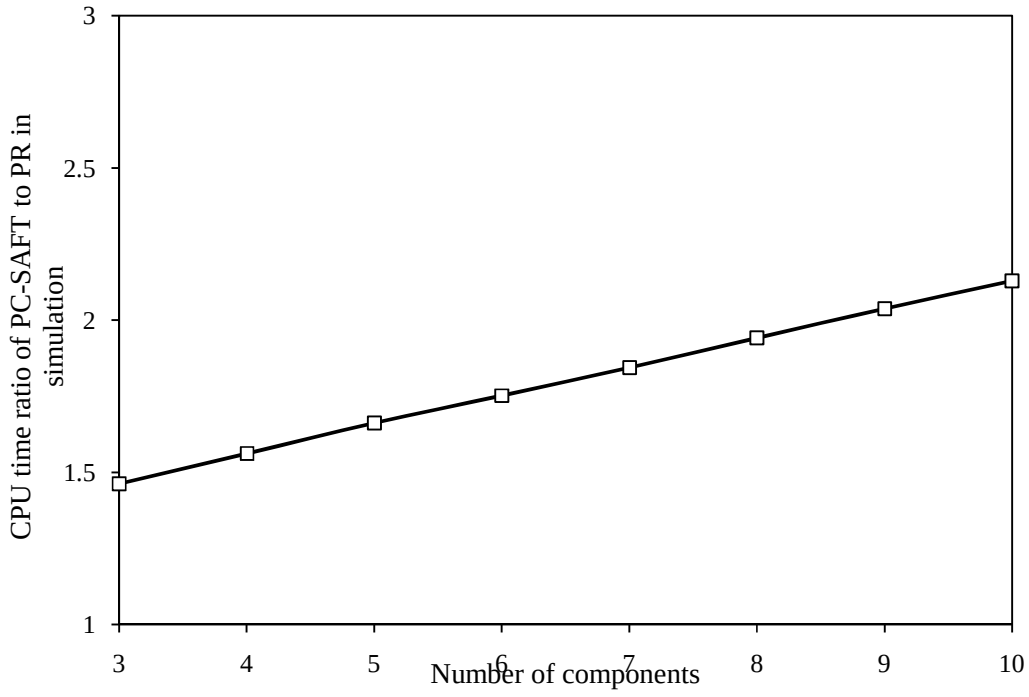

Figure 3-13: CPU-time ratio of simulations with PC-SAFT to PR EOS

The implementation of the PC-SAFT model in UTCOMP is verified by comparing the recovery factor and average reservoir pressure curves using PC-SAFT and PR EOS models in Figure 3-14 and Figure 3-15. As shown in Figure 3-14 and Figure 3-15, the recovery factor and average reservoir pressure curves using both EOS are in good agreement.

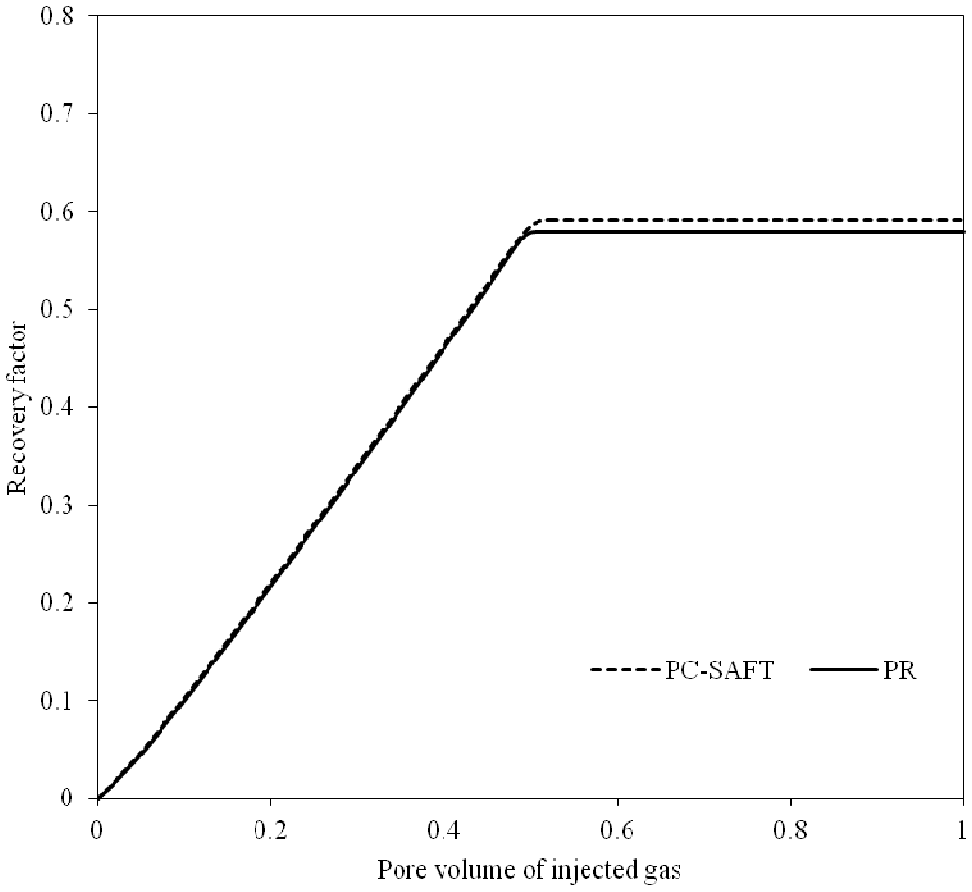

Figure 3-14: Recovery factor of the simulation case study 2 using PC-SAFT and PR EOS

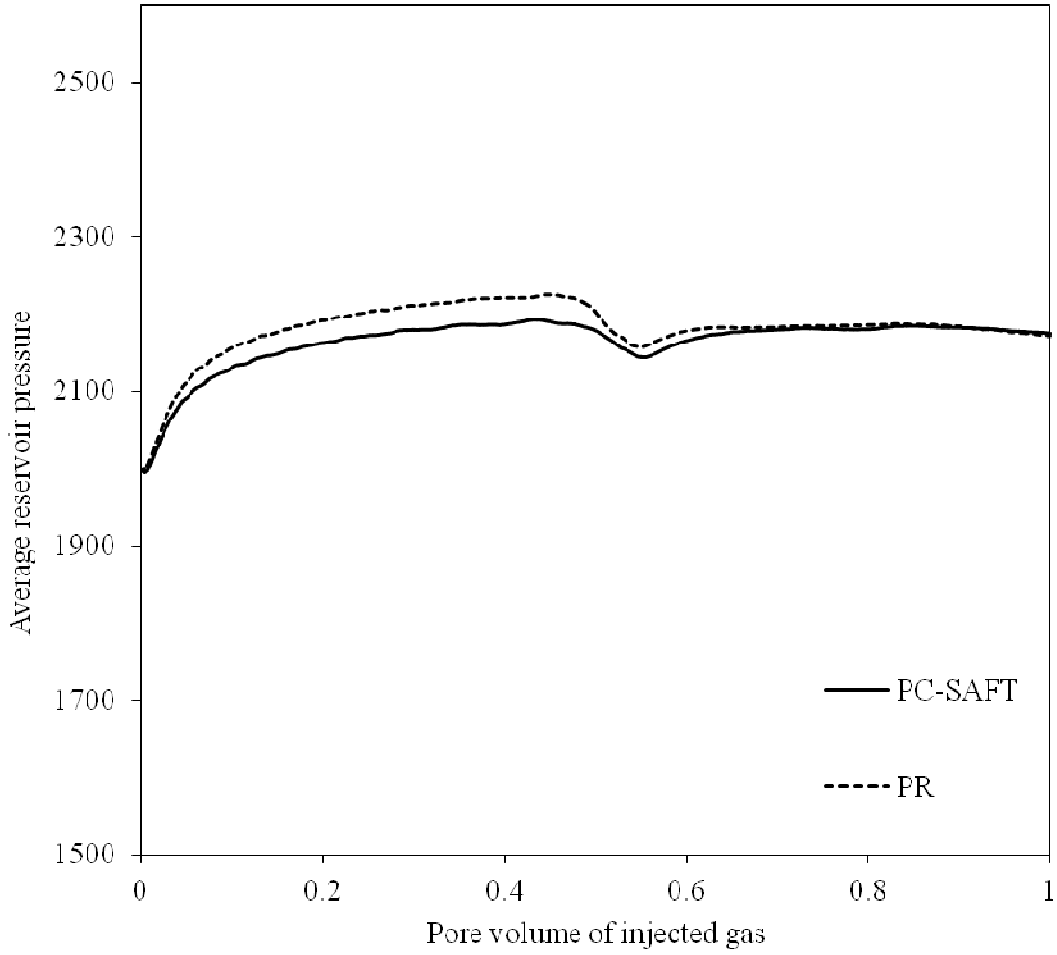

Figure 3-15: Average reservoir pressure for case study 2 using PC-SAFT and PR EOS

3.5. PC-SAFT LIMITATIONS

Beyond the qualitative efficiency of the PC-SAFT model, it has some limitations that must be taken into account to avoid erroneous predictions. Inaccurate predictions near critical regions and atypical behavior at low temperatures are two drawbacks of the PC-SAFT EOS, which are explained in the following subsections.

3.5.1. Inaccurate predictions at critical point

Pure-component parameters for SAFT family EOSs are traditionally obtained by fitting to the experimental vapor pressure and liquid volume data. This technique presents a major drawback: the SAFT-type EOSs cannot give an exact match with the experimental values of the critical temperature and pressure (T_c and P_c). The CEOSs, however, are forced to satisfy the experimental values of T_c and P_c.

The critical point of a pure component can be determined by finding a pressure-volume isotherm having an inflection point. In Figure 3-16, we have plotted three isotherms of pure CO_2 at a pressure-volume diagram using PC-SAFT and PR EOS. As is shown in this figure, PR EOS can exactly predict the critical temperature of CO_2 (i.e. 304.2 K). The PC-SAFT EOS, however, overpredicts the critical temperature by about 6 K.

Castro-Marcano *et al.* (2006) rescaled the PC-SAFT EOS parameters to force the model to match the critical temperature and pressure. They proposed three polynomial expressions to relate the PC-SAFT parameters to the critical temperature T_c, critical pressure P_c and acentric factor, ω. The polynomial expressions are given as

$$m = \sum_{i=0}^{3} p_i \omega^i \,, \tag{3.96}$$

$$\varepsilon / \kappa = T_c \sum_{i=-1}^{6} q_i m^i \,, \tag{3.97}$$

$$\sigma^3 = \kappa T_c / P_c \sum_{i=-1}^{6} s_i m^i \,, \tag{3.98}$$

with the coefficients listed in Table 3-6.

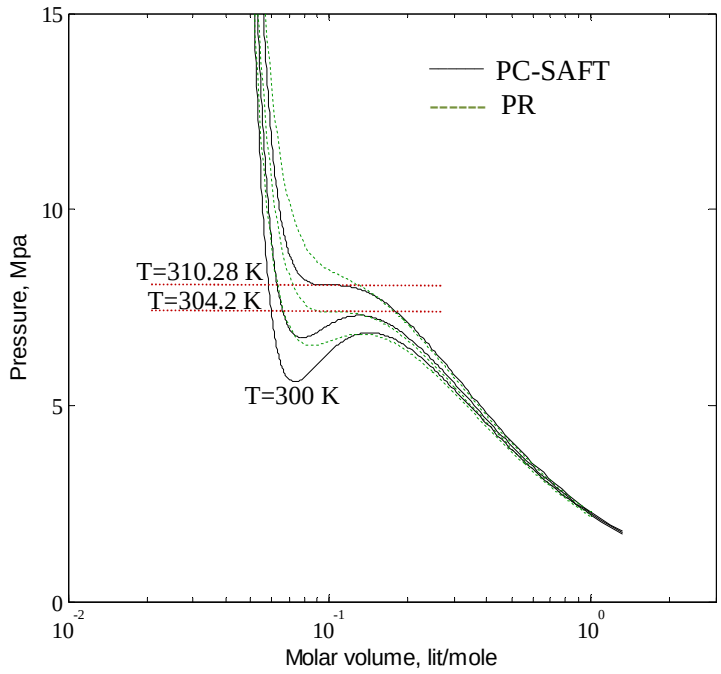

Figure 3-16: The pressure–volume diagrams of pure CO_2 at T = 300 K, 304.2 K, and 310.28 K

Table 3-6: Coefficients for Eqs. (3.96)-(3.98) (Castro-Marcano *et al.*, 2006).

i	p_i	q_i	s_i
-1	-	2.320996×10^{-1}	1.283708×10^{-1}
0	9.897355×10^{-1}	7.705073×10^{-1}	-7.443132×10^{-2}
1	7.484070	-2.932798×10^{-1}	4.984538×10^{-2}
2	6.022657×10^{-1}	8.978452×10^{-2}	-1.703190×10^{-2}
3	2.817746×10^{-2}	-1.575745×10^{-2}	3.177150×10^{-3}
4	-	1.574702×10^{-3}	-3.297430×10^{-4}
5	-	-8.316697×10^{-5}	1.786190×10^{-5}
6	-	1.798699×10^{-6}	-3.933074×10^{-7}

However, this technique causes deviations in the liquid density predictions. To show this, we have plotted the pressure-density diagram for pure ethane using PC-SAFT (with both original and rescaled pure-component parameters) and PR EOS in Figure 3-17. The results are compared with experimental data (Funke *et al.* 2002) in this figure. The original and rescaled pure-component parameters for ethane are given in Table 3-7.

Table 3-7: Original and rescaled pure-component parameters for ethane

	m	σ	ε / κ
Original parameter	1.6069	3.5206	191.42
Rescaled parameter	1.7366	3.4773	182.0190

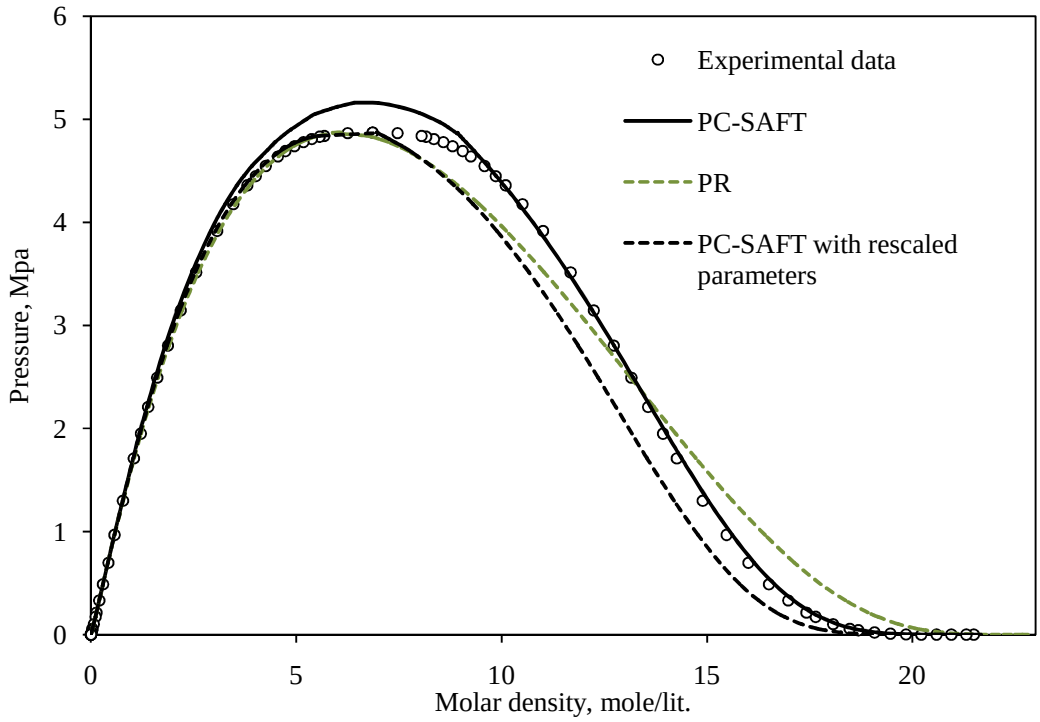

Figure 3-17: Pressure-density diagram for pure ethane. Experimental data are from Funke *et al.* (2002).

As is shown in Figure 3-17, the density predictions by PC-SAFT with the original pure-components are in excellent agreement with experimental data in regions far from the critical point. However, PC-SAFT with original pure-components overestimates the critical point. While the rescaled parameters result in better predictions in the critical region, they cause deviations in liquid density results.

3.5.2. Atypical behavior at very low temperatures

As first reported by Privat *et al.* (2010), the PC-SAFT equation may exhibit a physically inconsistent behavior at low temperatures. They showed that the PC-SAFT EOS can give up to five density roots at low temperatures, which consequently results in two different fluid–fluid coexistence lines (i.e., VL and LL equilibrium lines) and two critical points. In Figure 3-18, we have regenerated the P-η isotherms for pure n-decane using PC-SAFT at four different temperatures, which was originally illustrated by Privat *et al.* (2010).

As is shown, PC-SAFT gives five different real roots at 135 K. This behavior is more evident for heavier components. In Figure 3-19, the P-η diagrams for a range of n-alkanes (*i.e.*, from C_1 to C_{19}) are plotted at T=135 K. This atypical behavior is not a major concern in reservoir simulations, as it happens only at very low temperatures, which are far from the operation reservoir conditions.

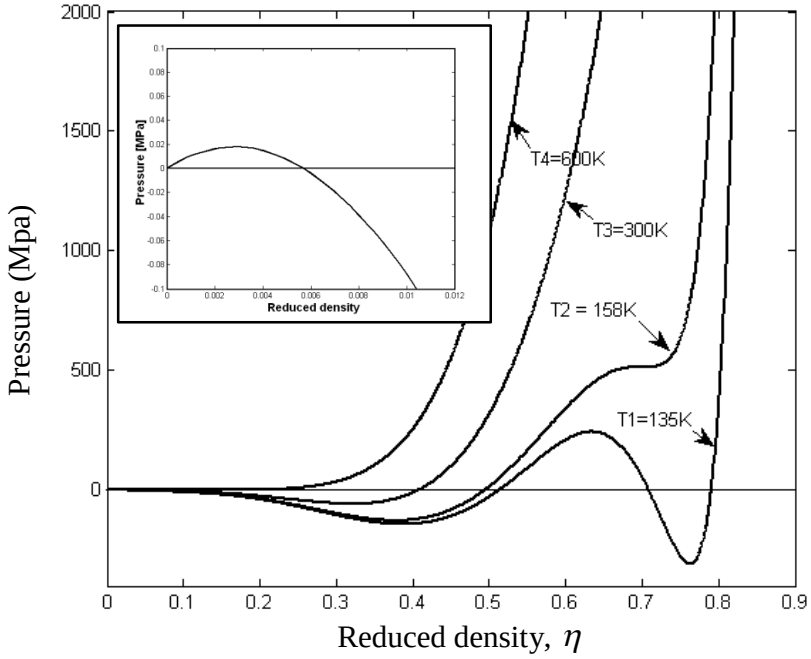

Figure 3-18: Regenerated isotherms of the pure n-decane based on PC-SAFT EOS, originally illustrated by Privat *et al.* (2010).

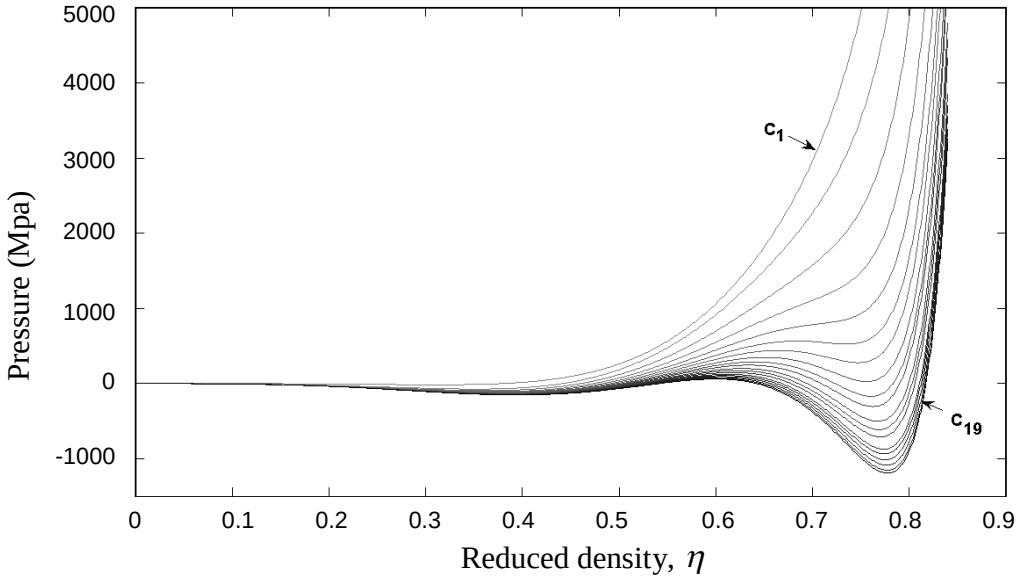

Figure 3-19: The pressure-density diagram of pure n-alkanes at T=135 K.

3.6. CHAPTER SUMMARY

PC-SAFT was effectively implemented in UTCOMP using a reasonable computational time. The additional computational time of PC-SAFT is decreased by improving the root finding algorithm and calculating the derivatives analytically. Results show that the increased computational time using PC-SAFT compared to PR EOS for a two-phase flash calculation of a mixture, containing 3 to10 components, ranges from a factor of 5 to 6 in stand-alone mode and 1.5 to 2.1 in simulations. Results suggest the feasibility of implementing PC-SAFT in compositional simulator, although its match at critical points is not as good as a CEOS.

Chapter 4. Asphaltene precipitation and deposition modeling

The purpose of this chapter is to simulate asphaltene deposition in the reservoir under gas injection. Deposition modeling in porous media includes two main aspects: (1) the thermodynamics of the asphaltene precipitation and (2) the dynamics of the precipitated solids. To model the thermodynamics of precipitation, we used the developed phase behavior algorithm using PC-SAFT EOS explained in Chapter 3. Then, the thermodynamic model is sequentially integrated with the deposition and plugging models to simulate the dynamics of precipitated asphaltenes during the simulation.

In this chapter, we describe the phase behavior approach to model asphaltene precipitation, fluid characterization with the PC-SAFT model, phase identification, and the deposition of asphaltene particles in porous media. Then simulation case studies are presented to show the effect of gas injection on asphaltene precipitation and deposition in the reservoir.

4.1. PHASE BEHAVIOR OF ASPHALTENE PRECIPITATION

Asphaltene precipitation is modeled here as forming an asphaltene-rich phase from the reservoir fluid at liquid/liquid equilibrium (LLE) or vapor/liquid/liquid equilibrium (VLLE). The asphaltene-rich phase is assumed to be a liquid phase containing asphaltene component, in micro-aggregate form, with some amounts of other crude oil components.

Some authors assumed that the asphaltene-rich phase does not interfere with VLE and, therefore, they modeled asphaltene precipitation using a sequential flash algorithm consisting of separate VLE and LLE calculations (Burke *et al.* 1990, Nor-Azlan and Adewumi 1993, Hirschberg *et al.* 1984). In the sequential flash, VLE calculations are performed first to obtain compositions and fluid properties of the vapor and oleic phases.

LLE calculations are then conducted to model an equilibrium state between the oleic-phase, which behaves as a solvent for asphaltenes, and a pseudo-liquid asphaltene-rich phase. This type of approach to solve a three-phase problem is not thermodynamically consistent and can cause errors in the equilibrium calculations. In this research, however, we modeled the three phases, i.e. the vapor (V), oil (L_1), and asphatene-rich phase (L_2), simultaneously in a unified framework by using the equilibrium calculations algorithm described in Chapter 3.

The formation of an asphaltene-rich phase from a given crude is a function of temperature and pressure, which can be represented in a P-T phase diagram (Leontaritis 1996) called the asphaltene precipitation envelope (APE). Such a diagram is schematically presented in Figure 4-1 which is composed of

(I) a bubble-point pressure curve

(II) an upper onset pressure curve at which the least soluble asphaltenes start to precipitate

(III) a lower onset curve below which the asphaltene aggregates redissolve into the oil phase.

Apshaltene stability zones are delimited by the upper and lower onset pressure curves. Once the operating condition of a given system falls into the window between the upper and lower onset pressures, the asphaltenes start to precipitate from the solution. Pressure depletion is one of the primary reasons favoring asphaltene precipitation from asphaltic crudes. A change in oil composition is another source of precipitation, which can occur during gas injection or the comingling of two incompatible oils. Gas injection can enlarge the precipitation window of the asphaltic crude oil and therefore increase the precipitation risk.

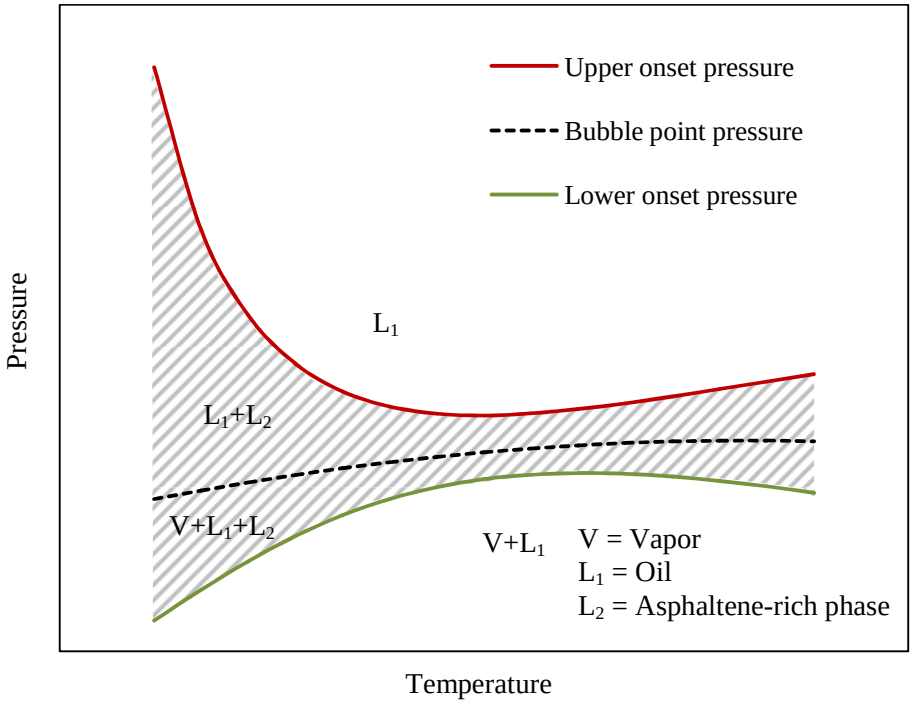

Figure 4-1: A schematic diagram of asphaltene precipitation envelope. The abbreviations V, L_1, and L_2 represent the vapor, oil, and asphaltene-rich phases, respectively.

The main assumptions made in this research to model asphaltene precipitation are summarized in the following:

(I) Asphaltene precipitation is considered as a thermodynamically reversible process.

(II) The asphaltene phase behavior can be sufficiently described by molecular size and van der Waals interactions (Ting 2003); therefore, we ignored the association term of the PC-SAFT EOS.

(III) The precipitate phase, L_2, is a liquid phase rich of asphaltene micro-aggregates, which can flow with other phases present in the porous media.

To capture the phase behavior of asphaltic crude systems using the PC-SAFT EOS, a suitable characterization scheme is required, which is described in the following section.

4.2. FLUID CHARACTERIZATION

Typical crude oils contain a very large number of hydrocarbon components which makes it impractical to consider all the components in phase behavior modeling. Therefore, for phase behavior modeling purposes, crude oils are usually characterized into a smaller number of hydrocarbon fractions or groups representing the blends of similar constituents.

Several techniques have been proposed in the literature to characterize crude oils (Katz and Firoozabadi 1978, Whitson 1983, Riazi 1997). The most widely applied procedure is based on subdividing the crude oil into different single carbon numbers (SCN) groups using their average boiling points (Whitson 1983). For asphaltic crude systems, Ting (2003) proposed a characterization scheme based on composition, saturates–aromatics–resins–asphaltenes (SARA) analysis, and gas-oil-ratio (GOR) data. His characterization method consists of characterizing the flashed gas and stock tank oil (STO) and then recombining them according to GOR to simulate the live oil. The recombined live oil is subdivided into six pseudo-components containing methane, nitrogen + carbon dioxide, light alkanes, saturates, aromatics + resins, and asphaltenes. The “saturates” pseudo-component represents normal, branched, and cyclo alkanes.

Ting also proposed a set of correlations to calculate PC-SAFT EOS parameters for saturates and aromatic + resins pseudo-components based on their average molecular weights, *MW* (Table 4-1). He lumped the aromatics and resins into a single pseudo component, which is characterized by linearly weighting the parameters of ploy-nuclear-

aromatic and benzene derivatives components with aromaticity parameter, γ, as the weighting factor.

Table 4-1: PC-SAFT parameter correlations as proposed by Ting (2003)

Saturates pseudo-component:

$$m = 0.253MW + 0.9263 \tag{4.1}$$

$$\sigma = \frac{1}{m}\left[0.1037MW + 2.7985\right] \tag{4.2}$$

$$\varepsilon / \kappa = 32.81\ln\left(MW\right) + 80.398 \tag{4.3}$$

Aromatics + Resins pseudo-component:

$$m = \gamma\left(0.0201MW + 0.7860\right) + \left(1-\gamma\right)\left(0.0139MW + 1.2988\right) \tag{4.4}$$

$$\sigma = \frac{1}{m}\left[\gamma\left(0.0782MW + 2.466\right) + \left(1-\gamma\right)\left(0.0597MW + 4.2015\right)\right] \tag{4.5}$$

$$\varepsilon / \kappa = \gamma\left(40.65\ln\left(MW\right) + 112.4\right) + \left(1-\gamma\right)\left(119.41\ln\left(MW\right) - 230.21\right) \tag{4.6}$$

Gonzalez (2008) proposed a new set of correlations for estimating the pure-component parameters of saturates and aromatic + resins pseudo-components (Table 4-2). Panuganti *et al.* (2012) extended Ting's characterization method by characterizing the gas phase as a seven component mixture containing N_2, CO_2, H_2S, C_1, C_2, C_3, and heavy gas (i.e. C_4+ components) and the liquid phase into saturates, aromatics + resins, and asphaltenes. They reported that a single set of component parameters, obtained with the proposed characterization method, can sufficiently describe the phase behavior of asphaltene precipitation at various gas injection amounts.

Table 4-2: PC-SAFT parameter correlations as proposed by Gonzalez (2008)

Saturates pseudo-component:

$$m = 0.0257MW + 0.844 \tag{4.7}$$

$$\sigma = 4.047 - 4.8013\ln\left(MW\right)/MW \tag{4.8}$$

$$\ln\left(\varepsilon/\kappa\right) = 5.5769 - 9.523/MW,\ \left[K\right] \tag{4.9}$$

Aromatics + Resins pseudo-component:

$$m = \left(1-\gamma\right)\left(0.0223MW + 0.751\right) + \gamma\left(0.0101MW + 1.7296\right) \tag{4.10}$$

$$\sigma = \left(1-\gamma\right)\left(4.1377 - 38.1483/MW\right) + \gamma\left(4.6169 - 93.98/MW\right) \tag{4.11}$$

$$\varepsilon/\kappa = \left(1-\gamma\right)\left(0.00436MW + 283.93\right) + \gamma\left(508 - 234100/MW^{1.5}\right) \tag{4.12}$$

4.3. PHASE IDENTIFICATION

The compositional simulation of a multiphase system requires a phase identification algorithm capable of consistently identifying the phases that appear or disappear during phase split calculations. Fluid phase properties, such as capillary pressures and relative permeabilities, are modeled according to the identity of the phases existing in gridblocks. For asphaltene precipitation simulation, it is also required to identify the asphaltene-rich phase at which the aggregation and consequently the deposition of asphaltene particles can happen.

The method implemented with this research is similar to the Perschke's algorithm (Perschke 1988) for three-phase mixtures. We changed this algorithm to include an asphaltene-rich phase, instead of a second-liquid hydrocarbon phase considered in Perschke's algorithm.

The algorithm implemented by Perschke for the phase identification in UTCOMP consists of two main parts: (1) phase classification and (2) phase tracking. The phase classification is a process of classifying a phase as oil, gas, or second liquid at the initial condition of the reservoir or when a new phase emerges during flash calculations. After the phases have been classified, the phase tracking is applied to consistently label the phases during the simulation. Perschke used the combination of mass density and phase composition for the phase classification procedure. For phase tracking, however, he applied only phase composition.

At the initial condition of the reservoir, the phase equilibrium calculations are employed to determine the number and composition of the phases initially present. The phase classification is then applied to label the phases resulting from the phase split calculations. For three hydrocarbon phase mixtures, Perschke assumed that the phase with the largest composition of the heaviest hydrocarbon component is the oil phase. Of the remaining two phases, the denser phase is labeled as the second-liquid phase and the other one is the vapor phase. For two-phase mixtures, the same labeling criterion is used for the oleic phase, if an oil phase has been specified. The other phase is labeled based on its mass density as either a gas or second liquid phase. If the mass density is less than a threshold value, the phase is labeled as a gas phase. Otherwise, it is considered as a second liquid phase. The single-phase mixtures at initial conditions are labeled by the user based on the experimental phase behavior data.

After the phases have been classified, they are tracked and labeled during the simulation such that the composition values of a selected component at the current time-step are closest to the values at the previous time-step. If a new phase appears during the simulation, it is labeled by the phase classification method.

Perschke's algorithm for the phase classification is modified in this research considering the possibilities of forming oil, gas, oil/gas, oil/asphaltene-rich phase, and oil/gas/asphaltene-rich phase systems. In these systems, the phase with the highest mole fraction of the heaviest hydrocarbon component is not always the oil phase. If an asphaltene-rich phase appears, it has the highest composition of the heaviest component (i.e., asphaltene) among other phases.

Similar to Perschke's algorithm, the liquid phases are differentiated from the gas phase by comparing the phase mass density with a threshold value. When two liquid phases are recognized to exist at equilibrium (whether it is LLE or VLLE), the one with the highest composition of the asphaltene component is labeled as the asphaltene-rich phase and the other one is considered as the oil phase. For two-phase mixtures at the VLE state, the liquid phase is labeled as oil. Based on the asphaltene precipitation envelope, we assumed that the combination of gas/asphaltene-rich phase in not possible to form.

4.4. DYNAMICS OF ASPHALTENE PARTICLES IN POROUS MEDIA

As explained in Chapter 2, asphaltene particles can deposit in the porous medium in two different modes (Minssieux 1997):

(I) adsorption onto the rock surface,

(II) mechanical entrapment.

Therefore, it is assumed that the total precipitated asphaltenes is composed of three parts (Nghiem 1999):

(I) moles of asphaltene component that adsorb onto active sites of the reservoir rock surface, N_{ads},

(II) moles of asphaltene component that deposit on the rock through mechanical entrapment, N_{me},

(III) moles of asphaltene component that remain suspended in the bulk and can flow with other phases, N_{sus}.

From the material balance, we have

$$N_{prec} = N_{ads} + N_{me} + N_{sus}\,, \tag{4.13}$$

where N_{prec} accounts for the total moles of precipitated asphaltenes in a gridblock. The procedure used in this research to calculate the three parts of the precipitated solids in Eq. (4.13) is adopted from Nghiem (1999) and described in the following sections.

4.4.1. Adsorption

In order to predict the amount of asphaltenes adsorbed to the rock surface, the Langmuir adsorption isotherm is used. The basic assumption in the Langmuir model is that the process occurs by monolayer adsorption on a homogeneous surface. The Langmuir equation can be expressed as follows:

$$w_{ads} = \frac{w_{ads,\max} K_a C_{sus}}{K_a C_{sus} + 1}, \tag{4.14}$$

where,

w_{ads} = the mass of asphaltene particles adsorbed per mass of rock [mg/g],

$w_{ads,max}$ = the maximum amount of asphaltene particles adsorbed per mass of rock [mg/g],

K_a = Langmuir equilibrium adsorption constant [g/μg],

C_{sus} = the concentration of the suspended asphaltenes in the oil phase [μg/g].

The concentration of suspended asphaltenes in the oil phase, C_{sus}, is calculated as

$$C_{sus} = \frac{N_{sus} M_{asph}}{N_o M_o} \times 10^6, \tag{4.15}$$

where

M_{asph} = the molecular weight of the asphaltene

M_o = the molecular weight of the oil phase

N_o = the number of moles of the oil

We assumed that only asphaltene components can be adsorbed on the rock surface; therefore the molecular weight of the deposited solid is assumed to be equal to the molecular weight of the asphaltene component. The number of moles of adsorbed asphaltenes per unit bulk volume, N_{abs}, is calculated through the equation

$$N_{ads} = \frac{(1-\phi)\tilde{\rho}_R w_{ads}}{M_{asph}}, \tag{4.16}$$

where $\tilde{\rho}_R$ is the rock mass density [kg/m^3].

4.4.2. Mechanical entrapment

The moles of deposited asphaltenes through mechanical entrapment are determined by solving the differential Eq. (2.42). The discrete form of this equation is as follows:

$$\sigma_{me}{}^{n+1} = \sigma_{me}{}^{n} + \Delta t\left[(\alpha_0 + \alpha_1\sigma_{me})|u_o|\hat{C}_{sus}\right]^n. \tag{4.17}$$

The volume of the deposited asphaltenes because of mechanical entrapment per unit initial pore volume, σ_{me}, is given by

$$\sigma_{me} = \frac{N_{me}v_s}{\phi_0}, \tag{4.18}$$

where v_s is the solid molar volume and ϕ_0 is the initial porosity. The volume concentration of suspended asphaltenes in the oil phase is given by

$$\hat{C}_{sus} = \frac{N_{sus}v_s}{(N_o/\rho_o)}. \tag{4.19}$$

Eqs. (4.13)-(4.19) are solved together to determine N_{ads}, N_{me}, and N_{sus}.

We assumed that the suspended solids have enough time from one time-step to the next to reach a thermodynamic equilibrium state with other hydrocarbons; therefore, they are added to other components present in a gridblock to calculate the overall mole fraction in the next time-step.

4.4.3. Plugging

Reis and Acock (1994) showed that the permeability reduction caused by the asphaltene deposition can be represented by a power-law model given by

$$k = c\phi^b, \tag{4.20}$$

where the exponent b ranges from 3 to 7. Kohse and Nghiem (2004) used the power-law model to define a resistance factor, R_f, as the ratio of the original permeability, k_0, to the instantaneous permeability, k:

$$R_f = \frac{k_0}{k} = \left(\frac{\phi_0}{\phi}\right)^b. \tag{4.21}$$

The instantaneous porosity, ϕ, is obtained by subtracting the volume of deposited asphaltenes from the initial porosity:

$$\phi = \phi_0 - \sigma_d, \tag{4.22}$$

where σ_d is defined as the volume of the deposited asphaltenes per unit volume of a gridblock. The power-law model, Eq. (4.21), is used in this research to model the permeability reduction because of asphaltene deposition.

4.4.4. Wettability alteration

Wettability is a key factor in determining the degree of the oil recovery as it determines the reservoir fluid distribution, which controls relative permeability values. Asphaltenes can act as a wettability modifier and change the wettability of reservoir rocks from water-wet to mixed-wet or oil-wet.

In order to model the asphaltene deposition-induced wettability alteration, we adopted the existing method in the UTCHEM simulator (Delshad *et al.* 1996) for surfactant and alkali-induced wettability alteration. This model is based on interpolating the relative permeability and capillary pressure between two extreme sets of relative permeability curves defined for each wetting phase as input parameters (Anderson 2006, Goudarzi *et al.* 2012). This method was implemented in UTCOMP by Kazeminia (2013) primarily to model the wettability alteration in low salinity water injection.

During the simulation, the extreme relative permeability and capillary pressure values are calculated at each time-step and then the altered values are determined by interpolating between these two extremes, i.e. initial and final states, as follows:

$$k_{r\ell}^{altered} = \Omega_1 k_{r\ell}^{final} + \left(1-\Omega_1\right) k_{r\ell}^{initial}, \tag{4.23}$$

$$P_{cap}^{altered} = \Omega_2 P_{cap}^{final} + \left(1-\Omega_2\right) P_{cap}^{initial}, \tag{4.24}$$

where Ω_1 and Ω_2 represent the process dependent interpolation factors, $k_{r\ell}$ is the relative permeability of phase ℓ, and P_{cap} is the capillary pressure. The interpolating parameter is usually defined as a function of adsorbed chemicals or organic species on the rock surface.

Assuming that the adsorbed asphaltenes form a monolayer coating on the rock surface, we can correlate the surface of the rock coated by asphaltenes to the mass of adsorbed solids. Therefore, the interpolating parameters can be defined as follows

$$\Omega_1 = \Omega_2 = \frac{S_{coated}}{S_{coated,\max}} = \frac{w_{ads}}{w_{ads,\max}}, \tag{4.25}$$

where S_{coated} represents the area of the rock surface which is coated by adsorbed asphaltenes and $S_{coated,max}$ is the maximum surface of the rock, which can be coated by asphaltenes. When the amount of adsorbed asphaltenes reaches its maximum value, i.e. $w_{ads,max}$, maximum wettability alteration occurs.

4.4.5. Oil viscosity

To account for the effect of asphaltene precipitation on the viscosity of the oil phase, we used the Gillespie (1983) model, which is proposed to correlate the viscosity of the suspensions to the volume fraction of the solid particles:

$$\eta_r = \frac{1 + \Phi_{eff} / 2}{\left(1 - \Phi_{eff}\right)^2}, \tag{4.26}$$

where η_r is defined as the ratio of the dynamic viscosity of the suspension to the viscosity of the oil and Φ_{eff} is the effective volume fraction of the solid particles (i.e. equal to $\hat{C}_{sus}$) in oil phase. We assumed that the dynamic viscosity value of the asphaltene-rich phase is equal to those of the bulk phase.

4.5. SIMULATION CASE STUDIES

Three simulation case studies were set up to investigate the asphaltene precipitation under gas injection in porous media. Two different asphaltic crude samples (i.e., fluids ‘A’ and ‘B’) and three gases (i.e., CO_2, N_2, and a lean gas) were used in the simulations.

4.5.1. Case study 1: CO_2 injection

A gas injection case study was set up to study the effect of CO_2 injection on asphaltene precipitation from an asphaltic reservoir fluid (oil 'A') in a two-dimensional reservoir. The sample fluid is a live oil taken from a reservoir, which was known to have asphaltene precipitation problem during primary production (Jamaluddin *et al.* 2002). The fluid properties and compositions are summarized in Table 4-3 and Table 4-4.

Table 4-3: Composition of reservoir fluid 'A' (Jamaluddin *et al.* 2002)

		Mole %	
Components	Flashed liquid	Flashed liquid	Recombined oil
Nitrogen	0.00	0.77	0.49
Carbon dioxide	0.00	17.67	11.37
Hydrogen sulfide	0.00	5.00	3.22
Methane	0.00	42.49	27.36
Ethane	0.14	14.54	9.41
Propane	0.66	10.05	6.70
i-butane	0.23	1.13	0.81
n-butane	1.48	4.11	3.17
i-pentane	1.17	1.26	1.22
n-pentane	2.71	1.57	1.98
Pseudo-C_6H_{14}	5.32	0.92	2.49
Pseudo-C_7H_{16}	7.38	0.37	2.87
Pseudo-C_8H_{18}	8.62	0.10	3.14
Pseudo-C_9H_{20}	7.67	0.02	2.74
Pseudo-$C_{10}H_{22}$	6.49	0.01	2.32
Pseudo-$C_{11}H_{24}$	5.31	0.01	1.90
C_{12}+	58.82	0.01	18.82
Total	100.00	100.00	100.00
MW	229.21	31.69	102.04
Mole ratio	0.3562	0.6438	
Molar mass: C_{12}+	337.98	167.11	337.94
Density (g/cc): C_{12}+	0.906		0.906

Table 4-4: The properties of oil 'A' (Jamaluddin *et al.* 2002)

GOR (scf/stb)	900
Oil API gravity	32
Wax content (%,w/w)	12
Cloud point (°F)	72
SARA contents (ASTM D4124-97):	
Saturates (wt %)	57.4
Aromatics (wt %)	30.8
Resins (wt %)	10.4
Asphaltenes (n-pentane insoluble) (wt %)	1.4

Jamaluddin *et al.* (2002) carried out an experimental study to evaluate the risk of asphaltene precipitation from fluid 'A' under N_2 injection. Later on, Gonzalez *et al.* (2005, 2008) characterized this oil as a recombined oil containing seven pseudo-components (Table 4-5). They described the separator gas as a four-component fluid (i.e. N_2, CO_2, C_1, and light n-alkanes) and recombined it with the stock tank oil which was characterized by three subfractions comprising saturates, aromatics + resins, and asphaltenes. They used PC-SAFT EOS to model the asphaltene precipitation from this system. Binary interaction parameters used for this mixture are presented in Table 4-6 (Gonzalez *et al.* 2008).

The asphaltene precipitation envelope for this crude oil was generated by Gonzalez *et al.* (2008) using the PC-SAFT EOS. Gonzalez *et al.* (2008) modeled the asphaltene precipitation as a LLE state. They found that the experimental data are well-correlated by the PC-SAFT EOS model. The APE for oil 'A' is regenerated in this research (Figure 4-2) assuming that the precipitation occurs in the LLE state between the upper onset and bubble point region and VLLE state between the bubble point and lower onset pressure.

Table 4-5: PC-SAFT characterization of oil ‘A’ (Gonzalez *et al.* 2008)

Component	Overall mole fraction	MW	*m*	σ	ε/k
N_2	0.004950	28.01	1.2053	3.3130	90.96
CO_2	0.145830	44.01	2.0729	2.7852	169.21
C_1	0.273340	16.04	1.0000	3.7039	150.03
Light	0.219170	44.60	2.0546	3.6130	204.96
Saturates	0.238530	207.6	5.9670	3.9320	254.05
Aromatics+Resins	0.117500	270.5	6.4730	3.8700	332.52
Asphaltene	0.000676	1700	29.500	4.3000	392.56

Table 4-6: Binary interaction parameters for oil ‘A’ (Gonzalez *et al.* 2008)

Component	N_2	CO_2	C_1	Light	Saturates	Aromatics + Resins	Asphaltenes
N_2	0.000	0.000	0.030	0.060	0.120	0.120	0.250
CO_2		0.000	0.050	0.010	0.120	0.110	0.110
C_1			0.000	0.000	0.030	0.029	0.029
Light				0.000	0.010	0.010	0.010
Saturates					0.000	0.007	0.007
Aromatics + Resins						0.000	0.000
Asphaltene							0.000

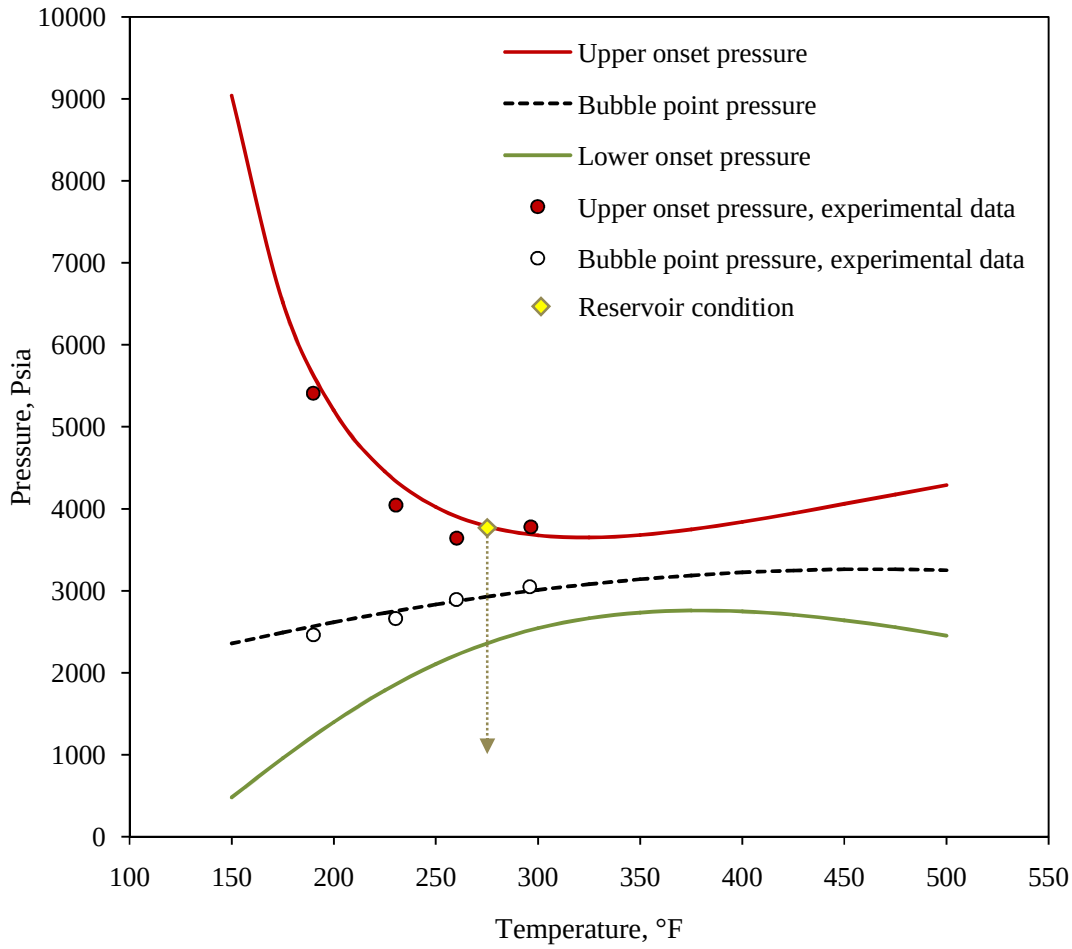

Figure 4-2: The APE for crude 'A' generated using PC-SAFT EOS. Same results as Gonzalez *et al.* (2008). The experimental data are from Jamaluddin *et al.* (2002).

The effect of CO_2 addition on the asphaltene precipitation boundaries is plotted in Figure 4-3 (same results as Gonzalez *et al.*, 2008). As is shown, CO_2 addition enlarges the APE and consequently increases the asphaltene precipitation risk. However, there is a crossover point (i.e., around 200 °F) below which the addition of CO_2 increases the asphaltene stability in the mixture compared to the original oil.

Gonzalez *et al.* (2008) explained this exceptional behavior of CO_2 using the concept of solubility parameter. They stated that below the crossover temperature the CO_2 solubility parameter is larger than the solubility parameter of the crude oil and therefore, CO_2 injection into the oil can increase the solubility of asphaltenes in the mixture. On the contrary, CO_2 injection above the crossover temperature reduces the solubility parameter of the oil and thus, increases the asphaltene precipitation risk.

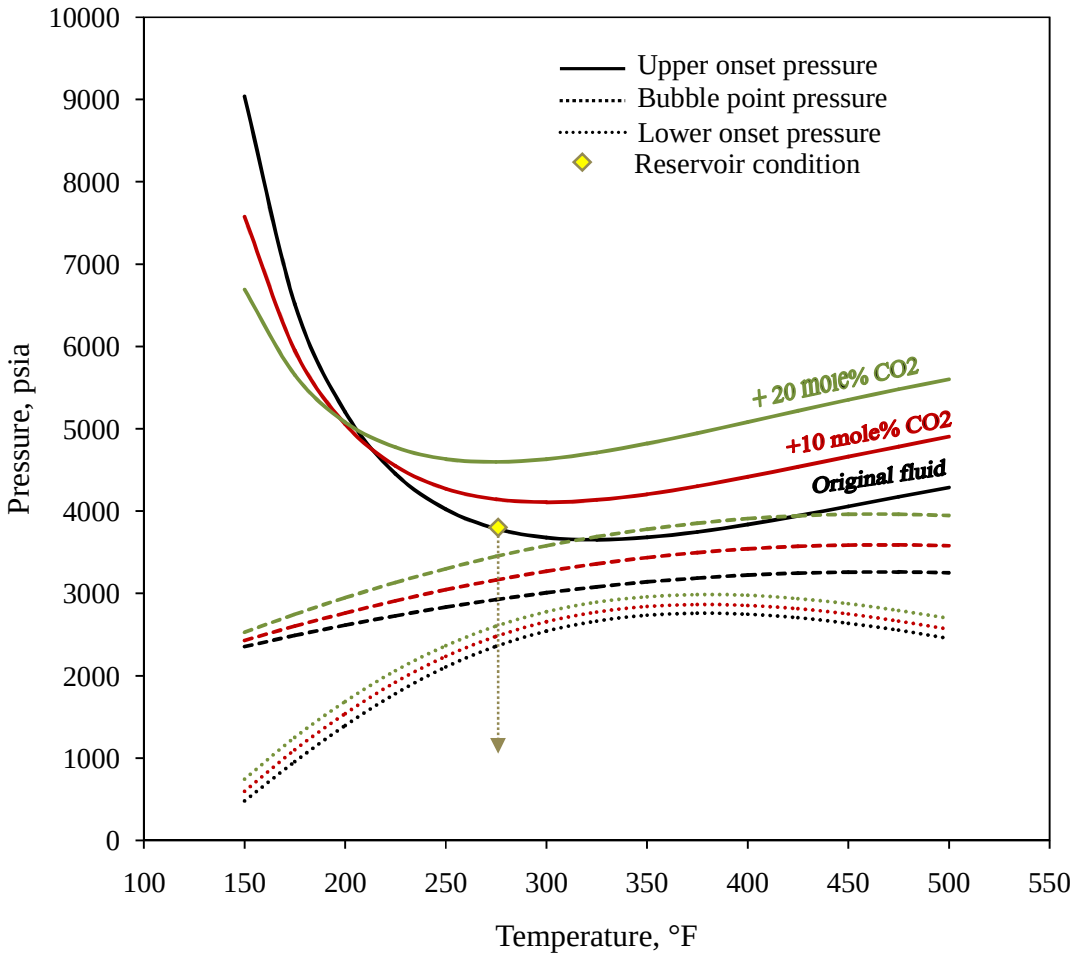

Figure 4-3: The APE of oil 'A' after addition of different amounts of CO_2. Same results as Gonzalez *et al.* (2008).

Figure 4-4 represents a P-x diagram illustrating CO_2-oil mixture phase boundaries at reservoir temperature (i.e. 275 °F). Results indicate that CO_2 injection at this temperature promotes asphaltene precipitation in the reservoir.

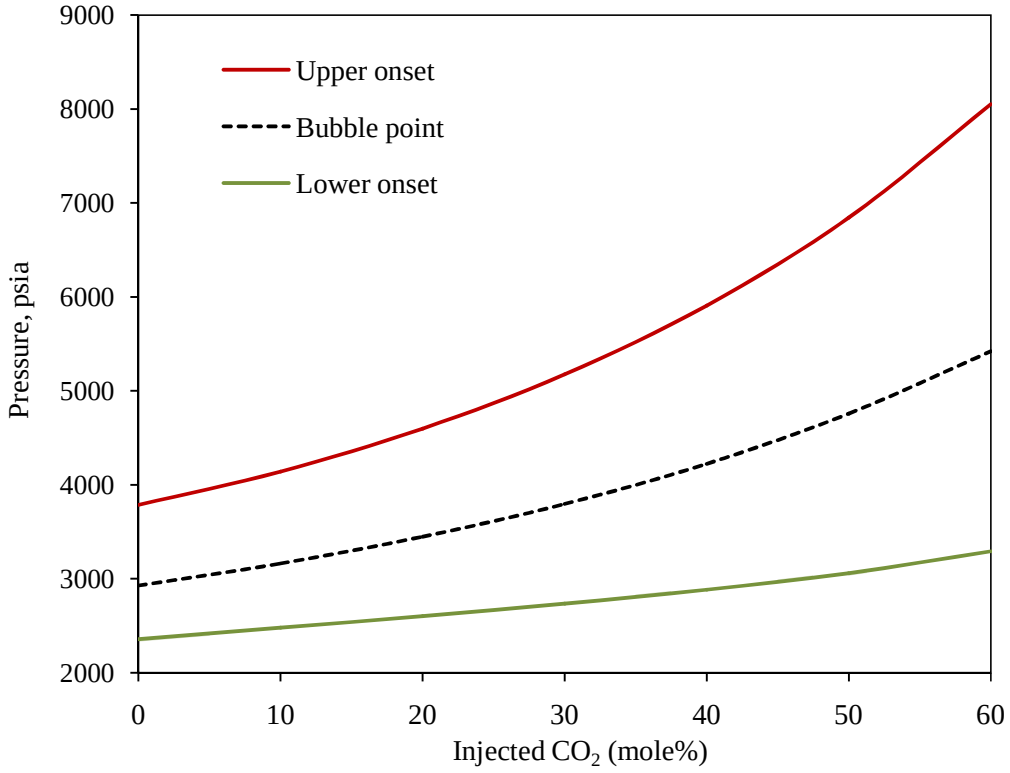

Figure 4-4: P-x diagram for CO_2 addition to oil 'A' at 275 °F.

The percentage of precipitated asphaltenes with respect to the original asphaltene content of the oil is illustrated in Figure 4-5. Three key points are evident in this figure:

(I) As CO_2 increases, the reservoir oil is prone to asphaltene precipitation over a wider pressure range.

(I) The maximum amount of asphaltene precipitation occurs at the bubble-point.

(II) The maximum amount of asphaltene precipitation increases with the amount of CO_2 injected.

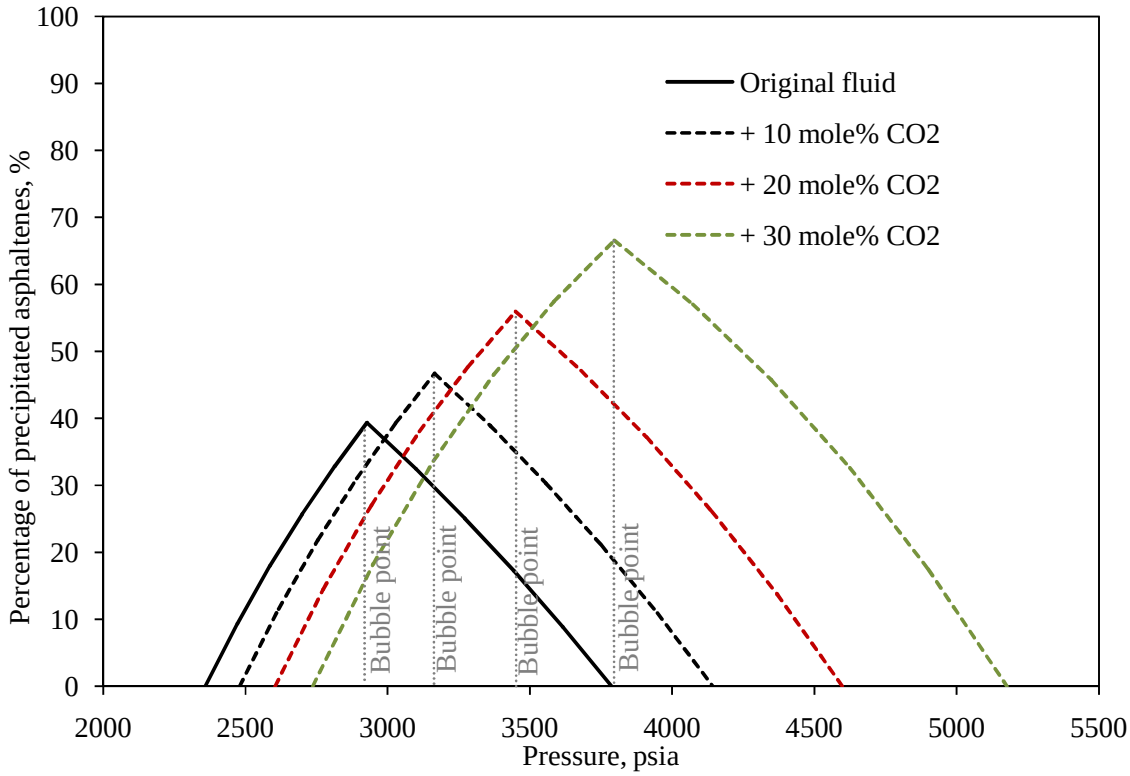

Figure 4-5: The percentage of asphaltenes precipitated under pressure depletion at 275 °F for different CO_2 amounts.

Oil 'A' was used to set up a simulation case in order to investigate asphaltene precipitation in a reservoir under gas injection. The parameters for the deposition model and the reservoir properties are summarized in Table 4-7 and Table 4-8.

Table 4-7: Parameters for the deposition model for case study 1

Deposition model constants		Reference
Maximum asphaltene adsorption, $w_{ads,max}$	0.1 [mg/g rock]	(Nghiem 1999)
Ratio of adsorption/desorption reaction, K_a	2500 [g/μg]	(Almehaideb 2004)
α_0	1000 [1/m]	(Nghiem 1999)
α_1	20 [1/m]	(Nghiem 1999)
Rock density, $\tilde{\rho}_R$	2650 [kg/m^3]	

Table 4-8: Reservoir properties for case study 1

Reservoir fluid	Oil 'A'
Injected gas	CO_2
Number of gridblocks	40×40
Constant bottomhole injection pressure	4800 psia
Constant bottomhole production pressure	3000 psia
Initial reservoir pressure	3800 psia
Reservoir temperature	275 °F
Initial water saturation	0.25
Initial porosity	0.25
Initial homogeneous permeability in x and y directions	100 mD
Relative permeability model	Corey's model
Constant gridblock size in x and y directions	25 ft

Figure 4-6 and Figure 4-7 show different snapshots of: (i) the dimensionless volume of deposited asphaltenes, σ_d, (left column) profile and (ii) the gas saturation profile (right column) throughout one areal quarter of a five spot injection pattern. A logarithmic color-map scheme is used to show the asphaltene deposition profile in these figures. As expected from the APE, the asphlatene precipitation and therefore deposition starts at both injection and production wells. The damaged area grows with time in the reservoir domain. The radius of the damaged area around the production well becomes constant at some point, which is around 0.1 PV of gas injection for this case.

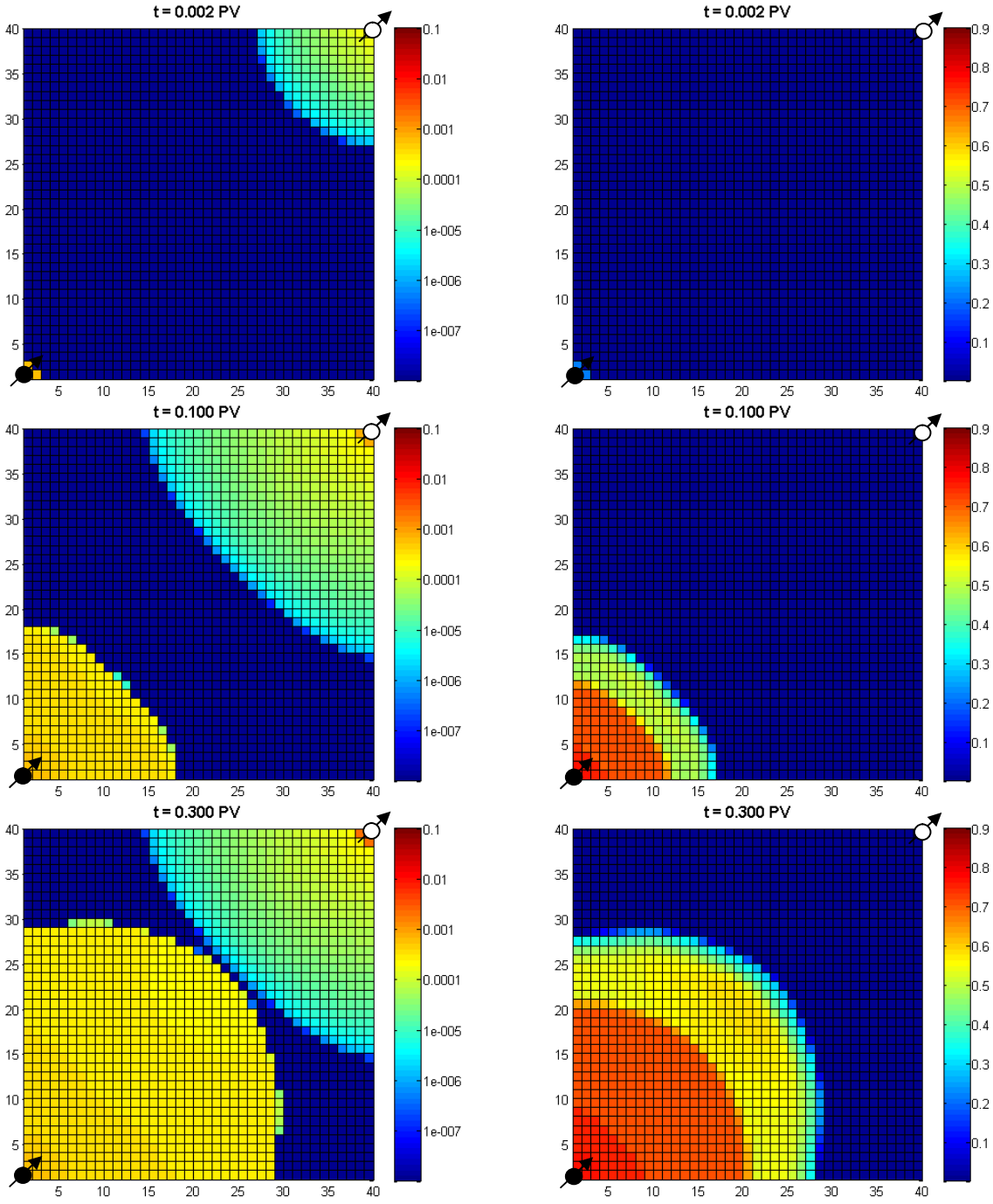

Figure 4-6: Asphaltene deposition and gas saturation profiles for case study 1 at 0.002, 0.1, and 0.3 PV gas injection. Left: the dimensionless volume of deposited asphaltenes σ_d ; right: gas saturation

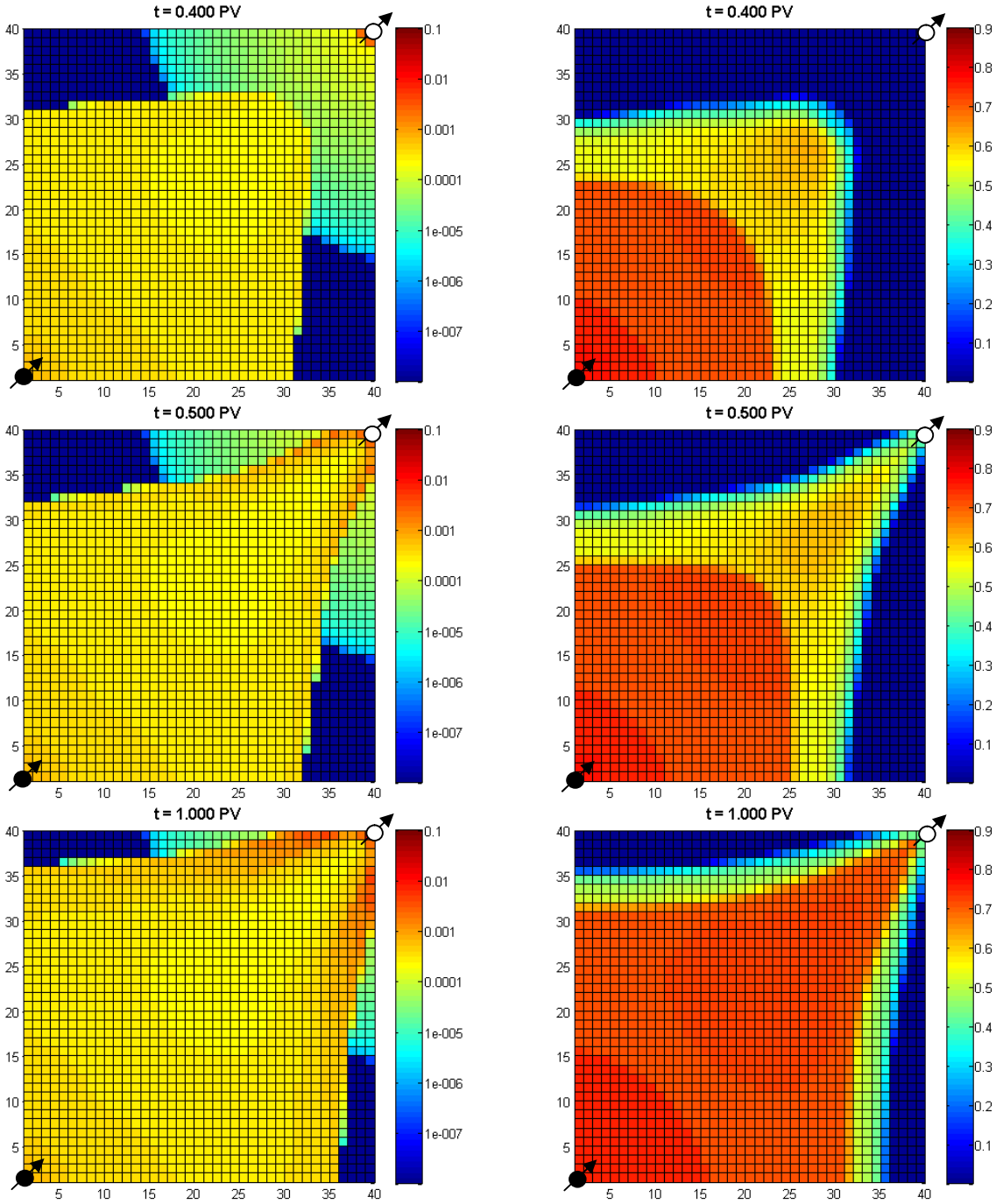

Figure 4-7: Asphaltene deposition and gas saturation profiles for case study 1 at 0.4, 0.5, and 1.0 PV gas injection. Left: the dimensionless volume of deposited asphaltenes, σ_d; right: gas saturation

The consequences of asphaltene deposition in porous media are (i) the pore throat plugging, which results in a reduction in the absolute permeability values and (ii) the wettability alteration, which changes the relative permeability of the formation fluids. To show the effect of pore throat plugging on the absolute permeability, the permeability values of three gridblocks near the production well are plotted in Figure 4-8 versus pore volume of the injected gas. The positions of the target gridblocks in *x* and *y* directions are (40, 37), (40, 38), and (40, 39), which are represented in Figure 4-9 by the color code.

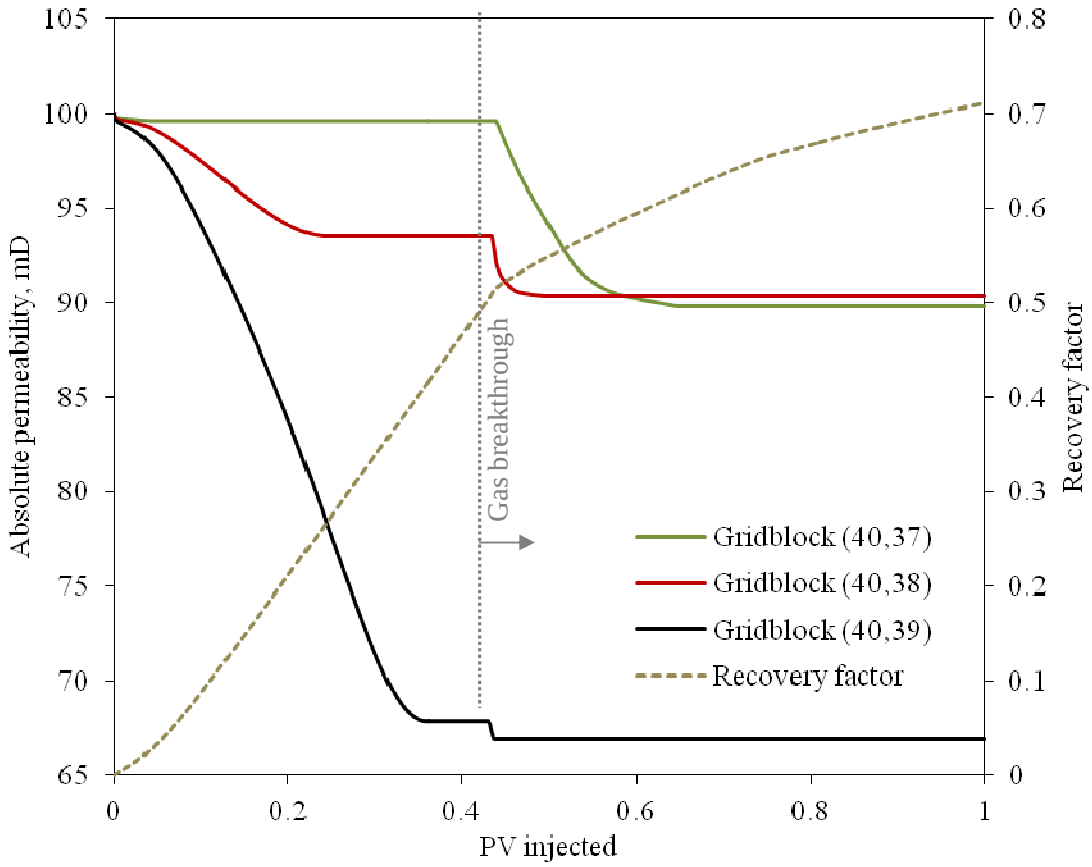

Figure 4-8: Permeability reduction curves for three gridblocks around the production well. Points (40, 37), (40, 38), and (40, 39) represent the position of the target girdblocks with respect to the injection well.

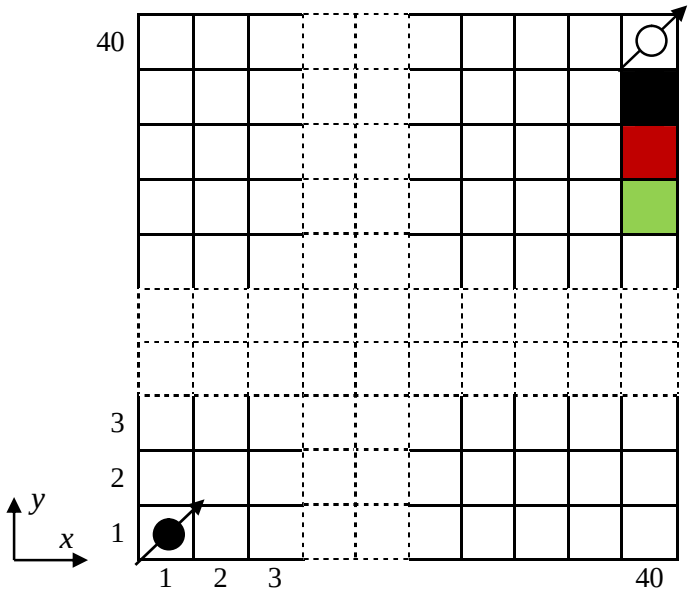

Figure 4-9: The positions of the gridblocks in Figure 4-8.

Figure 4-8 reveals two contributions to the permeability reduction process: (i) pressure depletion (mainly around the production well) and (ii) mixing of oil with the injection gas at the arrival of the gas front to the target gridlocks. When the fluid front reaches the target gridblocks, contacting the reservoir fluid with injected gas augments asphaltene precipitation and leads to a further permeability reduction. The fluid front reaches these gridblocks around the gas breakthrough time. Figure 4-8 also indicates that for the gridblocks neighboring the production well, the role of pressure depletion in the deposition-induced permeability reduction is larger than that of the gas injection. However, as we move further away from the production well, the contribution of the pressure depletion diminishes.

The consequence of the permeability reduction around the production well is decline in the ability of the production well to produce oil. To show the effect of plugging on oil production, we have plotted the productivity index, i.e. defined as the ratio of the oil flow rate to the pressure drawdown, versus the pore volume of the gas injected (Figure 4-10) for two simulation situations: (i) considering the asphaltene deposition, (ii) ignoring the asphaltene deposition. Figure 4-10 shows considerable decline in the productivity index, PI, curve in the simulation in which the asphaltene deposition is considered. The maximum difference between these two curves occurs around the breakthrough time. Before gas breakthrough, the slope of the PI curve considering asphaltene deposition is negative, which indicates the significant effect of permeability reduction on production rate.

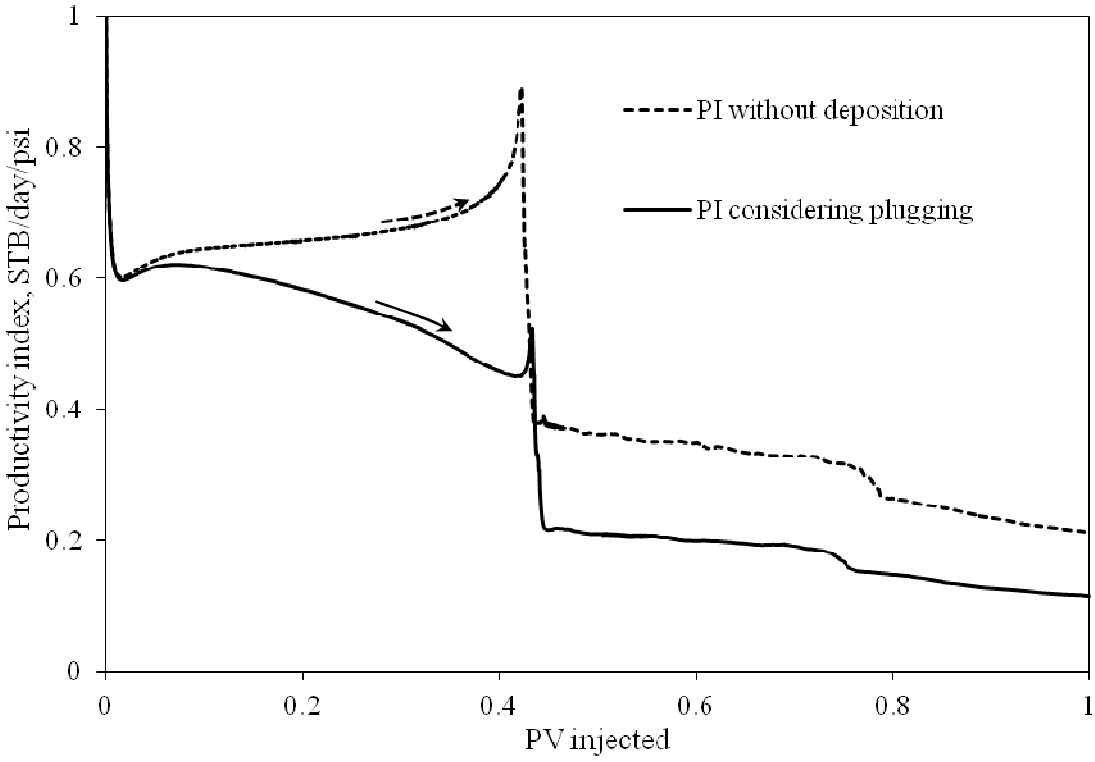

Figure 4-10: Productivity index versus the PV of CO_2 injected

Pore throat plugging becomes insignificant in the gridblocks far from the production well. However, as we mentioned earlier, plugging is not the only consequence of the asphaltene deposition. Even a small amount of asphaltene adsorption can influence the wettability of the rock and therefore the relative permeabilities. The wettability alteration is modeled by interpolating the relative permeability and capillary pressure between two extreme sets of relative permability curves during the simulation. The initial and final characteristics of the relative permeability sets are presented in Table 4-9 and Figure 4-11.

Table 4-9: Relative permeability parameters

	Initial state		Final state	
	Oil	Water	Oil	Water
Residual saturation	0.2	0.25	0.25	0.25
Relative permeability endpoint	0.7	0.21	0.6	0.3
Relative permeability exponent	2.5	1.5	3.5	2

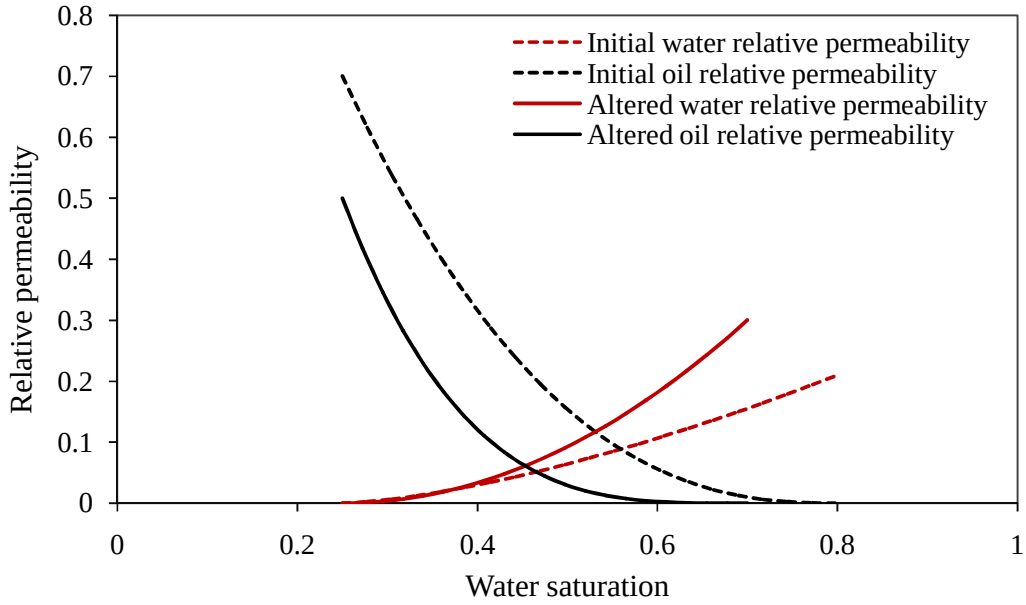

Figure 4-11: Initial and final characteristics of relative permeability

We assumed that asphaltene deposition can change the wettability of the formation from a water-wet state (i.e., initial state) toward a mixed-wet condition (i.e., final state). The effect of wettability alteration on the PI curve is illustrated in Figure 4-12. At early production times, considering the wettability alteration caused a decline in the productivity index. However, there is a crossover point above which the wettability alteration diminishes the effect of plugging. In general, wettability alteration flattens the PI curve slightly. The reason is the reduction in the mobility of the oleic-phase. As stated earlier, plugging because of mechanical entrapment is a flow-dependent process. Decreasing the oil rate lessens mechanical entrapment and therefore decreases pore throat plugging.

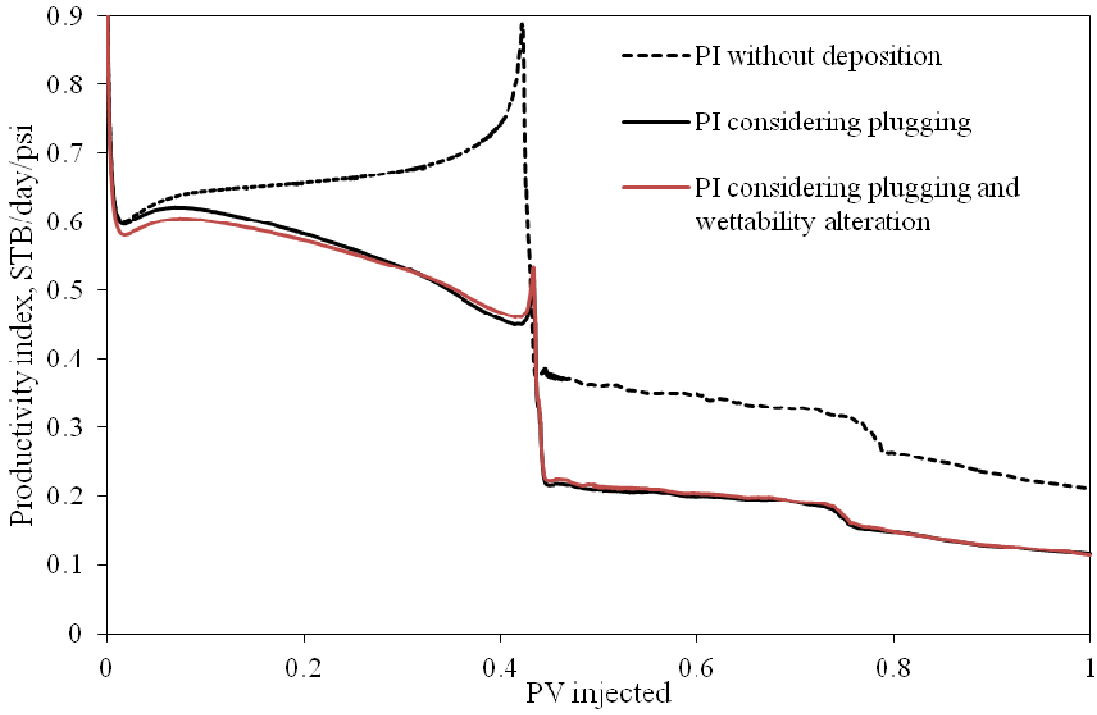

Figure 4-12: Productivity index curves for case study 1.

4.5.2. Case study 2: N_2 injection

Another simulation case study was set up by displacing oil 'A' by N_2 at the same reservoir conditions presented in Table 4-8. The effect of 10 mole percent N_2 injection on the APE is illustrated in Figure 4-13. Comparing this figure with Figure 4-3 for 10 mole% CO_2, the effect of N_2 on asphaltene precipitation boundaries is more severe than that of CO_2.

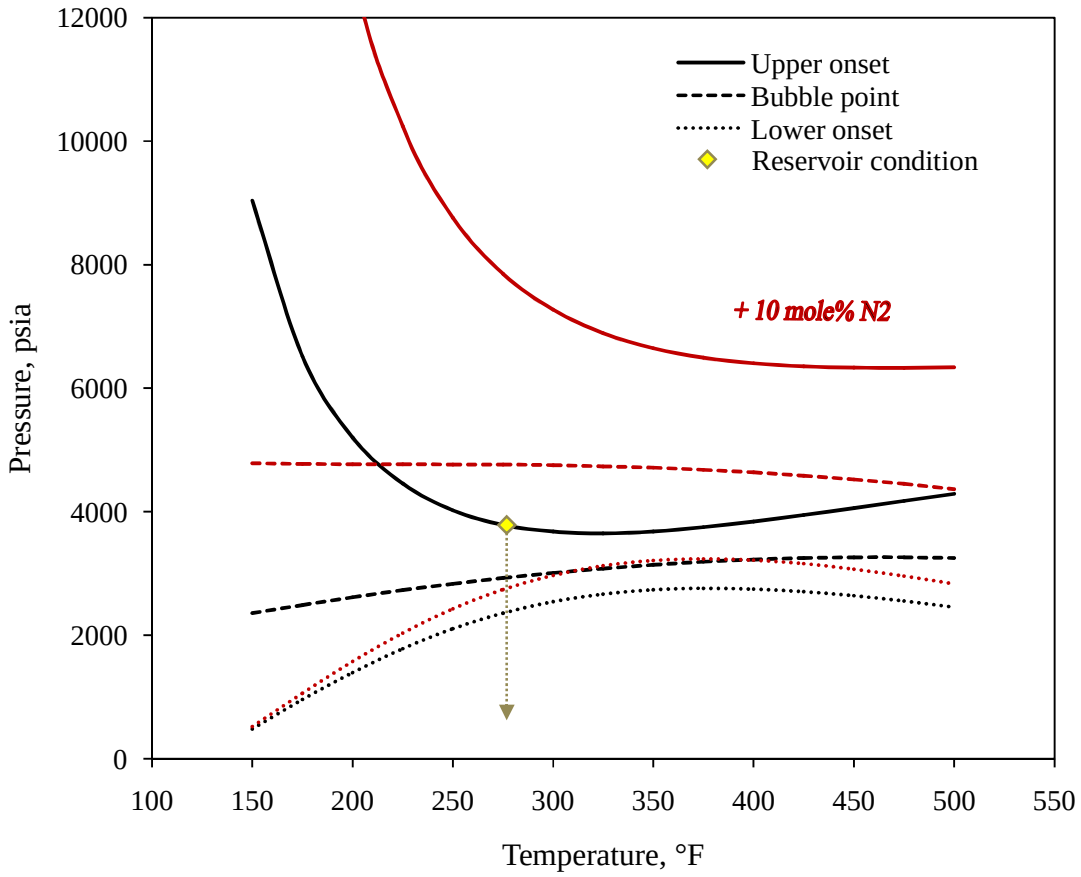

Figure 4-13: Representation of the effect of 10 mole% N_2 addition to oil 'A' on the APE.

Figure 4-14 represents the PI curves for this case study with and without considering asphaltene deposition. Comparing these results with those of the CO_2 injection, we found that while N_2 injection results in more severe effect on the APE, the effect of CO_2 injection on the PI curves is more profound. The reason is that CO_2 is generally more miscible with hydrocarbons and therefore the breakthrough time in CO_2 injection is longer than in the N_2 injection case study. Since the maximum permeability reduction occurs before the breakthrough time and there is more time for case 1 with CO_2 injection to reduce the permeability than case 2 with N_2 injection, asphaltene deposition in case 1 has a more severe effect on the productivity of the production well.

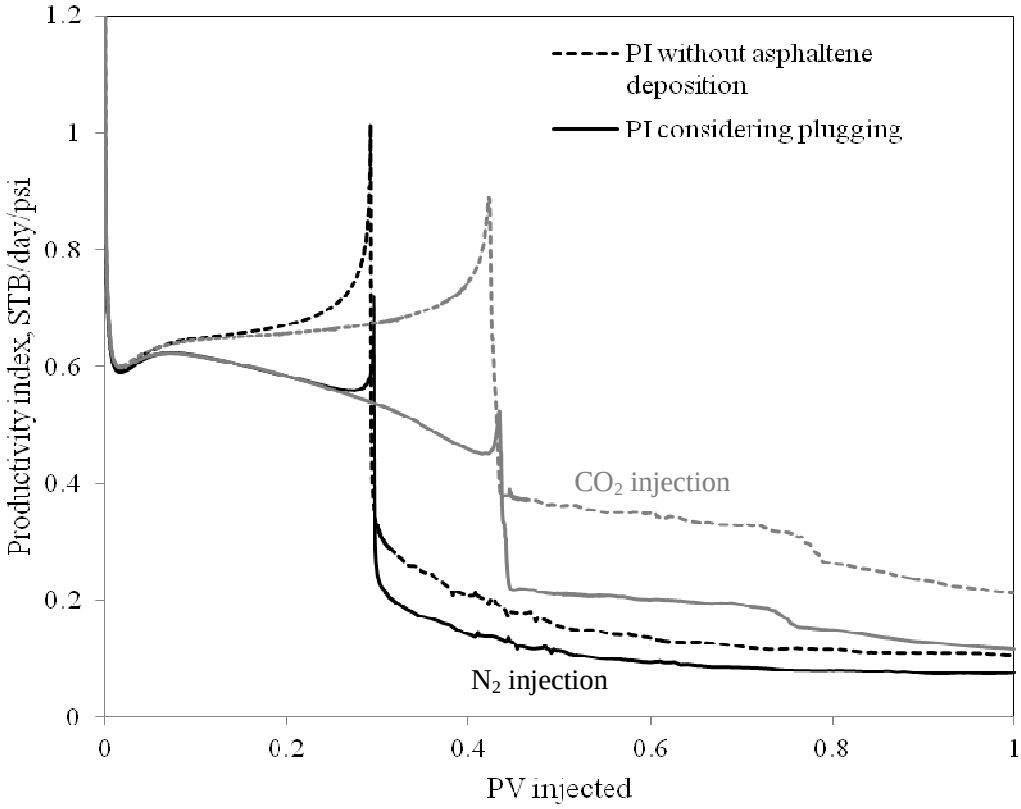

Figure 4-14: Productivity index curves for case study 1 and case study 2. Black lines show the productivity index of N_2 injection (case study 2) and gray lines represent productivity index of CO_2 injection (case study 1).

To test the effect of wettability alteration in this case study, we used the same characteristics for initial and final relative permeability curves (Table 4-9). The effect of wettability alteration on the PI curve is represented in Figure 4-15. Again, wettability alteration decreases the slope of the PI curve. In this case study, wettability alteration causes a slight lag in the gas breakthrough.

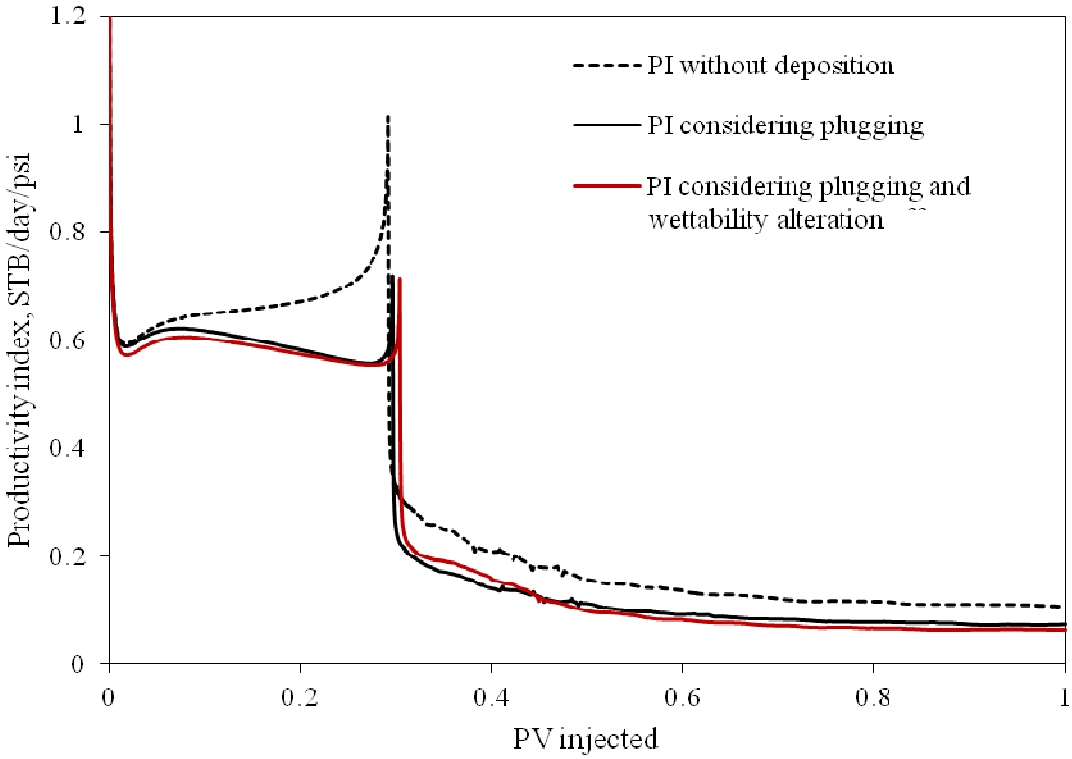

Figure 4-15: Productivity index for case study 2.

4.5.3. Case study 3: lean gas injection

The third case study injects a lean gas into a reservoir with a recombined oil taken from Panuganti *et al.* (2012). The fluid properties and characterization are described in Table 4-10 and Table 4-11. The binary interaction parameters for this system are summarized in Table 4-12.

Table 4-10: Properties of oil ‘B’ (Panuganti *et al.* 2012)

GOR(scf/stb)	798
Mw of reservoir fluid (g/mole)	96.15
Mw of flashed gas (g/mole)	28.54
Mw of STO (g/mole)	191
STO density (g/cc)	0.823
SARA contents:	
Saturates (wt %)	75.56
Aromatics (wt %)	20.08
Resins (wt %)	4.13
Asphaltenes (n-pentane insoluble) (wt %)	0.21

Table 4-11: PC-SAFT characterization of oil ‘B’ (Panuganti *et al.* 2012)

	Overall mole fraction					
Component	Oil	Injected gas	MW	*m*	σ	ε/k
N_2	0.00169	0.004	28.04	1.206	3.313	90.96
CO_2	0.02096	0.039	44.01	2.073	2.785	169.21
C_1	0.34865	0.714	16.04	1.000	3.704	150.03
C_2	0.07578	0.120	30.07	1.607	3.520	191.42
C_3	0.06042	0.072	44.10	2.002	3.618	208.11
Heavy gas	0.07560	0.051	67.12	2.750	3.750	229.32
Saturates	0.34152		176.08	5.370	3.910	250.36
Aromatics+Resins	0.07527		256.14	6.360	4.000	293.30
Asphaltene	0.00010		1700.00	37.220	4.493	413.54

Figure 4-16 represents the APE for this crude oil generated using PC-SAFT EOS. At temperatures ranging from 175 °F to 250 °F, the upper onset, bubble point, and lower onset pressure curves coincide, indicating no asphaltene precipitation risk under pressure depletion at this temperature range.

Table 4-12: Binary interaction parameters for oil ‘B’ (Panuganti *et al.* 2012)

	CO_2	C_1	C_2	C_3	Heavy gas	Saturates	Aromatics + Resins	Asphaltenes
N_2	0.000	0.030	0.040	0.060	0.075	0.140	0.158	0.160
CO_2		0.050	0.097	0.100	0.120	0.130	0.100	0.100
C_1			0.000	0.000	0.030	0.030	0.029	0.070
C_2				0.000	0.020	0.012	0.025	0.060
C_3					0.015	0.010	0.010	0.010
Heavy gas						0.005	0.012	0.010
Saturates							0.007	-0.004
Aromatics + Resins								0.000

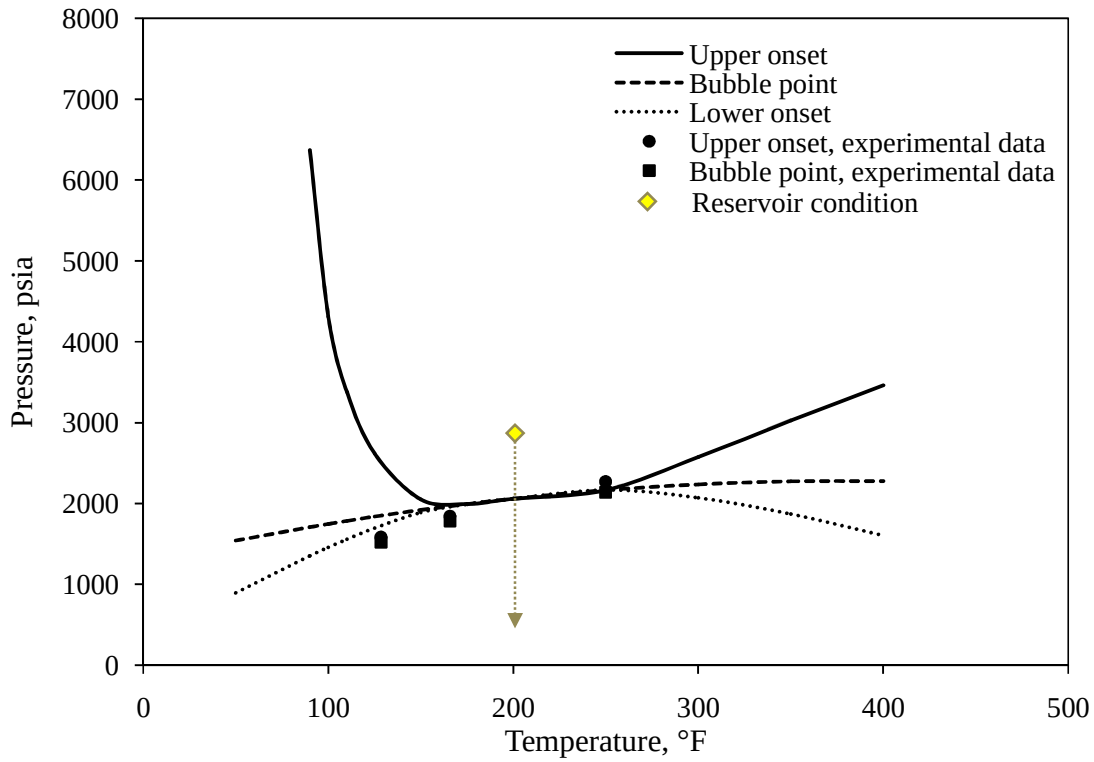

Figure 4-16: The APE for crude ‘B’ generated using PC-SAFT EOS. Same results as Panuganti *et al.* (2012). Experimental data are from Panuganti *et al.* (2012).

The effect of gas injection on the asphaltene precipitation boundaries for this crude oil is plotted in Figure 4-17. As is shown, gas injection results in a larger asphaltene instability zone. It also causes a precipitation window to appear at temperatures ranging from 175 °F to 250 °F.

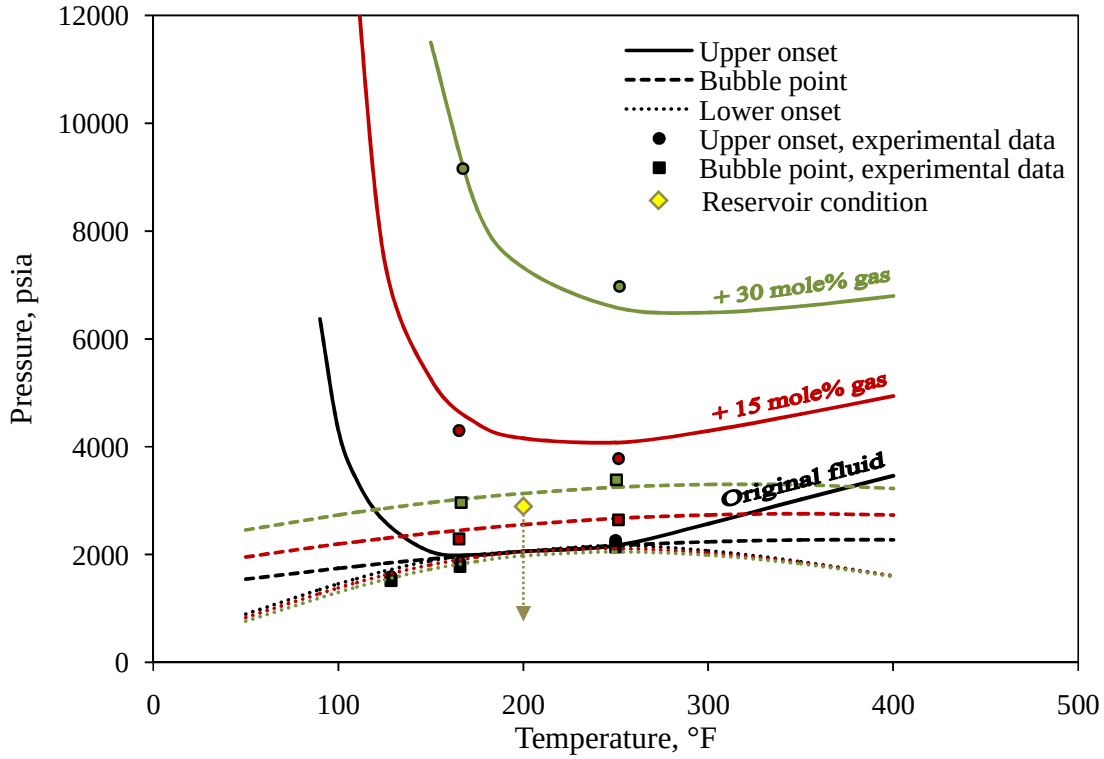

Figure 4-17: The APE of oil 'B' after addition of different amounts of lean gas. Same results as Panuganti *et al.* (2012).

A gas injection process was simulated by injecting the lean gas described in Table 4-11 to crude 'B' at 200 °F. As mentioned above, the original oil at this temperature does not have the precipitation risk under pressure depletion. A summary of the reservoir properties and conditions is provided in Table 4-13. The deposition model constants are the same as in case study 1.

Table 4-13: Reservoir properties for case study 3

Number of gridblocks	40×40
Constant bottomhole injection pressure	4000 psia
Constant bottomhole production pressure	2100 psia
Initial reservoir pressure	3000 psia
Reservoir temperature	200 °F
Initial water saturation	0.25
Initial porosity	0.25
Initial homogeneous permeability in x and y directions	100 mD
Relative permeability model	Corey's model
Constant gridblock size at x and y directions	25 ft

Figure 4-18 and Figure 4-19 represent: (i) the dimensionless volume of deposited asphaltenes, σ_d, profile (left column) and (ii) the gas saturation profile (right column). A logarithmic color-map scheme is used again to show the asphaltene deposition profile in these figures.

As expected, precipitation and deposition start only at the injection well. The maximum plugging occurs around the production well at gas breakthrough. The effect of plugging on the PI curve is illustrated in Figure 4-20. As is shown, the PI curve considering the plugging effect coincides with the PI curve without asphaltene deposition. This indicates that the amount of pore throat plugging is negligible in this case study.

Figure 4-20 also shows the PI curve considering the effect of wettability alteration. The initial and final relative permeability sets are given in Table 4-9. The wettability alteration causes a considerable decline in the PI curve, especially before the breakthrough time.

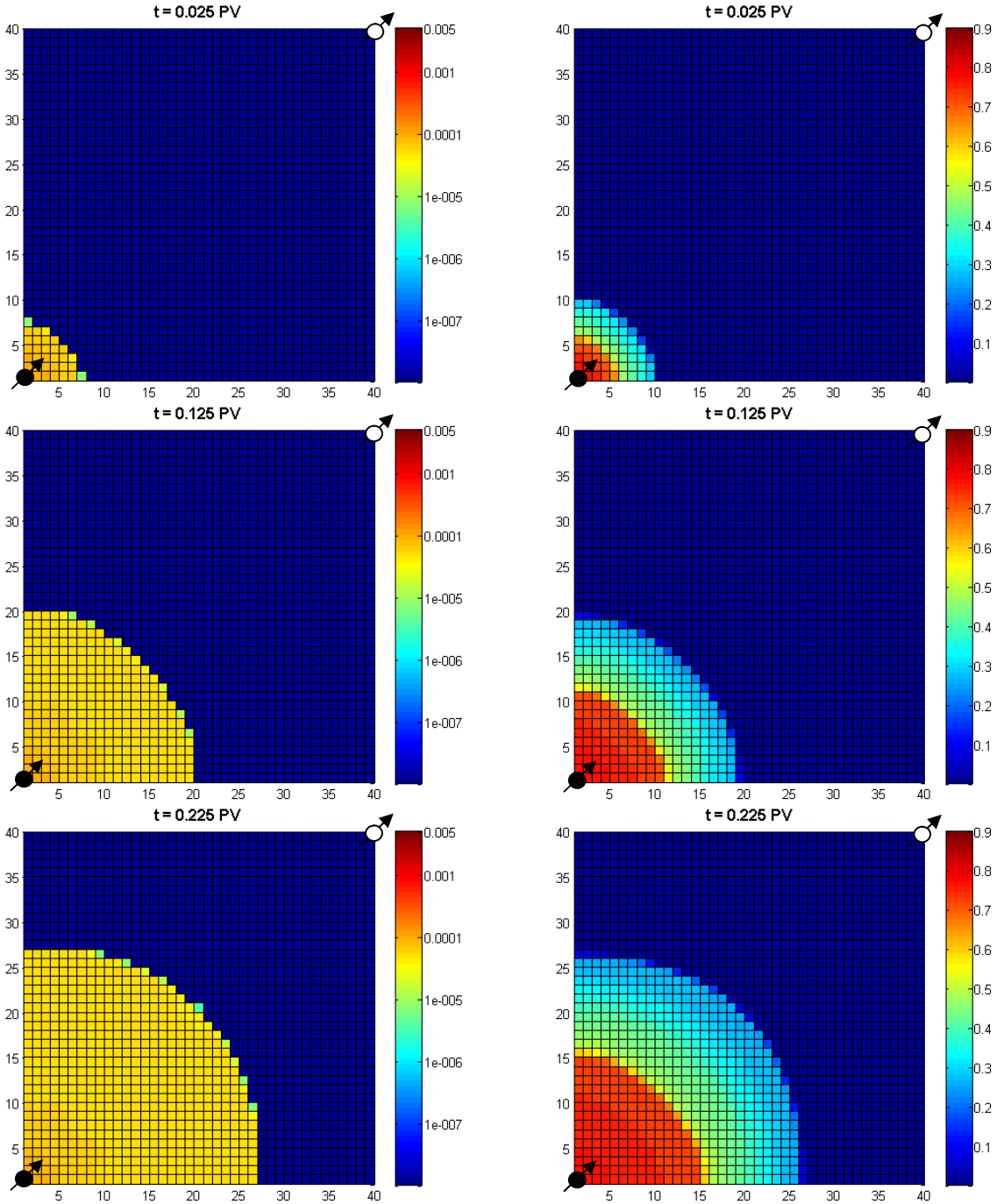

Figure 4-18: Asphaltene deposition and gas saturation profiles for case study 3 at 0.025, 0.125, and 0.225 PV of gas injection. Left: the dimensionless volume of deposited asphaltenes, σ_d ; right: gas saturation.

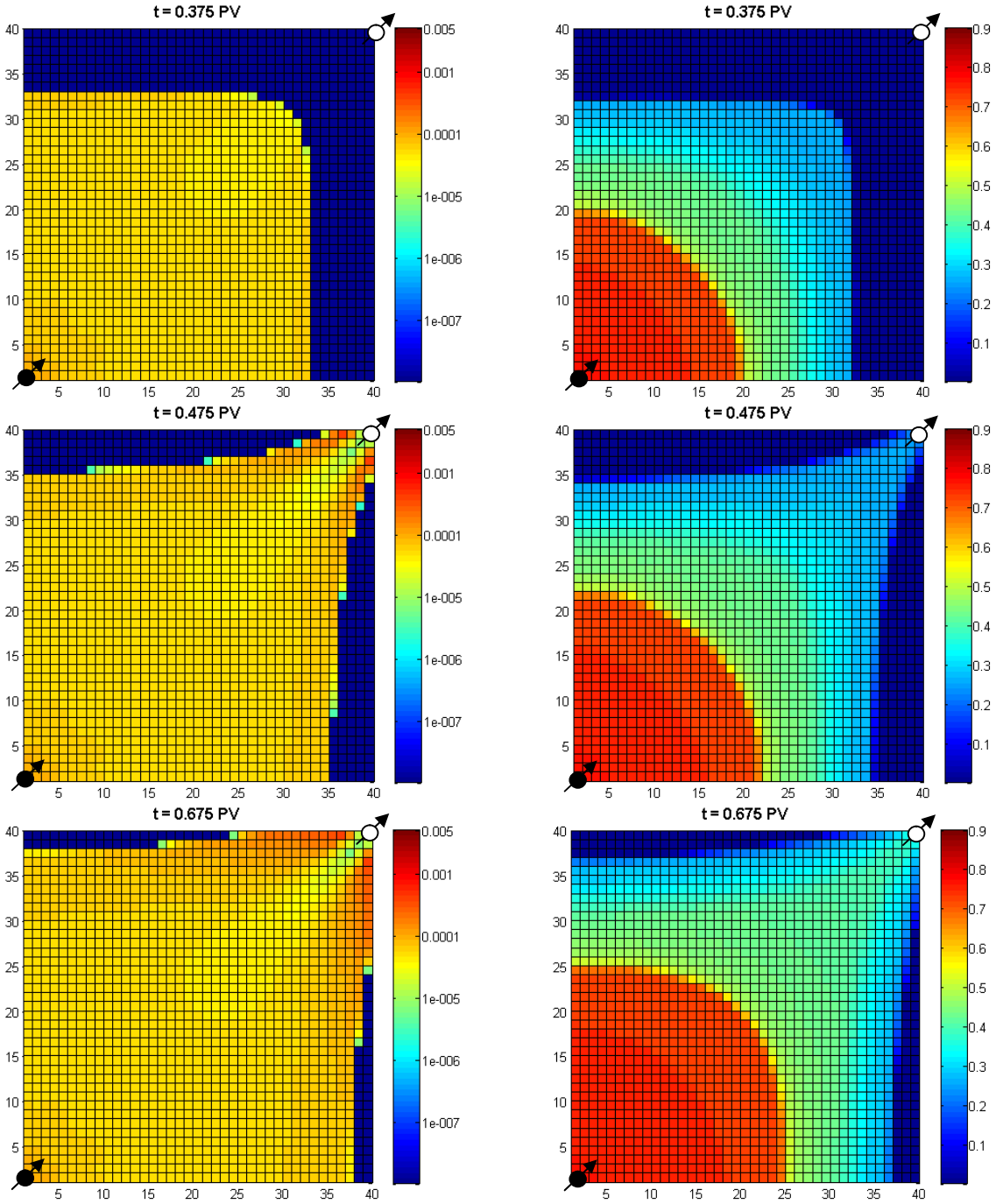

Figure 4-19: Asphaltene deposition and gas saturation profiles for case study 3 at 0.375, 0.475, and 0.675 PV of gas injection. Left: the dimensionless volume of deposited asphaltenes, σ_d ; right: gas saturation.

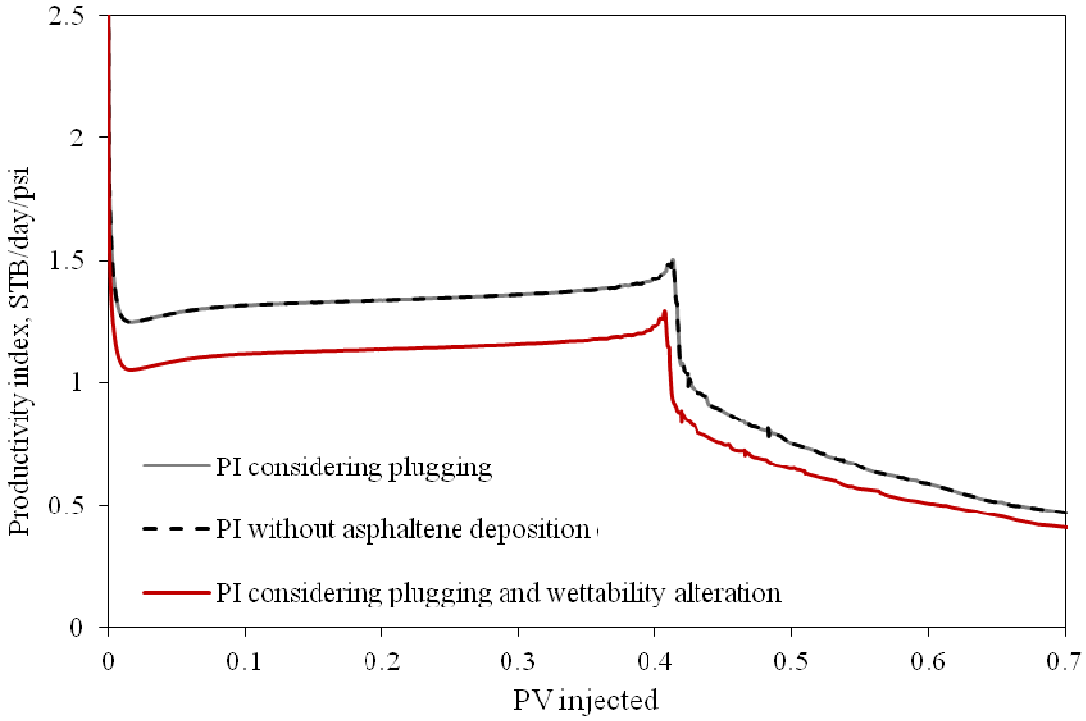

Figure 4-20: Productivity index for case study 3.

4.6. KEY FINDINGS

Asphaltenes are shown to be destabilized with pressure depletion around the production well and or with gas injection everywhere in the reservoir domain, which is swept by injected gas. The profile of asphaltene deposition in the reservoir depends on the reservoir fluid. Based on the observations in the previous section, we can categorize the reservoir fluids into two classes:

- Fluid type-I: Oils with inherent potential of asphaltene precipitation.
- Fluid type-II: Oils without initial asphaltene precipitation risk

Fluid type-I and -II can be recognized based on their asphaltene precipitation envelopes (APE). A typical APE for fluid type-I would be similar to the APE of oil ‘A’.

In these oils, there is always a window between the upper onset and lower onset pressures for all temperature ranges. For fluid type-II, however, the upper onset and lower onset pressures coincide in a range of temperature. Therefore, pressure depletion at that temperature range would not result in asphaltene deposition. For these crude oils, gas injection can open the precipitation window and therefore can cause asphaltene deposition.

Based on the PI curves, pore throat plugging around the production well is more severe in fluid type-I because of the contribution of pressure depletion to asphaltene deposition before gas breakthrough. The contribution of gas injection to pore throat plugging is generally small. However, the adsorption of asphaltenes to the rock surface can cause a considerable effect on the wettability of the formation and therefore on the mobility of hydrocarbons.

Comparing the results for CO_2 and N_2 injection indicates that the more miscible gas, i.e. CO_2, causes more damage through pore plugging due to asphaltene deposition. Although N_2 addition has more severe effect on the APE of the crude oil, the effect of CO_2 injection on the productivity of the production well is higher than N_2 flood because of the longer breakthrough time in CO_2 injection. Results show that the maximum plugging happens around the breakthrough time; because before gas breakthrough, the gridblocks around the production well are constantly exposed to the oil, which is not de-asphalted by the injected gas. Therefore, longer breakthrough time means more pore throat plugging around the production well.

Chapter 5. Aqueous phase modeling

The purpose of this chapter is to propose an algorithm for the phase equilibrium calculations of CO_2/hydrocarbon/water systems. In order to model the aqueous and hydrocarbon phases in a unified framework, we need to extend the available three-phase equilibrium calculations in UTCOMP to four phases. In UTCOMP, the aqueous phase is modeled using Henry's law approximation (Henry 1803). Water is allowed to be present only in the aqueous phase. Including the aqueous phase in the phase behavior calculations allows hydrocarbon components to enter the aqueous phase and water to the hydrocarbon phases. In order to extend the available three-phase flash algorithm to four phases in UTCOMP, it is required to modify the phase behavior algorithm as well as material balance, volumetric derivatives, and coefficients of pressure equations to be consistent with the new equilibrium calculation modules.

5.1. PR EOS FOR AQUEOUS PHASE

PR EOS is applied in this research with Søreide and Whitson's modifications (Søreide and Whitson 1992) to describe the equilibrium between the aqueous and hydrocarbon phases. This model is chosen because of its simplicity and reasonable predictions of solubilities between light hydrocarbons and water, and between CO_2 and water (Yan and Stenby 2009). Søreide and Whitson proposed a specific α-function for water/brine to fit vapor pressure data as follows:

$$\alpha^{1/2} = 1 + 0.4530[1 - T_r(1 - 0.0103c_{sw}^{1.1})] + 0.0034(T_r^{-3} - 1), \quad (5.1)$$

where T_r is the pure water reduced temperature and c_{sw} is the molality of NaCl in brine. They used two sets of BIPs for aqueous and non-aqueous phases, k_{ij}^{AQ} and k_{ij}^{NA}, resulting

in two different attraction terms in the EOS, which can be expressed as a function of their respective phase BIPs:

$$a_{ij}^{NA} = \sum_i \sum_j x_i x_j \sqrt{a_i a_j}(1-k_{ij}^{NA}), \tag{5.2}$$

$$a_{ij}^{AQ} = \sum_i \sum_j x_i x_j \sqrt{a_i a_j}(1-k_{ij}^{AQ}). \tag{5.3}$$

To correct the PR EOS predictions for the gas solubility in the aqueous phase, Søreide and Whitson (1992) proposed two correlations to find BIPs between brine/hydrocarbon and brine/CO_2 binaries as a function of reduced temperature, acentric factor and salinity of the brine:

$$\begin{aligned} k_{iw}^{AQ} &= (1.112 - 1.7369\omega_i^{-0.1}) \times (1 + 0.017407 c_{sw}) + (1.1001 + 0.836\omega_i) \times T_{ri} \times \\ &(1 + 0.033516 c_{sw}) + (-0.15742 - 1.0988\omega_i) \times T_{ri}^2 \times (1 + 0.011478 c_{sw}), \end{aligned} \tag{5.4}$$

$$\begin{aligned} k_{CO_2 w}^{AQ} &= -0.31092(1 + 0.15587 c_{sw}^{0.7505}) + 0.2358(1 + 0.17837 c_{sw}^{0.979}) \times T_{rCO_2} \\ &-21.2566 \exp(-6.7222 T_{rCO_2} - c_{sw}). \end{aligned} \tag{5.5}$$

Søreide and Whitson also proposed constant values for non-aqueous phase interaction parameters for light components and water binaries, k_{iw}^{NA} (Table 5-1). Later on, Yan *et al.* (2011) showed that the Søreide and Whitson model under predicts the CO_2 solubility in high salinity brines. They corrected this deficiency by refitting the expression for $k_{CO_2 w}^{AQ}$ for CO_2 solubility in high salinity NaCl brines. Their new expression for $k_{CO_2 w}^{AQ}$ is given by

$$\begin{aligned} k_{CO_2 w}^{AQ} &= 0.30823655 + 0.11820367 c_{sw} - 9.5381166 \times 10^{-4} c_{sw}^2 \\ &-126.42095 / T - 6.2924435 \times 10^{-4} c_{sw} T + 9.2946667 \times 10^{-7} c_{sw} T^2 \end{aligned} \tag{5.6}$$

Table 5-1: Non-aqueous phase interaction parameters for light components and water binaries

Component	k_{iw}^{NA}
C_1	0.4850
C_2	0.4920
C_3	0.5525
nC_4	0.5091
N_2	0.4778
CO_2	0.1896

Yan *et al.* (2011) also proposed a new value for $k_{CO_2w}^{NA}$, i.e. 0.18756, corresponding to the new expression for $k_{CO_2w}^{AQ}$. In this research, we used the Søreide and Whitson model with modified correlations proposed by Yan *et al.* (2011) to model the gas solubility in the aqueous phase. We validated the developed algorithm by comparing the results obtained for CO_2 solubility in pure water with experimental data (Yan *et al.* 2011). Figure 5-1 and Figure 5-2 represent the CO_2 solubility versus pressure at 373.2 K and 413.2 K, which are in a good agreement with experimental data.

This approach, however, has some limitations. It is limited to the tuning of the BIPs and application of the flash calculations. Moreover, identification of the aqueous phase is always required upfront in the calculations because the BIPs in the aqueous phase are different from those in the non-aqueous phases.

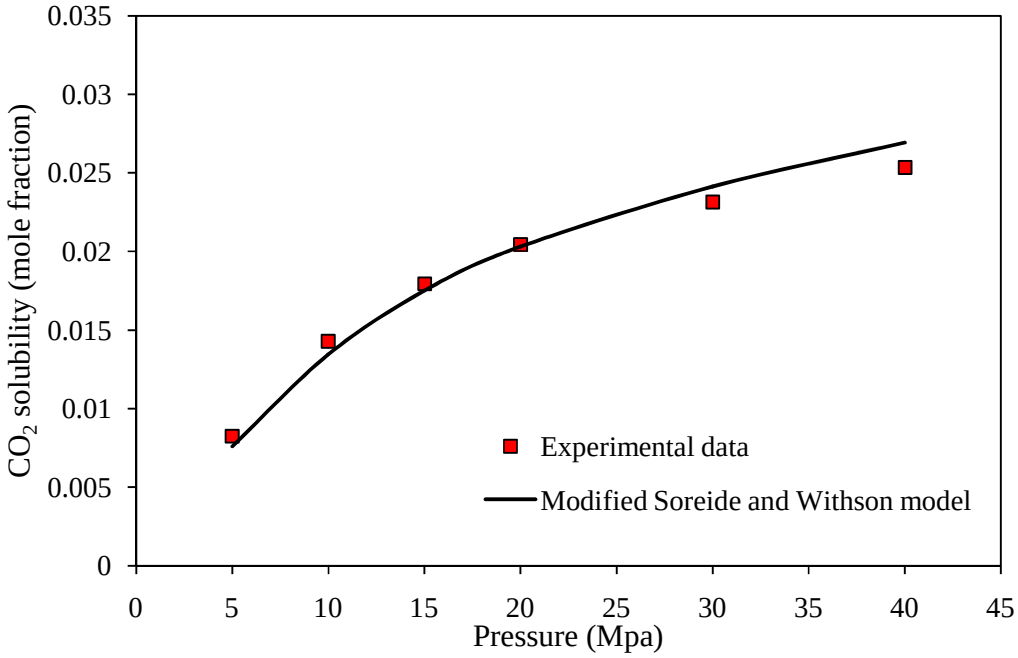

Figure 5-1: CO_2 solubility in pure water using the modified Søreide and Whitson model at T = 373.2 K. Experimental data are from Yan *et al.* (2011).

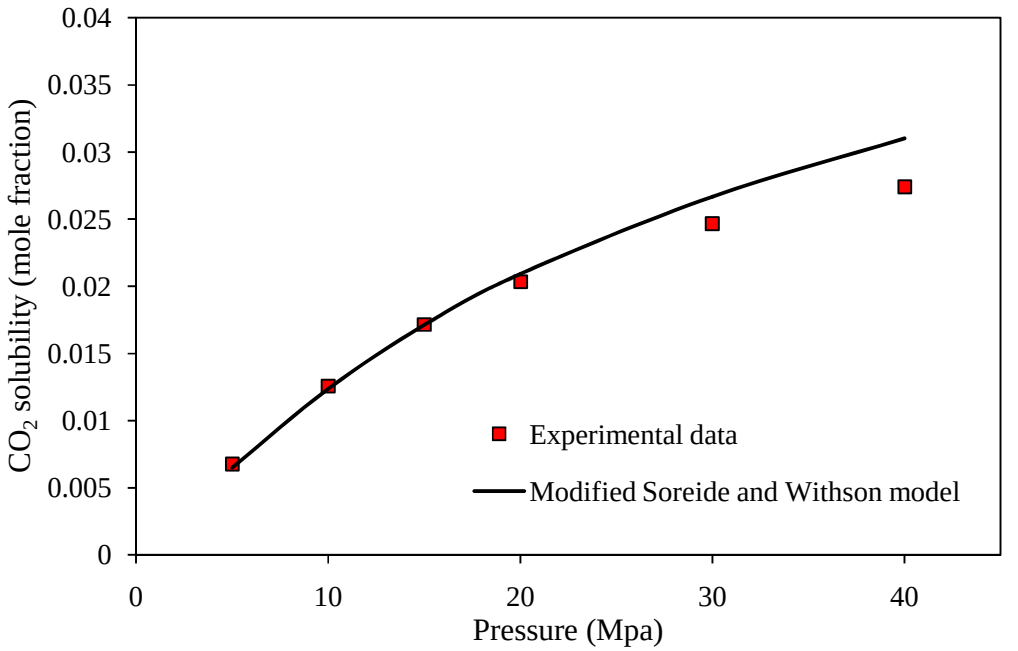

Figure 5-2: CO_2 solubility in pure water using the modified Søreide and Whitson model at T = 413.2 K. Experimental data are from Yan *et al.* (2011).

5.2. FOUR-PHASE FLASH IMPLEMENTATION IN UTCOMP

In compositional simulations, phase equilibrium calculations are coupled with mass conservation and pressure equations. The overall solution scheme of UTCOMP is based on the standard IMPEC method (i.e. implicit-pressure and explicit-composition) in which the pressure equations for each gridblock are solved explicitly first and then the mass change of each component is calculated explicitly from the conservation equations. In order to extend the available three-phase flash calculations to four phases, the phase behavior algorithm must be modified to consider the aqueous phase in the equilibrium calculations. Besides the phase behavior, other parts of the solution algorithm such as pressure equation coefficients must be adjusted to be consistent with the four-phase equilibrium calculations.

5.2.1. Four phase flash calculation methodology

The equations which form the basis of the flash calculations in UTCOMP and the algorithm to solve the equations were described in Chapter 3. The most important parts of the algorithm which must be modified to consider four phases at equilibrium are (i) constant-K flash calculation in SS iterations and (ii) the Hessian matrix in the minimization of Gibbs free energy iterations.

5.2.1.1. Constant-K flash calculations

As mentioned earlier, the procedure for flash calculations using SS method is to solve the fugacity equations subject to the material-balance constraints in the form of Rachford-Rice equations. Rachford-Rice equations are solved to determine the phase composition and mole fractions for a given set of overall mole fraction and constant K-values. The procedure to solve Rachford-Rice equations is often called constant-K flash

calculation (Okuno *et al.* 2010a). The minimization of Gibbs free energy algorithm does not contain the constant-K flash calculation because the independent variables (i.e. the mole numbers of the components) are chosen so that they give the phase compositions and phase mole fractions explicitly (Michelsen 1982a, Okuno *et al.* 2010a).

As the number of phases increases, the behavior of Rachford-Rice equations becomes more implicit and complicated. Implementing a four-phase flash calculation in compositional simulator requires a robust and efficient algorithm for four-phase constant-K flash calculations. Okuno *et al.* (2010a) developed an algorithm for multiphase constant-K flash calculation for compositional simulation, which is guaranteed to converge to the correct solution for both negative and positive flash calculations. In this research, we used the Okuno *et al.* (2010a) algorithm for the four-phase constant-K flash calculations described briefly in the following.

The material balance equations in the flash calculations are

$$z_i = \sum_{j=1}^{N_P} \beta_j x_{ij} \quad \text{for } i = 1,...,N_C, \tag{5.7}$$

$$\sum_{j=1}^{N_P} \beta_j = 1, \tag{5.8}$$

and

$$\sum_{i=1}^{N_C} x_{ij} = 1 \quad \text{for } j = 1,...,N_P, \tag{5.9}$$

where β_j represents the mole fraction of phase *j*. Eqs. (5.7)-(5.9) along with the definition of *K*-values result in

$$x_{iN_P} = z_i / t_i, \tag{5.10}$$

where t_i is defined as

$$t_i = 1 - \left[\sum_{j=1}^{N_P - 1} \left(1 - K_{ij}\right) \beta_j \right] \quad \text{for } i = 1, ..., N_C . \tag{5.11}$$

Phase N_P is selected as the reference phase. Eq. (5.9) is equivalent to

$$\sum_{i=1}^{N_C} \left(1 - K_{ij}\right) x_{i4} = 0 \quad \text{for } j = 1, ..., N_P - 1 . \tag{5.12}$$

Multiphase Rachford-Rice equations, $f_j(\beta)$, are then derived by combining Eqs. (5.10) and (5.12):

$$f_j\left(\beta\right) = \sum_{i=1}^{N_C} \left(1 - K_{ij}\right) z_i / t_i \quad \text{for } j = 1, ..., N_P - 1 , \tag{5.13}$$

where β is a vector comprised of elements β_j. Okuno *et al.* (2010a) developed an algorithm to solve Eqs. (5.13) based on a minimization of a convex function with N_C linear constraints. Okuno explained that since the Jacobian matrix to solve Eq. (5.13) is symmetric, a scalar function $F(\beta)$ exists for which the gradient vector consists of the Rachford-Rice equations. The iteration schemes for Newton's method based on root finding and minimization techniques are as follows:

$$\beta^{n+1} = \beta^n - \left[\nabla f\left(\beta^n\right)^T \right]^{-1} f\left(\beta^n\right) \quad \text{for root finding algorithm,} \tag{5.14}$$

and

$$\beta^{n+1} = \beta^n - \left[\nabla^2 F\left(\beta^n\right) \right]^{-1} \nabla F\left(\beta^n\right) \quad \text{for minimization algorithm.} \tag{5.15}$$

Newton's iteration scheme for minimization could be treated as a special case of the root finding technique. The function F to be minimized is constructed by integrating the elements of f_j with respect to β_j:

$$F\left(\beta\right) = \sum_{i=1}^{N_C} \left(-z_i \ln\left|t_i\right|\right) . \tag{5.16}$$

The main advantage of using the minimization technique for solving the constant-K flash problem is that the function F defined in Eq. (5.16) is a convex function as its Hessian matrix is positive semi-definite. Another feature of this function is that if the region $t_i > 0$ (i=1,...,N_C) is unbounded, there would be no solution to the multiphase constant-K flash because the function becomes monotonic and therefore it does not have any minimum.

The simplest feasible region for the solution of a constant-K flash calculation is defined by the non-negative values of t_i. Okuno *et al.* (2010a) developed a smaller feasible region, which does not contain any pole. They derived the new feasible region based on the non-negativity of the component mole fractions, which is mathematically expressed as

$$0 \le x_{ij} \le 1 \ \left(i = 1,..., N_C \text{ and } j = 1,..., N_P\right). \tag{5.17}$$

The non-negativity of the component mole fractions condition results in the following inequalities

$$0 \le z_i \le t_i, \tag{5.18}$$

and

$$0 \le K_{ij} z_i \le t_i. \tag{5.19}$$

Okuno *et al.* (2010a) derived the final form of the constraints as

$$a_{RR,i}^T \beta \le b_{RR,i}, \tag{5.20}$$

where

$$a_{RR,i} = \left\{1 - K_{ij}\right\}, \tag{5.21}$$

$$\beta = \left\{\beta_j\right\}, \tag{5.22}$$

and

$$b_{RR,i} = \min\left\{1 - z_i, \min_j \left\{1 - K_{ij} z_i\right\}\right\} \quad \text{for } i = 1,\ldots,N_C \text{ and } j = 1,\ldots,N_P - 1. \tag{5.23}$$

The set of constraints $S = \left\{\beta \mid a_{RR,i}^T \beta \le b_{RR,i},\ i = 1,\ldots,N_C\right\}$ would then lead to a smaller-sized feasible region compared to that on the basis of $t_i \ge 0$. As mentioned earlier, this new set would not contain any pole and thus excludes the region with poor minimization convergence. The detailed algorithm, which is used to solve multiphase constant-K flash calculation, can be found in Okuno *et al.* (2010a).

5.2.1.2. Minimization of Gibbs free energy

In this research, we extend the Perschke's algorithm for three-phase flash calculations based on the minimization of Gibbs free energy to four phases. The main modification is the extension of the Hessian matrix for four-phase systems. As described previously, the elements of the Hessian matrix are determined by taking the derivatives of the Gibbs free energy function with respect to the independent mole numbers. Assuming the first phase as the reference phase, the Hessian matrix has the following forms for two- and three-phase mixtures

$$H^{2-phase} \equiv \left[\frac{\partial^2}{\partial n_{s2} \partial n_{i2}}\left(\frac{G^t}{RT}\right)\right] \quad \text{for } s \text{ and } i = 1,\ldots,N_C, \tag{5.24}$$

and

$$H^{3-phase} \equiv \begin{bmatrix} \dfrac{\partial^2}{\partial n_{s2} \partial n_{i2}}\left(\dfrac{G^t}{RT}\right) & \dfrac{\partial^2}{\partial n_{s3} \partial n_{i2}}\left(\dfrac{G^t}{RT}\right) \\ \dfrac{\partial^2}{\partial n_{s2} \partial n_{i3}}\left(\dfrac{G^t}{RT}\right) & \dfrac{\partial^2}{\partial n_{s3} \partial n_{i3}}\left(\dfrac{G^t}{RT}\right) \end{bmatrix}. \tag{5.25}$$

The extension of the Hessian matrix for four-phase mixtures results in

$$H^{4-phase}=\begin{bmatrix} \frac{\partial^2}{\partial n_{s2}\partial n_{i2}}\left(\frac{G^t}{RT}\right) & \frac{\partial^2}{\partial n_{s3}\partial n_{i2}}\left(\frac{G^t}{RT}\right) & \frac{\partial^2}{\partial n_{s4}\partial n_{i2}}\left(\frac{G^t}{RT}\right) \\ \frac{\partial^2}{\partial n_{s2}\partial n_{i3}}\left(\frac{G^t}{RT}\right) & \frac{\partial^2}{\partial n_{s3}\partial n_{i3}}\left(\frac{G^t}{RT}\right) & \frac{\partial^2}{\partial n_{s4}\partial n_{i3}}\left(\frac{G^t}{RT}\right) \\ \frac{\partial^2}{\partial n_{s2}\partial n_{i4}}\left(\frac{G^t}{RT}\right) & \frac{\partial^2}{\partial n_{s3}\partial n_{i4}}\left(\frac{G^t}{RT}\right) & \frac{\partial^2}{\partial n_{s4}\partial n_{i4}}\left(\frac{G^t}{RT}\right) \end{bmatrix}, \tag{5.26}$$

where $\frac{\partial^2}{\partial n_{sj}\partial n_{ik}}\left(\frac{G^t}{RT}\right)$ is a $N_C \times N_C$ matrix whose elements are determined from the following relations:

$$\frac{\partial^2}{\partial n_{sj}\partial n_{ij}}\left(\frac{G^t}{RT}\right)=\frac{\partial \ln f_{ij}}{\partial n_{sj}}+\frac{\partial \ln f_{i1}}{\partial n_{s1}} \quad \text{for } s,i, \text{ and } j=1,...,N_C, \tag{5.27}$$

and

$$\frac{\partial^2}{\partial n_{sj}\partial n_{ik}}\left(\frac{G^t}{RT}\right)=\frac{\partial \ln f_{i1}}{\partial n_{s1}} \quad \text{for } s,i,j, \text{ and } k=1,...,N_C \ (j\neq k). \tag{5.28}$$

The partial derivatives in Eqs. (5.27) and (5.28) are determined analytically and can be found in Perschke (1988).

5.2.2. Derivatives of total fluid volume

The most complicated part in the solution of pressure equations is to analytically compute the partial derivatives of the total fluid volume with respect to component moles and pressure. The calculation procedure of these derivatives has been described by Chang (1990) for three hydrocarbon phases assuming no mass transfer between the aqueous phase and hydrocarbon phases. In this section, we describe the extension of the total fluid volume derivatives to four phases considering mass transport between all phases.

5.2.2.1. Derivatives of total fluid volume with respect to component moles

The derivatives of the total fluid volume with respect to component moles can be written as

$$\dot{V}_{t_i} = \left(\frac{\partial V_t}{\partial N_i}\right)_{P,N_{r(r\neq i)}} = \frac{\partial}{\partial N_i}\left(\sum_{j=1}^{N_P} n_j v_j\right) \quad \text{for } i = 1,...,N_C, N_C+1, \tag{5.29}$$

where V_t is the total fluid volume. In UTCOMP, the water component is indexed as the $(N_C+1)^{th}$ component and the hydrocarbon components are numbered from 1 to N_C. The aqueous phase is assumed as a single component and a slightly compressible phase. Hydrocarbon phases are modeled using an EOS. The derivative for the hydrocarbon components can be written as

$$\left(\frac{\partial V_t}{\partial N_i}\right)_{P,N_{r(r\neq i)}} = \sum_{j=2}^{N_P}\sum_{k=1}^{NC}\left[v_j + n_j\frac{RT}{P}\left(\frac{\partial Z_j}{\partial n_{kj}}\right)\right]\left(\frac{\partial n_{kj}}{\partial N_i}\right)_{P,N_r(r\neq i)} \qquad \text{for } i = 1,...,N_C. \tag{5.30}$$

In UTCOMP, the index of the summation term in Eq. (5.30) starts from phase 2. In this research, however, we modeled all the phases using the EOS; therefore, the derivative of the total volume is equal to the summation of the derivatives of components in all phases including the aqueous phase, which is indexed as the first phase in UTCOMP.

The partial derivative of the compressibility factor in Eq. (5.30) can be computed analytically from an EOS. The equilibrium constraints (*i.e.* the equality of the fugacity coefficients) are used to evaluate the second derivative term in Eq. (5.30), which is the partial derivative of the phase mole number with respect to the total component mole in the mixture. For a four-phase system, the equilibrium conditions are as follows:

$$\ln f_{s1} - \ln f_{sj} = 0 \qquad \text{for} \quad s = 1,...,N_C \quad \text{and} \quad j = 2,...,4, \tag{5.31}$$

where the first phase is considered as the reference phase. By taking the derivatives of Eq. (5.31) with respect to the components mole numbers, we obtain

$$\frac{\partial}{\partial N_i}\left(\ln f_{s1} - \ln f_{sj}\right) = \sum_{k=1}^{N_C}\left(\frac{\partial \ln f_{s1}}{\partial n_{k1}}\right)\left(\frac{\partial n_{k1}}{\partial N_i}\right) - \sum_{k=1}^{N_C}\left(\frac{\partial \ln f_{sj}}{\partial n_{kj}}\right)\left(\frac{\partial n_{kj}}{\partial N_i}\right) = 0\,, \tag{5.32}$$

for $s = 1,...,N_C$ and $j = 2,...,4.$

Material balance also gives the following relationship between the derivatives of mole numbers:

$$\frac{\partial n_{k2}}{\partial N_i} = \delta_{i,k} - \frac{\partial n_{k1}}{\partial N_i} - \frac{\partial n_{k3}}{\partial N_i} - \frac{\partial n_{k4}}{\partial N_i} \qquad \text{for} \qquad k = 1,...,N_C\,, \tag{5.33}$$

Eqs. (5.32) and (5.33) result in a set of simultaneous equations of the form of *Ax* = *B*, where

$$x = \left[\frac{\partial \vec{n}_1}{\partial N_i}, \frac{\partial \vec{n}_3}{\partial N_i}, \frac{\partial \vec{n}_4}{\partial N_i}\right]^T, \tag{5.34}$$

$$A = \begin{bmatrix} \left(\dfrac{\partial \ln \vec{f}_1}{\partial \vec{n}_1} + \dfrac{\partial \ln \vec{f}_2}{\partial \vec{n}_2}\right) & \dfrac{\partial \ln \vec{f}_2}{\partial \vec{n}_2} & \dfrac{\partial \ln \vec{f}_2}{\partial \vec{n}_2} \\ \dfrac{\partial \ln \vec{f}_1}{\partial \vec{n}_1} & -\dfrac{\partial \ln \vec{f}_3}{\partial \vec{n}_3} & 0 \\ \dfrac{\partial \ln \vec{f}_1}{\partial \vec{n}_1} & 0 & -\dfrac{\partial \ln \vec{f}_4}{\partial \vec{n}_4} \end{bmatrix}, \tag{5.35}$$

and (5.36)

$$B = \left[\frac{\partial \ln \vec{f}_2}{\partial n_{i2}}, 0, 0 \right]^T .$$

The solution of this system of equations is then used in Eq. (5.30) to compute the derivatives of the total fluid volume. In general, matrix *A* is not symmetric. As proposed by Trangenstein (1987), by rearranging the set of equations we can find a symmetric positive definite matrix for this system. Here, by subtracting the first row of the matrix *A* (and *B*) from row 2 and 3, a new set of equations is obtained as follows:

$$\left[\frac{\partial \vec{n}_1}{\partial N_i}, \frac{\partial \vec{n}_3}{\partial N_i}, \frac{\partial \vec{n}_4}{\partial N_i} \right]^T = \left(\vec{\vec{G}} \right)^{-1} \left[\frac{\partial \ln \vec{f}_2}{\partial n_{i2}}, \frac{\partial \ln \vec{f}_2}{\partial n_{i2}}, \frac{\partial \ln \vec{f}_2}{\partial n_{i2}} \right], \tag{5.37}$$

where matrix *G* is a symmetric positive definite matrix (Trangenstein 1987), which has the following form:

$$G = \begin{bmatrix} \left(\frac{\partial \ln \vec{f}_1}{\partial \vec{n}_1} + \frac{\partial \ln \vec{f}_2}{\partial \vec{n}_2} \right) & \frac{\partial \ln \vec{f}_2}{\partial \vec{n}_2} & \frac{\partial \ln \vec{f}_2}{\partial \vec{n}_2} \\ \frac{\partial \ln \vec{f}_2}{\partial \vec{n}_2} & \left(\frac{\partial \ln \vec{f}_2}{\partial \vec{n}_2} + \frac{\partial \ln \vec{f}_3}{\partial \vec{n}_3} \right) & \frac{\partial \ln \vec{f}_2}{\partial \vec{n}_2} \\ \frac{\partial \ln \vec{f}_2}{\partial \vec{n}_2} & \frac{\partial \ln \vec{f}_2}{\partial \vec{n}_2} & \left(\frac{\partial \ln \vec{f}_2}{\partial \vec{n}_2} + \frac{\partial \ln \vec{f}_4}{\partial \vec{n}_4} \right) \end{bmatrix}. \tag{5.38}$$

The solution procedure for this set of equations is similar to the solution method reported by Chang (1990) for three hydrocarbon phases.

5.2.2.2. Derivatives of total fluid volume with respect to pressure

The derivative of the total fluid volume with respect to pressure is expressed as

$$\left(\frac{\partial V_t}{\partial P} \right)_{N_i} = \left(\frac{\partial V_1}{\partial P} \right)_{N_i} + \sum_{j=2}^{N_P} \left(\frac{\partial V_j}{\partial P} \right)_{N_i} . \tag{5.39}$$

As stated earlier, the aqueous phase is treated differently in UTCOMP. The first term in the right hand side of Eq. (5.39) is the derivative of the aqueous phase volume with respect to pressure and the second term is the summation of the partial derivatives of the hydrocarbon phases. In this research, we used the EOS model for all of the phases; therefore, Eq. (5.39) is written in its general form as follows:

$$\left(\frac{\partial V_t}{\partial P}\right)_{N_i} = \sum_{j=1}^{N_P}\left(\frac{\partial V_j}{\partial P}\right)_{N_i} . \tag{5.40}$$

The required partial derivatives in the right hand side of Eq. (5.40) are given by

$$\left(\frac{\partial V_j}{\partial P}\right)_{N_i} = \sum_{k=1}^{N_C}\left[v_j + n_j \frac{RT}{P}\left(\frac{\partial Z_j}{\partial n_{kj}}\right)\right]\left(\frac{\partial n_{kj}}{\partial P}\right)_{N_i} + n_j\left(\frac{\partial v_j}{\partial P}\right)_{n_{rj}} \quad \text{for} \quad j = 1,...,4 . \tag{5.41}$$

The partial derivative of the molar volume with respect to pressure in Eq. (5.41) can be obtained as

$$\left(\frac{\partial v_j}{\partial P}\right)_{n_{rj}} = RT\frac{\partial}{\partial P}\left(\frac{Z_j}{P}\right) = \frac{RT}{P^2}\left[P\left(\frac{\partial Z_j}{\partial P}\right) - z_j\right] \quad \text{for} \quad j = 1,...,4 . \tag{5.42}$$

By applying the same procedure described in the previous section, a system of equations of the form $Ax = B$ is obtained to find the derivatives of mole numbers with respect to pressure, where

$$x = \left[\frac{\partial \vec{n}_1}{\partial P_i}, \frac{\partial \vec{n}_3}{\partial P_i}, \frac{\partial \vec{n}_4}{\partial P_i}\right]^T , \tag{5.43}$$

$$B = \left[\frac{\partial \ln \vec{f}_2}{\partial P} - \frac{\partial \ln \vec{f}_1}{\partial P}, \frac{\partial \ln \vec{f}_3}{\partial P} - \frac{\partial \ln \vec{f}_1}{\partial P}, \frac{\partial \ln \vec{f}_4}{\partial P} - \frac{\partial \ln \vec{f}_1}{\partial P}\right]^T , \tag{5.44}$$

and

$$A=\begin{bmatrix} \left(\frac{\partial \ln \vec{f}_1}{\partial \vec{n}_1}+\frac{\partial \ln \vec{f}_2}{\partial \vec{n}_2}\right) & \frac{\partial \ln \vec{f}_2}{\partial \vec{n}_2} & \frac{\partial \ln \vec{f}_2}{\partial \vec{n}_2} \\ \frac{\partial \ln \vec{f}_1}{\partial \vec{n}_1} & -\frac{\partial \ln \vec{f}_3}{\partial \vec{n}_3} & 0 \\ \frac{\partial \ln \vec{f}_1}{\partial \vec{n}_1} & 0 & -\frac{\partial \ln \vec{f}_4}{\partial \vec{n}_4} \end{bmatrix}. \tag{5.45}$$

Again, it is required to convert matrix *A* into a symmetric matrix which can be done by the same procedure described in the previous section.

5.3. EFFECT OF WATER ON THE PHASE BEHAVIOR OF CO_2/HYDROCARBON SYSTEMS

The developed four-phase flash algorithm is used to investigate the effect of introducing water on the phase behavior of two West Texas oil/CO_2 mixtures. These mixtures are selected because they form four phases at relatively low temperatures.

5.3.1. Case study 1: North Ward Estes oil

The first case study is made by mixing water with the North Ward Estes (NWE) oil based on the Khan *et al.* (1992) fluid characterization. In this example, we examine the effect of water on changing the phase behavior of CO_2 with hydrocarbons. The fluid properties are given in Table 5-2. The BIPs presented in Table 5-3 are the non-aqueous phase BIPs. For the aqueous phase, we use Eqs. (5.4) and (5.6). All hydrocarbon-hydrocarbon and CO_2-hydrocarbon BIPs in the aqueous phase are set to zero. This is a reasonable assumption because at low temperatures, the hydrocarbon solubilities in the aqueous phase are generally small.

Table 5-2: Fluid properties of NWE oil (Khan *et al.*, 1992)

Component	Mole%	T_c (°R)	P_c (psia)	ω
CO_2	0.77	547.560	1069.87	0.225
C_1	20.25	343.080	667.20	0.008
C_{2-3}	11.80	618.547	653.37	0.130
C_{4-6}	14.84	839.538	485.94	0.244
C_{7-14}	28.63	1085.530	351.54	0.600
C_{15-24}	14.90	1320.816	261.51	0.903
C_{25+}	8.81	1661.758	250.31	1.229

Table 5-3: Non-aqueous BIPs for CO_2/NWE oil mixture (Khan *et al.* 1992)

Component	$k^{NA}_{CO_2-i}$	k^{NA}_{w-i}
CO_2	0.00000	0.18756
C_1	0.12000	0.48500
C_{2-3}	0.12000	0.50000
C_{4-6}	0.12000	0.50000
C_{7-14}	0.09000	0.50000
C_{15-24}	0.09000	0.50000
C_{25+}	0.09000	0.50000
H_2O	0.18756	0.00000

The CO_2/NWE oil mixture has a large three-phase region at 83 °F and in the pressure range from 900 to 1300 psia. The three-phase region develops at CO_2 concentrations greater than 55% (Khan *et al.* 1992). The effect of water on the phase behavior of this system is examined by introducing different amounts of water to the original water-free CO_2/oil mixture. No salt is considered. The *p-x* diagrams for this

system at 83 °F for different amounts of water are presented in Figure 5-3. In this figure, water/(CO_2+oil) is the ratio of the moles of water to the combined moles of CO_2 and oil in the feed. As is shown, introducing water shifts the phase boundaries significantly toward larger mole fractions of CO_2. This effect occurs because CO_2 dissolution in the aqueous phase reduces the amount of CO_2 required for developing the liquid CO_2-rich phase, L_2.

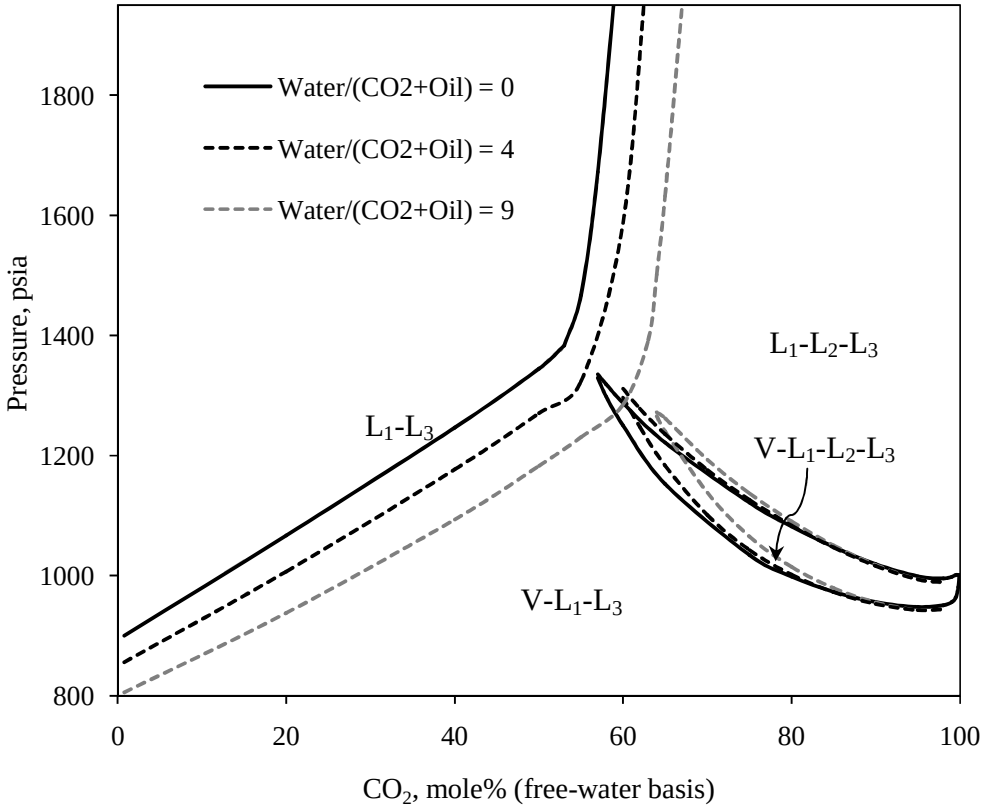

Figure 5-3: P-x diagram of water/CO_2/NWE oil mixtures at 83 °F. V is the vapor phase, L_1 is the oleic phase, L_2 is the CO_2-rich phase, and L_3 is the aqueous phase (Mohebbinia *et al.* 2013).

The experiments conducted by Pollack *et al.* (1988) show the same effect on the phase boundaries of the CO_2/Maljamar crude oil mixture by introducing water to the system. As is shown in Figure 5-3, the four-phase region on the right side of the figure has not changed much, because the amount of CO_2 loss is insignificant at high concentrations of CO_2. As the amount of water added increases, the magnitude of the shift in the phase boundaries also increases. This shows the importance of aqueous phase modeling to study the phase behavior of CO_2 floods at high saturations of water such as during water alternating gas (WAG) injections.

5.3.2. Case study 2: Bob Slaughter Block oil

Another case study was set up by including water in the phase behavior for Bob Slaughter Block (BSB) West Texas oil. The BSB oil fluid description generated by Khan *et al.* (1992) is listed in Table 5-4. The BIPs between CO_2-hydrocarbon binaries in the non-aqueous phases are presented in Table 5-5.

Table 5-4: Fluid properties of the BSB oil (Khan *et al.* 1992)

Component	Mole%	T_c (°R)	P_c (psia)	ω
CO_2	3.37	547.6	1069.87	0.225
C_1	8.61	288.0	667.20	0.008
C_{2-3}	15.03	619.6	652.56	0.131
C_{4-6}	16.71	833.8	493.07	0.240
C_{7-15}	33.04	1090.4	315.44	0.618
C_{16-27}	16.11	1351.8	239.90	0.957
C_{28+}	7.13	1696.5	238.12	1.268

The results obtained for the phase distribution of the water/CO_2/BSB oil mixture at 105 °F are shown in Figure 5-4. The phase mole fractions are normalized on a water-free basis to compare them with water-free calculations results (three-phase flash calculations shown by the dashed lines).

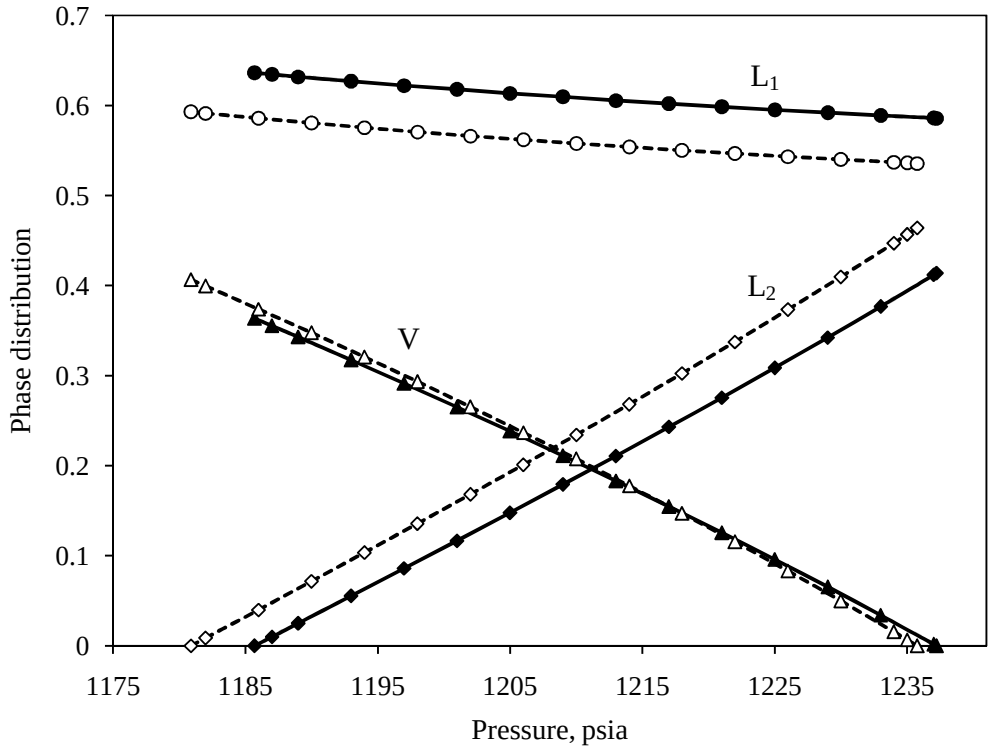

Figure 5-4: Phase distribution of water/CO_2/BSB oil mixture at 105 °F (Mohebbinia *et al.* 2013). The solid lines show the normalized phase distribution obtained by the four-phase reduced flash algorithm for (▲) vapor phase, (●) oleic phase, and (◆) CO_2-rich phase. The dashed lines depict the water-free calculations.

Figure 5-4 shows a shift in the phase boundaries toward higher pressures, which is identical to a shift in the *p-x* diagram toward greater CO_2 concentrations. By including water in the flash calculations, the amount of CO_2-rich phase decreases for all pressures, which is consistent with CO_2 loss into the aqueous phase.

The lower pressure boundary of the multiphase region increases from 1181 to 1185.6 psia. This means that the formation of an aqueous phase in contact with hydrocarbon phases makes the CO_2-rich phase disappear in this pressure range. A slight change from 1235.8 to 1236.2 psia can also be seen in the upper pressure boundary of the three-phase region. Phase boundary changes would decrease with brine salinity owing to decreasing CO_2 solubility. This trend was shown by Pollack *et al.* (1988) who demonstrated the effect of brine salinity on CO_2/Maljamar crude oil system phase boundaries.

Table 5-5: BIPs and reduced method specific parameters of water/CO_2/BSB oil mixture

Component	$k_{CO_2-i}^{NA}$	k_{w-i}^{NA}
CO_2	0.0000	0.1896
C_1	0.0550	0.4850
C_{2-3}	0.0550	0.5000
C_{4-6}	0.0550	0.5000
C_{7-15}	0.1050	0.5000
C_{16-27}	0.1050	0.5000
C_{28+}	0.1050	0.5000
H_2O	0.1896	0.0000

5.3.3. Case study-3: Effect of considering the aqueous phase on oil recovery

A gas injection simulation case was set up to examine the effect of considering the aqueous phase in equilibrium calculations on the oil recovery. The predicted oil recoveries from two types of simulations are compared in this case study: (i) simulations at which only the hydrocarbon phases are considered in flash calculations and (ii)

simulations at which the aqueous phase is also modeled with hydrocarbon phases. The reservoir fluid is the BSB oil with properties reported in Table 5-4 and Table 5-5. The oil displacement is simulated with injection gas consisting of 95% CO_2 and 5% C_1 in an areal two-dimensional reservoir model. Reservoir properties are given in Table 5-6.

Table 5-6: Reservoir properties for case study-3

Number of gridblocks	25×25
Constant bottomhole injection pressure	1300 psia
Constant bottomhole production pressure	900 psia
Initial reservoir pressure	1100 psia
Reservoir temperature	105 °F
Initial porosity	0.25
Homogeneous permeability in x and y directions	100 mD
Relative permeability model	Corey's model
Constant gridblock size at x and y directions	25 ft

Figure 5-5 illustrates the oil recoveries versus pore volume of injected gas for different amounts of initial water saturations (i.e. 0.3, 0.5, 0.6, and 0.7). Results show that considering water in the phase behavior calculations results in a lag in the oil recovery curves. That is, the simulations considering the CO_2 loss into the aqueous phase require a larger time to reach a given recovery factor. Final oil recoveries for both simulations are almost the same because the aqueous phase is eventually saturated with CO_2 and then the CO_2 loss will be replaced by the continuous gas injection. This behavior was also reported by Enick and Klara (1992).

Figure 5-5 also shows that including aqueous phase becomes more important at high water saturations because of the higher amount of CO_2 loss into the aqueous phase. The effect of CO_2 loss into the aqueous phase can be more pronounced in WAG processes as the saturated water in the formation are intermittently replaced with fresh slugs of water during the injection process.

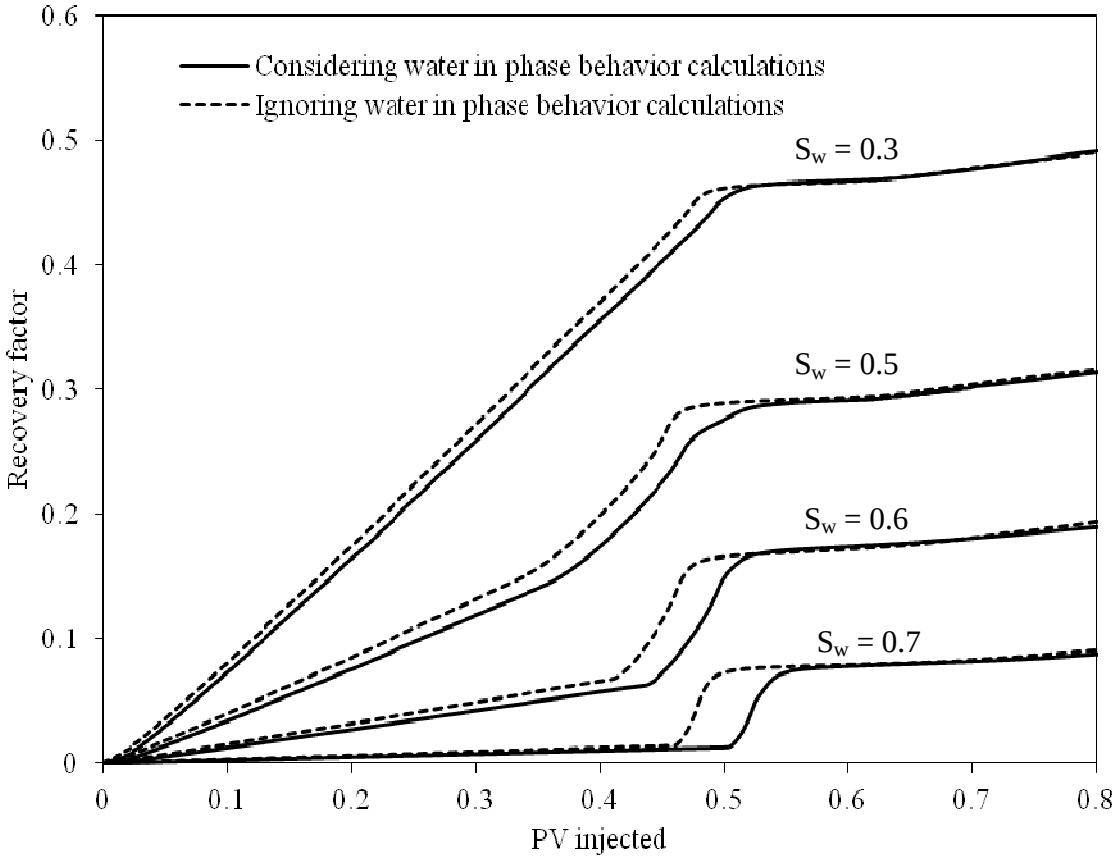

Figure 5-5: Oil recovery factor versus PV of CO_2 injection for various amounts of initial water saturations. Solid lines show the recovery factor considering water in the phase behavior calculations and dashed lines represent the recovery factor when water is ignored in the phase behavior calculations.

5.4. PR EOS VERSUS HENRY'S LAW

An alternative technique to find the gas solubility in the aqueous phase is using Henry's law, which mathematically is expressed as

$$f_i = k_H x_i, \tag{5.46}$$

where f_i is the fugacity of the gas component, x_i is the concentration of dissolved gas, and k_H is the Henry's law constant. Figure 5-6 and Figure 5-7 show the CO_2 solubility in pure water determined using Henry's law model in UTCOMP at 373.2 K and 413.2 K. As shown, Henry's law also gives a good match with experimental data. However, Henry's law has some limitations, which should be considered to avoid erroneous predictions. For example, Henry's law is only applicable for solutions in which the solvent does not chemically interact with the dissolved gases (Harvey and Smith 2007). CO_2 is one of the gases which reacts with water and converts to carbonic acid. Also, Henry's law only applies for solutions which are sufficiently dilute. EOS models have the advantage over Henry's law in that they are also able to determine other thermodynamic properties such as phase density.

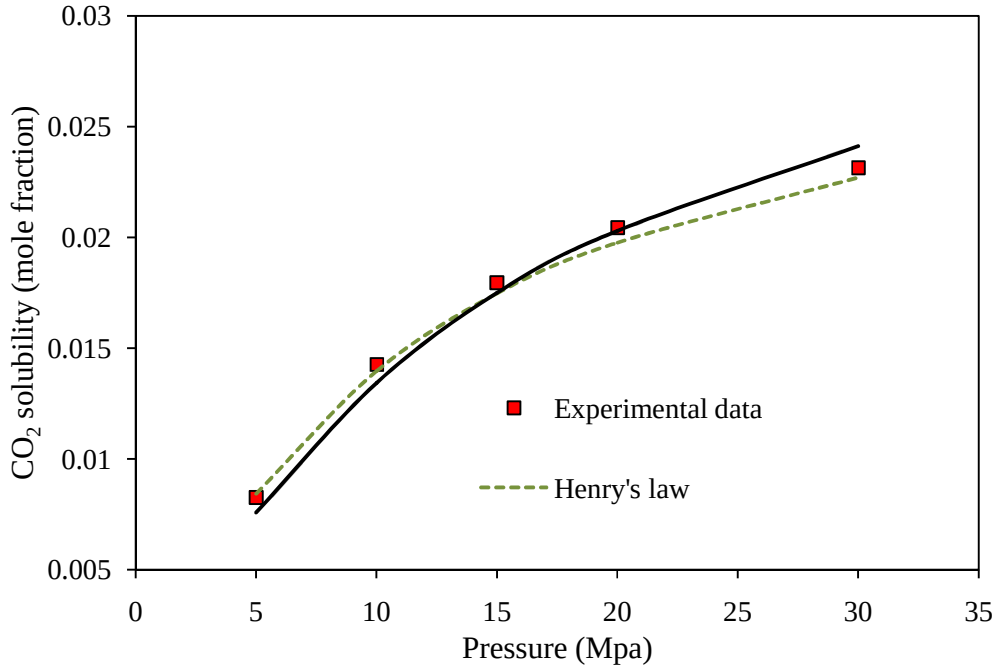

Figure 5-6: CO_2 solubility in pure water using Henry's law and modified Søreide and Whitson model at T=373.2 K. Experimental data are from Yan *et al.* (2011).

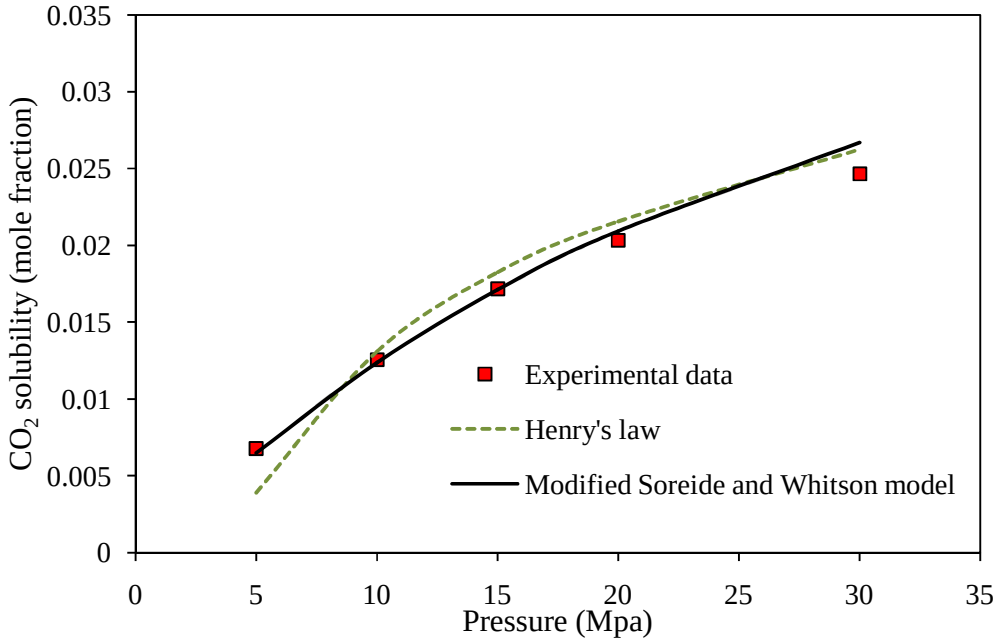

Figure 5-7: CO_2 solubility in pure water using Henry's law and modified Søreide and Whitson model at T=413.2 K. Experimental data are from Yan *et al.* (2011).

5.5. KEY FINDINGS

The results of this chapter show that the addition of water causes changes in the phase mole fractions and in the formation of the phase boundaries with pressure. Including water in the flash calculations for CO_2/hydrocarbon mixtures also causes a shift in the *p-x* diagram toward larger CO_2 concentrations because of the CO_2 loss into the aqueous phase. Moreover, the inclusion of water results in a reduction in the amount of the CO_2-rich phase, which is consistent with the CO_2 loss. The simulation case study shows that considering water in the phase behavior calculations results in a larger time to reach a given oil recovery. These phase behavior changes increase as more water is present in the system, and are likely more important in the compositional simulation of CO_2 WAG floods.

Chapter 6. Phase behavior speed up

The objective of this chapter is to speed up phase behavior calculations. As the number of phases and components increases, flash calculations become more difficult to converge and computationally more expensive, making it inefficient or even impractical for use in compositional simulators.

A possible approach to reduce the computational time of the phase equilibrium calculations is to use reduced methods. In this research, we extended the reduced flash calculations algorithm developed by Okuno *et al.* (2010b) to four phases (i.e. three hydrocarbon phases and an aqueous phase) in standalone mode. We also modified the equilibrium calculations algorithm in UTCOMP by changing the sequential steps in the flash calculation to skip more flash calculation and stability analysis without loss of accuracy.

6.1. REDUCED FLASH

The number of equations to be solved in flash calculations depends on the independent variables. In the conventional flash based on equi-fugacity equations, the equilibrium ratios are usually considered as independent variables. In this method, multi-phase flash calculations consist of $N_C \times (N_P\text{-}1)$ nonlinear equations; therefore, an increase in the number of components or number of phases increases the computational time of flash calculations. A significant part of the computational time in this method is spent on constructing the Jacobian matrix and calculating its inverse to solve the system of equations in Newton's iterations. Li and Johns (2006) proposed a reduced flash approach in which the number of independent variables is $6\times(N_p\text{-}1)$; accordingly, the size of the Jacobian matrix is $6\times(N_p\text{-}1)\times 6(N_p\text{-}1)$, regardless of the number of components. They

introduced a specific two-parameter form of the BIPs using a quadratic expression to handle non-zero BIPs:

$$k_{ij} = (h_{ri} - h_{rj}) g_{ri} g_{rj}; \quad i, j = 1, ..., N_C , \tag{6.1}$$

where h_{ri} and g_{ri} are tuning parameters that must be either tuned to BIPs determined from prior fluid characterization, or more ideally re-tuned to the experimental data.

Li and Johns' (2006) reduced method is implementable for Søreide and Whitson's model as they used van der Waals mixing rule. Using two sets of BIPs for the aqueous and non-aqueous phases results in two different sets of h_{ri} and g_{ri} for the corresponding phases. Therefore, we need to identify the aqueous phase in the calculations, which can be performed easily by comparing the concentration of water in all phases. Substitution of Eq. (6.1) into the attraction term of the EOS gives five reduced parameters for each phase:

$$\theta_{kj} = \sum_{i=1}^{N_C} \eta_{ki} x_{ij}, \eta_i = (B_i, \sqrt{A_i}, \sqrt{A_i} h_{ri} g_{ri}, \sqrt{A_i} h_{ri}^2 g_{ri}, \sqrt{A_i} g_{ri}), \quad j = 1, ..., N_P , \tag{6.2}$$

where A_i and B_i are dimensionless attraction and repulsion terms of the EOS, respectively. The fugacity coefficients of each phase are only a function of these five reduced parameters (Li and Johns 2006). The phase mole fraction is defined as the sixth reduced parameter for the corresponding phase. These parameters are adopted as independent variables for equilibrium calculations in the reduced approach. Assuming the fourth phase as the reference phase, the independent variables for the four-phase reduced flash calculations are

$$\psi = \{\theta_{11}, ..., \theta_{51}, \beta_1, \theta_{12}, ..., \theta_{52}, \beta_2, \theta_{13}, ..., \theta_{53}, \beta_3\} , \tag{6.3}$$

where β_j is the phase mole fraction of phase j.

As described by Okuno *et al.* (2010c), the equations to be solved for the reduced method are expressed as

$$F_m^R = \theta_{kj} - \sum_{i=1}^{N_C} \eta_{ki} x_{ij} = 0; \qquad m = k \times j \,, \tag{6.4}$$

and

$$F_m^R = \sum_{i=1}^{N_C} (x_{iN_P} - x_{ij}) = 0; \qquad m = 5(N_P - 1) + j \,. \tag{6.5}$$

These equations are solved for (N_P-1) number of phases by the NR method. The material balance constraint, Eq. (6.5), is a part of the system of equations and thus is satisfied once convergence is achieved. However, in the conventional method the material balance must be solved in an inner loop using the Rachford-Rice iterations. The derivatives required to make the Jacobian matrix are given by Okuno (2009). To find the reduced parameters for phase N_P (*i.e.*, the reference phase), Okuno *et al.* (2010c) suggested to use the following equation, which is derived from the material balance,

$$\theta_{kN_P} = (\theta_k^z - \sum_{j=1}^{N_P - 1} \beta_j \theta_{kj}) / \beta_{N_P} \,, \tag{6.6}$$

where θ^z is the reduced parameter using the feed composition, and θ_{kj} is the phase reduced parameters updated using Newton's method. Okuno *et al.* (2010c) used Eq. (6.2) to find the value of θ^z. However, Eq. (6.2) is not applicable to find θ^z in this research, because we cannot use either aqueous or non-aqueous h_{ri} and g_{ri} parameters for the overall feed composition. Instead of using θ^z to find the reference phase reduced parameters, we use Eq. (6.2) and employ the reference phase composition obtained from the following equation using the updated phase compositions:

$$x_{iN_P} = (z_i - \sum_{j=1}^{N_P - 1} \beta_j x_{ij}) / \beta_{N_P}; \quad i = 1, ..., N_C \tag{6.7}$$

To update the phase compositions, we use the following equation:

$$dx_{ij} = \sum_{k=1}^{6(N_P-1)} \frac{\partial x_{ij}}{\partial \psi_k} d\psi_k; \qquad i = 1,...,N_C; \quad j = 1,...,N_P - 1. \tag{6.8}$$

We also update the *K*-values in the NR iterations using the following equation:

$$dK_{ij} = \sum_{k=1}^{6(N_P-1)} \frac{\partial K_{ij}}{\partial \psi_k} d\psi_k; \qquad i = 1,...,N_C; \quad j = 1,...,N_P - 1. \tag{6.9}$$

The $(\partial x_{ij}/\partial \psi_k)$ and $(\partial K_{ij}/\partial \psi_k)$ derivatives have already been computed in the construction of the Jacobian matrix; therefore, we did not add additional calculations by using these derivatives. The algorithm used in this study is an extension and modification of the algorithm proposed by Okuno *et al.* (2010c) for three-phase flash calculations. We modified their algorithm so that different sets of specific reduced parameters, h_{ri} and g_{ri}, can be used for the phases. The main steps involved in the NR solution for the four-phase reduced flash are:

1. Specify the identity of each phase (aqueous and non-aqueous phases).
2. Set the h_{ri}^{AQ} and g_{ri}^{AQ} to the corresponding aqueous phase and h_{ri}^{NA} and g_{ri}^{NA} to the remaining non-aqueous phases.
3. Calculate the initial estimate for the independent variables, θ_{kj} and β_j using Eq. (6.2) and the results obtained from SS iterations.
4. Calculate the fugacity coefficients.
5. Check the residuals of the fugacity equations with the convergence criteria. If the residuals satisfy the convergence criteria, then stop; otherwise, go to step 6.
6. Update *K*-values using

$$K_{ij} = \phi_{ir} / \phi_{ij}; \qquad i = 1,...,N_C; \quad j = 1,...,N_P; \quad j \neq r. \tag{6.10}$$

7. Calculate the compositions using the updated *K*-values and old values for the phase mole fractions.
8. Calculate the residuals using Eq. (6.4).
9. Construct the Jacobian matrix.
10. Solve the system of equations and update the independent variables.
11. Update the phase compositions using Eq. (6.8).
12. Update the reference phase composition using Eq. (6.7).
13. Calculate the reference phase reduced parameters using Eq. (6.2).
14. Update *K*-values using Eq. (6.9).
15. Go to step 4.

The convergence criteria in all calculations are chosen to be 10^{-3} for the SS and 10^{-10} for the NR iteration loop in this research.

In the following sections, we compare the four-phase reduced flash calculation algorithm described above based on its accuracy and computational cost with the conventional approach using the same software optimization level and computer processors.

6.1.1. Reduced flash versus conventional flash

To compare the reduced method with the conventional flash, we made a case study using a synthetic quaternary mixture containing carbon dioxide, methane, normal-hexadecane, and water. At low temperatures, the ternary mixture of CO_2, C_1 and nC_{16} forms a three-phase hydrocarbon vapor-liquid-liquid region (Pan and Firoozabadi 1998a). Introducing water to this system results in the formation of an aqueous phase in equilibrium with the hydrocarbon phases. The addition of water may alter the two- and three-phase hydrocarbon phase boundaries.

The pure-component properties of the mixture are listed in Table 6-1, while the BIPs for the aqueous and non-aqueous phases are shown in Table 6-2. The reduced method specific parameters for non-aqueous phases (h_{ri}^{NA} and g_{ri}^{NA}) are determined by regression to give a reasonable fit with the original BIP matrix. In the aqueous phase, the only non-zero BIPs are assumed between water and other components, which are determined using Eqs. (5.4) and (5.6). In this example, we assume that water is pure and, therefore, the value of the brine salinity parameter, c_{sw}, in Eqs.(5.1), (5.4) and (5.6) is set to zero. The h_{ri}^{AQ} and g_{ri}^{AQ} values, listed in Table 6-2, give an exact match with the k_{ij}^{AQ} using Eq. (6.1).

Table 6-1: Fluid properties for the synthetic mixture of $CO_2/C_1/nC_{16}/H_2O$

Component	Mole%	T_c (°R)	P_c (psia)	ω
CO_2	75.0	547.56	1069.8	0.225
C_1	2.5	343.08	666.6	0.008
nC_{16}	2.5	1290.60	205.8	0.742
H_2O	20.0	1165.14	3197.8	0.344

Table 6-2: BIPs for the synthetic mixture of $CO_2/C_1/nC_{16}/H_2O$

	k_{ij}^{NA}				Reduce flash parameters			
	CO_2	CH_4	$nC_{16}H_{34}$	Ref.	h_r^{NA}	g_r^{NA}	h_r^{AQ}	g_r^{AQ}
CO_2				[1]	1.0000	1.0000	0.000	Eq. (5)
CH_4	0.1000			[1]	0.0000	0.1000	0.000	Eq. (4)
$nC_{16}H_{34}$	0.1250	0.0780		[1]	1.6676	0.2805	0.000	Eq. (4)
H_2O	0.1896	0.4850	0.5000	[2]	1.2465	3.1270	1.000	1.000

[1] From Pan and Firoozabadi (1998a)

[2] From Søreide and Whitson (1992)

Figure 6-1 gives the phase mole fractions that formed at equilibrium for a 75% CO_2, 2.5% C_1, 2.5% nC_{16} and 20% H_2O mixture at T = 299.7 K. A four-phase region exists at this temperature in the pressure range of 6.98-7.27 Mpa. Figure 6-2 represents the absolute error, i.e. the difference between the reduced flash and conventional flash results.

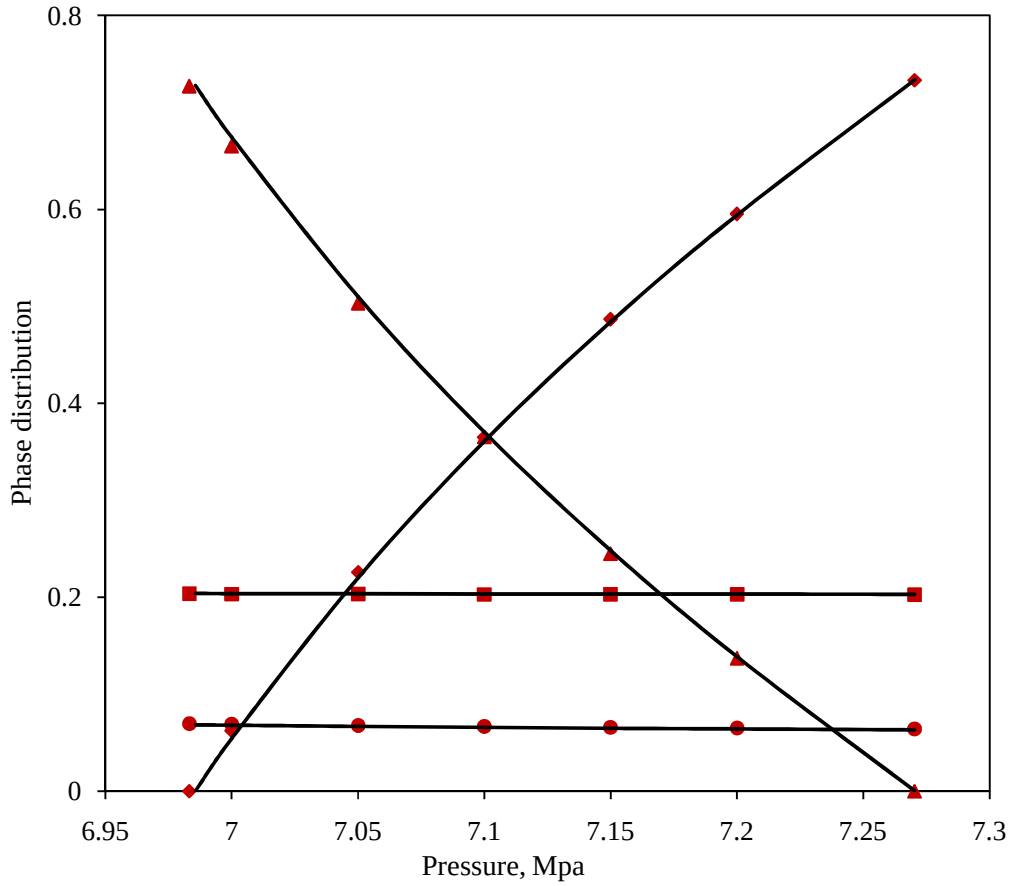

Figure 6-1: Phase mole fractions of mixture 1 at T=299.7 K (Mohebbinia *et al.* 2013); the symbols depict the results obtained by the four-phase reduced flash algorithm for the mole fractions of (▲) vapor phase, (●) oleic phase, (◆) CO_2-rich phase, and (■) aqueous phase. The solid lines give the phase mole fractions calculated by conventional flash calculations.

As shown in Figure 6-1 and Figure 6-2, the results obtained by the reduced flash are in good agreement with the conventional method results. The reduced flash method would give identical results as those of the conventional flash calculations, if the h_{ri} and g_{ri} values exactly matched the original BIP matrix. As stated by Li and Johns (2006), the best way to determine h_{ri} and g_{ri} is by tuning them to the available PVT data.

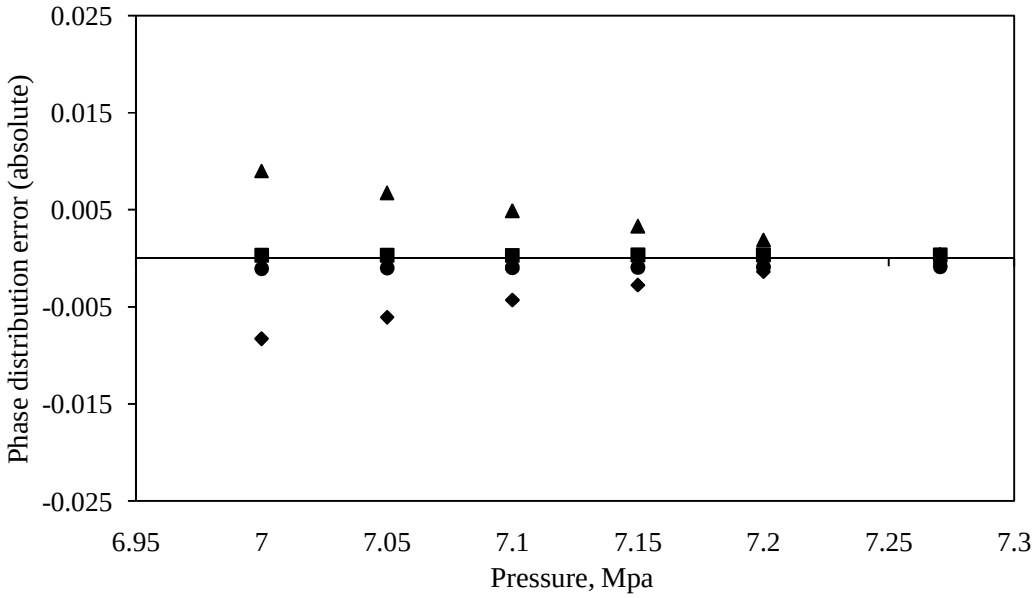

Figure 6-2: Absolute error of the reduced flash results (Mohebbinia *et al.* 2013). The symbols shows the (▲) vapor phase, (●) oleic phase, (◆) CO_2-rich phase, and (■) aqueous phase.

6.1.2. Computational time of reduced method

We demonstrate the computational time of the reduced method compared to the conventional method for the mixture given in Table 6-1, for a different number of phases and components. All of the computations are performed using an Intel(R) Xeon(R) processor at 2.0 GHz and 6.0 GB of RAM. The computations are performed with different number of components by splitting nC_{16} into as many components as needed with the same EOS properties as nC_{16}.

The calculations are initiated by conventional successive substitution (SS) iterations followed by the NR loop. The SS loop is the same in both methods; therefore, the only difference in the execution time is in the NR loop. The total computational time of iterative calculations is approximately equal to the product of the computational time per NR iteration and the number of iterations. The four-phase flash calculations take a few iterations to converge for this mixture independent of the number of components. The most time-consuming step in the NR iterations is to make the Jacobian matrix and its inverse in order to solve the systems of equations. Figure 6-3 shows the computational time required for the Jacobian matrix construction for both methods, versus the number of components for two-, three-, and four- phase flash calculations.

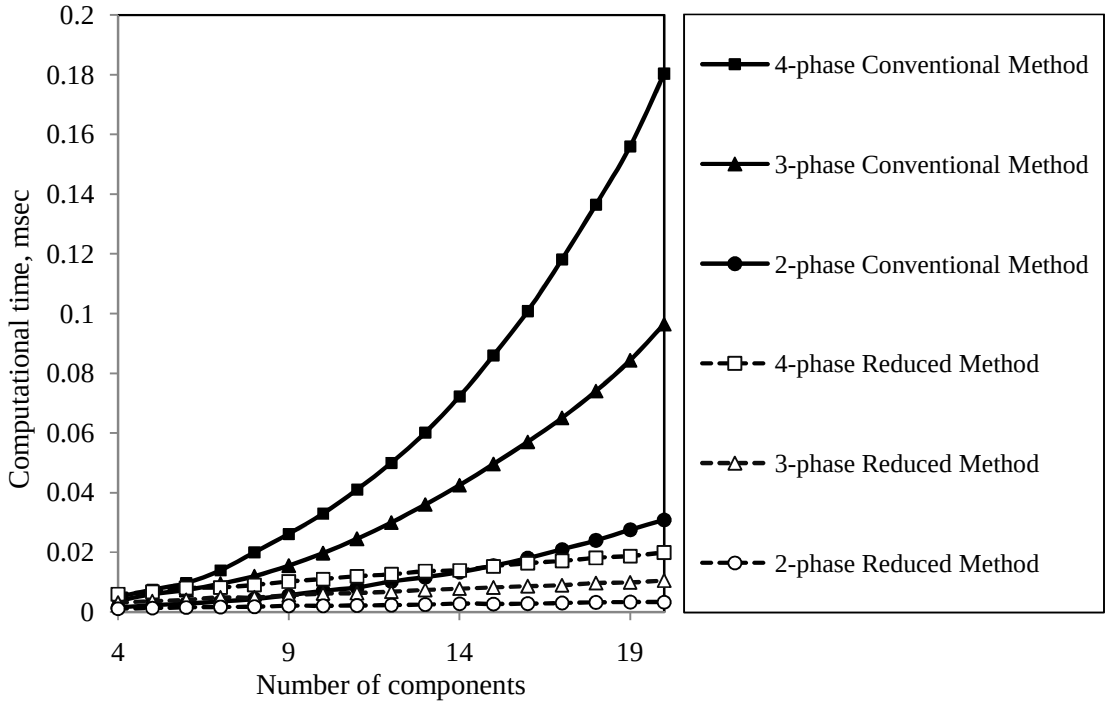

Figure 6-3: Computational time required for Jacobian matrix construction using reduced flash and conventional flash, for two-, three-, and four- phase flash calculations (Mohebbinia *et al.* 2013).

As is shown in Figure 6-3, the CPU time required to build the Jacobian matrix in conventional flash increases quickly with an increase in the number of phases and components. However, the computational time of the reduced method increases modestly, because the number of equations to be solved is independent of the number of components. Further, the four-phase reduced flash is approximately as fast as the two-phase conventional flash calculations for about 14 components. The total computational time per NR iteration for four-phase flash calculations is plotted versus the number of components in Figure 6-4.

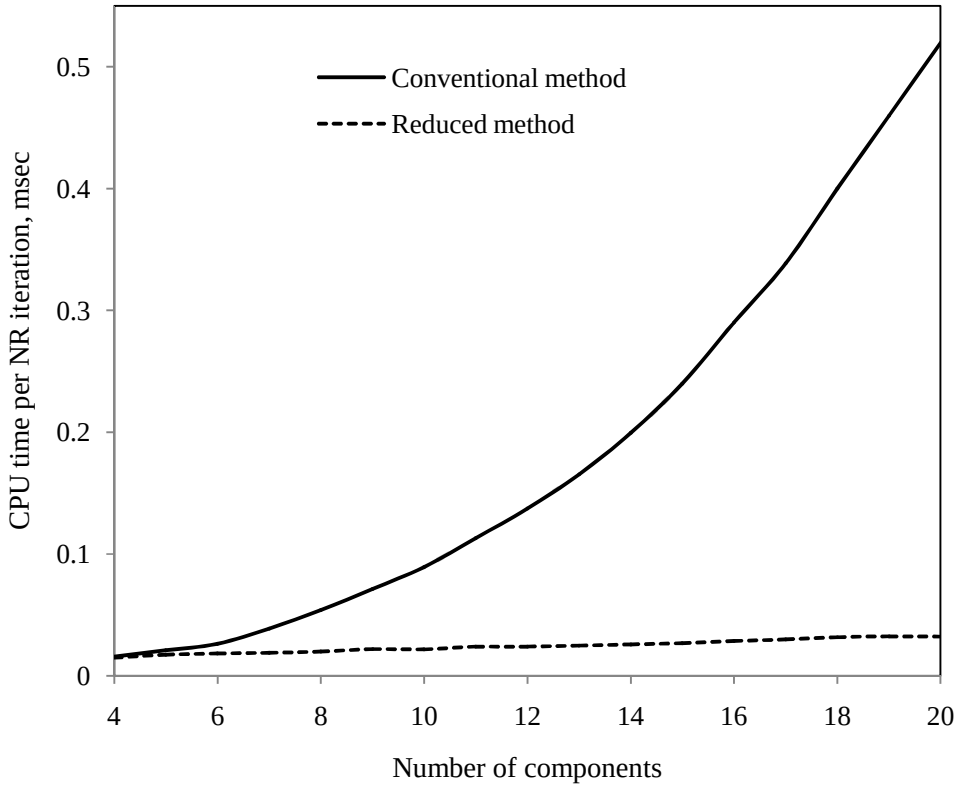

Figure 6-4: Average computational time per NR iteration for four-phase flash calculations (Mohebbinia *et al.* 2013).

While it is expected to have similar CPU time values at six components, there is a difference between the two methods owing to the computational time for solving the Rachford-Rice iterations in the conventional method. Figure 6-5 represents the speed-up obtained using the reduced method compared to the conventional approach per NR iterations. As is shown, the speed-up increases rapidly with an increase in the number of components, largely because of the reduction in the number of equations to be solved in the reduced method. For four-phase flash calculations, the number of equations to be solved is always 18 in the reduced algorithm, while it is $3N_c$ in the conventional method.

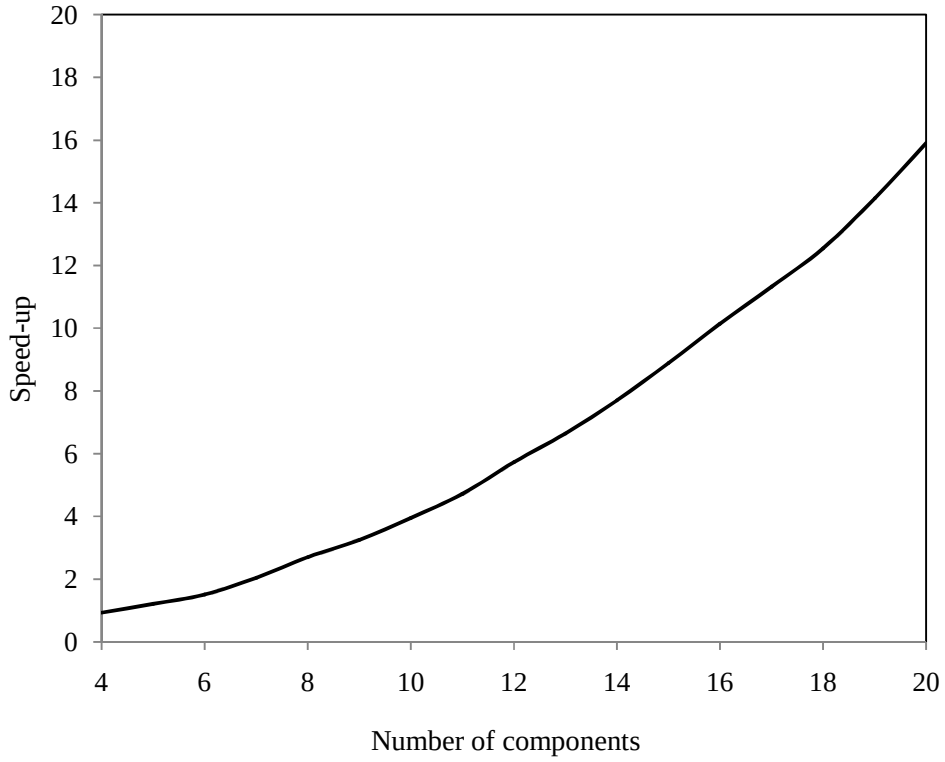

Figure 6-5: Speed-up for NR iteration in four-phase flash calculations using the reduced method (Mohebbinia *et al.* 2013).

Figure 6-6 shows the portion of the CPU time associated with solving the Rachford-Rice equations in the conventional method for four-phase flash calculations. To show the speed-up obtained just by using reduced parameters, the CPU time needed for solving Rachford-Rice equations is subtracted from the total CPU time of NR iterations in the conventional method.

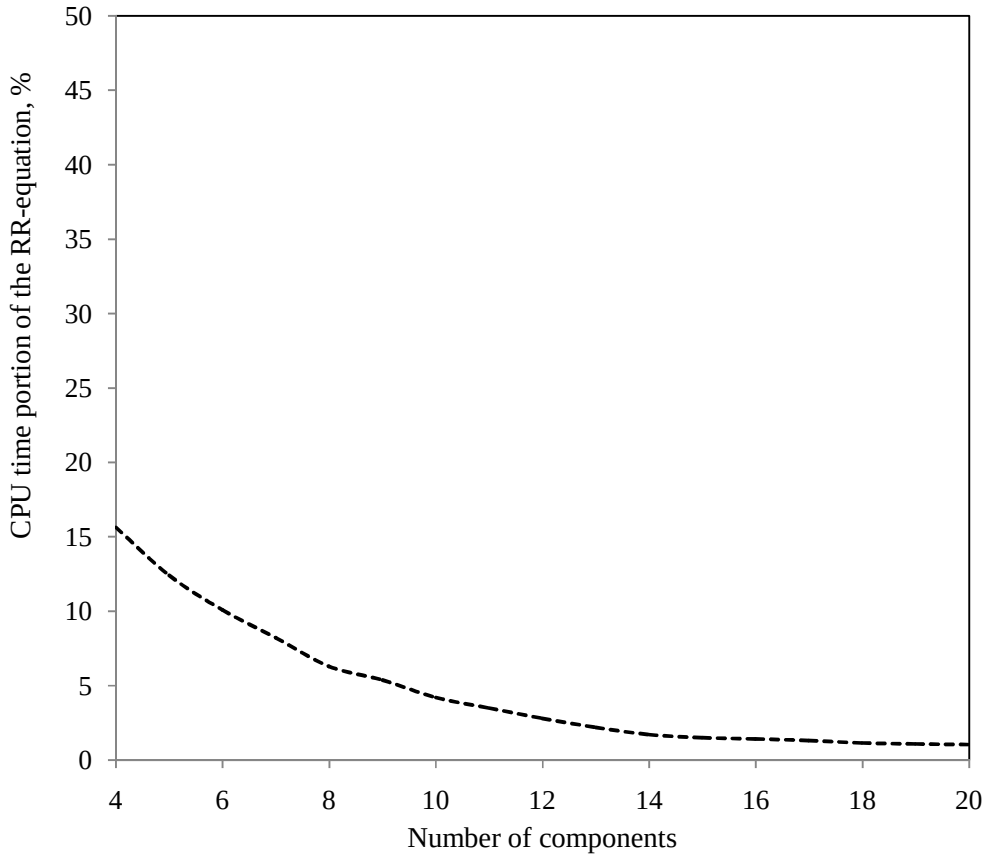

Figure 6-6: The percentage of the CPU time spent to solve Rachford-Rice equations in the NR iteration loop in the conventional method (Mohebbinia *et al.* 2013).

Figure 6-7 shows the comparison between the CPU times per NR in two methods excluding the Rachford-Rice CPU time from the time for the conventional method. Figure 6-7 shows that even after subtracting Rachford-Rice CPU time from the conventional method, our reduced method is still much faster. When this time is subtracted, the computational times for both the conventional and reduced methods become nearly the same at six components. However, when the number of components increases to values beyond six, the difference between two methods increases significantly. Figure 6-8 shows the percentage of total four-phase flash calculation CPU time spent for the NR iterations in the conventional method.

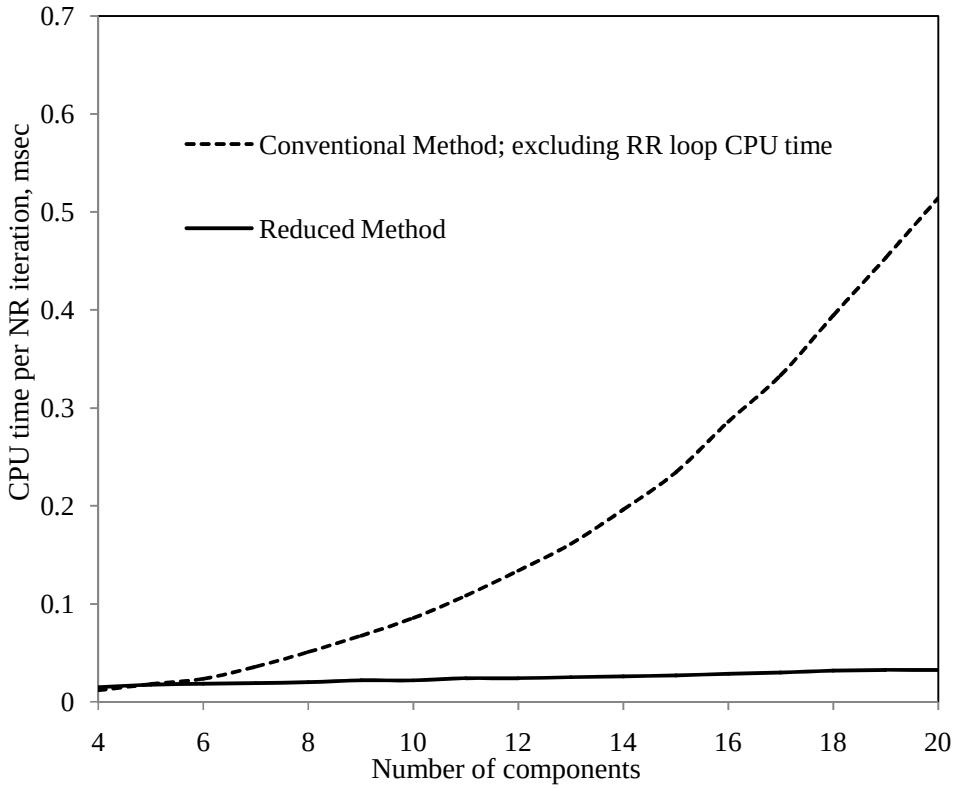

Figure 6-7: Comparison of the CPU time per NR iteration of the two methods after excluding the Rachford-Rice (RR) CPU time from the conventional method (Mohebbinia *et al.* 2013).

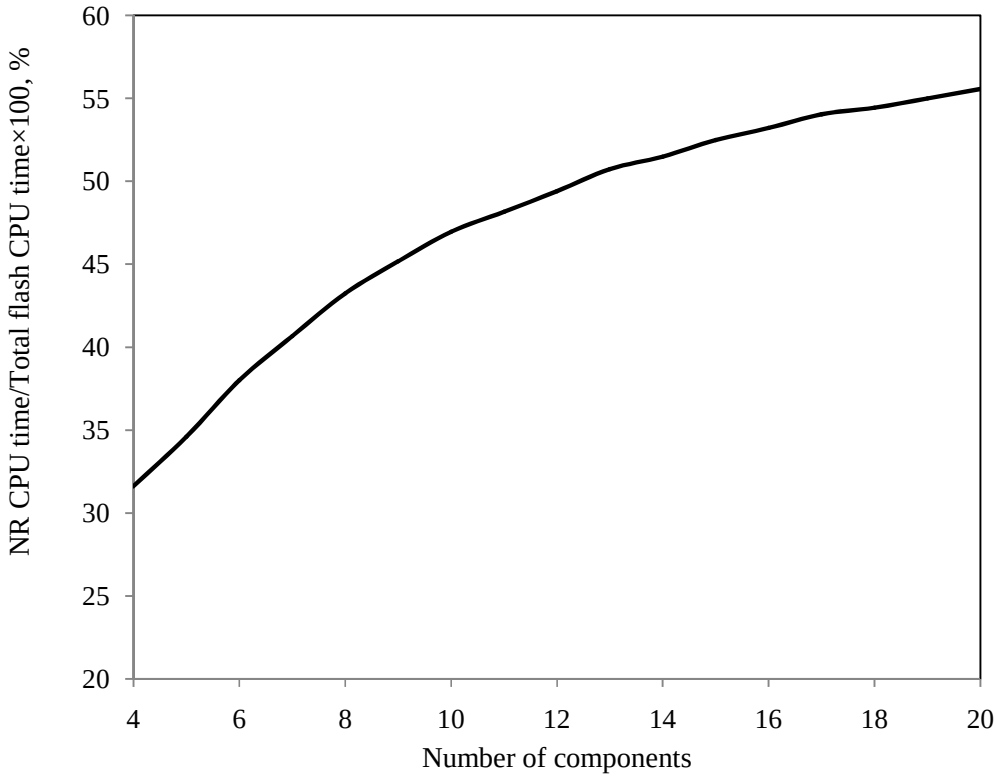

Figure 6-8: Percentage of the four-phase flash CPU time spent for the NR iterations (Mohebbinia *et al.* 2013).

The remaining CPU time is associated with SS iterations and intrinsic functions to initialize the Rachford-Rice iterations. Evidently, a considerable portion of the total flash calculations CPU time, *i.e.* 30-55%, is spent on NR iterations. Therefore, speeding up NR iterations can save substantial amount of time in performing flash calculations.

6.2. SPEED-UP OF THE EQUILIBRIUM CALCULATIONS ALGORITHM IN UTCOMP

In this section, the phase equilibrium calculations algorithm in UTCOMP is modified to save more computational time in the simulation of four-phase and three-phase systems. The new algorithm has been evaluated based on its computational time and accuracy.

6.2.1. Modifying the sequential steps in the flash calculation algorithm

Conventionally, multi-phase equilibrium calculations are sequences of stability analyses and flash calculations. Four-phase flash calculation starts with single-phase stability analysis for a specified overall composition. If the stability analysis detects the fluid as an unstable mixture, two-phase flash calculation is carried out using the results of the stability analysis as initial guess. Then, the stability analysis is done on one of the resulting phases to check its stability. If the test phase is unstable, three-phase flash calculations are performed. Again, the stability of one of the resulting phases is checked and if the instability of the test phase is detected, a four-phase flash calculation is carried out.

An essential preliminary step in doing phase equilibrium calculations is to find an initial estimate of the independent variables for the flash calculations. Using the results of the stability analysis calculations is a standard approach to initiate flash calculations. In compositional simulation, the resulting mole fractions from previous time-step can be another source of the initial guess for the current time-step flash calculation. UTCOMP can take the advantage of the phase compositions in a grid-block at previous time-step for flash calculation initiation in the following time-step, which can save one stability analysis calculation (Perschke 1988). The flowchart of the four-phase equilibrium calculation is given in Appendix C. As stated by Perschke (1988), before using the previous time-step results as initial guess for the current time-step, two conditions must be checked and satisfied:

1. A physically meaningful solution must be available for

$$\sum_{i=1}^{N_C} \frac{z_i(\frac{1}{K_{ij}}-1)}{1+\sum_{k=1}^{N_P}\beta_k(\frac{1}{K_{ik}}-1)} = 0 \qquad \text{for } j = 1,...,N_P. \tag{6.11}$$

To check this condition, it is enough to test the endpoints (*i.e.*, $\beta_i = 0$ and $\beta_i = 1$) at z^{n+1} using the following non-equalities:

$$\sum_{i=1}^{N_C} \frac{z_i^{n+1}}{K_i^n} \geq 1, \tag{6.12}$$

and

$$\sum_{i=1}^{N_C} z_i^{n+1} K_i^n \geq 1. \tag{6.13}$$

2. The Gibbs free energy of the two-phase/three-phase mixture determined by the previous time-step *K*-values (K^n) must be less than the Gibbs free energy corresponding to a single-phase/two-phase mixture having the composition of z^{n+1}. This condition is met when,

$$\sum_{j=1}^{N_P}\sum_{i=1}^{N_C} \beta_j x_{ij}\left(\ln x_{ij} + \ln \phi_{ij}\left(x_j\right)\right) < \sum_{i=1}^{N_C} z_i\left(\ln z_i + \ln \phi_i\left(z\right)\right). \tag{6.14}$$

If these two conditions are satisfied, then the previous time-step results can be used as the initial guess for the new time-step and, therefore, one stability analysis step can be skipped. When a gridblock had two phases at equilibrium at previous time-step, the checking process indicated above would contain solving a Rachford-Rice equation to split the current mixture to two phases using K^n and calculating its Gibb's free energy; however, if the gridblock had three phases at equilibrium at previous time-step, the checking procedure would involve a single-phase stability analysis, a two-phase flash using z^{n+1}, and three-phase Rachford-Rice equations solution using K^n.

In a four-phase gridblock, the steps required to check the conditions for using the previous time-step results are

(I) single-phase stability analysis

(II) two-phase flash calculation

(III) two-phase stability analysis

(IV) three-phase flash calculation, and

(V) four-phase Rachford-Rice equations solution.

If the time-steps are small enough, the conditions in Eq. (6.12) – Eq. (6.14) are satisfied, frequently; because the changes in the phase compositions from one time-step to the next one are often small. Therefore, it seems that the steps mentioned by Perschke (1988) to check the conditions in Eq. (6.12) – Eq. (6.14) are often redundant and unnecessary.

We modified the sequential steps in the flash calculation algorithm in UTCOMP to save more computational time. We can skip the checking steps, which are redundant calculations in the majority of the time-steps, and proceed to the flash calculations using the previous time-step results. If the flash calculation converges to negative mole fractions or it fails to converge using previous time-step results, we go back to single-phase stability analysis and go through all the steps of a standard multiphase flash calculation. Failure in a flash calculation for a grid-block costs more computational time compared to the Perschke's algorithm as it requires a restart of the calculations from the single-phase stability analysis. However, the number of successful flash calculations using the previous time-step results dominates. The reason is that the probability of being on the phase boundaries (i.e., where the phase change can happen) is much lower than the probability of being in the multi-phase regions (i.e., where the phases and number of phases do not change). Therefore, by skipping the checking steps we can save more

computational effort, especially for three- and four-phase gridblocks. The dashed lines in Figure D-1 in Appendix D show the modifications to the original flash calculation algorithm in UTCOMP to skip the checking steps.

6.2.2. Computational time of the modified phase behavior algorithm

Two gas injection case studies were set up to study the speed-up obtained by modifying the flash calculation algorithm. In the first case study, which is a three phase system, only hydrocarbon phases are considered in the flash calculations. In the second case study, water is also included in the flash calculations to study the computational time of a four-phase system.

6.2.2.1. Case study 1, simulation of a three-phase system

The reservoir fluid in this case study is the BSB oil with properties reported in Table 5-4 and Table 5-5. The oil displacement is simulated with an injection gas consisting of 95% CO_2 and 5% C_1 in an areal two-dimensional reservoir model. Reservoir properties are given in Table 6-3.

Table 6-3: Reservoir properties for case study 1

Dimensions	750×750×20
Number of grid cells	30×30×1
Porosity	0.25
Relative permeability	100 mD
Reservoir temperature	105 (°F)
Initial reservoir pressure	1100 (psi)
Relative permeability model	Corey
Constant bottom hole pressure of the injection well	1200 (psi)
Constant bottom hole pressure of the producer	1100 (psi)
Initial water saturation	0.5

In this case study, three hydrocarbon phases are considered in flash calculations and water is considered an isolated phase not contributing to equilibrium calculations. The number of single-phase stability analysis and two-phase flash calculations are plotted in Figure 6-9 using both old and modified algorithms up to 1 PV of gas injection. The results show a significant reduction in the number of equilibrium calculations using the new algorithm.

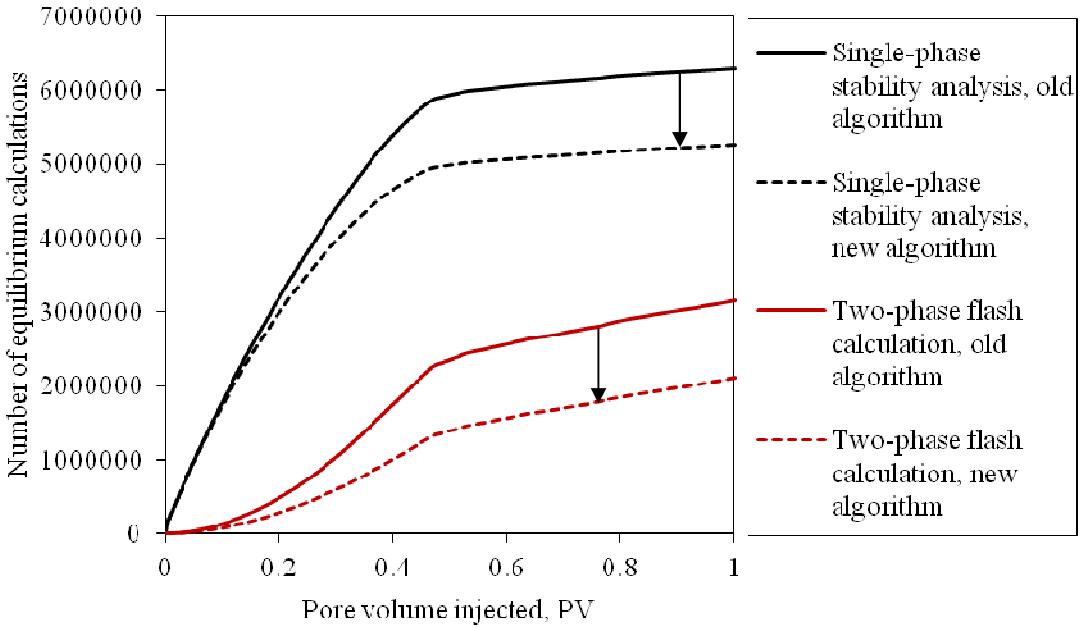

Figure 6-9: Number of single-phase stability analysis and two-phase flash calculations versus pore volume of gas injected for case study 1.

In this example the maximum number of phases in each grid-block is three. Therefore, the new algorithm skips a two-phase Rachford-Rice solution step for two-phase grid blocks, and a single-phase stability analysis and a two-phase flash calculation step for three-phase grid blocks to use the previous times step results.

The number of two-phase stability analysis and three-phase flash calculations should remain almost the same in both methods, because they are not involved in the checking steps. Figure 6-10 shows the number of two-phase stability analysis and three-phase flash calculations obtained by the old and new equilibrium calculation algorithms. As expected, the number of two-phase stability analysis and three-phase flash calculations obtained by the two methods is almost identical.

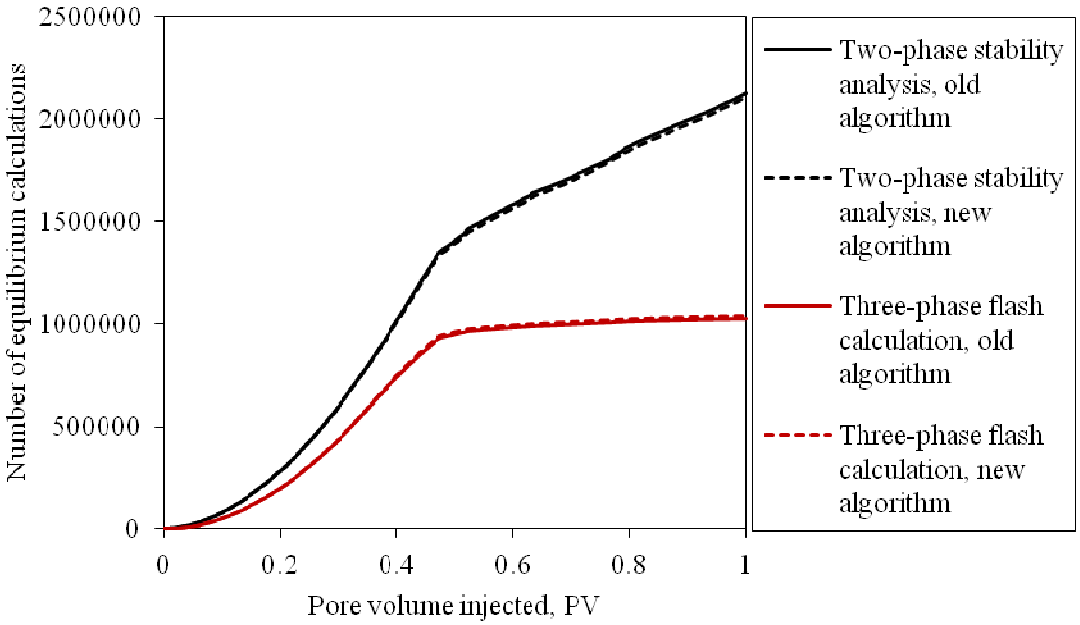

Figure 6-10: Number of two-phase stability analysis and three-phase flash calculations versus pore volume of gas injection, case study 1.

As reported in Table 6-4, skipping the checking steps causes a 33.1% reduction in the number of two-phase flash and 16.3% reduction in the number of single phase stability analysis calculations, which are identical to avoid two million equilibrium calculations.

The number of three-phase flash calculations increases by 1% due to failed three-phase flash calculations. While the number of three-phase flash calculations increased by 1%, the total simulation CPU time decreased by a factor of 29.4%, which is a significant amount of computational time. These results show that in the majority of cases, the conditions in Eq. (6.12) – Eq. (6.14) are satisfied and the checking steps to use previous time-step results are redundant.

Table 6-4: CPU time and number of equilibrium calculations, case study 1

	Number of calculations		
	New algorithm	Old algorithm	Percent change by using new algorithm, %
Two-phase flash calculations	2,108,718	3,151,339	-33.1
Three-phase flash calculations	1,034,304	1,022,552	1.2
Single-phase stability analysis	5,266,926	6,291,379	-16.3
Two-phase stability analysis	2,108,713	2,129,336	-1.0
	CPU time, sec.		
	New algorithm	Old algorithm	Percent change by using new algorithm, %
Total CPU time	687.5	973.8	-29.4

In Figure 6-11, the recovery factor curves are plotted using both algorithms. As shown in this figure, the new algorithm gives exactly the same recovery factor curve as the one obtained by the old algorithm. These results show that the new algorithm can save a significant computational time without loss of accuracy.

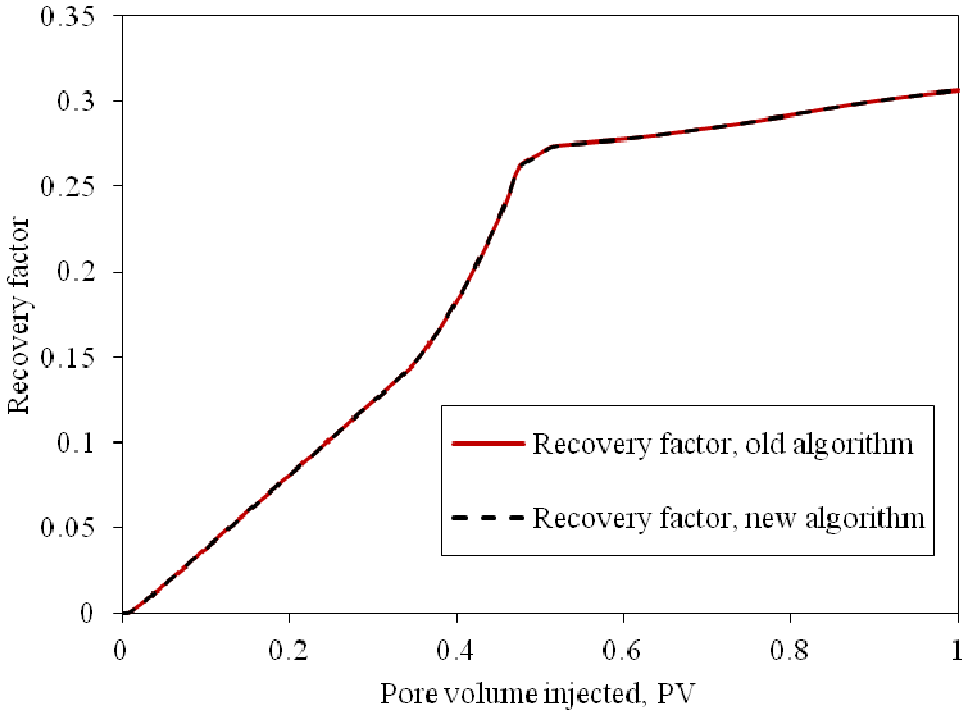

Figure 6-11: Recovery factor versus pore volume of gas injection, case study 1.

6.2.2.2. Case study 2, simulation of a four-phase system

In this case study, water is included in equilibrium calculations and a maximum of four phases is allowed to be present in the grid blocks. Fluid and reservoir properties are similar to those of case study 1. Figure 6-12-Figure 6-14 show the comparisons of the number of equilibrium calculations using the new and old algorithms. As expected, in four-phase system, the new algorithm skips more number of flash calculations and stability analysis steps than in the three-phase system.

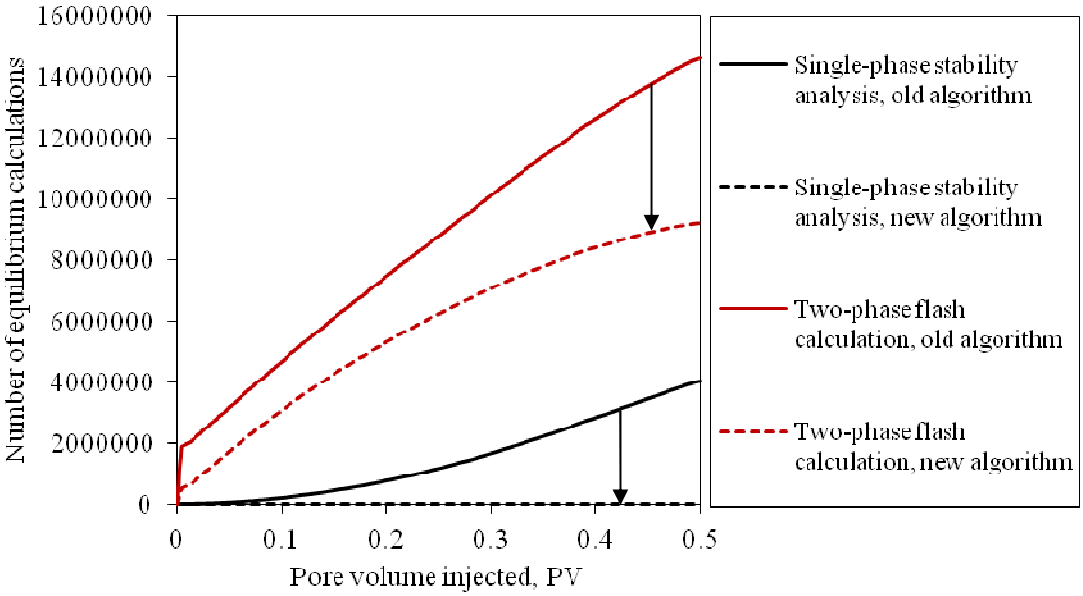

Figure 6-12: Number of single-phase stability analysis and two-phase flash calculations versus pore volume of gas injected, case study 2.

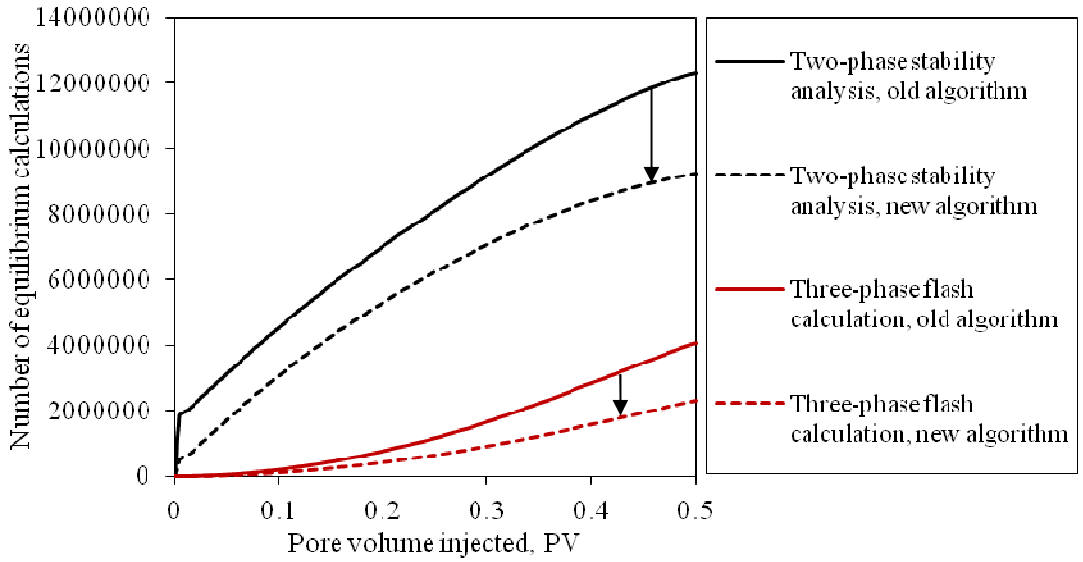

Figure 6-13**:** Number of two-phase stability analysis and three-phase flash calculations versus pore volume of gas injected, case study 2.

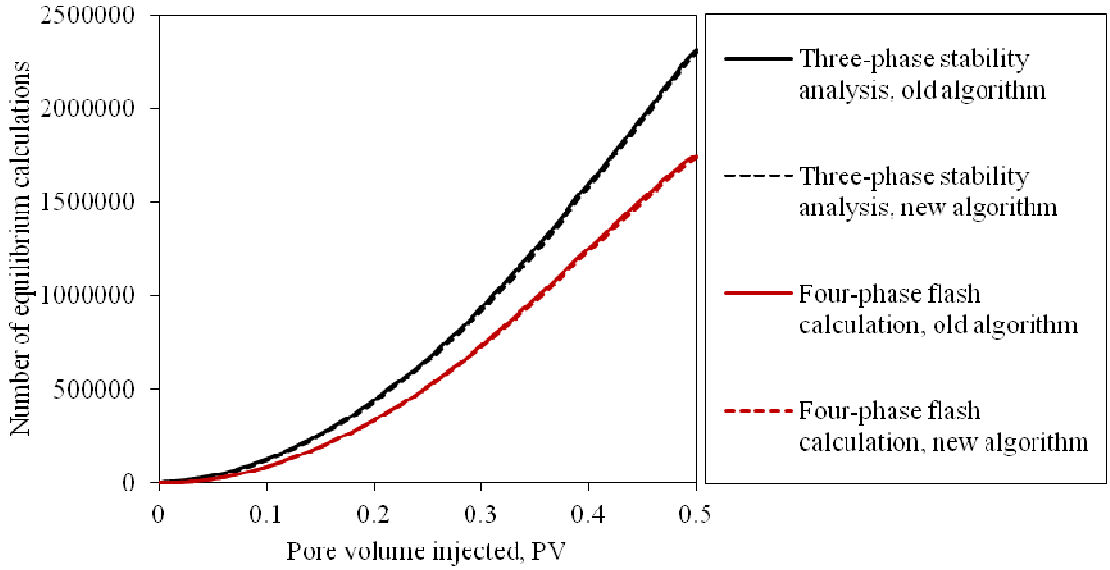

Figure 6-14**:** Number of three-phase stability analysis and four-phase flash calculations versus pore volume of gas injection, case study 2.

The total number of equilibrium calculations and the computational time of the simulation for 0.5 PV of gas injection are reported in Table 6-5. In this case study, the total speed-up by using the new algorithm for flash calculations is 46.6%.

Table 6-5: Number of equilibrium calculation steps in new and old algorithm

	Number of calculations		
	New algorithm	Old algorithm	Percent change (%)
Two-phase flash calculations	9232661	14629501	-36.9
Three-phase flash calculations	2305080	4061652	-43.3
Four-phase flash calculations	1738043	1747594	-0.6
Single-phase stability analysis	3899	4063657	-99.9
Two-phase stability analysis	9231759	12316110	-25.0
Three-phase stability analysis	2304031	2311332	-0.3
CPU time (sec.)			
Total CPU time	3879.6	7266.7	-46.6

The recovery factor for this case study is plotted in Figure 6-15 to show the accuracy of the results obtained by new algorithm. Again, there is a very good agreement between the recovery factor curves obtained by the two algorithms.

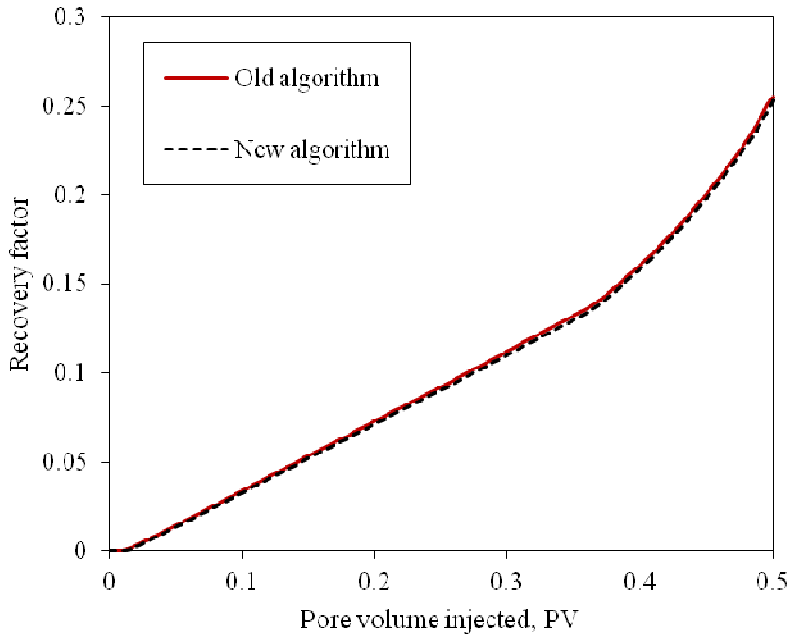

Figure 6-15**:** Recovery factor versus pore volume of gas injection, case study 2.

6.3. CHAPTER SUMMARY

A four-phase flash calculation algorithm was developed based on the reduced method of Li and Johns (2006). Their method was modified to apply the PR EOS modifications for water-containing mixtures. The developed algorithm was evaluated based on its computational time, and the results showed significant speed-up in the flash calculations using the reduced method compared to the conventional flash approach. Therefore, one significant advantage of using the reduced method is that more components can be used to properly characterize the four-phase region without loss of speed and accuracy.

Phase equilibrium calculations algorithm in UTCOMP has been improved by changing the sequential steps in the flash calculations and stability analyses. Results show that the new algorithm can save a significant computational time. The new algorithm has been evaluated based on its accuracy by comparing the recovery factor curves resulted by two algorithms. The results show a very good match between the two recovery curves.

Chapter 7. Conclusions and recommendations for future research

7.1. SUMMARY AND CONCLUSIONS

In this research, the PC-SAFT EOS was implemented in the UTCOMP simulator to model asphaltene precipitation. PC-SAFT has shown promise in modeling the phase equilibrium of asphaltic crude systems. However, it requires more computational efforts than CEOSs to perform phase behavior calculations. The additional computational time of PC-SAFT was decreased by improving the root finding algorithm and calculating the derivatives analytically. Results of a two-phase flash calculation for a mixture containing 3 to 10 components show that the increased CPU time using PC-SAFT compared to PR EOS ranges from a factor of 1.5 to 2.1 in simulation. These results suggest the feasibility of implementing the PC-SAFT EOS in a compositional simulator.

A deposition and wettability alteration model is then integrated with the thermodynamic model to simulate the dynamics of precipitated asphaltenes. Two recombined oils and three gases (CO_2, N_2 and a lean gas) were used to simulate three gas injection scenarios. Asphaltene deposition is shown to occur with pressure depletion around the production well or with gas injection everywhere in the reservoir domain swept by the injected gas. It is observed that the profile of the damaged area by asphaltene deposition depends on the reservoir fluid type. In one scenario, asphaltene deposition occurred only in the swept area by the injected gas, indicating no precipitation risk without gas injection in that case.

We defined two types of fluids in terms of the potential of asphaltene precipitation: (I) Oils with inherent potential of asphaltene precipitation, (II) Oils without initial asphaltene precipitation risk. In the asphaltene precipitation envelope of type-I fluids, a persistent window between the upper onset and lower onset pressures exists

regardless of the temperature. For type-II fluids, however, the upper and lower onset pressures coincide over a certain temperature range. Introduction of gas to the latter fluid type can create a precipitation window leading to asphaltene deposition.

The damaged caused by asphaltene deposition, through plugging and wettability alteration, was revealed as a decline in productivity index in each case. Comparison of the PI curves for reservoirs of fluid type-I and type-II suggests that the pore throat plugging around the production well is more severe in reservoirs with type-I fluid, owing to the initial asphaltene deposition around the production well because of pressure depletion.

Based on the results obtained for the CO_2 and N_2 injections, the degree of miscibility is also an important factor for the damaged caused by asphaltene deposition. While the effect of N_2 addition on APE is more severe than the effect of CO_2 injection, the CO_2 injection had a more pronounced effect on the productivity of the production well than the N_2 flood because of the longer breakthrough time in CO_2 injection.

Implementing a comprehensive phase behavior model such as PC-SAFT in a reservoir simulator makes it a valuable tool to predict asphaltene deposition potential damage. To the best of our knowledge, UTCOMP is the first reservoir simulator which uses PC-SAFT to model asphaltene precipitation.

The aqueous phase was modeled using a modification of the PR EOS. A four-phase flash calculation considering three hydrocarbon phases and an aqueous phase is developed and implemented in UTCOMP. Results of the flash calculations for CO_2/hydrocarbon mixtures reveal that the introduction of water to the system affects the phase mole fractions as well as formation of the phase boundaries with pressure. The presence of water in the flash calculations and the loss of CO_2 into the aqueous phase shifts the *p-x* diagram toward larger CO_2 concentrations. Similarly, inclusion of the

aqueous phase in flash calculation reduces the amount of the CO_2-rich phase. The simulation case studies confirm that the presence of water causes a lag in oil recovery curve. Such phase behavior changes increase with the amount of water present in the system, and are expected to be even more severe in the compositional simulation of CO_2 WAG floods.

A four-phase reduced flash algorithm was developed by using the reduced method of Li and Johns (2006). Their algorithm was modified in this research in order to apply the PR EOS to water-containing mixtures. The developed algorithm was then evaluated based on its computational time. The reduced method provided a significant speed-up in the flash calculations compared to the conventional flash approach. One crucial advantage of the reduced method is that it allows for considering more components to correctly characterize the four-phase region without considerable loss of accuracy.

The computational time of the phase equilibrium calculations algorithm in UTCOMP was improved through modifying the sequential steps in the flash calculations and stability analyses. Results show that the new algorithm decreases the computational time significantly by skipping the checking procedure based on the results from the previous time-step. The accuracy of the new algorithm was assessed by comparing the recovery factor curves achieved by the two algorithms. The results show an excellent agreement between the two recovery curves.

7.2. RECOMMENDATIONS FOR FUTURE RESEARCH

7.2.1. Tuning PC-SAFT for critical region

The drawback of PC-SAFT near critical regions can be important for miscible gas floods. Example of such gas floods is CO_2 injection. The CO_2/oil mixtures are usually found to be in the near-critical region.

To correct the behavior of SAFT-type EOSs near critical regions, several 'crossover SAFT' models (Kiselev and Ely 2000, McCabe and Kiselev 2004) have been proposed in the literature, but at the cost of additional adjustable parameters and therefore more computational time. Tuning PC-SAFT EOS for critical regions by using rescaled parameters or incorporating crossover functions is still an open research area.

7.2.2. Saving more CPU-time by switching between PR EOS and PC-SAFT during simulations

As mentioned earlier, the PC-SAFT EOS takes more computational time than the PR EOS. There are many gridblocks at which asphaltene does not precipitate. These girdblocks include single-phase hydrocarbon mixtures or two phase mixtures at the VLE state. Based on APEs, we considered that the gridblocks, which are at the VLE state, do not include the asphaltene-rich phase. The PR EOS is sufficiently accurate for gaseous and oleic phases. Therefore, a possible technique to save more computational time during simulations would be to switch from PC-SAFT to PR EOS in the gridblocks at which asphaltenes does not precipitate.

7.2.3. Developing a coupled reservoir/wellbore simulator considering asphaltene precipitation

Implementing the asphaltene precipitation model using PC-SAFT in a wellbore model and coupling it to the reservoir simulator would bring about a comprehensive tool

to study and design an optimum solution for reservoir development. A coupled reservoir/wellbore simulator can address flow restrictions in the reservoir domain as well as in the wellbore.

7.2.4. Implementing a compositional grading algorithm

Reservoir fluids are often graded because of gravity. Significant changes in fluid properties such as oil viscosity can happen because of asphaltene compositional grading. In extreme cases, the gravitational segregation of asphaltenes can lead to tar-mat formation (Panuganti *et al.* 2012), which is considered a fluid barrier in a reservoir. An algorithm for compositional grading that makes use of the PC-SAFT EOS would be a valuable tool to study the asphaltene compositional grading and tar-mat formation.

7.2.5. Incorporating the geochemical reactions into the phase behavior calculations

In this research, we did not consider chemical reactions which can take place in the aqueous phase during CO_2 EOR. It is well known that water chemistry may have a significant effect on the oil recovery process. Therefore, it would be of interest to incorporate the kinetics of potential dissolution/precipitation reactions in the aqueous phase in the compositional simulation of CO_2 floods.

7.2.6. Implementing the four-phase reduced flash in UTCOMP

Our results showed a significant speed-up in four-phase flash calculations by using a reduced method in standalone mode. We recommend implementing the four-phase reduced method in UTCOMP to reduce the additional computational time of considering the aqueous phase in phase equilibrium calculations.

Appendix A: Flowchart for density root search in PC-SAFT model

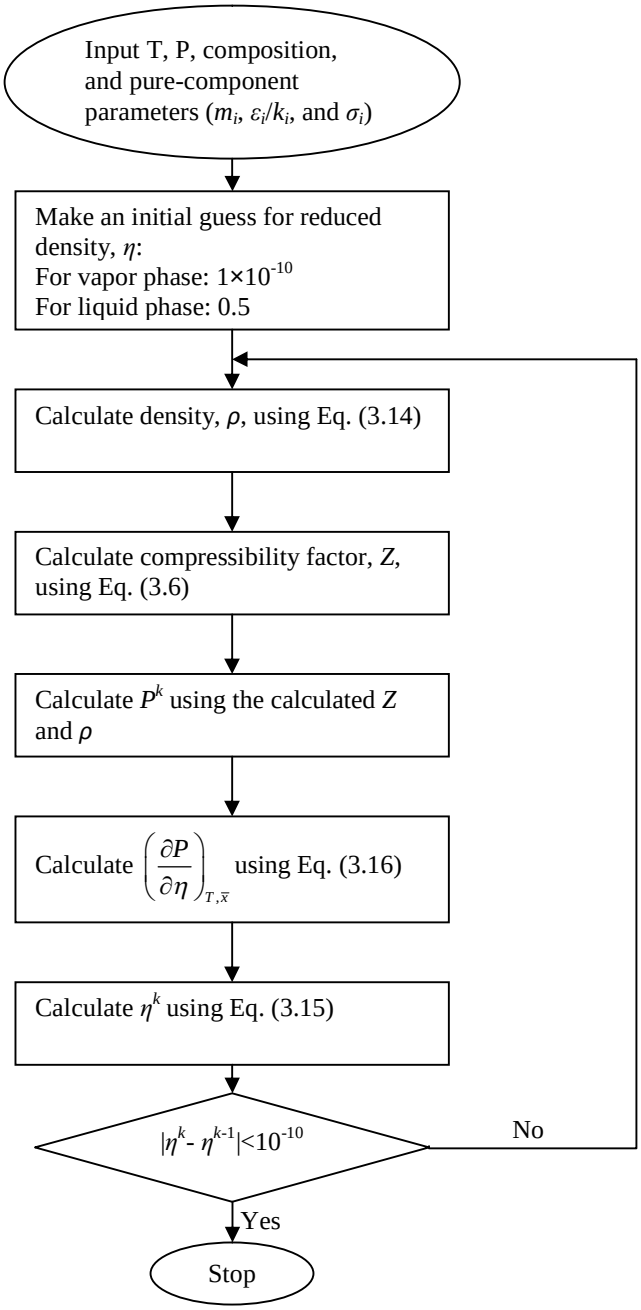

Figure A-1: Flowchart for density root search in PC-SAFT model

Appendix B: Derivatives of the chemical potential with respect to mole fraction

Taking the derivatives of Eq. (3.44) results in

$$\left[\frac{\partial}{\partial x_j}\left(\frac{\mu_i^{res}(T,v)}{\kappa T}\right)\right]_{T,P,x_{k\neq j}} = \underbrace{\left(\frac{\partial \tilde{a}^{res}}{\partial x_j}\right)_{T,P,x_{k\neq j}}}_{(1)} + \left(\frac{\partial Z}{\partial x_j}\right)_{T,P,x_{k\neq j}} + \underbrace{\left(\frac{\partial}{\partial x_j}\left(\left(\frac{\partial \tilde{a}^{res}}{\partial x_i}\right)_{T,v.x_{k\neq i}}\right)\right)_{T,P,x_{k\neq j}}}_{(2)} - \sum_{k=1} x_k \left(\frac{\partial}{\partial x_j}\left(\left(\frac{\partial \tilde{a}^{res}}{\partial x_k}\right)_{T,v,x_{m\neq k}}\right)\right)_{T,P,x_{m\neq j}} - \left(\frac{\partial \tilde{a}^{res}}{\partial x_j}\right)_{T,v,x_{k\neq j}}. \tag{B.1}$$

The expressions assigned by (1) and (2) are the only unknowns in Eq. (B.1). Term (1) is determined by taking the derivatives of Eq. (2.20) with respect to the mole fraction at constant temperature and pressure as follows:

$$\left(\frac{\partial \tilde{a}^{res}}{\partial x_j}\right)_{T,P,x_{k\neq j}} = m_j \tilde{a}^{hs} + \bar{m}\left(\frac{\partial \tilde{a}^{hs}}{\partial x_j}\right)_{T,P,x_{k\neq j}} + \left(\frac{\partial \tilde{a}^{chain}}{\partial x_j}\right)_{T,P,x_{k\neq j}} + \left(\frac{\partial \tilde{a}^{disp}}{\partial x_j}\right)_{T,P,x_{k\neq j}}. \tag{B.2}$$

The hard sphere term of the Helmholtz is a function of $\xi_n\,(n=0,...,3)$. Therefore, its derivatives are calculated as

$$\left(\frac{\partial \tilde{a}^{hs}}{\partial x_j}\right)_{T,P,x_{k\neq j}} = \sum_{n=0}^{3}\left(\frac{\partial \tilde{a}^{hs}}{\partial \xi_n}\right)\left(\frac{\partial \xi_n}{\partial x_j}\right)_{T,P,x_{k\neq j}}, \tag{B.3}$$

where,

$$\frac{\partial \tilde{a}^{hs}}{\partial \xi_0} = \frac{1}{\xi_0^2}\left[\ln(1-\xi_3)\times\left(\xi_0 - \frac{\xi_2^3}{\xi_3^2}\right) - \frac{\xi_2^3}{\xi_3(\xi_3-1)^2} + \frac{3\xi_1\xi_2}{(\xi_3-1)}\right] - \frac{1}{\xi_0}\ln(1-\xi_3), \tag{B.4}$$

$$\frac{\partial \tilde{a}^{hs}}{\partial \xi_1} = \frac{-3\xi_2}{\xi_0\left(\xi_3 - 1\right)}, \tag{B.5}$$

$$\frac{\partial \tilde{a}^{hs}}{\partial \xi_2} = \frac{1}{\xi_0}\left[\frac{3\xi_2^2}{\xi_3\left(\xi_3 - 1\right)^2} - \frac{3\xi_1}{\left(\xi_3 - 1\right)} + \frac{3\xi_2^2 \ln\left(1-\xi_3\right)}{\xi_3^2}\right], \tag{B.6}$$

$$\frac{\partial \tilde{a}^{hs}}{\partial \xi_3} = \frac{-1}{\xi_0}\left[\frac{\xi_0 - \xi_2^3/\xi_3^2}{\left(\xi_3 - 1\right)} + \frac{2\xi_2^3}{\xi_3\left(\xi_3 - 1\right)^3} + \frac{\xi_2^3}{\xi_3^2\left(\xi_3 - 1\right)^2} - \frac{3\xi_1\xi_2}{\left(\xi_3 - 1\right)^2} + \frac{2\xi_2^3 \ln\left(1-\xi_3\right)}{\xi_3^3}\right]. \tag{B.7}$$

The expression $\left(\frac{\partial \xi_n}{\partial x_j}\right)_{T,P,x_{k\neq j}}$ in Eq. (B.3) is previously determined in Eq. (3.66).

The derivatives of the chain and dispersion contributions to the Helmholtz free energy are given by

$$\left(\frac{\partial \tilde{a}^{chain}}{\partial x_j}\right)_{T,P,x_{k\neq j}} = -\left(m_j - 1\right)\ln g_{jj}^{hs} - \sum_i x_i\left(m_i - 1\right)\frac{1}{g_{ii}^{hs}}\left(\frac{\partial g_{ii}^{hs}}{\partial x_j}\right)_{T,P,x_{k\neq j}}, \tag{B.8}$$

and

$$\begin{aligned}\left(\frac{\partial \tilde{a}^{disp}}{\partial x_j}\right)_{T,P,x_{k\neq j}} &= \frac{\tilde{a}^{disp}}{\rho}\left(\frac{\partial \rho}{\partial x_j}\right)_{T,P,x_{k\neq j}} - \left(2\pi\rho\right)\overline{m^2\varepsilon\sigma^3}\left(\frac{\partial I_1}{\partial x_j}\right)_{T,P,x_{k\neq j}} - \\ &2\pi\rho I_1\left(\frac{\partial\left(\overline{m^2\varepsilon\sigma^3}\right)}{\partial x_j}\right)_{T,P,x_{k\neq j}} - \pi\rho m_j C_1 I_2\overline{m^2\varepsilon^2\sigma^3} - \pi\rho\bar{m}\left(\frac{\partial C_1}{\partial x_j}\right)_{T,P,x_{k\neq j}} I_2\overline{m^2\varepsilon^2\sigma^3} \\ &-\pi\rho\bar{m}C_1\left(\frac{\partial I_2}{\partial x_j}\right)_{T,P,x_{k\neq j}}\overline{m^2\varepsilon^2\sigma^3} - \pi\rho\bar{m}C_1 I_1\left(\frac{\partial\left(\overline{m^2\varepsilon^2\sigma^3}\right)}{\partial x_j}\right)_{T,P,x_{k\neq j}},\end{aligned} \tag{B.9}$$

where,

$$\left(\frac{\partial I_1}{\partial x_j}\right)_{T,P,x_{k\neq j}} = \sum_{i=0}^{6} a_{i,x_j}\eta^i + \sum_{i=0}^{6} a_i i\eta^{i-1}\left(\frac{\partial \eta}{\partial x_j}\right)_{T,P,x_{k\neq j}} . \tag{B.10}$$

Other partial derivatives required in Eqs (B.8) and (B.9) have been already determined through the calculation of the compressibility factor derivative. Term (2) of Eq. (B.1) is determined by taking the derivatives of Eq. (3.45) at constant temperature and pressure as follows:

$$\begin{aligned}\left(\frac{\partial}{\partial x_j}\left(\left(\frac{\partial \tilde{a}^{res}}{\partial x_i}\right)_{T,v,x_{k\neq i}}\right)\right)_{T,P,x_{k\neq j}} &= m_i\left(\frac{\partial \tilde{a}^{hs}}{\partial x_j}\right)_{T,P,x_{k\neq j}} + m_j\left(\frac{\partial \tilde{a}^{hs}}{\partial x_i}\right)_{T,v,x_{k\neq i}} + \\ \underbrace{\bar{m}\left(\frac{\partial}{\partial x_j}\left(\left(\frac{\partial \tilde{a}^{hs}}{\partial x_i}\right)_{T,v,x_{k\neq i}}\right)\right)_{T,P,x_{k\neq j}}}_{D_1} &+ \underbrace{\left(\frac{\partial}{\partial x_j}\left(\left(\frac{\partial \tilde{a}^{chain}}{\partial x_i}\right)_{T,v,x_{k\neq i}}\right)\right)_{T,P,x_{k\neq j}}}_{D_2} + \\ \underbrace{\left(\frac{\partial}{\partial x_j}\left(\left(\frac{\partial \tilde{a}^{disp}}{\partial x_i}\right)_{T,v,x_{k\neq i}}\right)\right)_{T,P,x_{k\neq j}}}_{D_3} &.\end{aligned} \tag{B.11}$$

For convenience, we have defined three abbreviations, D_1, D_2, and D_3 for the last three partial derivatives in Eq. (B.11). Referring to Eq. (3.46), $\left(\frac{\partial \tilde{a}^{hs}}{\partial x_i}\right)_{T,v,x_{k\neq i}}$ can be defined as a function of nine parameters:

$$\left(\frac{\partial \tilde{a}^{hs}}{\partial x_i}\right)_{T,v,x_{k\neq i}} = f_1\left(\xi_n, \xi_{n,x_i}, \tilde{a}^{hs}\right) \quad \text{where } n = 0,...,3. \tag{B.12}$$

Therefore, the first derivative, D_1, can be calculated using the chain rule as follows

$$D_1 = \left(\frac{\partial f_1}{\partial \tilde{a}^{hs}}\right)\left(\frac{\partial \tilde{a}^{hs}}{\partial x_j}\right)_{T,P,x_{k\neq j}} + \sum_{n=0}^{3}\left(\frac{\partial f_1}{\partial \xi_n}\right)\left(\frac{\partial \xi_n}{\partial x_j}\right)_{T,P,x_{k\neq j}} + \sum_{n=0}^{3}\left(\frac{\partial f_1}{\partial \xi_{n,x_i}}\right)\left(\frac{\partial \xi_{n,x_i}}{\partial x_j}\right)_{T,P,x_{k\neq j}} . \quad \text{(B.13)}$$

where

$$\frac{\partial f_1}{\partial \tilde{a}^{hs}} = \frac{-\xi_{0,x_i}}{\xi_0}, \quad \text{(B.14)}$$

$$\frac{\partial f_1}{\partial \xi_0} = \frac{\xi_{0,x_i}}{\xi_0^2}\tilde{a}^{hs} - \frac{\xi_{3,x_i}}{\xi_0(\xi_3-1)} + \frac{1}{\xi_0^2}\left[\frac{3\xi_1\xi_{2,x_i} + 3\xi_{1,x_i}\xi_2}{(\xi_3-1)} + \right.$$
$$\ln(1-\xi_3)\times\left(\xi_{0,x_i} + \frac{2\xi_2^3\xi_{3,x_i} - 3\xi_2^2\xi_3\xi_{2,x_i}}{\xi_3^3}\right) + \frac{\xi_{3,x_i}\left(\xi_0 - \xi_2^3/\xi_3^2\right)}{(\xi_3-1)} - \quad \text{(B.15)}$$
$$\left.\frac{3\xi_2^2\xi_{2,x_i}}{\xi_3(\xi_3-1)^2} - \frac{3\xi_1\xi_2\xi_{3,x_i}}{(\xi_3-1)^2} + \frac{\xi_2^3\xi_{3,x_i}(3\xi_3-1)}{\xi_3^2(\xi_3-1)^3}\right],$$

$$\frac{\partial f_1}{\partial \xi_1} = \frac{-1}{\xi_0}\left[\frac{3\xi_{2,x_i}}{\xi_3-1} - \frac{3\xi_2\xi_{3,x_i}}{(\xi_3-1)^2}\right], \quad \text{(B.16)}$$

$$\frac{\partial f_1}{\partial \xi_2} = \frac{-1}{\xi_0}\left[\frac{3\xi_{1,x_i}}{\xi_3-1} + \frac{1}{\xi_3^3}\ln(1-\xi_3)\times\left(6\xi_2^2\xi_{3,x_i} - 6\xi_2\xi_{2,x_i}\xi_3\right) - \frac{3\xi_1\xi_{3,x_i}}{(\xi_3-1)^2} - \frac{3\xi_2^2\xi_{3,x_i}}{\xi_3^2(\xi_3-1)}\right.$$
$$\left. - \frac{6\xi_2\xi_{2,x_i}}{\xi_3(\xi_3-1)^2} + \frac{3\xi_2^2\xi_{3,x_i}(3\xi_3-1)}{\xi_3^2(\xi_3-1)^3}\right], \quad \text{(B.17)}$$

$$\frac{\partial f_1}{\partial \xi_3}=\frac{-1}{\xi_0}\Bigg\{\frac{1}{(\xi_3-1)}\left(\xi_{0,x_i}+\frac{1}{\xi_3^3}\left(2\xi_2^3\xi_{3,x_i}-3\xi_2^2\xi_{2,x_i}\xi_3\right)\right)-\ln(1-\xi_3)\times$$

$$\left[\frac{3\xi_2^2\xi_{2,x_i}}{\xi_3^3}+\frac{3}{\xi_3^4}\left(2\xi_2^3\xi_{3,x_i}-3\xi_2^2\xi_{2,x_i}\xi_3\right)\right]-\frac{3\xi_1\xi_{2,x_i}+3\xi_{1,x_i}\xi_2}{(\xi_3-1)^2}-\frac{\xi_{3,x_i}}{(\xi_3-1)^2}\times$$

$$\left(\xi_0-\frac{\xi_2^3}{\xi_3^2}\right)+\frac{6\xi_2^2\xi_{2,x_i}}{\xi_3(\xi_3-1)^3}+\frac{3\xi_2^2\xi_{2,x_i}}{\xi_3^2(\xi_3-1)^2}+\frac{2\xi_2^3\xi_{3,x_i}}{\xi_3^3(\xi_3-1)}+\frac{3\xi_2^3\xi_{3,x_i}}{\xi_3^2(\xi_3-1)^3}+$$

$$\frac{6\xi_1\xi_2\xi_{3,x_i}}{(\xi_3-1)^3}-\frac{3\xi_2^3\xi_{3,x_i}(3\xi_3-1)}{\xi_3^2(\xi_3-1)^4}-\frac{2\xi_2^3\xi_{3,x_i}(3\xi_3-1)}{\xi_3^3(\xi_3-1)^3}\Bigg\}, \tag{B.18}$$

$$\frac{\partial f_1}{\partial \xi_{0,x_i}}=\frac{-1}{\xi_0}\left[\tilde{a}^{hs}+\ln(1-\xi_3)\right], \tag{B.19}$$

$$\frac{\partial f_1}{\partial \xi_{1,x_i}}=-\frac{3\xi_2}{\xi_0(\xi_3-1)}, \tag{B.20}$$

$$\frac{\partial f_1}{\partial \xi_{2,x_i}}=\frac{1}{\xi_0}\left[\frac{3\xi_2^2}{\xi_3^2}\ln(1-\xi_3)-\frac{3\xi_1}{(\xi_3-1)}+\frac{3\xi_2^2}{\xi_3(\xi_3-1)^2}\right], \tag{B.21}$$

$$\frac{\partial f_1}{\partial \xi_{3,x_i}}=-\frac{1}{\xi_0}\left[\frac{1}{(\xi_3-1)}\left(\xi_0-\frac{\xi_2^3}{\xi_3^2}\right)+\frac{2\xi_2^3\ln(1-\xi_3)}{\xi_3^3}-\frac{3\xi_1\xi_2}{(\xi_3-1)^2}+\frac{\xi_2^3(3\xi_3-1)}{\xi_3^2(\xi_3-1)^3}\right], \tag{B.22}$$

and

$$\left(\frac{\partial \xi_{n,x_i}}{\partial x_j}\right)_{T,P,x_{k\neq j}}=\frac{\pi}{6}m_i d_i^n\left(\frac{\partial \rho}{\partial x_j}\right)_{T,P,x_{k\neq j}}. \tag{B.23}$$

The second derivative, D_2, is determined by taking the derivative of Eq. (3.48) with respect to mole fraction at constant temperature and pressure as follows:

$$\left(\frac{\partial}{\partial x_j}\left(\left(\frac{\partial \tilde{a}^{chain}}{\partial x_i}\right)_{T,v,x_{k\neq i}}\right)\right)_{T,P,x_{k\neq j}} = (1-m_i)\frac{1}{g_{ii}^{hs}}\left(\frac{\partial g_{ii}^{hs}}{\partial x_j}\right)_{T,P,x_{k\neq j}} -$$

$$(m_j-1)\frac{1}{g_{jj}^{hs}}\left(\frac{\partial g_{jj}^{hs}}{\partial x_i}\right)_{T,v,x_{k\neq i}} - \sum_k x_k(m_k-1)\frac{-1}{\left(g_{kk}^{hs}\right)^2}\left(\frac{\partial g_{kk}^{hs}}{\partial x_j}\right)_{T,P,x_{k\neq j}}\left(\frac{\partial g_{kk}^{hs}}{\partial x_i}\right)_{T,v,x_{k\neq i}} \quad \text{(B.24)}$$

$$-\sum_k \frac{x_k(m_k-1)}{g_{kk}^{hs}}\left(\frac{\partial}{\partial x_j}\left(\left(\frac{\partial g_{kk}^{hs}}{\partial x_i}\right)_{T,v,x_{k\neq i}}\right)\right)_{T,P,x_{k\neq j}},$$

where,

$$\left(\frac{\partial g_{kk}^{hs}}{\partial x_i}\right)_{T,v,x_{k\neq i}} = f_2\left(\xi_2,\xi_3,\xi_{2,x_i},\xi_{3,x_i}\right). \quad \text{(B.25)}$$

Therefore,

$$\left(\frac{\partial}{\partial x_j}\left(\left(\frac{\partial g_{kk}^{hs}}{\partial x_i}\right)_{T,v,x_{k\neq i}}\right)\right)_{T,P,x_{k\neq j}} = \sum_{n=2}^{3}\left(\frac{\partial f_2}{\partial \xi_n}\right)\left(\frac{\partial \xi_n}{\partial x_j}\right)_{T,P,x_{k\neq j}} + \sum_{n=2}^{3}\left(\frac{\partial f_2}{\partial \xi_{n,x_i}}\right)\left(\frac{\partial \xi_{n,x_i}}{\partial x_j}\right)_{T,P,x_{k\neq j}}, \quad \text{(B.26)}$$

where

$$\frac{\partial f_2}{\partial \xi_2} = -\frac{d_k^2}{4}\left[\frac{4\xi_{2,x_i}}{(\xi_3-1)^3} - \frac{12\xi_2\xi_{3,x_i}}{(\xi_3-1)^4}\right] - \frac{3\xi_{3,x_i}d_k}{(\xi_3-1)^3}, \quad \text{(B.27)}$$

$$\frac{\partial f_2}{\partial \xi_3} = \frac{-2\xi_{3,x_i}}{(\xi_3-1)^3} - \frac{d_k}{2}\left[\frac{6\xi_{2,x_i}}{(\xi_3-1)^3} - \frac{18\xi_2\xi_{3,x_i}}{(\xi_3-1)^4}\right] - \frac{d_k^2}{4}\left[\frac{24\xi_2^2\xi_{3,x_i}}{(\xi_3-1)^5} - \frac{12\xi_2\xi_{2,x_i}}{(\xi_3-1)^4}\right], \quad \text{(B.28)}$$

$$\frac{\partial f_2}{\partial \xi_{2,x_i}} = \frac{3d_k}{2(\xi_3-1)^2} - \frac{\xi_2 d_k^2}{(\xi_3-1)^3}, \quad \text{(B.29)}$$

and (B.30)

$$\frac{\partial f_2}{\partial \xi_{3,x_i}} = \frac{1}{\left(\xi_3 - 1\right)^2} - \frac{3\xi_2 d_k}{\left(\xi_3 - 1\right)^3} + \frac{3\xi_2^2 d_k^2}{2\left(\xi_3 - 1\right)^4}.$$

In order to determine the third derivative, D_3, we considered $\left(\frac{\partial \tilde{a}^{disp}}{\partial x_i}\right)_{T,v,x_{k\neq i}}$ as

$$\left(\frac{\partial \tilde{a}^{disp}}{\partial x_i}\right)_{T,v.x_{k\neq i}} = f_3\left(\begin{array}{c}\rho, I_1, I_2, I_{1,x_i}, I_{2,x_i}, \overline{m^2\varepsilon\sigma^3}, \overline{m^2\varepsilon^2\sigma^3}, \\ \left(\overline{m^2\varepsilon\sigma^3}\right)_{x_i}, \left(\overline{m^2\varepsilon^2\sigma^3}\right)_{x_i}, \bar{m}, C_1, C_{1,x_i}\end{array}\right). \tag{B.31}$$

Therefore, we can differentiate $\left(\frac{\partial \tilde{a}^{disp}}{\partial x_i}\right)_{T,v,x_{k\neq i}}$ at constant temperature and pressure by applying the chain rule to Eq. (B.31) as follows:

$$\left(\frac{\partial}{\partial x_j}\left(\left(\frac{\partial \tilde{a}^{disp}}{\partial x_i}\right)_{T,v,x_{k\neq i}}\right)\right)_{T,P,x_{k\neq j}} = \left(\frac{\partial f_3}{\partial \rho}\right)\left(\frac{\partial \rho}{\partial x_j}\right)_{T,P,x_{k\neq j}} + \left(\frac{\partial f_3}{\partial I_1}\right)\left(\frac{\partial I_1}{\partial x_j}\right)_{T,P,x_{k\neq j}} +$$

$$\left(\frac{\partial f_3}{\partial I_2}\right)\left(\frac{\partial I_2}{\partial x_j}\right)_{T,P,x_{k\neq j}} + \left(\frac{\partial f_3}{\partial I_{1,x_i}}\right)\left(\frac{\partial I_{1,x_i}}{\partial x_j}\right)_{T,P,x_{k\neq j}} + \left(\frac{\partial f_3}{\partial I_{2,x_i}}\right)\left(\frac{\partial I_{2,x_i}}{\partial x_j}\right)_{T,P,x_{k\neq j}} +$$

$$\left(\frac{\partial f_3}{\partial \overline{m^2\varepsilon\sigma^3}}\right)\left(\frac{\partial \overline{m^2\varepsilon\sigma^3}}{\partial x_j}\right)_{T,P,x_{k\neq j}} + \left(\frac{\partial f_3}{\partial \overline{m^2\varepsilon^2\sigma^3}}\right)\left(\frac{\partial \overline{m^2\varepsilon^2\sigma^3}}{\partial x_j}\right)_{T,P,x_{k\neq j}} +$$

$$\left(\frac{\partial f_3}{\partial \left(\overline{m^2\varepsilon\sigma^3}\right)_{x_i}}\right)\left(\frac{\partial \left(\overline{m^2\varepsilon\sigma^3}\right)_{x_i}}{\partial x_j}\right)_{T,P,x_{k\neq j}} + \left(\frac{\partial f_3}{\partial \left(\overline{m^2\varepsilon^2\sigma^3}\right)_{x_i}}\right)\left(\frac{\partial \left(\overline{m^2\varepsilon^2\sigma^3}\right)_{x_i}}{\partial x_j}\right)_{T,P,x_{k\neq j}} +$$

$$\left(\frac{\partial f_3}{\partial \bar{m}}\right)\left(\frac{\partial \bar{m}}{\partial x_j}\right)_{T,P,x_{k\neq j}} + \left(\frac{\partial f_3}{\partial C_1}\right)\left(\frac{\partial C_1}{\partial x_j}\right)_{T,P,x_{k\neq j}} + \left(\frac{\partial f_3}{\partial C_{1,x_i}}\right)\left(\frac{\partial C_{1,x_i}}{\partial x_j}\right)_{T,P,x_{k\neq j}}. \tag{B.32}$$

The partial derivatives of f_3 are given in the following:

$$\frac{\partial f_3}{\partial \rho} = \frac{1}{\rho}\left(\frac{\partial \tilde{a}^{disp}}{\partial x_i}\right)_{T,v.x_{k\neq i}}, \tag{B.33}$$

$$\frac{\partial f_3}{\partial I_1} = -2\pi\rho\left(\overline{m^2\varepsilon\sigma^3}\right)_{x_i}, \tag{B.34}$$

$$\frac{\partial f_3}{\partial I_2} = -\pi\rho\left(\overline{m^2\varepsilon^2\sigma^3}\right)\left(m_i C_1 + \bar{m}C_{1,x_i}\right) - \pi\rho\left(\overline{m^2\varepsilon^2\sigma^3}\right)_{x_i} \times \bar{m}C_1, \tag{B.35}$$

$$\frac{\partial f_3}{\partial I_{1,x_i}} = -2\pi\rho\left(\overline{m^2\varepsilon\sigma^3}\right), \tag{B.36}$$

$$\frac{\partial f_3}{\partial I_{2,x_i}} = -\pi\rho\bar{m}C_1\left(\overline{m^2\varepsilon^2\sigma^3}\right), \tag{B.37}$$

$$\frac{\partial f_3}{\partial \overline{m^2\varepsilon\sigma^3}} = -2\pi\rho I_{1,x_i}, \tag{B.38}$$

$$\frac{\partial f_3}{\partial \overline{m^2\varepsilon^2\sigma^3}} = -\pi\rho\left(m_i C_1 I_2 + \bar{m}C_{1,x_i} I_2 + \bar{m}C_1 I_{2,x_i}\right), \tag{B.39}$$

$$\frac{\partial f_3}{\partial\left(\overline{m^2\varepsilon\sigma^3}\right)_{x_i}} = -2\pi\rho I_1, \tag{B.40}$$

$$\frac{\partial f_3}{\partial\left(\overline{m^2\varepsilon^2\sigma^3}\right)_{x_i}} = -\pi\rho\bar{m}C_1 I_2, \tag{B.41}$$

$$\frac{\partial f_3}{\partial \bar{m}} = -\pi\rho\left(C_{1,x_i} I_2 + C_1 I_{2,x_i}\right)\overline{m^2\varepsilon^2\sigma^3} - \pi\rho C_1 I_2\left(\overline{m^2\varepsilon^2\sigma^3}\right)_{x_i}, \tag{B.42}$$

$$\frac{\partial f_3}{\partial C_1} = -\pi\rho\left(m_i I_2 + \bar{m}I_{2,x_i}\right)\overline{m^2\varepsilon^2\sigma^3} - \pi\rho\bar{m}I_2\left(\overline{m^2\varepsilon^2\sigma^3}\right)_{x_i}, \tag{B.43}$$

$$\frac{\partial f_3}{\partial C_{1,x_i}} = -\pi\rho\bar{m}I_2\overline{m^2\varepsilon^2\sigma^3}, \tag{B.44}$$

The other partial derivatives required in Eq. (B.32) are given through equations (B.45)-(B.51).

$$\left(\frac{\partial I_{1,x_k}}{\partial x_j}\right)_{T,P,x_{m\neq j}} = \sum_{i=0}^{6}[a_{i,x_j} i\xi_{3,x_k}\eta^{i-1} + a_i i\left(\frac{\partial \xi_{3,x_k}}{\partial x_j}\right)_{T,P,x_{m\neq j}}\eta^{i-1} +$$

$$a_i i\xi_{3,x_k}(i-1)\eta^{i-2}\left(\frac{\partial \eta}{\partial x_j}\right)_{T,P,x_{m\neq j}} + \left(\frac{\partial a_{i,x_k}}{\partial x_j}\right)_{T,P,x_{m\neq j}}\eta^{i} + \tag{B.45}$$

$$a_{i,x_k} i\eta^{i-1}\left(\frac{\partial \eta}{\partial x_j}\right)_{T,P,x_{m\neq j}}],$$

where,

$$\left(\frac{\partial a_{i,x_k}}{\partial x_j}\right)_{T,P,x_{m\neq j}} = \frac{-2m_k m_j}{\bar{m}^3}a_{1i} + \frac{-2m_k m_j}{\bar{m}^3}\left(3-\frac{4}{\bar{m}}\right)a_{2i} + \frac{m_k}{\bar{m}^2}\left(\frac{4m_j}{\bar{m}^2}\right)a_{2i}, \tag{B.46}$$

$$\left(\frac{\partial I_{2,x_k}}{\partial x_j}\right)_{T,P,x_{m\neq j}} = \sum_{i=0}^{6}[b_{i,x_j} i\xi_{3,x_k}\eta^{i-1} + b_i i\left(\frac{\partial \xi_{3,x_k}}{\partial x_j}\right)_{T,P,x_{m\neq j}}\eta^{i-1} +$$

$$b_i i\xi_{3,x_k}(i-1)\eta^{i-2}\left(\frac{\partial \eta}{\partial x_j}\right)_{T,P,x_{m\neq j}} + \left(\frac{\partial b_{i,x_k}}{\partial x_j}\right)_{T,P,x_{m\neq j}}\eta^{i} + \tag{B.47}$$

$$b_{i,x_k} i\eta^{i-1}\left(\frac{\partial \eta}{\partial x_j}\right)_{T,P,x_{m\neq j}}],$$

where,

$$\left(\frac{\partial b_{i,x_k}}{\partial x_j}\right)_{T,P,x_{m\neq j}} = \frac{-2m_k m_j}{\bar{m}^3}b_{1i} + \frac{-2m_k m_j}{\bar{m}^3}\left(3-\frac{4}{\bar{m}}\right)b_{2i} + \frac{m_k}{\bar{m}^2}\left(\frac{4m_j}{\bar{m}^2}\right)b_{2i}, \tag{B.48}$$

$$\left(\frac{\partial\left(\overline{m^2\varepsilon\sigma^3}\right)_{x_i}}{\partial x_j}\right)_{T,P,x_{k\neq j}} = 2m_i m_j\left(\frac{\varepsilon_{ij}}{\kappa T}\right)\sigma_{ij}^3, \tag{B.49}$$

$$\left(\frac{\partial\left(\overline{m^2\varepsilon^2\sigma^3}\right)_{x_i}}{\partial x_j}\right)_{T,P,x_{k\neq j}} = 2m_i m_j\left(\frac{\varepsilon_{ij}}{\kappa T}\right)^2\sigma_{ij}^3, \tag{B.50}$$

and

$$\begin{aligned}\left(\frac{\partial C_{1,x_i}}{\partial x_j}\right)_{T,P,x_{k\neq j}} &= \left(\frac{\partial C_2}{\partial x_j}\right)_{T,P,x_{k\neq j}}\xi_{3,x_i} + C_2\left(\frac{\partial \xi_{3,x_i}}{\partial x_j}\right)_{T,P,x_{k\neq j}} - \\ &2C_1\left(\frac{\partial C_1}{\partial x_j}\right)_{T,P,x_{k\neq j}}\left[m_i\frac{8\eta-2\eta^2}{(1-\eta)^4} - m_i\frac{20\eta-27\eta^2+12\eta^3-2\eta^4}{(1-\eta)^2(2-\eta)^2}\right] \\ &-C_1^2 m_i\left[\frac{2\left(-2\eta^4+12\eta^3-27\eta^2+20\eta\right)}{(\eta-1)^2(\eta-2)^3} - \frac{4\left(8\eta-2\eta^2\right)}{(\eta-1)^5} - \frac{4\eta-8}{(\eta-1)^4} + \right. \\ &\left.\frac{2\left(-2\eta^4+12\eta^3-27\eta^2+20\eta\right)}{(\eta-1)^3(\eta-2)^2} + \frac{\left(8\eta^3-36\eta^2+54\eta-20\right)}{(\eta-1)^2(\eta-2)^2}\right]\left(\frac{\partial\eta}{\partial x_j}\right)_{T,P,x_{k\neq j}}.\end{aligned} \tag{B.51}$$

Appendix C: Derivatives of the fugacity with respect to pressure

Taking the derivatives of Eq. (3.43) at constant temperature and mole fractions results in

$$\left(\frac{\partial \ln \phi_i}{\partial P}\right)_{T,\bar{x}} = \left[\frac{\partial}{\partial P}\left(\frac{\mu_i^{res}(T,v)}{\kappa T}\right)\right]_{T,\bar{x}} - \frac{1}{Z}\left(\frac{\partial Z}{\partial P}\right)_{T,\bar{x}}. \tag{C.1}$$

The steps to calculate the partial derivatives in Eq. (C.1) are similar to those for calculating the derivatives with respect to mole number. As the compressibility factor also required finding the chemical potential, we should start with taking the derivatives of the compressibility factor.

B.1. DERIVATIVES OF THE COMPRESSIBILITY FACTOR WITH RESPECT TO PRESSURE

By taking the derivatives of the both sides of Eq. (3.6) we have

$$\left(\frac{\partial Z}{\partial P}\right)_{T,\bar{x}} = \left(\frac{\partial Z^{hc}}{\partial P}\right)_{T,\bar{x}} + \left(\frac{\partial Z^{disp}}{\partial P}\right)_{T,\bar{x}}. \tag{C.2}$$

The left-hand side of Eq. (C.2) is given by

$$\left(\frac{\partial Z}{\partial P}\right)_{T,\bar{x}} = \left(10^{-10}\,\frac{\mathrm{m}}{\text{Å}}\right)^3 \frac{-P}{\kappa T \rho^2}\left(\frac{\partial \rho}{\partial P}\right)_{T,\bar{x}} + \frac{Z}{P}. \tag{C.3}$$

The partial derivatives of the hard-chain term of the compressibility factor are obtained as follows:

$$\left(\frac{\partial Z^{hc}}{\partial P}\right)_{T,\bar{x}} = \bar{m}\left(\frac{\partial Z^{hs}}{\partial P}\right)_{T,\bar{x}} - \sum_i x_i\left(m_i - 1\right)\{\left(\frac{\partial\left(g_{ii}^{hs}\right)^{-1}}{\partial P}\right)_{T,\bar{x}} \rho\frac{\partial g_{ii}^{hs}}{\partial\rho} + \left(g_{ii}^{hs}\right)^{-1}\left(\frac{\partial}{\partial P}\left(\rho\frac{\partial g_{ii}^{hs}}{\partial\rho}\right)\right)_{T,\bar{x}}\}. \tag{C.4}$$

The derivative of the hard-sphere can be found using the chain rule as follows:

$$\left(\frac{\partial Z^{hs}}{\partial P}\right)_{T,\bar{x}} = \sum_{n=0}^{3}\left(\frac{\partial Z^{hs}}{\partial\xi_n}\right)\left(\frac{\partial\xi_n}{\partial P}\right)_{T,\bar{x}}, \tag{C.5}$$

where

$$\left(\frac{\partial\xi_n}{\partial P}\right)_{T,\bar{x}} = \frac{\pi}{6}\left(\frac{\partial\rho}{\partial P}\right)_{T,\bar{x}}\sum_i x_i m_i d_i^n = \frac{\xi_n}{\rho}\left(\frac{\partial\rho}{\partial P}\right)_{T,\bar{x}}. \tag{C.6}$$

The partial derivatives of the hard-sphere term of the compressibility factor with respect to ξ_n are given by Eqs. (3.67)-(3.70). The derivatives of $\left(g_{ii}^{hs}\right)^{-1}$ with respect to pressure is given as follows:

$$\left(\frac{\partial\left(g_{ii}^{hs}\right)^{-1}}{\partial P}\right)_{T,\bar{x}} = \frac{-1}{\left(g_{ii}\right)^2}\left(\frac{\partial g_{ii}^{hs}}{\partial P}\right)_{T,\bar{x}}, \tag{C.7}$$

where,

$$\left(\frac{\partial g_{ii}^{hs}}{\partial P}\right)_{T,\bar{x}} = \sum_{n=0}^{3}\left(\frac{\partial g_{ii}^{hs}}{\partial\xi_n}\right)\left(\frac{\partial\xi_n}{\partial P}\right)_{T,\bar{x}} = \left[\sum_{n=0}^{3}\left(\frac{\partial g_{ii}^{hs}}{\partial\xi_n}\right)\left(\frac{\xi_n}{P}\right)\right]\left(\frac{\partial\rho}{\partial P}\right)_{T,\bar{x}}. \tag{C.8}$$

The partial derivatives $\frac{\partial g_{ii}^{hs}}{\partial\xi_n}$ required in Eq. (C.8) are given by Eqs. (3.73)-(3.75). Term $\rho\frac{\partial g_{ii}^{hs}}{\partial\rho}$ is also a function of ξ_n, therefore

$$\left(\frac{\partial}{\partial P}\left(\rho\frac{\partial g_{ii}^{hs}}{\partial\rho}\right)\right)_{T,\bar{x}}=\sum_{n=0}^{3}\frac{\partial}{\partial\xi_n}\left(\rho\frac{\partial g_{ii}^{hs}}{\partial\rho}\right)\left(\frac{\partial\xi_n}{\partial P}\right)_{T,\bar{x}}$$
$$=\left[\sum_{n=0}^{3}\frac{\partial}{\partial\xi_n}\left(\rho\frac{\partial g_{ii}^{hs}}{\partial\rho}\right)\frac{\xi_n}{P}\right]\left(\frac{\partial\rho}{\partial P}\right)_{T,\bar{x}}, \tag{C.9}$$

where the derivatives of $\rho\frac{\partial g_{ii}^{hs}}{\partial\rho}$ with respect to ξ_n are determined previously through Eqs. (3.77)-(3.79).

Taking the derivatives of the dispersion term of the compressibility factor (i.e. given by Eq. (3.10)) with respect to pressure results in

$$\left(\frac{\partial Z^{disp}}{\partial P}\right)_{T,\bar{x}}=-2\pi\left(\frac{\partial\rho}{\partial P}\right)_{T,\bar{x}}\frac{\partial(\eta I_1)}{\partial\eta}\overline{m^2\varepsilon\sigma^3}-2\pi\rho\left(\frac{\partial}{\partial P}\left(\frac{\partial(\eta I_1)}{\partial\eta}\right)\right)_{T,\bar{x}}\overline{m^2\varepsilon\sigma^3}$$
$$-2\pi\rho\frac{\partial(\eta I_1)}{\partial\eta}\left(\frac{\partial\overline{m^2\varepsilon\sigma^3}}{\partial P}\right)_{T,\bar{x}}-\pi\bar{m}\left(\frac{\partial\rho}{\partial P}\right)_{T,\bar{x}}\left[C_1\frac{\partial(\eta I_2)}{\partial\eta}+C_2\eta I_2\right]\overline{m^2\varepsilon^2\sigma^3}$$
$$-\pi\rho\bar{m}\left[\left(\frac{\partial C_1}{\partial P}\right)_{T,\bar{x}}\frac{\partial(\eta I_2)}{\partial\eta}+C_1\left(\frac{\partial}{\partial P}\left(\frac{\partial(\eta I_2)}{\partial\eta}\right)\right)_{T,\bar{x}}\right. \tag{C.10}$$
$$\left.+\left(\frac{\partial C_2}{\partial P}\right)_{T,\bar{x}}\eta I_2+C_2\left(\frac{\partial\eta}{\partial P}\right)_{T,\bar{x}}I_2+C_2\eta\left(\frac{\partial I_2}{\partial P}\right)_{T,\bar{x}}\right]\overline{m^2\varepsilon^2\sigma^3}$$
$$-\pi\rho\bar{m}\left[C_1\frac{\partial(\eta I_2)}{\partial\eta}+C_2\eta I_2\right]\left(\frac{\partial\overline{m^2\varepsilon^2\sigma^3}}{\partial P}\right)_{T,\bar{x}}.$$

The unknowns in Eq. (C.10) are calculated through Eqs. (C.11)-(C.16). Note that the reduced density, η, is equal to ξ_3 whose derivatives with respect to pressure is previously determined in Eq. (C.6).

$$\left(\frac{\partial}{\partial P}\left(\frac{\partial(\eta I_1)}{\partial \eta}\right)\right)_{T,\bar{x}} = \sum_{i=0}^{6} a_i (i+1) i \eta^{i-1} \left(\frac{\partial \eta}{\partial P}\right)_{T,\bar{x}}, \tag{C.11}$$

$$\left(\frac{\partial \overline{m^2 \varepsilon \sigma^3}}{\partial P}\right)_{T,\bar{x}} = \left(\frac{\partial \overline{m^2 \varepsilon^2 \sigma^3}}{\partial P}\right)_{T,\bar{x}} = 0, \tag{C.12}$$

$$\left(\frac{\partial C_1}{\partial P}\right)_{T,\bar{x}} = \left(\frac{\partial C_1}{\partial \eta}\right)\left(\frac{\partial \eta}{\partial P}\right)_{T,\bar{x}}, \tag{C.13}$$

$$\left(\frac{\partial}{\partial P}\left(\frac{\partial(\eta I_2)}{\partial \eta}\right)\right)_{T,\bar{x}} = \sum_{i=0}^{6} b_i (i+1) i \eta^{i-1} \left(\frac{\partial \eta}{\partial P}\right)_{T,\bar{x}}, \tag{C.14}$$

$$\left(\frac{\partial C_2}{\partial P}\right)_{T,\bar{x}} = \left(\frac{\partial C_2}{\partial \eta}\right)\left(\frac{\partial \eta}{\partial P}\right)_{T,\bar{x}} = \left(\frac{\partial^2 C_1}{\partial \eta^2}\right)\left(\frac{\partial \eta}{\partial P}\right)_{T,\bar{x}}, \tag{C.15}$$

$$\left(\frac{\partial I_2}{\partial P}\right)_{T,\bar{x}} = \sum_{i=0}^{6} b_i i \eta^{i-1} \left(\frac{\partial \eta}{\partial P}\right)_{T,\bar{x}}, \tag{C.16}$$

where $\frac{\partial C_1}{\partial \eta}$ and $\frac{\partial^2 C_1}{\partial \eta^2}$ are given in Eqs. (3.88) and (3.90).

Substituting Eq. (C.3) and the derivatives of the hard-chain and dispersion terms of the compressibility factor into Eq. (C.2) results in a linear equation in which the only unknown is $\left(\partial \rho / \partial P\right)_{T,\bar{x}}$. The derivative of the compressibility factor is then calculated from Eq. (C.3) using the calculated $\left(\partial \rho / \partial P\right)_{T,\bar{x}}$.

B.2. DERIVATIVES OF THE CHEMICAL POTENTIAL WITH RESPECT TO PRESSURE

Taking the derivatives of Eq. (3.44) with respect to pressure at constant temperature and mole fractions results in

$$\left(\frac{\partial}{\partial P}\left(\frac{\mu_i^{res}}{\kappa T}\right)\right)_{T,\bar{x}} = \underbrace{\left(\frac{\partial \tilde{a}^{res}}{\partial P}\right)_{T,\bar{x}}}_{(1)} + \left(\frac{\partial Z}{\partial P}\right)_{T,\bar{x}} + \underbrace{\left(\frac{\partial}{\partial P}\left(\left(\frac{\partial \tilde{a}^{res}}{\partial x_i}\right)_{T,v,x_{k\neq i}}\right)\right)_{T,\bar{x}}}_{(2)}$$
$$-\sum_{k=1} x_k \left(\frac{\partial}{\partial P}\left(\left(\frac{\partial \tilde{a}^{res}}{\partial x_k}\right)_{T,v,x_{m\neq k}}\right)\right)_{T,\bar{x}} . \qquad \text{(C.17)}$$

The only unknowns in Eq. (C.17) are the expressions (1) and (2). Term (1) is determined by taking the derivatives of Eq. (2.20) with respect to pressure at constant temperature and mole fractions as follows:

$$\left(\frac{\partial \tilde{a}^{res}}{\partial P}\right)_{T,\bar{x}} = \bar{m}\left(\frac{\partial \tilde{a}^{hs}}{\partial P}\right)_{T,\bar{x}} + \left(\frac{\partial \tilde{a}^{chain}}{\partial P}\right)_{T,\bar{x}} + \left(\frac{\partial \tilde{a}^{disp}}{\partial P}\right)_{T,\bar{x}}, \qquad \text{(C.18)}$$

where

$$\left(\frac{\partial \tilde{a}^{hs}}{\partial P}\right)_{T,\bar{x}} = \sum_{n=0}^{3}\left(\frac{\partial \tilde{a}^{hs}}{\partial \xi_n}\right)\left(\frac{\partial \xi_n}{\partial P}\right)_{T,\bar{x}} = \sum_{n=0}^{3}\left(\frac{\partial \tilde{a}^{hs}}{\partial \xi_n}\right)\left(\frac{\xi_n}{\rho}\right)\left(\frac{\partial \rho}{\partial P}\right)_{T,\bar{x}}, \qquad \text{(C.19)}$$

$$\left(\frac{\partial \tilde{a}^{chain}}{\partial P}\right)_{T,\bar{x}} = -\sum_i x_i \left(m_i - 1\right)\frac{1}{g_{ii}^{hs}}\left(\frac{\partial g_{ii}^{hs}}{\partial P}\right)_{T,\bar{x}}, \qquad \text{(C.20)}$$

and

$$\left(\frac{\partial \tilde{a}^{disp}}{\partial P}\right)_{T,\bar{x}} = \left(\frac{\tilde{a}^{disp}}{\rho}\right)\left(\frac{\partial \rho}{\partial P}\right)_{T,\bar{x}} - 2\pi\rho\left(\frac{\partial I_1}{\partial P}\right)_{T,\bar{x}}\overline{m^2\varepsilon\sigma^3}$$
$$-\pi\rho\bar{m}\left(\frac{\partial C_1}{\partial P}\right)_{T,\bar{x}} I_2\overline{m^2\varepsilon^2\sigma^3} - \pi\rho\bar{m}C_1\left(\frac{\partial I_2}{\partial P}\right)_{T,\bar{x}}\overline{m^2\varepsilon^2\sigma^3}. \qquad \text{(C.21)}$$

The only undetermined expression in Eqs. (C.19)-(C.21) is $\left(\partial I_1/\partial P\right)_{T,\bar{x}}$, which is calculated as follows:

$$\left(\frac{\partial I_1}{\partial P}\right)_{T,\bar{x}} = \sum_{i=0}^{6} a_i i\eta^{i-1}\left(\frac{\partial \eta}{\partial P}\right)_{T,\bar{x}} . \tag{C.22}$$

Term (2) in Eq. (C.17) is determined by taking the derivatives of Eq. (3.45) at constant temperature and mole fractions as follows:

$$\left(\frac{\partial}{\partial P}\left(\left(\frac{\partial \tilde{a}^{res}}{\partial x_i}\right)_{T,v,x_{k\neq i}}\right)\right)_{T,\bar{x}} = m_i\left(\frac{\partial \tilde{a}^{hs}}{\partial P}\right)_{T,\bar{x}} + \underbrace{\bar{m}\left(\frac{\partial}{\partial P}\left(\left(\frac{\partial \tilde{a}^{hs}}{\partial x_i}\right)_{T,v,x_{k\neq i}}\right)\right)_{T,\bar{x}}}_{D_1} +$$
$$\underbrace{\left(\frac{\partial}{\partial P}\left(\left(\frac{\partial \tilde{a}^{chain}}{\partial x_i}\right)_{T,v,x_{k\neq i}}\right)\right)_{T,\bar{x}}}_{D_2} + \underbrace{\left(\frac{\partial}{\partial P}\left(\left(\frac{\partial \tilde{a}^{disp}}{\partial x_i}\right)_{T,v,x_{k\neq i}}\right)\right)_{T,\bar{x}}}_{D_3} . \tag{C.23}$$

Three abbreviations, D_1, D_2, and D_3 are defined here for the last three partial derivatives in Eq. (C.23). Referring to Eq. (B.12), we have

$$D_1 = \sum_{n=0}^{3}\left(\frac{\partial f_1}{\partial \xi_n}\right)\left(\frac{\partial \xi_n}{\partial P}\right)_{T,\bar{x}} + \sum_{n=0}^{3}\left(\frac{\partial f_1}{\partial \xi_{n,x_i}}\right)\left(\frac{\partial \xi_{n,x_i}}{\partial P}\right)_{T,\bar{x}} + \left(\frac{\partial f_1}{\partial \tilde{a}^{hs}}\right)\left(\frac{\partial \tilde{a}^{hs}}{\partial P}\right)_{T,\bar{x}} , \tag{C.24}$$

where

$$\left(\frac{\partial \xi_{n,x_i}}{\partial P}\right)_{T,\bar{x}} = \frac{\pi}{6} m_i d_i^n \left(\frac{\partial \rho}{\partial P}\right)_{T,\bar{x}} . \tag{C.25}$$

The second derivative, D_2, is determined by taking the derivative of Eq. (3.48) with respect to pressure at constant temperature and mole fractions as follows:

$$D_2 = (1-m_i)\frac{1}{g_{ii}^{hs}}\left(\frac{\partial g_{ii}^{hs}}{\partial P}\right)_{T,\bar{x}} - \sum_k x_k (m_k - 1)\frac{-1}{(g_{kk})^2}\left(\frac{\partial g_{kk}^{hs}}{\partial P}\right)_{T,\bar{x}}\left(\frac{\partial g_{kk}^{hs}}{\partial x_i}\right)_{T,v,x_{m\neq i}}$$
$$-\sum_k x_i (m_k - 1)\frac{1}{g_{kk}^{hs}}\left(\frac{\partial}{\partial P}\left(\left(\frac{\partial g_{kk}}{\partial x_i}\right)_{T,v,x_{m\neq i}}\right)\right)_{T,\bar{x}}, \quad \text{(C.26)}$$

where

$$\left(\frac{\partial}{\partial P}\left(\left(\frac{\partial g_{kk}}{\partial x_i}\right)_{T,v,x_{k\neq i}}\right)\right)_{T,\bar{x}} = \sum_{n=2}^{3}\frac{\partial}{\partial \xi_n}\left(\left(\frac{\partial g_{kk}}{\partial x_i}\right)_{T,v,x_{k\neq i}}\right)\left(\frac{\partial \xi_n}{\partial P}\right)_{T,\bar{x}} +$$
$$\sum_{n=2}^{3}\frac{\partial}{\partial \xi_{n,x_i}}\left(\left(\frac{\partial g_{kk}}{\partial x_i}\right)_{T,v,x_{k\neq i}}\right)\left(\frac{\partial \xi_{n,x_i}}{\partial P}\right)_{T,\bar{x}}. \quad \text{(C.27)}$$

In order to find D_3, we can apply the chain rule to Eq. (B.31) as follows:

$$D_3 = \left(\frac{\partial f_3}{\partial \rho}\right)\left(\frac{\partial \rho}{\partial P}\right)_{T,\bar{x}} + \left(\frac{\partial f_3}{\partial I_1}\right)\left(\frac{\partial I_1}{\partial P}\right)_{T,\bar{x}} + \left(\frac{\partial f_3}{\partial I_2}\right)\left(\frac{\partial I_2}{\partial P}\right)_{T,\bar{x}} +$$
$$+\left(\frac{\partial f_3}{\partial I_{1,x_i}}\right)\left(\frac{\partial I_{1,x_i}}{\partial P}\right)_{T,\bar{x}} + \left(\frac{\partial f_3}{\partial I_{2,x_i}}\right)\left(\frac{\partial I_{2,x_i}}{\partial P}\right)_{T,\bar{x}} + \quad \text{(C.28)}$$
$$+\left(\frac{\partial f_3}{\partial C_1}\right)\left(\frac{\partial C_1}{\partial P}\right)_{T,\bar{x}} + \left(\frac{\partial f_3}{\partial C_{1,x_i}}\right)\left(\frac{\partial C_{1,x_i}}{\partial P}\right)_{T,\bar{x}},$$

where

$$\left(\frac{\partial I_{1,x_k}}{\partial P}\right)_{T,\bar{x}} = \sum_{i=0}^{6}\left[a_i i\left(\frac{\partial \xi_{3,x_k}}{\partial P}\right)_{T,\bar{x}}\eta^{i-1} + a_i i(i-1)\xi_{3,x_k}\eta^{i-2}\left(\frac{\partial \eta}{\partial P}\right)_{T,\bar{x}}\right.$$
$$\left. + a_{i,x_k} i\eta^{i-1}\left(\frac{\partial \eta}{\partial P}\right)_{T,\bar{x}}\right], \quad \text{(C.29)}$$

$$\left(\frac{\partial I_{2,x_k}}{\partial P}\right)_{T,\bar{x}} = \sum_{i=0}^{6}\left[b_i i\left(\frac{\partial \xi_{3,x_k}}{\partial P}\right)_{T,\bar{x}} \eta^{i-1} + b_i i(i-1)\xi_{3,x_k}\eta^{i-2}\left(\frac{\partial \eta}{\partial P}\right)_{T,\bar{x}} \right.$$
$$\left. + b_{i,x_k} i\eta^{i-1}\left(\frac{\partial \eta}{\partial P}\right)_{T,\bar{x}}\right], \tag{C.30}$$

and

$$\left(\frac{\partial C_{1,x_i}}{\partial P}\right)_{T,\bar{x}} = \left(\frac{\partial C_2}{\partial P}\right)_{T,\bar{x}} \xi_{3,x_i} + C_2\left(\frac{\partial \xi_{3,x_i}}{\partial P}\right)_{T,\bar{x}}$$
$$-2C_1\left(\frac{\partial C_1}{\partial P}\right)_{T,\bar{x}}\left[m_i \frac{8\eta - 2\eta^2}{(1-\eta)^4} - m_i \frac{20\eta - 27\eta^2 + 12\eta^3 - 2\eta^4}{(1-\eta)^2(2-\eta)^2}\right]$$
$$-C_1^2 m_i\left[\frac{2\left(-2\eta^4 + 12\eta^3 - 27\eta^2 + 20\eta\right)}{(\eta-1)^2(\eta-2)^3} - \frac{4\left(8\eta - 2\eta^2\right)}{(\eta-1)^5} - \frac{4\eta - 8}{(\eta-1)^4} + \right. \tag{C.31}$$
$$\left. + \frac{2\left(-2\eta^4 + 12\eta^3 - 27\eta^2 + 20\eta\right)}{(\eta-1)^3(\eta-2)^2} + \frac{\left(8\eta^3 - 36\eta^2 + 54\eta - 20\right)}{(\eta-1)^2(\eta-2)^2}\right]\left(\frac{\partial \eta}{\partial P}\right)_{T,\bar{x}}.$$

Appendix D: Flow chart of the flash calculation algorithm in UTCOMP

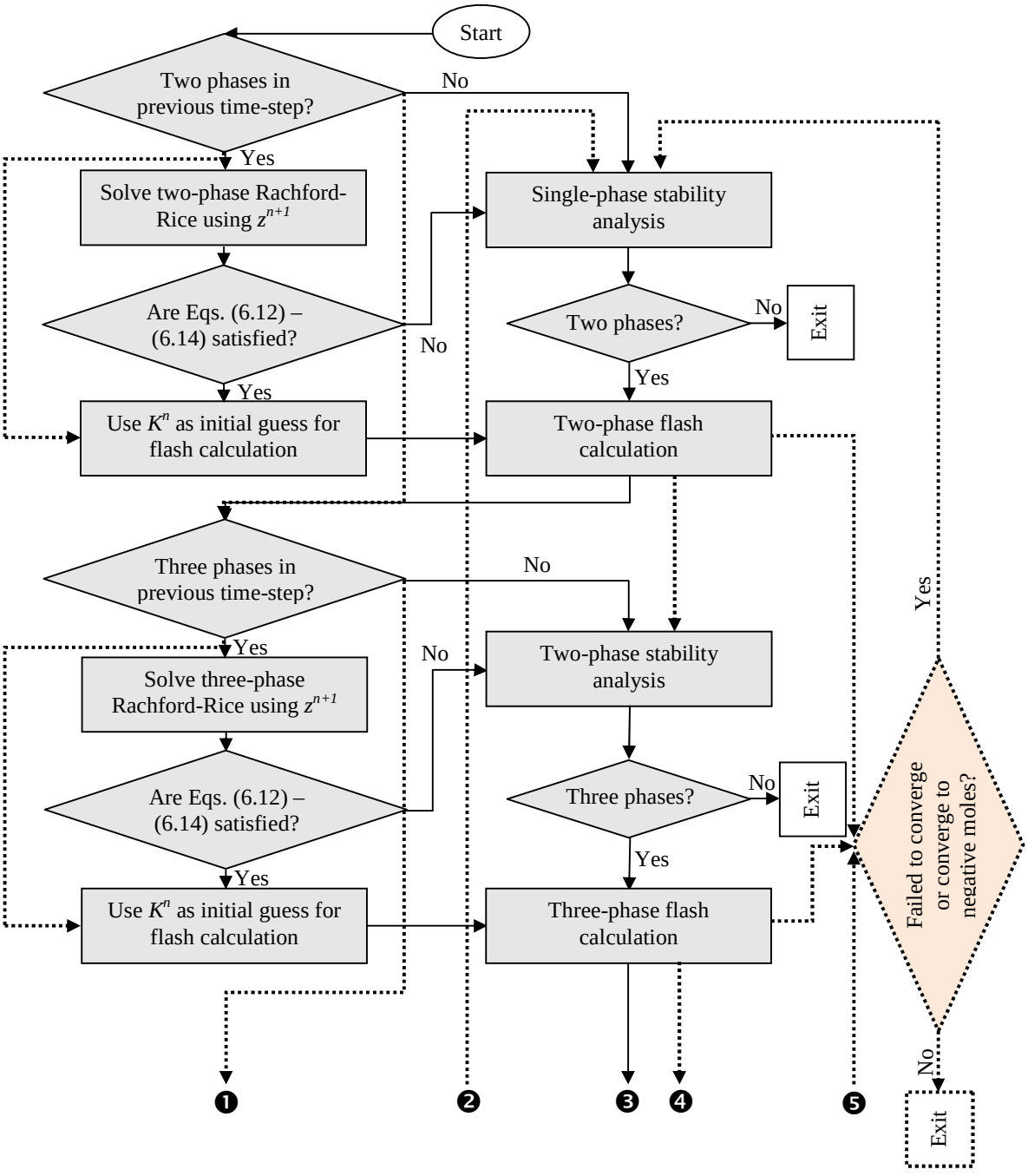

Figure D-1: Flow chart of the flash calculation algorithm in UTCOMP.

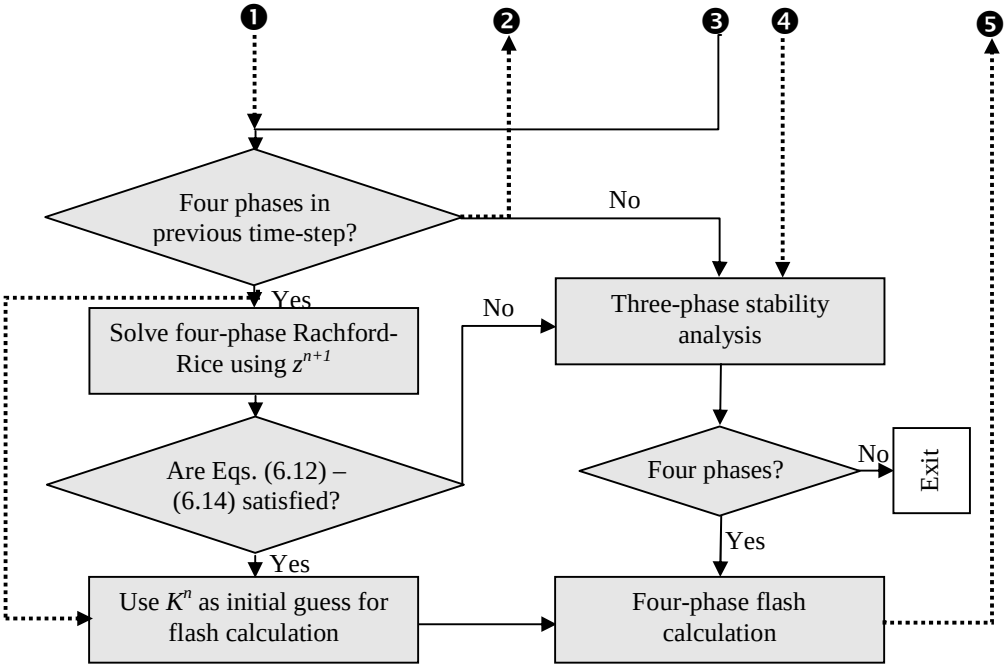

Figure D-1 (cont'd): Flow chart of the flash calculation algorithm in UTCOMP.

The dashed lines in this figure show the changes made in the original flash calculation algorithm of UTCOMP to skip the checking steps.

Glossary

Symbols

A	=	Helmholtz free energy, J
$\tilde{a}$	=	reduced Helmholtz free energy
a_i	=	attraction term in PR EOS for component *i*, Pa.m^3/mol
a_{01}, a_{02}, a_{03}	=	PC-SAFT EOS model constants
a_{RR}	=	abbreviation defined for the constraints in RR equations
b_{RR}	=	abbreviation defined for the constraints in RR equations
b_{01}, b_{02}, b_{03}	=	PC-SAFT EOS model constants
b_i	=	co-volume parameter in PR EOS, m^3/mol
C_{sus}	=	suspended asphaltene concentration in oil phase, μg/g
$\hat{C}_{sus}$	=	suspended asphaltene volume ratio in oil phase, m^3/m^3
c_{sw}	=	molality of NaCl in brine, mol/kg
d_i	=	temperature-dependent segment diameter of component *i*, Å
D_R	=	dimensionless tangent plane distance function
f_{ij}	=	fugacity of component *i* in phase *j*, Pa
G	=	Gibbs free energy function, J
$\bar{G}$	=	partial molar Gibbs free energy, J/mol
g^{hs}	=	hard-sphere radial distribution function
g_r	=	tuning parameter in reduced method
H	=	Hessian matrix
h_r	=	tuning parameter in reduced method
J	=	Jacobian matrix
k	=	absolute permeability, mD
$k_{r\ell}$	=	relative permeability of phase ℓ
K_a	=	ratio of adsorption/desorption rate constants, g/μg
k_H	=	Henry's law constant, Pa
K_{ij}	=	equilibrium ratio (*K*-value) of component *i* in phase *j*.
k_{ij}	=	binary interaction parameter between components *j* and *i*

M^{A_i} = number of association sites on molecule *i*

MW = molecular weight, kg/mol

m_i = number of segments in a chain of component *i*

$\bar{m}$ = mean segment number

N_{ads} = moles of asphaltenes adsorbed to the rock surface, mol

N_{sus} = moles of asphaltenes remained suspended in the bulk, mol

N_{me} = moles of asphaltenes deposited through mechanical entrapment, mol

N_C = number of components in the mixture

N_P = number of phases

n_{ij} = number of moles of component *i* in phase *j*, mol

P = absolute pressure, Pa

P_c = critical pressure, psia

P_{cap} = capillary pressure, psia

R = universal gas constant, J/K.mol

R_f = resistance factor

S_{coated} = area of the rock surface coated by adsorbed asphaltenes, m^3

T = absolute temperature, K

t = time, s

T_c = critical temperature, K

T_r = reduced temperature

u_o = oil Darcy velocity, m/s

v = molar volume, m^3/mol

V_t = total fluid volume, m^3

w_{ads} = mass of adsorbed solids per mass of rock, mg/g of rock

x = fluid composition

X^{A_i} = fraction of molecules *i* not bonded at site *A*

y = fluid composition

Z = compressibility factor

z = overall mole fraction

Greek letters

α_0 and α_1	=	empirical parameters for the mechanical entrapment equation, m^{-1}
β_j	=	mole fraction of phase *j*
ε_i	=	depth of square well potential for component *i*, J
ε^{AB}	=	association energy between site *A* and site *B*, J
ϕ	=	porosity
ϕ_i	=	fugacity coefficient of component *i*
Φ_{eff}	=	effective volume fraction of the solid particles
η	=	packing fraction
η_r	=	ratio of the viscosity of the suspension to the viscosity of the oil
θ_i	=	i^{th} reduced parameter
κ	=	Boltzmann's constant, J/K
κ^{AB}	=	association volume parameter
λ	=	acceleration factor in the successive substitution method
ρ	=	total number density of molecules, 1/Å
$\tilde{\rho}_R$	=	rock mass density, Kg/m^3
σ_i	=	temperature independent segment diameter of component *i*, Å
σ_{me}	=	volume of deposited asphaltenes through mechanical entrapment per initial pore volume, m^3/m^3
σ_d	=	volume of deposited asphaltenes per volume of a gridblock, m^3/m^3
ω	=	acentric factor
Ω_1 and Ω_2	=	interpolating parameters in the wettability alteration model
ψ_i	=	i^{th} independent variable for reduced method
ξ_n	=	abbreviation (n= 0, ..., 3) defined by Eq. (2.25), $Å^{n-3}$

Superscripts

AQ	=	aqueous phase
assoc	=	association
disp	=	contribution due to dispersive attraction

hc	=	hard-chain system residual contribution
hs	=	hard-sphere system residual contribution
k	=	Index for iteration steps
NA	=	non-aqueous phase
res	=	residual contribution

Subscripts

ads	=	adsorbtion
asph	=	asphaltene
me	=	deposition through mechanical entrapment
o	=	oil
R	=	rock
s	=	solid
sus	=	suspended asphaltenes
sys	=	system

Abbreviations

BIP	=	binary interaction parameter
BSB	=	Bob Slaughter Block oil
CEOS	=	cubic equation of state
CPA	=	cubic plus association
EOS	=	equation of state
IMPEC	=	implicit pressure explicit composition
NR	=	Newton-Raphson
NWE	=	North Ward Estes oil
PC-SAFT	=	perturbed-chain statistical associating fluid theory
PR	=	Peng-Robinson
PV	=	pore volume

RR	=	Rachford-Rice equations
SAFT	=	statistical associating fluid theory
SRK	=	Soave-Redlich-Kwong
SS	=	successive substitution
TPD	=	tangent plane distance function
UTCOMP	=	compositional simulator developed at The University of Texas at Austin

References

Abedini, A., S. Ashoori, F. Torabi, Y. Saki, and N. Dinarvand, 2011, "Mechanism of the Reversibility of Asphaltene Precipitation in Crude Oil," *J. Pet. Sci. Eng.*, no. 78:316-320.

Abhvani, A.S., and D.N. Beaumont, 1987, "Development of an Efficient Algorithm for the Calculation of Two-Phase Flash Equilibria," *SPE Res. Eng.*, no. 2 (4):695-702.

Agarwal, R., Y.K. Li, and L. Nghiem, 1993, "An Efficient Method for Modelling Gas Solubility in the Aqueous Phase for Compositional Simulators," *J. Can. Pet. Tech.*, no. 32 (2):44-49.

Allenson, S.J., and M.A. Walsh, 1997, "A Novel Way to Treat Asphaltene Deposition Problems Found in Oil Production," *International Symposium on Oilfield Chemistry*, Houston, Texas.

Almehaideb, R.A., 2004, "Asphaltene Precipitation and Deposition in the Near Wellbore Region: a Modeling Approach," *J. Pet. Sci. Eng.*, no. 42 (2-4):157-170.

Ammar, M.N., and H. Renon, 1987, "The Isothermal Flash Problem: New Methods for Phase Split Calculations," *AIChE J.*, no. 33 (6):926-939.

Anderko, A., 1991, "Phase Equilibria in Aqueous Systems from an Equation of State Based on the Chemical Approach," *Fluid Phase Equilibr.*, no. 65:89-110.

Andersen, S.I., and E.H. Stenby, 1996, "Thermodynamics of Asphaltene Precipitation and Dissolution Investigation of Temperature and Solvent Effects," *Fuel Sci. Technol. Int.*, no. 14 (1-2):261-287.

Anderson, W.G., 2006, "*Simulation of Chemical Flood Enhanced Oil Recovery Processes Including the Effects of Reservoir Wettability*," Master thesis, The University of Texas at Austin.

Aske, N., H. Kallevik, E.E. Johnsen, and J. Sjoblom, 2002, "Asphaltene Aggregation from Crude Oils and Model Systems Studied by High-Pressure NIR Spectroscopy," *Energy & Fuels*, no. 16 (5):1287-1295.

Baker, L.E., A.C. Pierce, and K.D. Luks, 1982, "Gibbs Energy Analysis of Phase Equilibria," *SPE J.*, no. 22 (5):731-742.

Barker, J.A., and D. Henderson, 1967, "Perturbation Theory and Equation of State for Fluids. II. A Successful Theory of Liquids," *J. Chem. Phys.*, no. 47 (11):4714-4722.

Beck, J., W.Y.S. Svrcek, and H.W. Yarranton, 2005, "Hysteresis in Asphaltene Precipitation and Redissolution," *Energy & Fuels*, no. 19 (3):944-947.

Beliveau, D., and D.A. Payne, 1991, "Analysis of a Tertiary CO_2 Flood Pilot in a Naturally Fractured Reservoir," *SPE Annual Technical Conference and Exhibition*, 6-9 October, Dallas, Texas.

Buckley, J.S., Y. Liu, X. Xie, and N.R. Morrow, 1997, "Asphaltenes and Crude Oil Wetting - The Effect of Oil Composition," *SPE J.*, no. 2 (2):107-119.

Burke, N., R. Hobbs, and S. Kashou, 1990, "Measurement and Modeling of Asphaltene Precipitation," *J. Pet. Tech.*, no. 42 (11):1440-1446.

Burya, Y.G., I.K. Yudin, V.A. Dechabo, and M.A. Anisimov, 2001, "Colloidal Properties of Crude Oil Studied by Dynamic Light-Scattering," *Int. J. Thermophy.*, no. 22:1397-1410.

Castro-Marcano, F., C.M. Colina, and C. Olivera-Fuentes, 2006, "Parametrization of Molecular-Based Equations of State: The PC-SAFT, soft-SAFT, PHSC and PSCT Models," *Polish J. Chem.*, no. 80:37–49.

Chang, Y.B., 1990, "*Development and Application of an Equation of State Compositional Simulator*," PhD dissertation, The University of Texas at Austin.

Chapman, W.G., K.E. Gubbins, G. Jackson, and M. Radosz, 1990, "New Reference Equation of State for Associating Liquids," *Ind. Eng. Chem. Res.*, no. 29 (8):1709-1721.

Collins, S.H., and J.C. Melrose, 1983, "Adsorption of Asphaltenes and Water on Reservoir Rock Minerals," *SPE Oilfield and Geothermal Chemistry Symposium*, 1-3 June, Denver, Colorado.

Crocker, M.E., and L.M. Marchin, 1988, "Wettability and Adsorption Characteristics of Crude-Oil Asphaltene and Polar Fractions," *J. Pet. Tech.*, no. 40 (4):470-474.

Delshad, M., G.A. Pope, and K. Sepehrnoori, 1996, "A Compositional Simulator for Modeling Surfactant Enhanced Aquifer Remediation," *J. Contam. Hydrol.*, no. 23 (4):303-327.

Doolittle, A., 1964, "Specific Volumes of n-Alkanes," *J. Chem. Eng. Data*, no. 9 (2):275-279.

Dubey, S.T., and M.H. Waxman, 1991, "Asphaltene Adsorption and Desorption from Mineral Surfaces," *SPE Res. Eng.*, no. 6 (3):389-395.

Enick, R.M., and S.M. Klara, 1992, "Effects of CO_2 solubility in Brine on the Compositional Simulation of CO_2 Floods," *SPE Res. Eng.*, no. 7 (2):253-258.

Escobedo, J., and A. Mansoori, 1997, "Viscometric Principles of Onsets of Colloidal Asphaltene Flocculation in Paraffinic Oils and Asphaltene Micellization in Aromatics," *SPE Prod. Facil.*, no. 12 (2):116-122.

Firoozabadi, A., and H. Pan, 2002, "Fast and Robust Algorithm for Compositional Modeling: Part I - Stability Analysis Testing," *SPE J.*, no. 7 (1):78-89.

Funke, M., R. Kleinrahm, and W. Wagne, 2002, "Measurement and Correlation of the (*P,ρ,T)* Relation of Ethane II. Saturated-Liquid and Saturated-Vapor Densities and Vapour Pressures Along the Entire Coexistence Curve," *J., Chem., Thermodyn.*, no. 34 (12):2017-2039.

Gautam, R., and W.D. Seider, 1979, "Computation of Phase and Chemical Equilibrium," *AIChE J.*, no. 25 (6):991-1007.

Gill, P.E., and W. Murray, 1974, "Newton-Type Methods for Unconstrained and Linearly Constrained Optimization," *Math. Prog.*, no. 7 (3):311-350.

Gillespie, T., 1983, "The Effect of Aggregation and Particle Size Distribution on the Viscosity of Newtonian Suspensions," *J. Colloid Int. Sci.*, no. 94 (1):166-173.

Gonzalez, D.L., 2008, "*Modeling of Asphaltene Precipitation and Deposition Tendency using the PC-SAFT Equation of State,*" PhD dissertation, Rice University.

Gonzalez, D.L., G.J. Hirasaki, J. Creek, and W.G. Chapman, 2007, "Modeling of Asphaltene Precipitation Due to Changes in Composition Using the Perturbed Chain Statistical Associating Fluid Theory Equation of State," *Energy Fuels*, no. 21 (3):1231-1242.

Gonzalez, D.L., P.D. Ting, G.J. Hirasaki, and W.G. Chapman, 2005, "Prediction of Asphaltene Instability under Gas Injection with the PC-SAFT Equation of State," *Energy Fuels*, no. 19 (4):1230-1234.

Gonzalez, D.L., F.M. Vargas, G.J. Hirasaki, and W.G. Chapman, 2008, "Modeling Study of CO_2-Induced Asphaltene Precipitation," *Energy Fuels*, no. 22:757–762.

Gonzalez, G., and A.M. Travalloni-Louvisse, 1993, "Adsorption of Asphaltene and its Effect on Oil Production," *SPE Prod. Facil.*, no. 8 (2):91-96.

Gorucu, S.E., and R.T. Johns, 2013, "Comparison of Reduced and Conventional Phase Equilibrium Calculations," *SPE Reservoir Simulation Symposium*, 18-20 February, Woodland, Texas.

Goudarzi, A., M. Delshad, K.K. Mohanty, and K. Sepehrnoori, 2012, “Impact of Matrix Block Size on Oil Recovery Response Using Surfactants in Fractured Carbonates,” *SPE Annual Technical Conference and Exhibition*, 8-10 October, San Antonio, Texas.

Gross, J., and G. Sadowski, 2001, "Perturbed-Chain SAFT: An Equation of State Based on a Perturbation Theory for Chain Molecules," *Ind. Eng. Chem. Res.*, no. 40 (4):1244–1260.

Gruesbeck, C., and R.E. Collins, 1982, "Entrainment and Deposition of Fine Particles in Porous Media," *SPE J.*, no. 22 (6):847-856.

Hammami, A., C.H. Phelps, T. Monger-Mcclure, and T.M. Little, 2000, "Asphaltene Precipitation from Live Oils: An Experimental Investigation of Onset Conditions and Reversibility," *Fuels*, no. 14 (1):14-18.

Harvey, A.H., and F.L. Smith, 2007, “Avoid Common Pitfalls When Using Henry's Law,” *Chem. Eng. Prog.*, 33-39.

Hendriks, E.M., and A.R.D. van Bergen, 1992, "Application of a Reduction Method to Phase Equilibria Calculations," *Fluid Phase Equilibr.*, no. 74:255-271.

Henry, R., and R. Metcalfe, 1983, "Multiple-Phase Generation During Carbon Dioxide Flooding," *SPE J.*, no. 23 (4):595-601.

Henry, W., 1803, “*Experiments on the Quantity of Gases Absorbed by Water at Different Temperatures and under Different Pressures*,” Vol. 93, *Philosophical Transactions*: Royal Society of London.

Hirschberg, A., L.N.J. deJong, B.A. Schipper, and J.G. Meijer, 1984, "Influence of Temperature and Pressure on Asphaltene Flocculation," *SPE J.*, no. 24 (3):283-293.

Huang, T., and J. Tracht, 1974, “The Displacement of Residual Oil By Carbon Dioxide,” *SPE Improved Oil Recovery Symposium*, Tulsa, Oklahoma.

Huron, M.J., and J. Vidal, 1979, "New Mixing Rules in Simple Equations of State for Representing Vapor-Liquid Equilibria of Strongly Non-ideal Mixtures," *Fluid Phase Equilibr.*, no. 3 (4):255-271.

Jamaluddin, A.K.M., N. Joshi, F. Iwere, and O. Gurpinar, 2002, “An Investigation of Asphaltene Instability Under Nitrogen Injection,” *SPE International Petroleum Conference and Exhibition in Mexico*, 10-12 February, Villahermosa, Mexico.

James, N.E., and A.K. Mehrotra, 1988, "V-L-S Multiphase Equilibrium in Bitumen-Diluent System," *Can. J. Chem. Eng.*, no. 66 (5):870-878.

Jensen, B.H., and A. Fredenslund, 1987, "A Simplified Flash Procedure for Multicomponent Mixtures Containing Hydrocarbons and One Non-Hydrocarbon Using Two-Parameter Cubic Equations of State," *Ind. Eng. Chem. Res.*, no. 26 (10):2129-2134.

Katz, D.L., and A. Firoozabadi, 1978, "Predicting Phase Behavior of Condensate/Crude-Oil Systems Using Methane Interaction Coefficients," *J. Pet. Tech.*, no. 30:1649-1655.

Kazeminia, A., 2013, "*Mechanistic Modeling of Low Salinity Water Injection*," Ongoing research project, The University of Texas at Austin.

Khan, S., G. Pope, and K. Sepehrnoori, 1992, "Fluid Characterization of Three-Phase CO_2/Oil Mixtures," *8th Symposium on Enhances Oil Recovery*, 22-24 April, Tulsa, Oklahoma.

Kiselev, S.B., and J.F. Ely, 2000, "Simplified Crossover SAFT Equation of State for Pure Fuids and Fuid Mixtures," *Fluid Phase Equilibr.*, no. 174: 93-113.

Kohse, B.F., and L.X. Nghiem, 2004, "Modelling Asphaltene Precipitation and Deposition in a Compositional Reservoir Simulator," *SPE/DOE Symposium on Improved Oil Recovery*, 17-21 April, Tulsa, Oklahoma.

Kontogeorgis, G.M., E.C. Voutsas, I.V. Yakoumis, and D.P. Tassios, 1996, "An Equation of State for Associating Fluids," *Ind. Eng. Chem. Res.*, no. 35 (11):4310–4318.

Kuznicki, T., J.H. Masliyah, and S. Bhattacharjee, 2008, "Molecular Dynamics Study of Model Molecules Resembling Asphaltene-Like Structures in Aqueous Organic Solvent Systems," *Energy & Fuels*, no. 22: 2379–2389

Leontaritis, K.J., 1988, "*Asphaltene Deposition: A Thermodynamic-Colloidal Model*," PhD dissertation, University of Illinois.

Leontaritis, K.J., 1996, "The Asphaltene and Wax Deposition Envelopes," *Fuel Sci. Tech. Int.*, no. 14 (1-2):13-39.

Leontaritis, K.J., 1998, "Asphaltene Near-wellbore Formation Damage Modeling," *SPE Formation Damage Control Conference*, 18-19 February, Lafayette, Louisiana.

Leontaritis, K.J., J.O. Amaefule, and R.E. Charles, 1994, "A Systematic Approach for the Prevention and Treatment of Formation Damage Caused by Asphaltene Deposition," *SPE Production & Facilities*, no. 9 (3):157-164.

Leontaritis, K.J., and G.A. Mansoori, 1987, “Asphaltene Flocculation During Oil Production and Processing: A Thermodynamic Colloidal Model,” *SPE International Symposium on Oilfield Chemistry*, 4-6 February, San Antonio, Texas.

Li, Y., and R.T. Johns, 2006, "Rapid Flash Calculations for Compositional Simulation," *SPE Res. Eval. Eng.*, no. 9 (5):521-529.

Li, Z., and A. Firoozabadi, 2009, "Cubic-Plus-Association Equation of State for Water-Containing Mixtures: Is Cross Association Necessary?" *AIChE J.*, no. 55 (7):1803-1813.

Li, Z., and A. Firoozabadi, 2010, "Cubic-Plus-Association Equation of State for Asphaltene Precipitation in Live Oils," *Energy & Fuels*, no. 24:2956–2963.

Lim, M.T., S.A. Khan, K. Sepehrnoori, and G.A. Pope, 1992, “Simulation of Carbon Dioxide Flooding Using Horizontal Wells,” *67th Annual Technical Conference and Exhibition of SPE*, 4-7 October, Washington, DC.

Lucia, A., D.C. Miller, and A. Kumar, 1985, "Thermodynamically Consistent Quasi-Newton Formulae," *AIChE J.*, no. 31 (8):1381-1388.

McCabe, C., and S.B. Kiselev, 2004, "A Crossover SAFT-VR Equation of State for Pure Fluids: Preliminary Results for Light Hydrocarbons," *Fluid Phase Equilibr.*, no. 219:3-9.

Mehra, R.K., R.A. Heidemann, and K. Aziz, 1983, "Accelerated Successive Substitution Algorithm," *Can. J. Chem. Eng.*, no. 61 (4):590-596.

Mehra, R.K., R.A. Heidemann, and K. Aziz, 1982, "Computation of Multiphase Equilibrium for Compositional Simulation," *SPE J.*, no. 22 (1):61-68.

Michelsen, M.L., 1982a, "The Isothermal FLash Problem. Part I. Stability," *Fluid Phase Equilibr.*, no. 9 (1):1-19.

Michelsen, M.L., 1982b, "The Isothermal Flash Problem. Part II. Phase-Split Calculation," *Fluid Phase Equilibr.*, no. 9 (1):21-40.

Michelsen, M.L., 1986, "Simplified Flash Calculations for Cubic Equations of state," *Ind. Eng. Chem. Process Des. Dev.*, no. 25 (1):184-188.

Minssieux, L., 1997, “Core Damage from Crude Asphaltene Deposition,” *International Symposium on Oilfield Chemistry*, 18-21 February , Houston, Texas.

Mohebbinia, S., K. Sepehrnoori, and R.T. Johns, 2013, "Four-Phase Equilibrium Calculations of Carbon Dioxide/Hydrocarbon/Water Systems With a Reduced Method," *SPE J.*, no. 18 (5):943-951.

Nagel, R.G., B.E. Hunter, J.K. Peggs, D.K. Fong, and E. Mazzocchi, 1990, "Tertiary Application of a Hydrocarbon Miscible Flood: Rainbow Keg River "B" Pool," *SPE Res. Eng.*, no. 5 (3):301-308.

Nellensteyn, F.J., 1924, "The Constitution of Asphalt," *J. Inst. Pet. Technol.*, no. 10:311-323.

Nghiem, L.X., 1999, "*Phase Behavior Modeling and Compositional Simulation of Asphaltene Deposition in Reservoirs*," PhD dissertation, University of Alberta.

Nghiem, L.X., K. Aziz, and Y.K. Li, 1983, "A Robust Iterative Method for Flash Calculations Using the Soave-Redlich-Kwong or the Peng-Robinson Equation of State," *SPE J.*, no. 23 (3):521-530.

Nghiem, L.X., and D.A. Coombe, 1997, "Modeling Asphaltene Precipitation During Primary Depletion," *Soc. Petrol. Eng. J.*, no. 2 (2):170-176.

Nghiem, L.X., and R.A. Heidemann, 1982, "General Acceleration Procedure for Multiphase Flash Calculation with Application to Oil-Gas-Water Systems," *2nd European Symposium on Enhanced Oil Recovery*, 8-10 November, Paris, France.

Nghiem, L.X., and Y.K. Li, 1984, "Computation of Multiphase Equilibrium Phenomena with an Equation of State," *Fluid Phase Equilibr.*, no. 17 (1):77-95.

Nghiem, L.X., and Y.K. Li, 1986, "Effect of Phase Behavior on CO_2 Displacement Efficiency at Low Temperatures: Model Studies with an Equation of State," *SPE Res. Eng.*, no. 1 (4):414-422.

Nichita, D.V., D. Broseta, and J.C. de Hemptinne, 2006, "Multiphase Equilibrium Calculation Using Reduced Variables," *Fluid Phase Equilibr.*, no. 246 (1-2):15-27.

Nor-Azlan, N., and M.A. Adewumi, 1993, "Development of Asphaltene Phase Equilibria Predictive Model," *SPE Eastern Regional Meeting*, 2-4 November, Pittsburgh, Pennsylvania.

Okuno, R., 2009, "*Modeling of Multiphase Behavior for Gas Flooding Simulation*," PhD dissertation, The University of Texas at Austin.

Okuno, R., R.T. Johns, and K. Sepehrnoori, 2010a, "A New Algorithm for Rachford-Rice for Multiphase Compositional Simulation," *SPE J.*, no. 15 (2):313-325.

Okuno, R., R.T. Johns, and K. Sepehrnoori, 2010b, "Three-Phase Flash in Compositional Simulation Using a Reduced Method," *SPE J.*, no. 15 (3):689-703.

Okuno, R., R.T. Johns, and K. Sepehrnoori, 2010c, "Application of a Reduced Method in Compositional Simulation," *SPE J.*, no. 15 (1):39-49.

Pan, H., and A. Firoozabadi, 1998a, "Complex Multiphase Equilibrium Calculations by Direct Minimization of Gibbs Free Energy by Use of Simulated Annealing," *SPE Res. Eval. & Eng.*, no. 1 (1):36-42.

Pan, H., and A. Firoozabadi, 1998b, "Thermodynamic Micellization Model for Asphaltene Aggregation and Precipitation in Petroleum Fluids," *SPE Production & Facilities*, no. 13 (2):118-127.

Pan, H., and A. Firoozabadi, 2003, "Fast and Robust Algorithm for Compositional Modeling: Part II - Two-Phase Flash Computations," *SPE J.*, no. 8 (4):380-391.

Panagiotopolous, A., and R. Reid, 1986, "A New Mixing Rule for Cubic Equations of State for Highly Polar, Asymmetric Systems," *Equation of State*, 571-582.

Panuganti, S.R., F.M. Vargas, and W.G. Chapman, 2012, "Modeling Reservoir Connectivity and Tar Mat Using Gravity-Induced Asphaltene Compositional Grading," *Energy & Fuels*, no. 26 (5):2548-2557.

Panuganti, S.R., F.M. Vargas, D.L. Gonzalez, A.S. Kurup, and W.G. Chapman, 2012, "PC-SAFT characterization of crude oils and modeling of asphaltene phase behavior," *Fuel*, no. 93:658-669.

Peng, D.Y., and D.B. Robinson, 1976, "A New Two-Constant Equation of State," *Ind. Eng. Chem. Fund.*, no. 15 (1):59-64.

Peng, D.Y., and D.B. Robinson, 1980, "Two- and Three-Phase Equilibrium Calculations for Coal Gasification and Related Processes," *Thermodynamics of Aqueous Systems with Industrial Applications*, 393-414.

Peramanu, S., C. Singh, M. Agrawala, and H.W. Yarranton, 2001, "Investigation on the Reversibility of Asphaltene Precipitation," *Energy & Fuels*, no. 15:910-917.

Pernyeszi, T., A. Patzko, O. Berkesi, and I. Dekani, 1998, "Asphaltene Adsorption on Clays and Crude oil Reservoir Rocks," *Coll. Surf. A*, no. 137 (1-3):373-384.

Perschke, D.R., 1988, "*Equation of State Phase Behavior Modeling for Compositional Simulation*," PhD dissertation, The University of Texas at Austin.

Pollack, N.R., R.M. Enick, D.J. Mangone, and B.I. Morsi, 1988, "Effect of an Aqueous Phase on CO_2/Tetradecane and CO_2/Maljamar-Crude-Oil Systems," *SPE Res. Eng.*, no. 3 (2):533-541.

Privat, R., R. Gani, and J. Jaubert, 2010, "Are Safe Results Obtained When the PC-SAFT Equation of State is Applied to Ordinary Pure Chemicals?," *Fluid Phase Equilibr.*, no. 295 (1):76-92.

Qin, X., P. Wang, K. Sepehrnoori, and G.A. Pope, 2000, "Modeling Asphaltene Precipitation in Reservoir Simulation," *Ind. Eng. Chem. Res.*, no. 39 (8):2644-2654.

Rachford, R.H., and J.D. Rice, 1952, "Procedure for Use of Electronic Digital Computers in Calculating Flash Vaporization Hydrocarbon Equilibrium," *J. Pet. Technol.*, no. 4 (10):327-328.

Rassamdana, H., B. Dabir, M. Nematy, M. Farhani, and M. Sahimi, 1996, "Asphalt Flocculation and Deposition: I. The Onset of Precipitation," *AIChE J.*, no. 42 (1):10-22.

Ravey, J.C., G. Ducouret, and D. Espinat, 1988, "Asphaltene Macrostructure by Small Angle Neutron Scattering," *Fuel*, no. 67:1560-1567.

Reis, J.C., and A.M. Acock, 1994, "Permeability Reduction Models for the Precipitation of Inorganic Solids in Berea Sandstone," *In Situ*, no. 18 (3):347-368.

Rezaveisi, M., K. Sepehrnoori, and R.T. Johns, 2013, "Tie-Simplex-Based Phase Behavior Modeling in an IMPEC Reservoir Simulator," *SPE Reservoir Simulation Symposium*, 18-20 February, Woodland, Texas.

Riazi, M.R., 1997, "A Continuous Model for C_7+ Fraction Characterization of Petroleum Fluids," *Ind. Eng. Chem. Res.*, no. 36 (10):4299-4307.

Rudrake, A., K. Karan, and J.H. Horton, 2009, "A Combined QCM and XPS Investigation of Asphaltene Adsorption on Metal Surfaces," *J. Coll. Interface Sci.*, no. 332 (1):22-31.

Sarma, H.K., 2003, "Can We Ignore Asphaltene in a Gas Injection Project for Light-Oils?," *SPE International Improved Oil Recover Conference in Asia Pacific*, 20-21 October, Kuala Lumpur, Malaysia.

Scotti, R., and L. Montanari, 1998, "Molecular Structure and Intermolecular Interaction of Asphaltenes by FT-IR, NMR," *Structure and Dynamics of Asphaltenes*, Plenum Press, New York.

Shelton, J., and L. Yarborough, 1977, "Multiple Phase Behavior in Porous Media During CO_2 or Rich-Gas Flooding," *J. Pet. Tech.*, no. 29 (9):1171-1178.

Shinta, A., and A. Firoozabadi, 1995, "Equation of State Representation of Aqueous Mixtures Using an Association Model," *Can. J. Chem. Eng.*, no. 73 (3):367-379.

Soave, G., 1972, "Equilibrium Constants from a Modified Redlich-Kwong Equation of State," *Chem. Eng. Sci.*, no. 27 (6):1197-1203.

Srivastava, R.K., and S.S. Huang, 1997, "Asphaltene Deposition During CO_2 Flooding: A Laboratory Assessment," *SPE Production Operations Symposium*, Oklahoma City, Oklahoma.

Stalkup, F., 1978, "Carbon Dioxide Miscible Flooding: Past, Present, and Outlook for the Future," *J. Pet. Tech.*, no. 30 (8):1102-1112.

Stenby, E., and P. Wang, 1993, "Noniterative Phase Equilibrium Calculation in Compositional Reservoir Simulation," *SPE Annual Technical Conference and Exhibition*, 3-6 October, Houston, Texas.

Syunyaev, R.Z., R.M. Balabin, I.S. Akhatov, and J.O. Safieva, 2009, "Adsorption of Petroleum Asphaltenes onto Reservoir Rock Sands Studied by Near-Infrared (NIR) Spectroscopy," *Energy & Fuels*, no. 23 (3):1230-1236.

Søreide, I., and C.H. Whitson, 1992, "Peng-Robinson Predictions for Hydrocarbons, CO_2, N_2, and H_2S with Pure Water and NaCl Brine," *Fluid Phase Equilibr.*, no. 77:217-240.

Ting, P.D., 2003, "*Thermodynamic Stability and Phase Behavior of Asphaltenes in Oil and of Other Highly Asymmetric Mixtures*," PhD dissertation, Rice University.

Ting, P.D., G.J. Hirasaki, and W.G. Chapman, 2003, "Modeling of Asphaltene Phase Behavior with the SAFT Equation of State," *Petroleum Science and Technology*, no. 21 (3-4):647-661.

Trangenstein, J.A., 1985, "Minimization of Gibbs Free Energy in Compositional Reservoir Simulation," *SPE Reservoir Simulation Symposium*, 10-13 February, Dallas, Texas.

Trangenstein, J.A., 1987, "Customized Minimization Techniques for Phase Equilibrium Computations in Reservoir Simulation," *Chem. Eng. Sci.*, no. 42 (12):2847-2863.

Vargas, F.M., 2009, "*Modeling of Asphaltene Precipitation and Arterial Deposition*," PhD dissertation, Rice University.

Vargas, F.M., D.L. Gonzalez, G.J. Hirasaki, and W.G. Chapman, 2009, "Modeling Asphaltene Phase Behavior in Crude Oil Systems Using the Perturbed Chain Form of the Statistical Associating Fluid Theory (PC-SAFT) Equation of State," *Energy Fuels*, no. 23:1140-1146.

Victorov, A.I., and A. Firoozabadi, 1996, "Thermodynamics of Asphaltene Precipitation in Petroleum Fluids by a Micellization Model," *AIChE J.*, no. 42 (6):1753-1764.

Voskov, D.V., and H.A. Tchelepi, 2007, "Compositional Space Parameterization for Flow Simulation," *SPE Reservoir Simulation Symposium*, 26-28 February, Houston, Texas.

Voskov, D.V., and H.A. Tchelepi, 2009, "Compositional Space Parameterization: Theory and Application for Immiscible Displacement," *SPE J.*, no. 14 (3):431-440.

Wang, X., and A. Strycker, 2000, "Evaluation of CO_2 Injection with Three Hydrocarbon Phases," *International Oil and Gas Conference and Exhibition*, 7-10 November, Beijing, China.

Werner, A., F. Behar, and E. Behar, 1998, "Viscosity and Phase Behavior of Petroleum Fluids with High Asphaltene Contents," *Fluid Phase Equilibr.*, no. 147 (1-2):343-349.

Wertheim, M.S., 1984a, "Fluids with Highly Directional Attractive Forces. I. Statistical Thermodynamics," *J. Stat. Phys.*, no. 35 (1-2):19-34.

Wertheim, M.S., 1984b, "Fluids with Highly Directional Attractive Forces. II. Thermodynamic Perturbation Theory and Integral Equations," *J. Stat. Phys.*, no. 35 (1-2):35-47.

Whitson, C.H., 1983, "Characterizing Hydrocarbon Plus Fractions," *SPE J.*, no. 23 (4):683-694.

Wilson, G.M., 1969, "A Modified Redlich-Kwong Equation of State-Application to General Physical Data Calculations," *65th National AIChE Meeting*, 4-7 May, Cleveland, Ohio.

Xie, K., and K. Karan, 2005, "Kinetics and Thermodynamics of Asphaltene Adsorption on Metal Surface: A Preliminary Study," *Energy & Fuels*, no. 19 (4):1252-1260.

Yan, W., S. Huang, and E.H. Stenby, 2011, "Measurement and Modeling of CO_2 Solubility in NaCl Brine and CO_2-saturated NaCl Brine Density," *Int. J. Greenh Gas Con*, no. 5 (6):1460-1477.

Yan, W., M.L. Michelsen, and E.H. Stenby, 2011, "On Application of non-cubic EOS to Compositional Reservoir Simulation," *SPE EUROPEC/EAGE Annual Conference and Exhibition*, Vienna, Austria.

Yan, W., and E.H. Stenby, 2009, "The Influence of CO_2 Solubility in Brine on CO_2 Flooding Simulation," *Annual Technical Conference and Exhibition of SPE*, 4-7 October, New Orleans, Louisiana.

Yan, W., and E.H. Stenby, 2010, "The Influence of CO_2 Solubility in Brine on Simulation of CO_2 Injection into Water Flooded Reservoir and CO_2 WAG," *EUROPEC/EAGE Annual Conference and Exhibition*, 14-17 June, Barcelona, Spain.